NASA TN D-1792

TECHNICAL NOTE

D-1792

STATIC LONGITUDINAL AERODYNAMIC CHARACTERISTICS OF AN ELASTIC CANARD-FUSELAGE CONFIGURATION AS MEASURED IN AIR AND IN FREON-12 AT MACH NUMBERS UP TO 0.92

By E. Carson Yates, Jr., and Maynard C. Sandford

Langley Research Center
Langley Station, Hampton, Va.

NATIONAL AERONAUTICS AND SPACE ADMINISTRATION

WASHINGTON

July 1963

NATIONAL AERONAUTICS AND SPACE ADMINISTRATION

TECHNICAL NOTE D-1792

STATIC LONGITUDINAL AERODYNAMIC CHARACTERISTICS OF AN ELASTIC CANARD-FUSELAGE CONFIGURATION AS MEASURED IN AIR AND IN FREON-12 AT MACH NUMBERS UP TO 0.92

By E. Carson Yates, Jr., and Maynard C. Sandford

SUMMARY

Longitudinal aerodynamic characteristics of a geometrically, dynamically, and elastically scaled model of the clipped-delta canard and forward fuselage of a projected nuclear-powered airplane have been investigated by means of force tests conducted in air and in Freon-12 (dichlorodifluoromethane) in the Langley transonic dynamics tunnel. The statically balanced canard was tested in both restrained and free-floating conditions at several levels of dynamic pressure.

The aerodynamic trends of the restrained canard were found to be generally typical of those for delta and clipped-delta planforms. Canard normal-force coefficients measured in Freon-12 were higher than corresponding values measured in air, particularly at the higher Mach numbers. Moreover, the pitching-moment coefficients indicated that canard centers of pressure in Freon-12 were farther aft than those in air. The latter result, however, may be associated with large differences in Reynolds number between the tests in air and in Freon-12. The principal aeroelastic deformations observed were twisting of the torque tube and chordwise deflections of the canard.

As Mach number increased, the free canard experienced appreciable reductions of normal-force coefficient and pitch angle. This behavior could lead to a severe tuck-under problem for the airplane.

INTRODUCTION

The use of canard surfaces for airplane stability, trim, and control has recently attracted increased interest because of proposed applications to supersonic bombers and transport planes. In these applications the canard has frequently been considered only as a trimming and stabilizing device with longitudinal control being provided by elevons on the main lifting surface. The canard was also selected for use on a projected nuclear-powered airplane for operation at high subsonic speeds. This latter canard configuration is the subject of the present investigation. In this installation the canard provides longitudinal

control as well as trim and stability. The canard seems especially appropriate for this type of airplane for several reasons, two of which are (1) the canard configuration permits the crew compartment and the control surfaces to be located as far as possible from the nuclear reactor, and (2) the canard configuration is not subject to the large downward trim loads frequently required by conventionally located tail surfaces at high subsonic and transonic speeds.

The subject canard was statically balanced about its pitch axis and was originally intended to be free floating and to be positioned by servotabs. However, the results of preliminary tests of the free canard led to subsequent consideration of the possibility of using a restrained canard which is positioned by the pitch-axis torque tube.

Although the subsonic longitudinal characteristics of restrained canards have been extensively investigated (refs. 1 to 10, for example), little aerodynamic data appear to be available for free-floating canards except at very low speeds (refs. 11 and 12). Further, no information appears to be available on the effects of static aeroelastic deformations on the subsonic aerodynamic characteristics of canards. In order to provide specific information for the present configuration, an investigation of these characteristics has been conducted in the Langley transonic dynamics tunnel. The model employed (fig. 1) was a geometrically, dynamically, and elastically scaled model of the clipped-delta canard and forward fuselage of a projected nuclear airplane. This model was also used in a flutter investigation of the canard.

Canard lift, bending moment, and pitching moment and servotab hinge moment were measured at Mach numbers up to 0.92 and at several levels of dynamic pressure. The canard was tested in both the free-floating and restrained conditions. Finally, tests of the restrained canard were conducted both in air and in Freon-12 (dichlorodifluoromethane) so that comparisons could be made between the aerodynamic characteristics associated with the two media. Freon-12 is sometimes used as an alternate to air as a test medium because, for a given Mach number and tunnel power, use of Freon-12 results in significant increases in Reynolds number and flow density. (See ref. 13.) The former increase is advantageous for aerodynamic testing, whereas the latter is desirable for aeroelastic experiments. The effects of the aerodynamic differences between air and Freon-12 have not previously been investigated for low-aspect-ratio surfaces.

SYMBOLS

b_c exposed span of one canard panel

$\bar{c}_c$ mean aerodynamic chord of exposed canard

$\bar{c}_t$ mean aerodynamic chord of tab

C_b bending-moment coefficient for canard measured about a spanwise station 10.450 inches outboard of model center line (electric center of bending strain gate), positive for positive normal force, $\frac{\text{Bending moment}}{qS_c b_c}$

C_m pitching-moment coefficient for canard measured about the 24-percent-mean-aerodynamic-chord position (pitch-axis location), positive moment tends to raise leading edge, $\frac{\text{Pitching moment}}{qS_c \bar{c}_c}$

C_h hinge-moment coefficient for tab measured about tab hinge line, positive moment tends to depress trailing edge, $\frac{\text{Hinge moment}}{qS_t \bar{c}_t}$

C_N normal-force coefficient for canard, positive upward, $\frac{\text{Normal force}}{qS_c}$

EI stiffness of fuselage in vertical bending

GJ stiffness of fuselage in torsion

M Mach number

q dynamic pressure

R Reynolds number based on mean aerodynamic chord of exposed canard

S_c exposed area of one canard panel including tab

S_t tab area (each tab)

α_b fuselage angle of attack at canard pitch axis, positive nose up

α_s sting angle of attack, positive nose up

δ_c canard incidence (deflection) angle relative to fuselage reference line at canard pitch axis, positive leading edge up

δ_t tab deflection angle relative to canard chord plane, positive trailing edge down

MODEL

Geometry

As indicated previously this investigation employed a geometrically, elastically, and dynamically scaled model of the canard and forward fuselage of

a proposed nuclear-powered airplane. The general arrangement of the model is shown in figure 1, and some pertinent geometrical properties of the canard and servotab surfaces are given in table I. Photographs of the model are shown as figure 2.

Construction

Canard.- The canard surfaces were built up by a core-plus-balsa-fill type of construction (fig. 3). The core (fig. 3(a)) consisted of streamwise aluminum ribs with end-grain balsa fill. Lead ballast weights were embedded in the core to provide the required mass distribution which resulted in static balance for the canard (canard center of gravity lying on the pitch axis). The core skins (fig. 3(b)) were 0.091-inch-thick aluminum with integral spar and rib caps which projected outward from the skin. The ribs, rib caps, and spar caps were located to provide the required stiffness distribution. End-grain balsa fill was cemented to the outside of the core to build up the required airfoil contour. The exterior of the canard surfaces consisted of squares of balsa sheet with alternating grain orientation.

Tabs.- A core-plus-fill type of construction was also employed for the tabs (fig. 4). However, no ribs, rib caps, nor spar caps were used. The tab core was end-grain balsa, the core skin was 0.016-inch magnesium sheet, and the contour was built up with end-grain balsa. Tab leading and trailing edges were wrapped with one layer of fiber-glass cloth. The tabs were held in fixed position during the static tests by means of turnbuckle-type links between tab and canard core fittings.

Fuselage.- The fuselage was of spar-and-pod construction (figs. 1, 2, and 5). The depth and width of the rectangular aluminum spar were varied along the spar length to yield required distributions of stiffness in vertical bending and torsion. Lateral aluminum flanges were added to the sides of the spar to obtain the required level of lateral bending stiffness.

The nine fuselage sections or pods were constructed of plastic impregnated fiber glass and suspended from the spar so as not to affect the fuselage stiffness. Joints between the sections were sealed with thin sheet rubber and faired with hard wax. The desired distributions of fuselage mass and rolling moment of inertia were attained by mounting lead ballast weights to the spar within the fuselage sections as shown in figure 6.

The canard panels were mounted to the fuselage by means of a spliced torque tube which was supported by four self-alining ball bearings (figs. 5 and 7). Figures 5 and 7 show the clevis and linear actuator arrangement used for remote positioning of the restrained canard. For the free-floating condition this canard-positioner assembly was removed.

Instrumentation

The canard normal force, bending moment, and pitching moment were measured by temperature-compensated strain gages on the canard torque tube. Measurements were made on the left canard panel only. Tab hinge moment was measured by a strain-gage force beam in the tab-positioner linkage.

For both restrained and free conditions the canard incidence angle relative to the fuselage was sensed by a linear variable differential transformer located beside the canard torque tube positioner (fig. 5). Tab angles were preset. The fuselage angle of attack at the canard pitch-axis location was measured by a temperature-compensated pendulum-type inclinometer.

Physical Properties

Distributions of the vertical bending stiffness and the torsional stiffness of the fuselage are indicated in figure 8. Distribution of model weight and moment of inertia in roll are presented in table II.

Structural influence coefficients for the canard surfaces were not measured; however, although the present tests were steady state, the measured natural vibration mode shapes (fig. 9) and natural frequencies of the model (table III) are presented to illustrate the elastic characteristics of the model. In addition to the natural frequencies for the complete model, table III also includes the natural frequencies for each canard plus torque tube mounted in rigidly supported bearings. It may be seen from the values given that the frequency characteristics of the left and right canard panels were close together and that fuselage and sting flexibilities did not greatly alter these characteristics.

APPARATUS AND TESTS

Wind Tunnel

The Langley transonic dynamics tunnel, shown in figure 2 herein and in figure 11 of reference 14, is a return-flow, variable-pressure, slotted-throat tunnel having a test section 16 feet square (with cropped corners). It is capable of operation at stagnation pressures from near vacuum to slightly above atmospheric and at Mach numbers from 0 to 1.2 using either air or Freon-12 as the test medium. The tunnel is particularly suited to both static and dynamic aeroelastic testing because Mach number and dynamic pressure can be varied independently.

Tests

The test conditions for the present investigation are shown in comparison with the tunnel operating curves for both air and Freon-12 in figure 10. For testing, the model was mounted on a massive steel sting support, the pitch angle

of which was adjustable from the tunnel control room. During the tests the outputs of the model strain gages, the fuselage inclinometer, and the canard-position transformer were digitized and recorded in print and on IBM cards. Tunnel stagnation temperature and stagnation and test-section static pressures were recorded in the same way. For tests in Freon-12 the Freon purity was measured by a purity meter which sensed the variation of magnetic susceptibility of the oxygen content of the testing medium. For the present tests, Freon-12 purity was always above 87 percent by volume (or 96.6 percent by weight).

Accuracy of Data

No corrections have been applied to the present data for wall interference, flow angularity, blockage, or differences in test media. However, on the basis of repeatability checks, instrument accuracies, and calibrations, the following uncertainties are considered to exist in the present measurements:

C_b	±0.003
C_m	±0.002
C_h	±0.006
C_N	±0.008
α_b, deg	±0.05
α_s, deg	±0.05
δ_c, deg	±0.10
δ_t, deg	±0.10

PRESENTATION OF RESULTS

Conditions for the present tests are given in tables IV and V, and the basic data are presented in figures 11 to 44. Some of these figures include the results of duplicate measurements which were made in order to indicate the repeatability of the data. Values of C_N, C_b, C_m, C_h, and the deformation $\alpha_s - \alpha_b$ obtained from tests of the restrained canard in air (figs. 11 to 23) and in Freon-12 (figs. 27 to 44) are plotted against $\alpha_b + \delta_c$, the geometric angle of attack (pitch angle) of the canard (relative to the free stream) as measured on the torque tube at the model plane of symmetry. For the free-floating canard, tested only in air (figs. 24 to 26), $\alpha_b + \delta_c$ and the quantities previously listed are plotted against α_b, the fuselage angle of attack measured at the canard pitch axis. For purposes of analysis some of these basic data have been combined or cross-plotted or both, and the results are shown in figures 45 to 54.

In addition to the measurements of aerodynamic forces and moments, unaided visual observations of shock-wave patterns near the model were possible in Freon-12 at high values of Mach number and dynamic pressure. A sketch of a

typical shock-wave pattern is shown in figure 55. Force measurements were not made over a range of pitch angle at these high dynamic pressures because model design load limits would have been exceeded even at relatively small angles.

DISCUSSION OF RESULTS

Restrained Canard in Air

General.- Test results for the restrained canard in air (figs. 11 to 23) indicate that the aerodynamic quantities measured had the same general trends and character regardless of whether the canard pitch angle was changed by varying α_b or δ_c. The normal-force-curve slope is essentially constant at the lower values of $\alpha_b + \delta_c$. Any increase in the slope which may result from the formation of a leading-edge separation vortex is generally small and usually appears at a value of $\alpha_b + \delta_c$ near 8° or 9° (fig. 12(a), for example). This angle may be lower, however, when the tabs are deflected upward (fig. 12(b)). Although no normal-force maximum appeared within the canard pitch-angle range investigated, the approach to stall was in all cases gradual as is typical for delta or clipped-delta planforms. The bending-moment curves are generally similar in shape to the normal-force curves.

The canard pitching-moment curves generally show two regions of reduced stability. One is indicated by a flattening of the pitching-moment curves at small values of the canard pitch angle $\alpha_b + \delta_c$. On some curves (figs. 17(a) and (d), 19(a) and (b), and 23(b)) this flattening becomes a slight depression, indicating a small region of instability. It should be noted that such depressions may exist in more cases than those actually shown because the number of points measured in many of the tests was not sufficient to define in detail the shape of the pitching-moment curve at small values of $\alpha_b + \delta_c$. Another region of reduced stability appears at large pitch angles (generally about 16°) and is indicated by a tendency of the pitching-moment curves to turn upward as $\alpha_b + \delta_c$ increases and the normal-force-curve slope decreases. Tests which included the largest pitch angles, however, showed that this tendency toward instability reverted to a stable trend as $\alpha_b + \delta_c$ was further increased $\left(\alpha_b + \delta_c > 16^\circ\right)$. (See figs. 13, 17, and 21, for example.) The resulting hump in the pitching-moment curve is more pronounced at the higher Mach numbers (figs. 21 and 23) but generally does not appear to be strongly affected by tab deflection. At the highest Mach numbers (0.90 and 0.92) and particularly at the lower dynamic pressure an additional hump occurs at more moderate pitch angles (about 8°). (See figs. 20 and 22.) This latter instability is much less pronounced at the higher dynamic pressure and appears to be associated with shock or boundary-layer phenomena which are sensitive to Reynolds number. (Compare figs. 20 and 22(a) with figs. 21(a) and 23(a), respectively.) The tests of the restrained canard in air cover Reynolds numbers from 0.68×10^6 ($M = 0.92$, $q = 50$ lb/sq ft) to 3.1×10^6 ($M = 0.40$, $q = 100$ lb/sq ft) based on the mean aerodynamic chord of the exposed canard panel. Elastic deformation of the canard at these moderate

pitch angles is not considered to be large enough to affect significantly the sharp instabilities shown.

As the canard pitch angle increases, there is a general trend of increasingl negative pitching moment which causes a progressive nose-down twisting of the torque tube and canard. Since the canard incidence angle δ_c is measured at the center of the fuselage, this increasing twist of torque tube and canard yields an effective angle between the canard surface and the free stream that is progressively less than δ_c. One consequence of this deformation is that the normal force values recorded for positive pitch angles in the present tests are in all cases lower than values that would be indicated for corresponding conditions on a rigid model. (See refs. 15 to 17 for more general discussions of the effects of aeroelastic deformations in the field of stability and control.)

With the tabs undeflected, the tab hinge moments are small except at the higher pitch angles where large nose-down tab moments develop. As the tabs are deflected ($\delta_t < 0$), however, these large nose-down moments are less evident in the data obtained and are generally delayed to higher pitch angles, particularly at the higher Mach number (figs. 17 and 21). Even at the highest pitch angles there is little evidence that any unloading of the tabs is imminent. At the higher Mach numbers (figs. 21 to 23) the large buildup of nose-down hinge moment is preceded, especially for the larger tab deflections, by a dip in the hinge-moment curve which may be associated with shock-induced separation over the tab.

The angle $\alpha_s - \alpha_b$ gives a measure of fuselage vertical bending. Figures 11 to 23 show that within the accuracy of the data, this angle varies approximately linearly with pitch angle, at least within the linear range of C_N. However, when C_N becomes negative, the deflection angle $\alpha_s - \alpha_b$ tends to increase sharply. This behavior may be associated with the changing carryover aerodynamic load on the fuselage. Since the canard is placed quite low on the fuselage and since the underside of the fuselage is relatively flat, the carryover loading on the lower fuselage surface at negative C_N may be greater than the corresponding loading on the upper surface at a positive C_N of the same magnitude. For comparison, it may be noted that the value of $\alpha_s - \alpha_b$ caused by gravity load alone (wind off) is 0.86°.

Effects of unporting and of fuselage flow field.- The canard surface investigated was untwisted and had a symmetrical airfoil section. Therefore, if it were tested in a midwing position on a vertically symmetrical fuselage with $\alpha_b = \delta_c = \delta_t = 0$, it would be expected to experience $C_N = C_m = C_h = 0$. Thus for the present tests the nonzero values of these aerodynamic coefficients which were measured with $\alpha_b = \delta_c = \delta_t = 0$ (figs. 11 to 23) are attributable to the asymmetry of the fuselage in the vertical plane and to the low mounting position of the canard. The effects of the fuselage flow field and of canard unporting[1] may be examined more extensively by comparing results of tests with δ_c varying ($\alpha_b = 0$) and with α_b varying ($\delta_c = 0$). (See fig. 45.) Figure 45 shows that

[1]Unporting refers to the opening of a gap between the canard root and the fuselage caused by angular deflection of the canard.

canard normal force, canard pitching moment, and tab hinge moment vary more rapidly with changes in α_b than with changes in δ_c, particularly at this higher pitch angle. The curves shown for C_N, C_m, and C_h have generally the same shapes regardless of whether α_b or δ_c is varied.

The differences shown in figure 45 are believed to be caused primarily by differing fuselage flow fields and to a lesser extent by unporting of the canard. This statement is supported, for example, by the fact that the difference in slope of the normal-force curves exists even at small pitch angles where no unporting occurs. Unfortunately, however, it is impractical to try to separate these two effects with only aerodynamic-force data. Moreover, the fuselage flow field alone involves two opposing effects. Thus for $\alpha_b > 0$ ($\delta_c = 0$), the inclination of the fuselage to the free stream induces a flow angularity (downwash) which tends to reduce the load on the canard. However, in this attitude the fuselage also induces a cross flow which creates an upwash at the canard and tends to increase the load on the canard, particularly inboard. Figure 45 indicates that the latter effect is dominant.

Although the effects of unporting are integrally combined with the effects of the fuselage flow field in the present data, some general observations can be made. As the canard incidence angle δ_c increases from 0, unporting begins at the trailing edge at about $\delta_c = 4^\circ$. No appreciable gap appears at the leading edge, however, until δ_c reaches about 14°. For negative canard incidence, unporting begins at the leading edge at about $\delta_c = -5^\circ$, but no unporting occurs at the trailing edge. At $\delta_c = 0$, the gap between canard and fuselage was about 1/16 inch. As δ_c increased, unporting would be expected to unload the inboard aft portion of the canard and consequently shift the center of pressure forward and outboard relative to its position at the same pitch angle with α_b varying ($\delta_c = 0$). Thus in comparison with results of tests at the same pitch angle with $\delta_c = 0$ (no unporting), the unporting which accompanied tests at $\alpha_b = 0$ would be expected to yield lower canard normal force and less nose-down moment on both canard and tab. Figure 45 shows that the results compare in this manner, although, as stated previously, the major portions of the differences shown are ascribed to differing fuselage flow fields rather than to unporting alone. With regard to the slope of the normal-force curve, it may also be noted that unloading due to unporting would begin to occur at moderately low pitch angles (4° to 6°) and hence would tend to offset any slope increase resulting from the formation of a leading-edge separation vortex. The test results for δ_c = Constant (0° or 8°) show some evidence of such vortex formation (figs. 12(a) and 13(c), for example), but the results for $\alpha_b = 0$ (gradual unporting) do not.

Figure 46 shows that for positive pitch angles, center-of-pressure positions for $\delta_c = 0$ and those for $\alpha_b = 0$ generally differ insignificantly except at low pitch angles. The asymptotes shown in figure 46 occur where the normal force becomes 0. Note, therefore, that, because of the previously discussed uncertainties in the data, the accuracies of the C_m/C_N and C_b/C_N

curves decrease as these asymptotes are approached. For $\alpha_b + \delta_c$ above 6° or 7° there is essentially no chordwise variation of center of pressure with pitch angle. Therefore, any unloading of the trailing edge due to unporting for $\alpha_b = 0$ must either be small or it must be accompanied by a compensating unloadin forward. For tests with $\delta_c = 0$, the center of pressure at high pitch angle $(\alpha_b + \delta_c > 10^\circ)$ moves inboard as the pitch angle increases. Such behavior is typical for delta and clipped-delta wings as the region of separated flow begins outboard and progresses inboard with increasing pitch angle. (See ref. 18, for example.) For tests with $\alpha_b = 0$, the center of pressure at high pitch angles does not move inboard with increasing pitch angle as rapidly as it does for $\delta_c = 0$. This behavior is probably caused by one or more of the following factors

(1) A relative unloading inboard for the case of $\alpha_b = 0$ due primarily to unporting

(2) A relative loading up inboard for the case of $\delta_c = 0$ caused by the fact that the fuselage cross flow (upwash) is strongest inboard

(3) A relative unloading outboard for the case of $\delta_c = 0$ caused by the presence of a relatively larger outboard region of separated flow for this case which in turn may be related to the differing fuselage flow fields

Pressure-distribution measurements or visual flow studies could define this behavior more completely.

Effects of tab deflection.- For the restrained canard, the effects of tab deflection on the aerodynamic coefficients are illustrated in figures 47(a) and (b). The reduction of normal force caused by progressive negative deflection of the tabs is seen to be relatively small and to vary little with Mach number. Fo $\alpha_b = 0$ (fig. 47(a)), canard pitching moment varies linearly with tab deflection at Mach numbers up to 0.90. For this condition, tab effectiveness in changing pitching moment increases slightly with increasing Mach number, as is indicated by the increasing slope of the curve of C_m against δ_t. For $\alpha_b = 8^\circ$ (fig. 47(b)), however, tab effectiveness decreases substantially as Mach number increases to 0.90. This loss of tab effectiveness at the higher Mach numbers and pitch angles may be caused by flow changes over the tab resulting from the appearance of a supersonic flow region over the upper surface of the canard. Since the boundary-layer thickness and to some extent the pressure distribution downstream of such a supersonic flow region may vary with Reynolds number, it should be remembered that all tests with deflected tabs were conducted in air at Reynolds numbers of 2.0×10^6 or less. (See table IV.)

The variation of tab hinge moment with tab deflection is characteristically nonlinear. The retarded buildup of hinge moment as tab deflection increases (negatively) from 0 is probably associated with the presence of a relatively thick boundary layer over the tab. This boundary layer must be effectively pene trated by the tab before appreciable buildup of hinge moment occurs. It is surprising to observe that for $\alpha_b = 8^\circ$ (fig. 47(b)) the tab hinge moment at small tab deflections is positive, that is, tends to depress the tab trailing edge.

The reason for the appearance of this indicated down load on the tab is not known.

Effects of Mach number.- Some effects of Mach number on the aerodynamic characteristics of the restrained canard are illustrated in figure 48. At zero canard pitch angle (fig. 48(a)), there is little effect of Mach number on the normal force up to $M = 0.90$. At 8° of pitch angle (fig. 48(c)), however, there is a characteristic monotonic increase of C_N amounting to about 13 percent as M increases from 0.40 to 0.85. Further increases of Mach number result in reduced normal force.

For all combinations of pitch angle and tab angle (fig. 48), increases of Mach number above about 0.60 result in appreciable increases of nose-down pitching moment. This behavior is also reflected by the pitching-moment curves of figure 47. Since these large changes of pitching moment are accompanied by only small changes in normal force, significant longitudinal movement of the center of pressure is indicated even at moderate Mach numbers. It should be remembered, however, that Reynolds numbers for these particular tests were relatively low. (See table IV.) Note that at $\alpha_b = 0$ (figs. 48(a) and (b)), the normal force is negative, so that an increase of nose-down pitching moment implies a forward center-of-pressure shift as M increases. At $\alpha_b = 8^\circ$ (figs. 48(c) and (d)), however, C_N is positive so that the indicated center-of-pressure shift is rearward.

Free Canard in Air

In addition to the test data for the free canard, figures 24 to 26 contain results for the restrained canard at $\alpha_b = 0$ with $\alpha_b + \delta_c$ the same as for the free canard tests. Comparisons of the free-canard results with corresponding values measured on the restrained canard give some indication of the consistency of the data.

Effect of fuselage angle.- With the canard free to rotate in pitch, the test results (figs. 24 to 26) show that, as expected, the pitching moment is quite small but in all cases slightly positive. This residual pitching moment is of the same sign and approximately of the same magnitude as the wind-off static-friction moment. The static-friction moment was found to be 2.60 lb-ft which corresponds to $C_m = 0.00182$ at $q = 100$ lb/sq ft. In these tests there was also generally little variation of tab hinge moment with fuselage angle of attack.

Figures 24 to 26 show that canard normal force generally increases as α_b increases. The rate of this increase, however, diminishes with increasing tab deflection and even vanishes entirely for the highest tab deflection $(\delta_t = -12^\circ)$ at $M = 0.90$. In comparison with this behavior of the normal force, note that the canard pitch angle relative to the free stream $(\alpha_b + \delta_c)$ also increases with α_b for small tab deflections. For large tab deflections, however, $\alpha_b + \delta_c$ actually decreases as α_b increases. The relations thus implied between C_N and $\alpha_b + \delta_c$ may be related to the effects of fuselage cross flow and to

unporting. Obviously as α_b increases, the fuselage cross flow increases thus yielding an increasing upwash at the canard. This increasing upwash would tend to generate a growing normal force on the canard at any given canard pitch angle. At small tab deflections, where this effect appears to be greatest, some unporting at the leading edge exists even at small values of α_b. It appears likely that as α_b then increases, further leading-edge unporting does not cause serious additional losses of normal force. At the larger tab deflections, $\alpha_b + \delta_c$ is positive even at low values of α_b. Thus with regard to unporting, the first effect of increasing α_b is to close the gap at the trailing edge; as α_b becomes large, unporting at the leading edge may begin. It should be emphasized, however, that the present force test data are not adequate to permit a detailed examination of the effects of these conditions.

Effects of tab deflection and Mach number.- Figures 47(c) and (d) show that the variations of canard normal force and pitch angle with tab deflection are decidedly nonlinear at Mach numbers up to 0.80 but become more nearly linear at $M = 0.90$. Furthermore, these figures, together with figure 48, show that, for a given tab angle, large reductions of C_N and $\alpha_b + \delta_c$ can occur as Mach number increases. The latter behavior is not surprising since figures 47(a) and (b) and 48 showed that for the restrained canard with a given tab deflection, C_m becomes more negative as M increases.

The curves of C_h against δ_t for the free canard (figs. 47(c) and (d)) show the same general shapes and magnitudes as the corresponding curves for the restrained canard with $\delta_c = 0$ (figs. 47(a) and (b)). Evidently the change of pitch angle with tab deflection on the free canard yields little relieving effect on the tab hinge moment. This behavior is consistent with the results for the restrained canard which generally did not show large variations of hinge moment with pitch angle except at the highest pitch angles.

This configuration of free canard and fuselage nose would, with increasing Mach number, contribute a severe tuck-under (nose-down) tendency to the airplane unless tab deflection is progressively increased (negatively) in order to maintain an approximately constant canard normal force. This requirement would be further complicated by the pronounced nonlinearities in the variation of C_N with δ_t (figs. 47(c) and (d)) and by the fact that even at a constant altitude the dynamic pressure varies as M^2. Even if the requirement could be met, the trim drag on the canard and tabs would constitute an undesirable penalty. It would be preferable aerodynamically to reshape the fuselage nose or to relocate the canard surface and pitch axis, in order to mitigate the changes in the aerodynamic forces resulting from increasing Mach number and in order to attain a configuration that would trim near $\delta_c = 0$ for zero tab deflection at small α_b. This trim requirement can be numerically investigated for the present configuration by examining the effects of adding ballast weight to the trailing edge of the free canard in order to adjust its trim position with $\delta_t = 0$. (See appendix.) The numerical example given in the appendix, however, shows that simple ballasting does not alleviate the tuck-under problem.

Restrained Canard in Freon-12

Comparison with results of tests in air.- The longitudinal aerodynamic characteristics of the restrained canard in Freon-12 (figs. 27 to 44) generally show the same trends and magnitudes as the corresponding quantities measured in air. Significant exceptions to this statement are indicated by the slopes of the normal-force curves and the behavior of the pitching moments at the higher Mach numbers. However, the latter differences are believed to be associated at least to some extent with differences in Reynolds number between tests in air and in Freon-12. Test results for the present elastic model in air and in Freon-12 are compared at the same Mach number and dynamic pressure. On the other hand, if aeroelastic deformations were not significant, the aerodynamic data should more logically be compared at the same Mach number and Reynolds number. Reynolds numbers for the tests in Freon-12 ranged from 1.9×10^6 ($M = 0.92$, $q = 50$ lb/sq ft) to 13.3×10^6 ($M = 0.92$, $q = 344$ lb/sq ft) as compared with 0.68×10^6 to 3.1×10^6 given previously for the tests in air.

Figures 50 and 51 show that for a given Mach number, the shape of the normal-force curve from tests in Freon-12 is essentially the same as that from tests in air. The slope of the curve for Freon-12, however, is greater than that for air, although the slope difference is small except at the highest Mach numbers. These results are in qualitative agreement with those of reference 13, which showed that transonic load levels for two-dimensional wings in Freon-12 were about 10 percent higher than corresponding values for air. No quantitative comparisons are given herein, however, because of the errors inherent in evaluating differences between nearly equal quantities and because of the magnitudes of uncertainties considered to exist in the present data.

The curves of pitching moment for the canard in air and in Freon-12 at $q = 100$ lb/sq ft (figs. 50 and 51) are essentially the same at M up to 0.80, but at higher Mach numbers significant differences appear. As previously indicated for the tests in air, the flat portion of the pitching-moment curve at small pitch angles develops into a depression as M increases to 0.92; this indicates a region of instability. For the tests in Freon-12, however, the pitching-moment curve at small values of $\alpha_b + \delta_c$ becomes steeper at the higher Mach numbers; this indicates a trend toward stability.

At moderate pitch angles (2° to 8°) for $M = 0.90$, pitching moments in Freon-12 are decidedly more negative than those in air. As $\alpha_b + \delta_c$ exceeds about 8°, this trend is terminated by the appearance of a region of near neutral stability which at still higher angles reverts to a stable trend. The unstable break which begins at about $\alpha_b = 12^\circ$ in air is not evident in the Freon-12 data. An increase of Mach number to 0.92 mitigates the differences between the pitching moments for air and for Freon-12 at moderate-to-high pitch angles.

The normal-force and pitching-moment characteristics for the canard in air and in Freon-12 (figs. 50 and 51) indicate that centers of pressure in the two media can differ significantly, particularly at the higher Mach numbers. This result is in contrast to the results of reference 13, which showed centers of pressure on swept and unswept wings of moderate-to-high aspect ratio to be

essentially the same in the two media. The deviations in the present case are believed to be to some extent caused by Reynolds number dependent boundary-layer and separation effects. (See fig. 52.) Figure 52 shows that an increase of dynamic pressure, and hence of Reynolds number, at either $M = 0.80$ or $M = 0.92$ reduces the pitching-moment discrepancies between air and Freon-12.

Another effect of the air Freon-12 pitching-moment difference may be noted. At Mach numbers for which this difference is appreciable, nose-down pitching moments for a given positive pitch angle are greater in Freon-12 than in air; hence, aeroelastic deformation, especially twisting of the torque tubes and canards, is greater in Freon-12. Under these conditions the normal forces measured in air and in Freon-12 at a given $\alpha_b + \delta_c$ are not only lower in magnitude but are closer together than they would be for a rigid model.

Unfortunately, the present force test data do not afford a detailed study of the air-Freon-12 pitching-moment discrepancy. Further investigation of this problem could employ pressure-distribution measurements and visual-flow technique most advantageously.

Effects of varying dynamic pressure.-Aerodynamic characteristics of the restrained canard were measured in Freon-12 at dynamic pressure levels of 50, 100, and 190 lb/sq ft, and the results are compared in figures 53 and 54. For the higher pitch angles, these figures show that both the normal-force coefficient and the pitching-moment coefficient vary less rapidly with pitch angle as q increases. This behavior is attributed primarily to progressive twisting of the torque tube and canard with increasing dynamic pressure or pitch angle or both, although some camber deformation also occurred. As q or $\alpha_b + \delta_c$ is increased, the nose-down pitching moment on the canard surface becomes larger. Under these conditions the canard and the torque tube between the canard and the variable transformer used to measure δ_c become progressively more twisted so that for a given value of $\alpha_b + \delta_c$, the true inclination of the canard to the free stream decreases as q increases.

For $q = 50$ lb/sq ft, however, the normal-force coefficients are close to the values for $q = 100$ lb/sq ft, whereas the corresponding pitching-moment coefficients for $q = 50$ lb/sq ft are decidedly lower (more negative) than those for $q = 100$ lb/sq ft. Some of this difference in pitching-moment coefficient remains even at small pitch angles. Torque-tube and canard twisting probably contributes little to the discrepancy at low pitch angles because values of C_m are not large in that range. Two other factors, however, may influence these results. First, at a given Mach number, the Reynolds number for $q = 50$ lb/sq ft is only about half that for $q = 100$ lb/sq ft. Second, the mechanical friction in the canard support system may account for part of the pitching-moment discrepancy. The friction torque (2.60 lb-ft) corresponds to $|C_m| = 0.00182$ at $q = 100$ lb/sq ft and to $|C_m| = 0.00364$ at $q = 50$ lb/sq ft.

At $M = 0.92$ (figs. 53(d) and 54(d)), the pitch angle for zero normal force with $q = 190$ lb/sq ft is about 0.3° to 0.6° larger than the values for $q = 100$ lb/sq ft. For $C_N = 0$ at $M = 0.92$, the pitching-moment coefficient is

about -0.03, so twisting of the torque tube could account for some of the difference in pitch angle. However, changes in tunnel flow angularity could also contribute.

Figures 34 and 44 show some further effects of q level on the characteristics of the restrained canard in Freon-12. Also included in these figures for comparison are some points reproduced from the data measured at discrete constant q levels. Although the data in figures 34 and 44 contain some scatter and the pitching-moment coefficients are not of large magnitude, the trends indicated for C_N and C_m are the same as those shown in figures 53 and 54. Also apparent in figures 34 and 44 is the progressive bending of the fuselage which occurs as q increases and the canard normal force grows. If these tests had been run at higher pitch angles, the nose-down pitching moments would have been of larger magnitude, and the effects of increasing q would have been more pronounced. Such tests were not conducted, however, because of model structural limitations.

For the tests shown in figures 34 and 44, the tab angle was held by means of the hydraulic actuators employed to oscillate the tabs during the previously mentioned flutter tests instead of by the rigid links used in the remainder of this investigation. The tab-angle accuracy with the hydraulic actuators was about $\pm 0.4^\circ$ instead of the $\pm 0.1^\circ$ applicable for the other test runs. This reduced accuracy undoubtedly contributes to the scatter in the data, particularly in the pitching moment.

SUMMARY OF RESULTS

Longitudinal aerodynamic characteristics of a dynamically and elastically scaled model of the clipped-delta canard and forward fuselage of a projected nuclear-powered airplane have been investigated by means of force tests conducted in air and in Freon-12 in the Langley transonic dynamics tunnel. The balanced canard was tested in both restrained and free-floating conditions at Mach numbers up to 0.92 and 0.90, respectively, and at several levels of dynamic pressure. Although a full understanding of the aerodynamic properties of the model would require pressure distributions and visual flow techniques, the following results are indicated by the present force tests.

For the restrained canard:

1. The aerodynamic trends obtained for the restrained canard are generally typical of those for delta and clipped-delta planforms and are the same regardless of whether fuselage angle of attack or canard incidence angle is varied. However, the cross flow generated by increasing the fuselage angle induces an upwash at the canard so that the resulting normal-force coefficient for a given geometric pitch angle is greater than when the incidence angle is varied.

2. Canard pitching-moment coefficient generally varies approximately linearly with tab deflection. However, tab effectiveness in changing pitching moment decreases markedly at the higher Mach numbers and pitch angles. As Mach

number increases, the pitching-moment coefficient becomes more negative for all pitch angles.

3. For a particular Mach number and dynamic pressure, the normal-force coefficient at a given canard pitch angle is greater in Freon-12 than in air, the larger differences occurring at the higher Mach numbers. Pitching-moment coefficients in air and in Freon-12 are essentially the same at the lower Mach numbers, but differ significantly at higher Mach numbers. The latter result, which indicates canard centers of pressure to be farther aft in Freon-12 than in air, is probably associated with large differences in Reynolds number between the tests in air and in Freon-12.

4. At all Mach numbers the variation of normal-force coefficient and pitching-moment coefficient with canard pitch angle becomes reduced as dynamic pressure is increased. These aeroelastic effects are attributed primarily to twisting of the torque tube and canard and to camber deformation of the canard.

For the free canard:

5. The normal-force coefficient for the free canard generally increases with increasing fuselage angle of attack; however, the rate of increase diminishes as Mach number or tab deflection is increased. The variation of normal-force coefficient with tab deflection is decidedly nonlinear.

6. As Mach number increases, the free canard experiences appreciable reductions of normal-force coefficient and canard pitch angle, in agreement with the buildup of nose-down pitching-moment coefficient observed for the restrained canard. This behavior could lead to a severe tuck-under problem for the airplan The tuck-under problem is not alleviated by ballasting, although at a particular Mach number, the canard can be brought to a desirable trim position with tab angle and canard incidence angle near zero by means of trailing-edge ballast.

Langley Research Center,
National Aeronautics and Space Administration,
Langley Station, Hampton, Va., February 25, 1963.

APPENDIX

EFFECT OF TRAILING-EDGE BALLAST WEIGHT

As a numerical example of the effect of trailing-edge ballast on the present canard, consider the following arbitrarily chosen requirements: The canard is required to trim at $\delta_c = 0$ for $\delta_t = 0$ and $\alpha_b = 0$ at $M = 0.60$ in air. Initially the dynamic pressure is assumed to be 100 lb/sq ft for all Mach numbers. Figure 13(b) indicates that for the stated conditions the restrained canard experiences $C_m = -0.00850$. The free canard, however, is assumed to experience $C_m = 0.00182$ due to the friction moment of 2.60 lb-ft. Therefore, for the canard to float free at $\delta_c = \delta_t = \alpha_b = 0$, an increase in nose-up pitching-moment coefficient of

$$\left[\Delta C_m\right]_{\delta_c=\alpha_b=0} = 0.00850 + 0.00182 = 0.01032$$

is required. At $q = 100$ lb/sq ft, the required ballast pitching moment is 14.74 lb-ft per side for $\delta_c = \alpha_b = 0$. For definiteness, consider the ballast weight to be located longitudinally at the tab hinge line. The moment arm about the pitch axis will then be 1.649 ft, and the corresponding ballast weight per side will be 8.940 lb or 42.36 percent of the average canard weight per side. The resulting corrections

$$\Delta C_m = 0.01032 \cos(\alpha_b + \delta_c)$$

and

$$\Delta C_N = -0.01693 \cos(\alpha_b + \delta_c)$$

are therefore to be added to the measured data for the restrained canard at a value of $\alpha_b + \delta_c$ such that the corrected pitching moment is 0.00182.

The aerodynamic properties of the canard with trailing-edge ballast (fig. 49) indicate that the addition of this type of ballast does not satisfactorily alleviate the increasing nose-down tendency as Mach number increases. Furthermore, in this example $q = 100$ lb/sq ft was assumed throughout. If the dynamic pressure were assumed to be proportional to M^2 (as for flight at a constant altitude), the correction to the pitching-moment and normal-force coefficients would decrease in magnitude with increasing M. In figure 49 then the resulting corrected curves would coincide with the corrected curves shown only at $M = 0.60$. For higher Mach numbers the corrected curves would deviate progressively from those shown, the deviation being in the direction of the uncorrected curves (i.e., curves for the balanced canard). Such a correction would indicate an even more pronounced nose-down tendency than that based on the assumption of constant q. If a calculated correction of this type (i.e., for varying dynamic pressure) were made in the present data, it should be remembered that the correction would be applied to aerodynamic characteristics measured at a constant q

and hence would not reflect any changes in aeroelastic effects which vary with dynamic pressure.

It appears that satisfactory solution of the tuck-under problem would require some other approach such as alteration of the flow field about the canard by a reshaping of the fuselage, by relocation of the canard, or both.

REFERENCES

1. Burrows, Dale L.: Large-Scale Low-Speed Wind-Tunnel Tests of a Model Having a 60° Delta Horizontal Canard Control Surface and Wing To Obtain Static-Longitudinal-Stability and Canard-Surface Hinge-Moment Data. NACA RM L54D16a, 1954.

2. Peterson, Victor L., and Menees, Gene P.: Static Stability and Control of Canard Configurations at Mach Numbers From 0.70 to 2.22 - Longitudinal Characteristics of a Triangular Wing and Unswept Canard. NACA RM A57K26, 1958.

3. Hall, Charles F., and Boyd, John W.: Effects of Canards on Airplane Performance and Stability. NACA RM A58D24, 1958.

4. Cone, Clarence D., Jr.: Low-Speed Static Longitudinal and Lateral Stability Characteristics of a Variable-Incidence Delta-Wing Canard Model With High-Lift Canard Surfaces. NASA TM X-72, 1959.

5. Croom, Delwin R., and Fournier, Paul G.: Aerodynamic Characteristics at Low Speed of a Canard Bomber Configuration Designed for Supersonic Cruise Flight. NASA TM X-264, 1960.

6. Kelly, Thomas C.: Aerodynamic Characteristics at Mach Numbers From 0.60 to 1.16 of a Canard Configuration Designed for Supersonic Cruise Flight. NASA TM X-265, 1960.

7. Peterson, Victor L.: Static Stability and Control of Canard Configurations at Mach Numbers From 0.70 to 2.22 - Triangular Wing and Canard With Twin Vertical Tails. NASA TN D-1033, 1961.

8. Mathews, Charles W.: Study of the Canard Configuration With Particular Reference to Transonic Flight Characteristics and Low-Speed Characteristics at High Lift. NACA RM L8G14, 1949.

9. Fournier, Paul G.: Aerodynamic Characteristics of a Canard and an Outboard-Tail Airplane Model at High Subsonic Speeds. NASA TN D-1002, 1961.

10. Brady, James A., Page, V. Robert, and Koenig, David G.: Large-Scale Low-Speed Wind-Tunnel Tests of a Delta Winged Supersonic Transport Model With a Delta Canard Control Surface. NASA TM X-643, 1962.

11. Bates, William R.: Low-Speed Static Longitudinal Stability Characteristics of a Canard Model Having a 60° Triangular Wing and Horizontal Tail. NACA RM L9H17, 1949.

12. Scallion, William I., and Cannon, Michael D.: The Low-Speed Static Longitudinal and Lateral Characteristics of a Delta-Wing Model With Fixed and Free-Floating Canard Surfaces. NASA TM X-120, 1959.

13. Von Doenhoff, Albert E., Braslow, Albert L., and Schwartzberg, Milton A.: Studies of the Use of Freon-12 as a Wind-Tunnel Testing Medium. NACA TN 3000, 1953.

14. Yates, E. Carson, Jr., Land, Norman S., and Foughner, Jerome T., Jr.: Measured and Calculated Subsonic and Transonic Flutter Characteristics of a 45° Sweptback Wing Planform in Air and In Freon-12 in the Langley Transonic Dynamics Tunnel. NASA TN D-1616, 1963.

15. J. B. Rea Co., Inc.: Aeroelasticity in Stability and Control. WADC Tech. Rep. 55-173, U.S. Air Force, Mar. 1957.

16. Taylor, A. S.: The Present Status of Aircraft Stability Problems in the Aeroelastic Domain. Tech. Note Aero.2538, British R.A.E., Dec. 1957.

17. Runyan, H. L., Pratt, K. G., and Bennett, F. V.: Effects of Aeroelasticity on the Stability and Control Characteristics of Airplanes. Presented to AGARD Specialists Meeting on Stability and Control (Brussels, Belgium), Apr. 10-14, 1961.

18. Yates, E. Carson, Jr.: Low-Speed Wind-Tunnel Investigation of Leading-Edge Porous Suction on a 4-Percent-Thick 60° Delta Wing. NACA RM L54L21, 1955.

TABLE I.- MODEL PROPERTIES

Canard:	
Exposed panel aspect ratio	0.954
Exposed panel taper ratio	0.1889
Leading-edge sweep angle, deg	50
Trailing-edge sweep angle, deg	-11.5
Airfoil section (streamwise)	NACA 0008-64
Thickness ratio	0.080
Full span, ft	6.153
Exposed panel span, b_c, ft	2.243
Mean aerodynamic chord of exposed area, $\bar{c}_c$, ft	2.706
Exposed panel area, S_c, sq ft	5.279
Pitch-axis location (percent of $\bar{c}_c$)	24
Panel weight:	
Left, lb	21.04
Right, lb	21.18
Tabs:	
Sweep angle of hinge line, deg	0
Span, ft	0.8333
Mean aerodynamic chord, $\bar{c}_t$	0.3928
Tab area (each), S_t, sq ft	0.3218
Tab weight (each):	
Left, lb	0.54
Right, lb	0.56
Torque tubes:	
Torsional stiffness:	
Left, ft-lb/radian	11,500
Right, ft-lb/radian	11,700

TABLE II.- DISTRIBUTIONS OF MODEL WEIGHT AND MOMENT OF INERTIA IN ROLL

Section (See fig. 1)	Weight, lb	Moment of inertia about spar center, $lb\text{-}ft^2$
1	8.6	1.132
2	27.4	10.069
a_3	186.0	129.438
a_4	268.8	134.868
5	153.0	89.347
6	52.4	20.424
7	94.4	46.875
8	192.7	48.778
9	70.4	21.854
Total	1,053.7	

[a]Canard weight and moment of inertia in roll are distributed between sections 3 and 4.

TABLE III.- NATURAL FREQUENCIES OF VIBRATION

Model component	Mode	Natural frequencies, cps, for -		
		Complete model in tunnel	Left canard on rigid support	Right canard on rigid support
Fuselage	First bending	4.2		
	Second bending	18.5		
	Third bending	26.7		
	First torsion	11.5		
Canard (restrained)	Symmetric pitch	12.5		
	Antisymmetric pitch	15.9	16.6	17.0
	First bending	36.3	38.3	38.5
	Third mode	67.1	67.2	69.1
	Fourth mode	96.8	103.4	100.0
Canard (free)	Antisymmetric pitch	15.9		
	First bending	36.1	34.0	35.0
	Third mode	67.4	66.0	68.2
	Fourth mode	96.8	91.7	92.7

TABLE IV.- SUMMARY OF TEST CONDITIONS IN AIR

(a) Restrained canard

M	q, lb/sq ft	R	δ_t, deg	δ_c, deg	α_b, deg	$\alpha_b + \delta_c$, deg	Figure
0.40	100	3.1×10^6	0	0	Varies	-2 to 10	11(a)
				Varies	0	-4 to 10	11(b)
0.60	50	1.0×10^6	0	0	Varies	-2 to 14	12(a)
			-12	0	Varies	-2 to 14	12(b)
				Varies	0	-8 to 16	12(c)
	100	2.0	0	0	Varies	-2 to 14	13(a)
				Varies	0	-8 to 16	13(b)
				8	Varies	6 to 20	13(c)
			-4	0	Varies	-2 to 14	13(d)
				Varies	0	-8 to 16	13(e)
				8	Varies	6 to 20	13(f)
			-8	0	Varies	-2 to 14	13(g)
				Varies	0	-8 to 16	13(h)
				8	Varies	6 to 20	13(i)
			-12	0	Varies	-2 to 14	13(j)
				Varies	0	-8 to 16	13(k)
0.70	50	0.92×10^6	0	0	Varies	-2 to 14	14(a)
				Varies	0	-8 to 16	14(b)
	100	1.8	0	0	Varies	-2 to 14	15(a)
				Varies	0	-8 to 16	15(b)
0.80	50	0.85×10^6	0	0	Varies	-2 to 14	16(a)
			-12	0	Varies	-2 to 14	16(b)
				Varies	0	-8 to 16	16(c)
	100	1.6	0	0	Varies	-2 to 14	17(a)
				Varies	0	-8 to 16	17(b)
				8	Varies	6 to 20	17(c)
			-4	0	Varies	-2 to 14	17(d)
				Varies	0	-8 to 16	17(e)
				8	Varies	6 to 20	17(f)
			-8	0	Varies	-2 to 14	17(g)
				Varies	0	-8 to 16	17(h)
				8	Varies	6 to 20	17(i)
			-12	0	Varies	-2 to 14	17(j)
				Varies	0	-8 to 16	17(k)
				8	Varies	6 to 20	17(l)
0.85	50	0.74×10^6	0	0	Varies	-2 to 14	18(a)
				Varies	0	-8 to 16	18(b)
	100	1.6	0	0	Varies	-2 to 14	19(a)
				Varies	0	-8 to 16	19(b)
0.90	50	0.79×10^6	0	0	Varies	-2 to 14	20
	100	1.5	0	0	Varies	-2 to 14	21(a)
				Varies	0	-8 to 16	21(b)
				8	Varies	6 to 20	21(c)
			-4	0	Varies	-2 to 14	21(d)
				Varies	0	-8 to 16	21(e)
				8	Varies	6 to 20	21(f)
			-8	0	Varies	-2 to 14	21(g)
				Varies	0	-8 to 16	21(h)
				8	Varies	6 to 20	21(i)
			-12	0	Varies	-2 to 14	21(j)
				Varies	0	-8 to 16	21(k)
				8	Varies	6 to 20	21(l)
0.92	50	0.68×10^6	0	0	Varies	-2 to 14	22(a)
				Varies	0	-8 to 16	22(b)
	100	1.5	0	0	Varies	-2 to 14	23(a)
				Varies	0	-8 to 16	23(b)
				12	Varies	10 to 26	23(c)

TABLE IV.- SUMMARY OF TEST CONDITIONS IN AIR - Concluded

(b) Free canard

M	q, lb/sq ft	R	δ_t, deg	α_b, deg	Figure
0.60	100	2.0×10^6	0	-2 to 12	24(a)
			-4	-2 to 12	24(b)
			-8	-2 to 12	24(c)
			-12	-2 to 12	24(d)
0.80	100	1.6×10^6	0	-2 to 12	25(a)
			-4	-2 to 12	25(b)
			-8	-2 to 12	25(c)
			-12	-2 to 12	25(d)
0.90	100	1.5×10^6	0	-2 to 12	26(a)
			-4	-2 to 12	26(b)
			-8	-2 to 12	26(c)
			-12	-2 to 12	26(d)

TABLE V.- SUMMARY OF TEST CONDITIONS IN FREON-12

[Restrained canard with $\delta_t = 0$]

M	q, lb/sq ft	R	δ_c, deg	α_b, deg	$\alpha_b + \delta_c$, deg	Figure
0.60	50	2.8×10^6	0	Varies	-2 to 14	27
	100	5.7	0	Varies	-2 to 14	28(a)
			Varies	0	-8 to 16	28(b)
0.70	50	2.5×10^6	0	Varies	-2 to 14	29(a)
			Varies	0	-2 to 8	29(b)
	100	5.1	0	Varies	-2 to 14	30(a)
			Varies	0	-8 to 16	30(b)
0.80	50	2.1×10^6	0	Varies	-2 to 14	31
	100	4.4	0	Varies	-2 to 14	32(a)
			Varies	0	-8 to 16	32(b)
	190	8.7	0	Varies	-2 to 12	33(a)
			Varies	0	-8 to 16	33(b)
	112 to 343	---	0	0	0	34(a)
			-4	0	-4	34(b)
0.85	50	2.0×10^6	0	Varies	-2 to 14	35(a)
			Varies	0	-2 to 8	35(b)
	100	4.1	0	Varies	-2 to 14	36(a)
			Varies	0	-8 to 16	36(b)
	190	8.2	0	Varies	-2 to 10	37(a)
			Varies	0	-8 to 12	37(b)
0.90	50	2.0×10^6	0	Varies	-2 to 14	38(a)
			Varies	0	-2 to 8	38(b)
	100	4.0	0	Varies	-2 to 14	39(a)
			Varies	0	-8 to 16	39(b)
	190	7.7	0	Varies	-2 to 4	40(a)
			Varies	0	-4 to 4	40(b)
0.92	50	1.9×10^6	0	Varies	-2 to 14	41(a)
			Varies	0	-2 to 8	41(b)
	100	4.0	0	Varies	-2 to 14	42(a)
			Varies	-2	-6 to 14	42(b)
			Varies	0	-8 to 16	42(c)
			Varies	2	-2 to 18	42(d)
			Varies	4	0 to 16	42(e)
			-8	Varies	-10 to 6	42(f)
	190	7.7	0	Varies	-2 to 4	43(a)
			Varies	0	-4 to 4	43(b)
	134 to 344	---	0	0	0	44

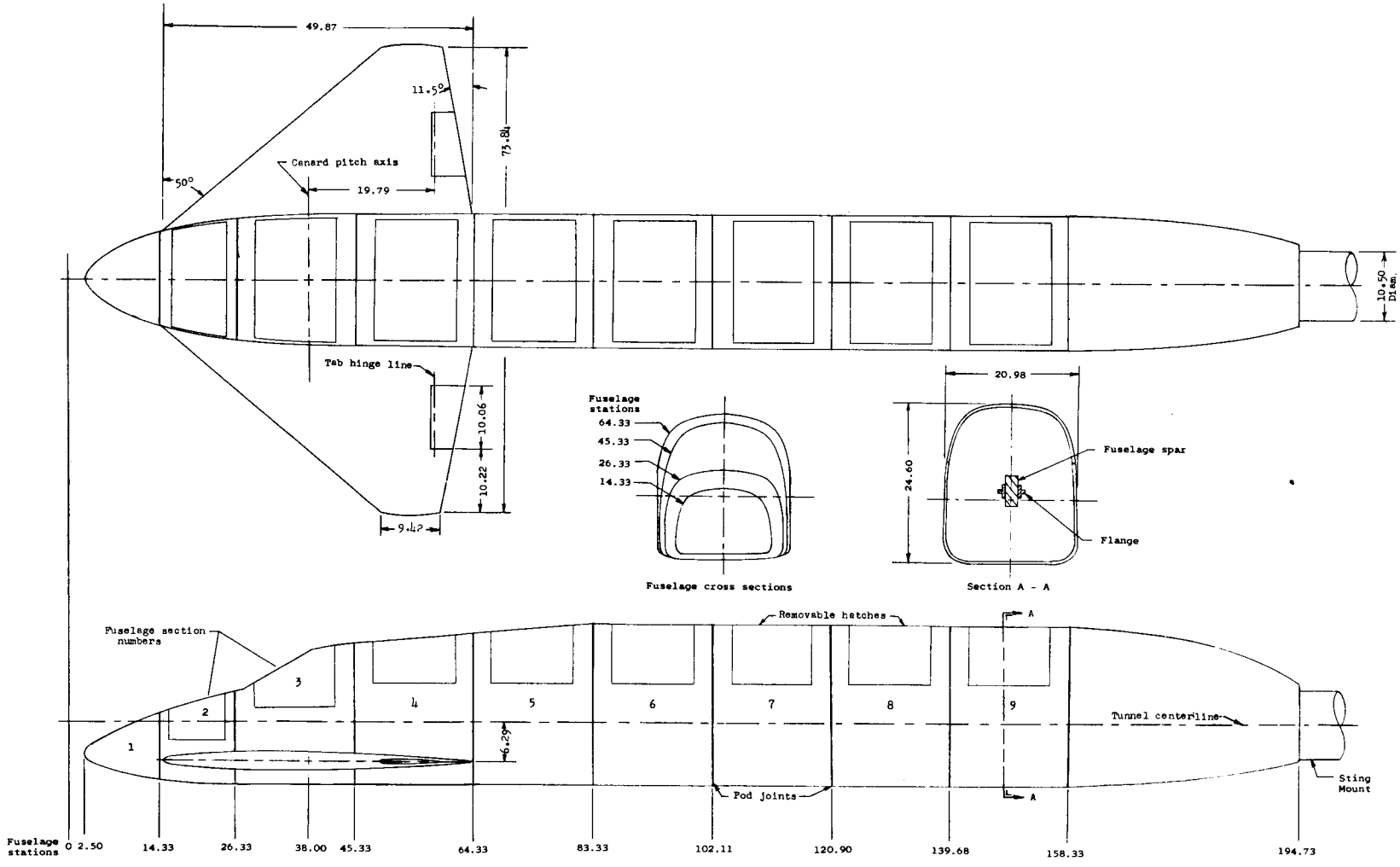

Figure 1.- Two-view drawing of the model. All dimensions are in inches unless otherwise specified.

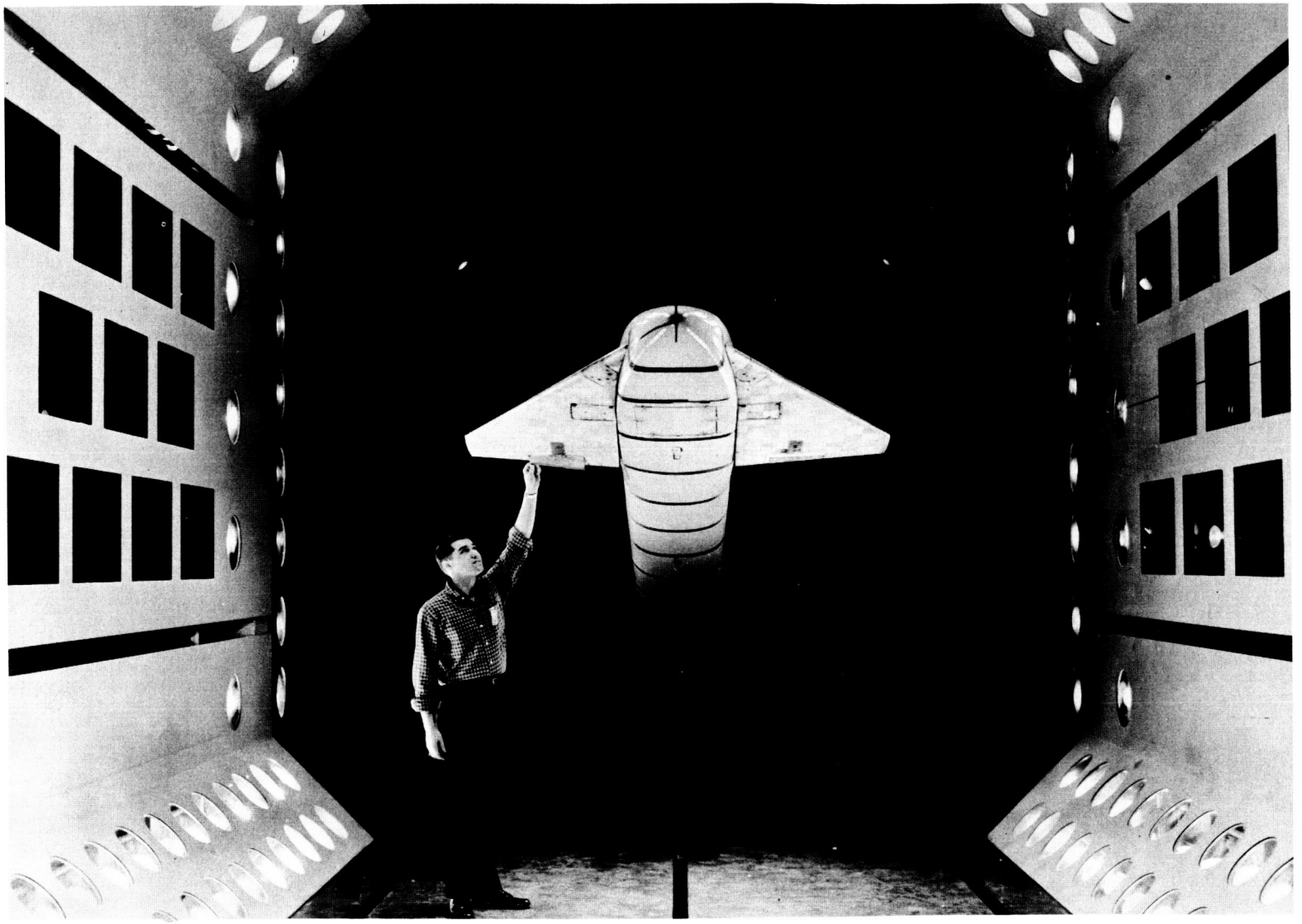

(a) Front view. L-61-2010

Figure 2.- Canard model in the Langley transonic dynamics tunnel.

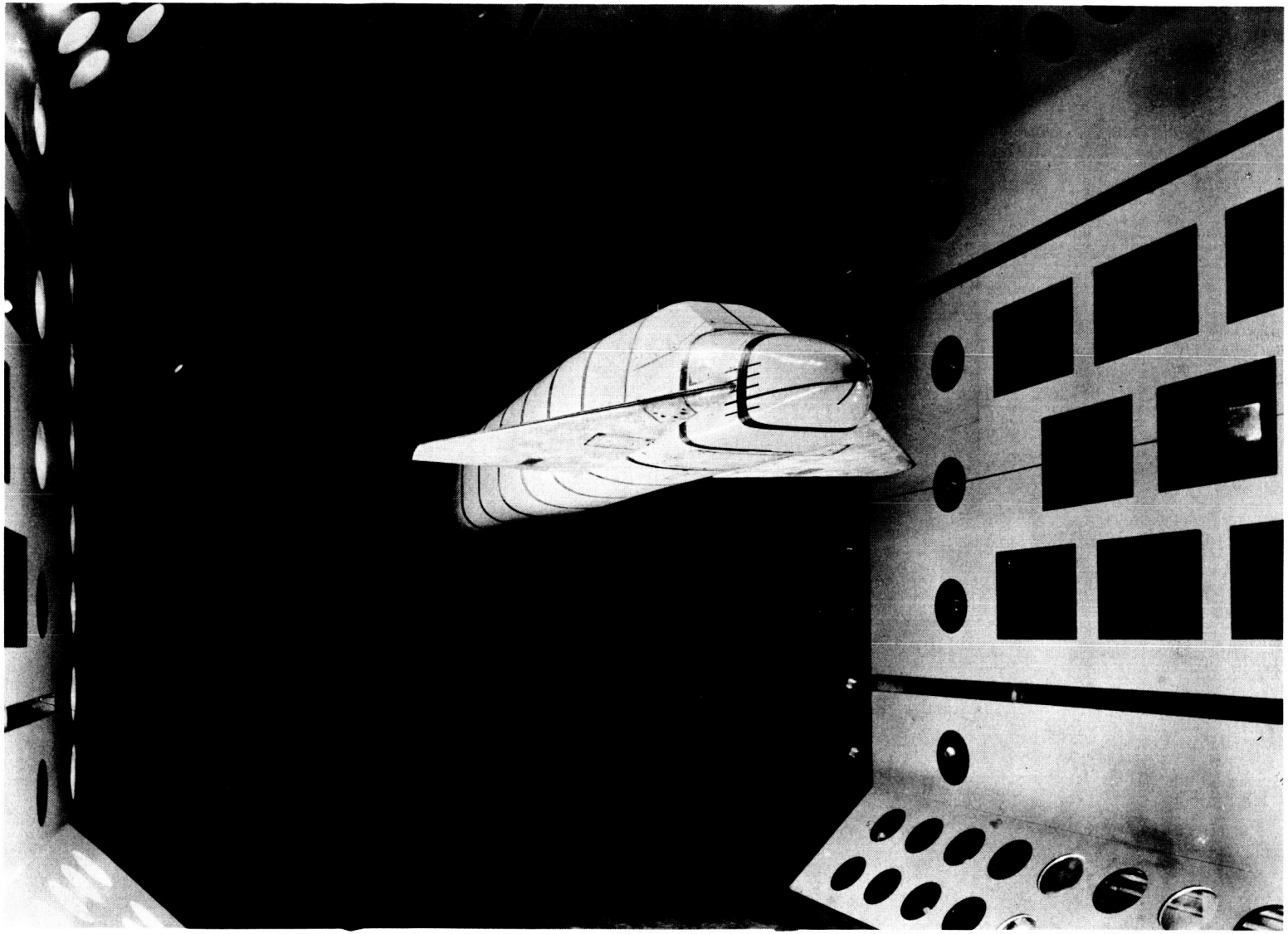

(b) Three-quarter front view. L-61-2014

Figure 2.- Concluded.

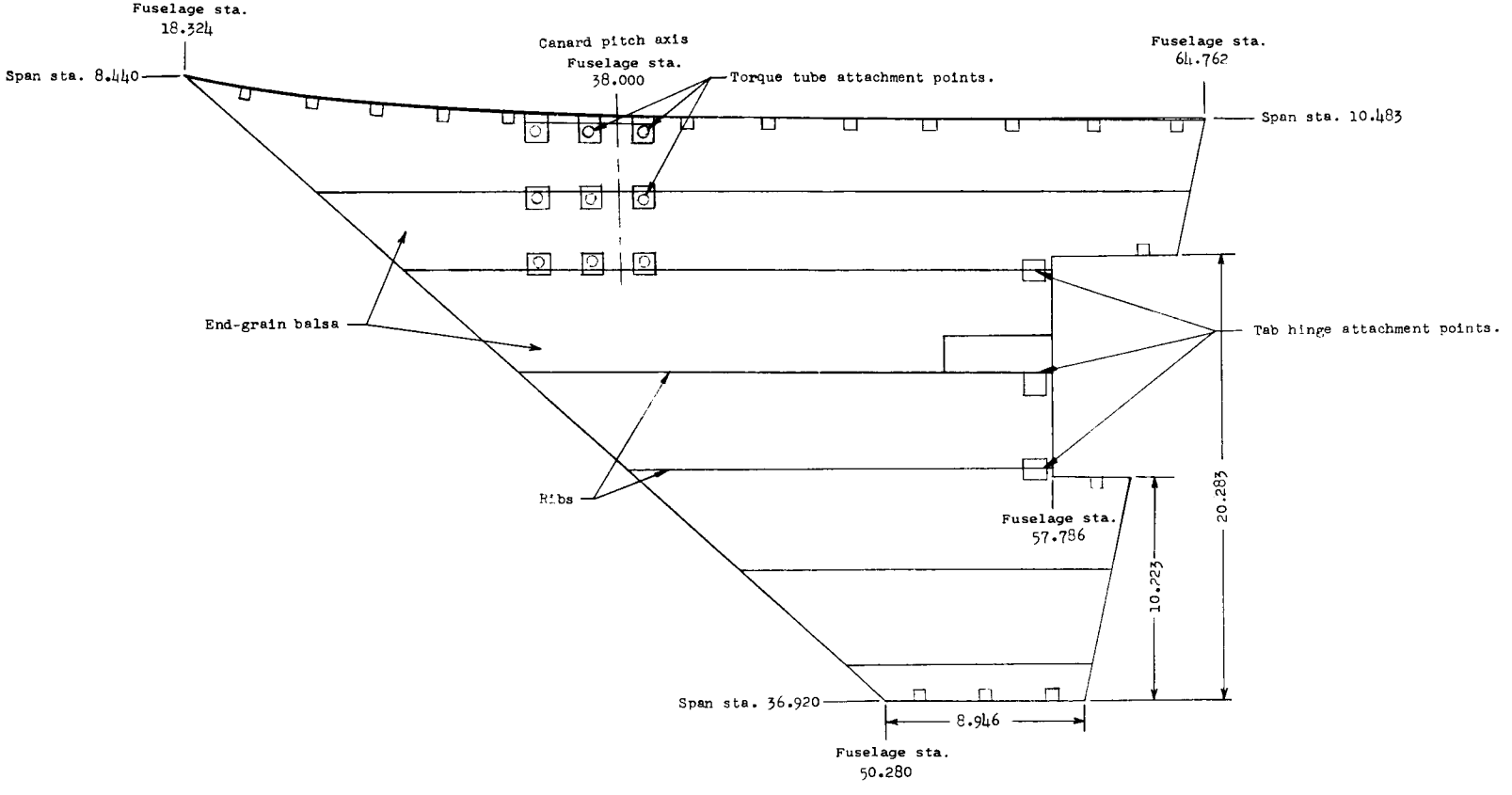

(a) Canard core.

Figure 3.- Internal structure of canard surface. All dimensions are in inches.

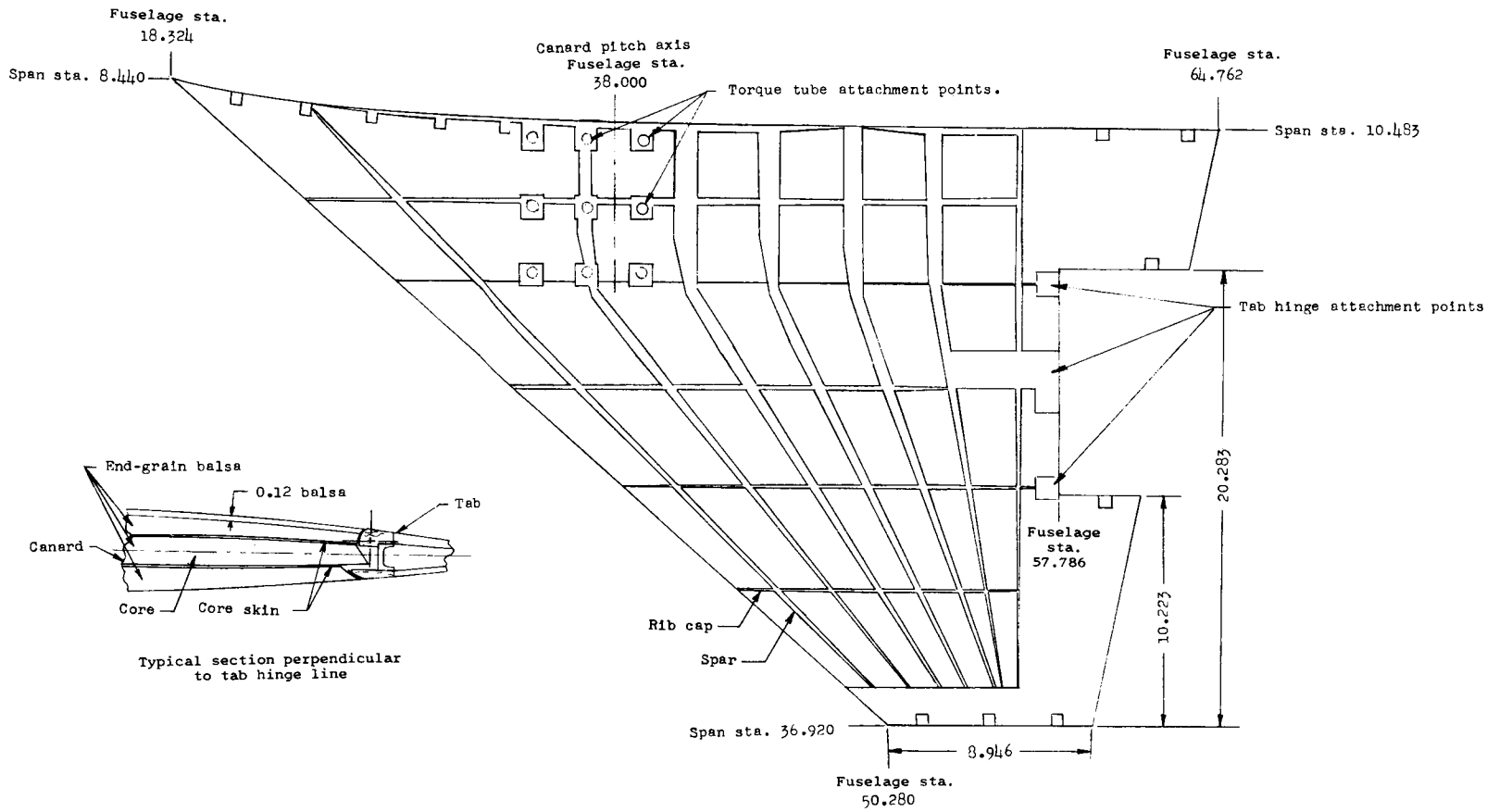

(b) Canard core skin with integral spars and rib caps.

Figure 3.- Concluded.

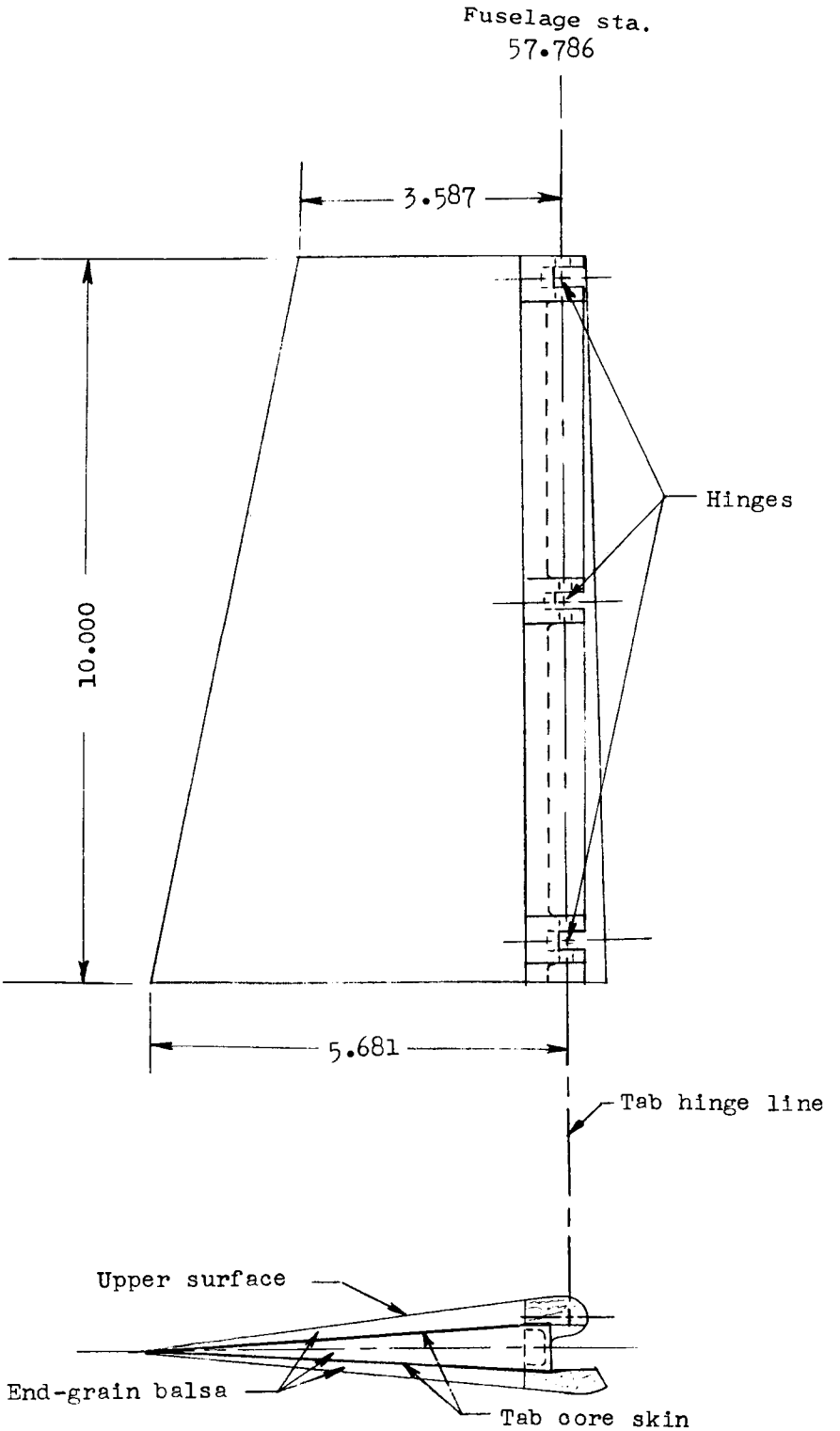

Figure 4.- Two-view drawing of tab. All dimensions are in inches.

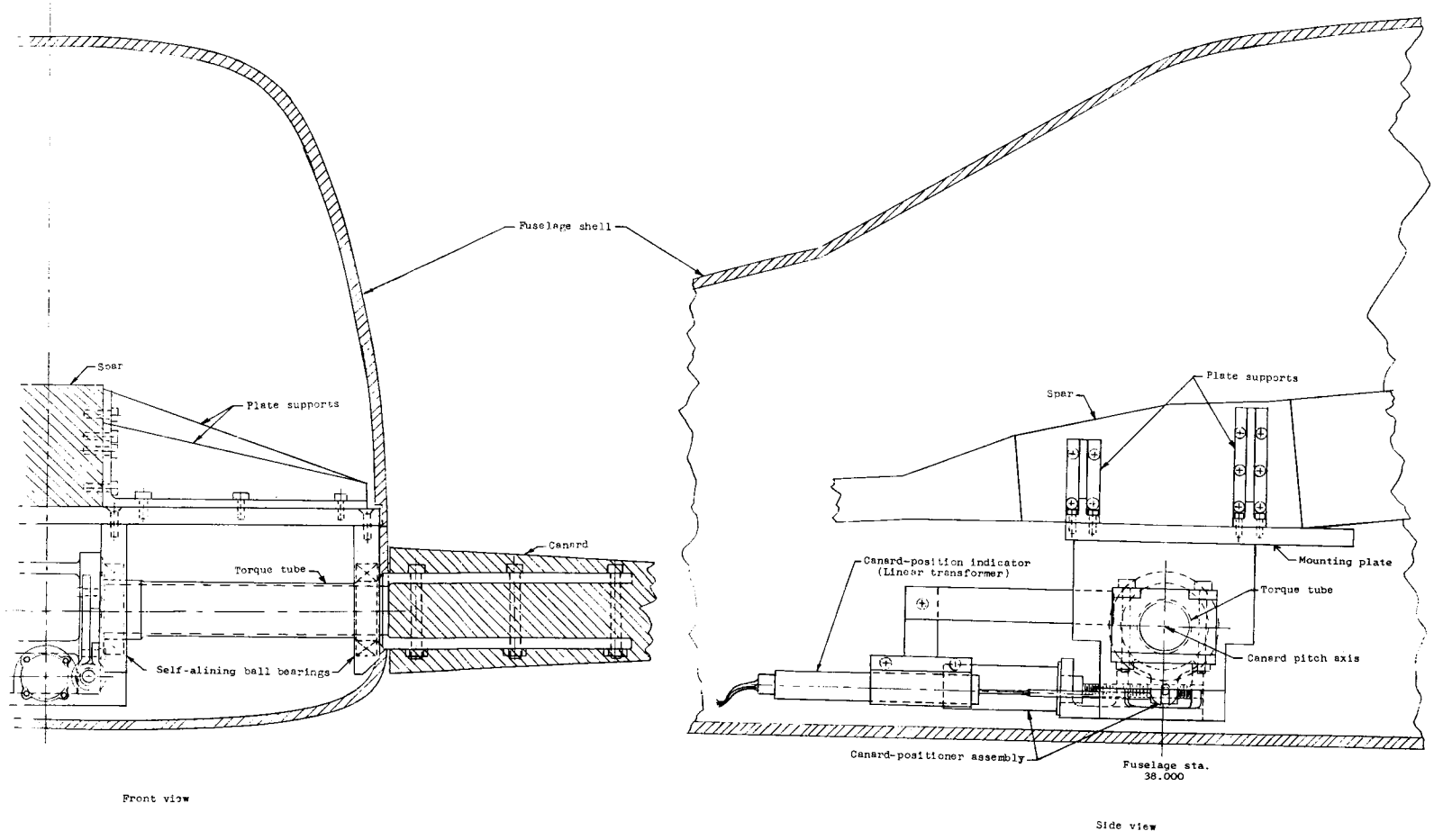

Figure 5.- Canard positioning mechanism.

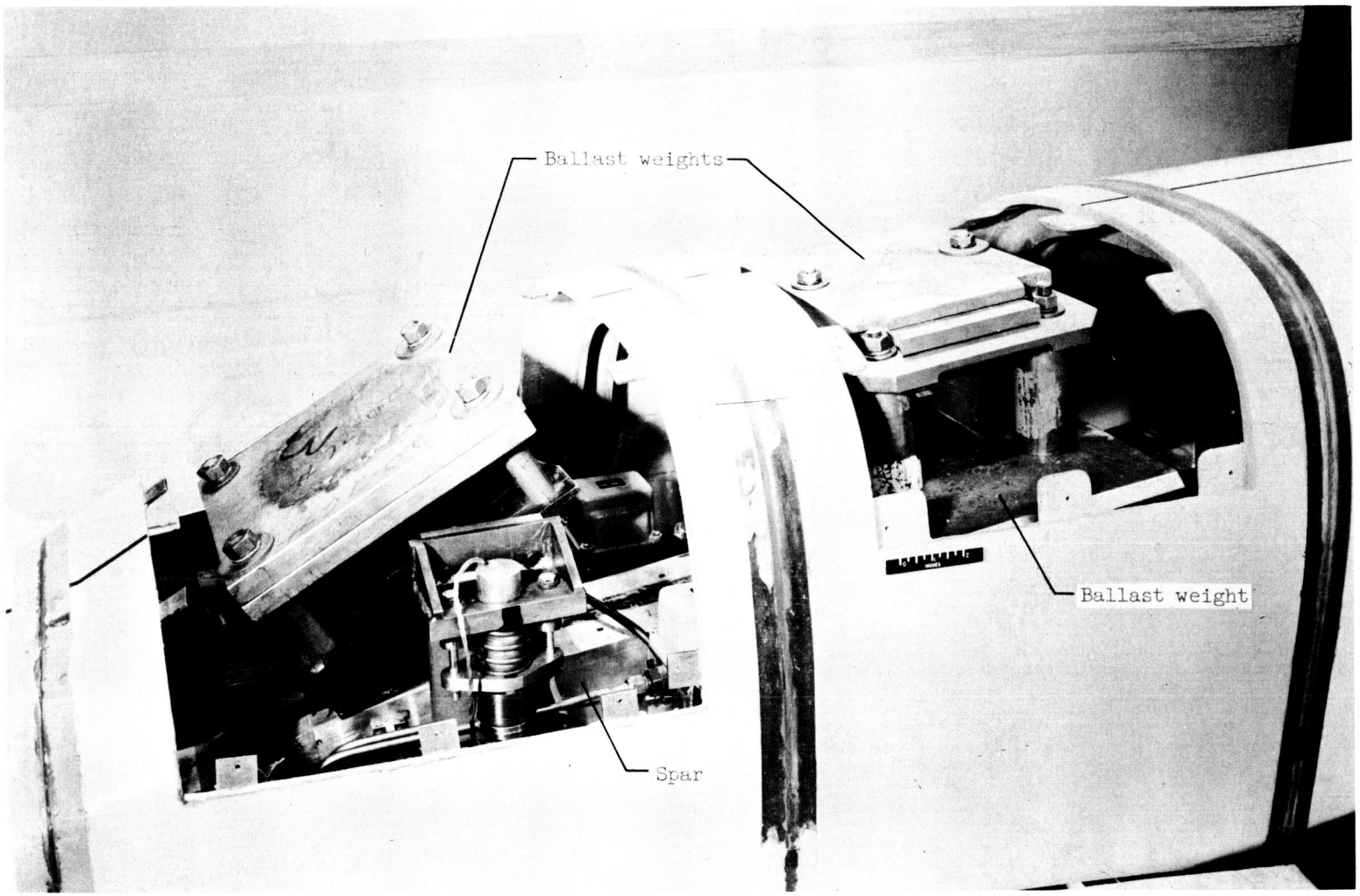

Figure 6.- Installation of ballast weights in model.

L-61-2017.1

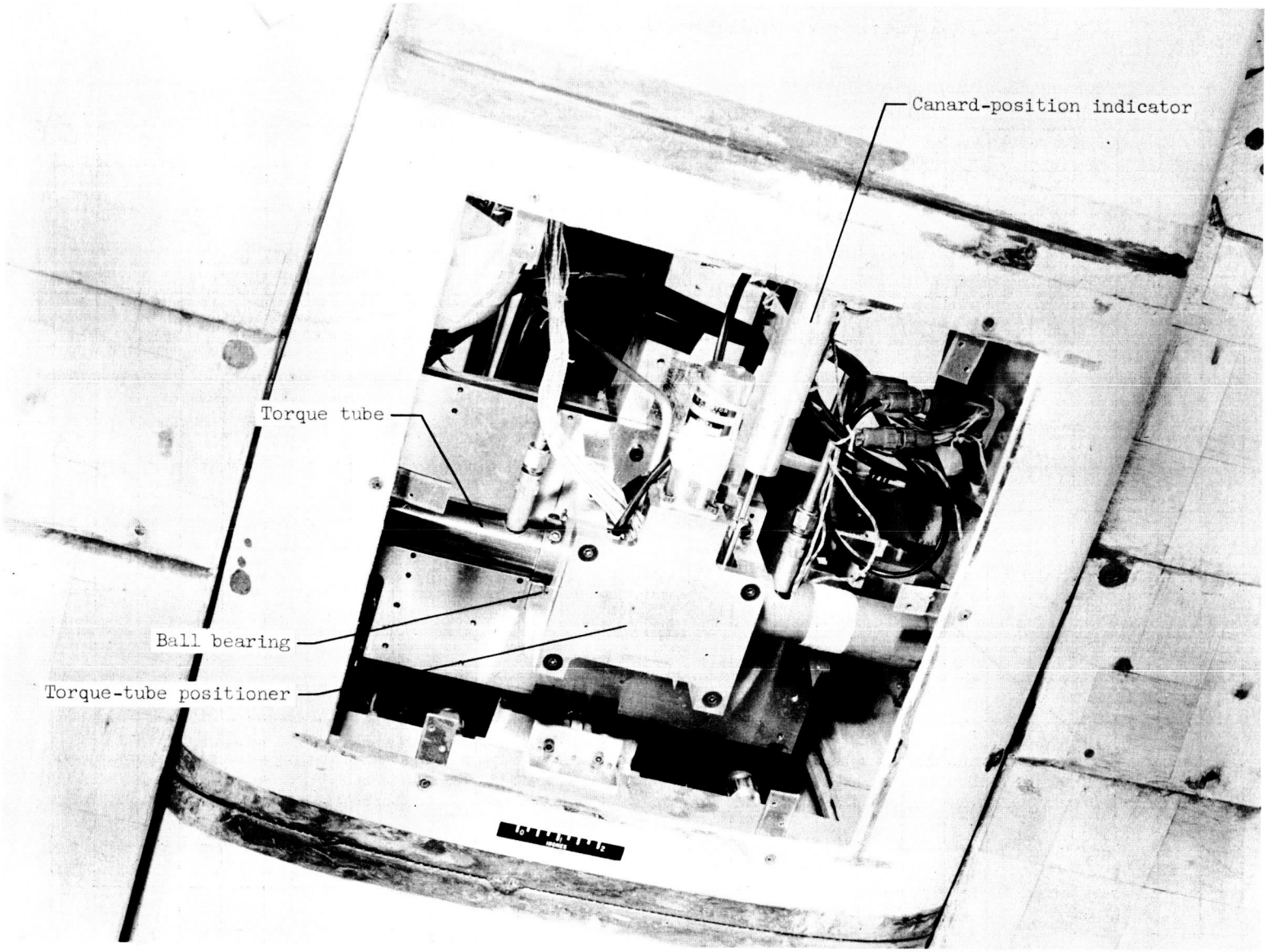

Figure 7.- Torque-tube and positioner assembly viewed from below. L-61-2019.1

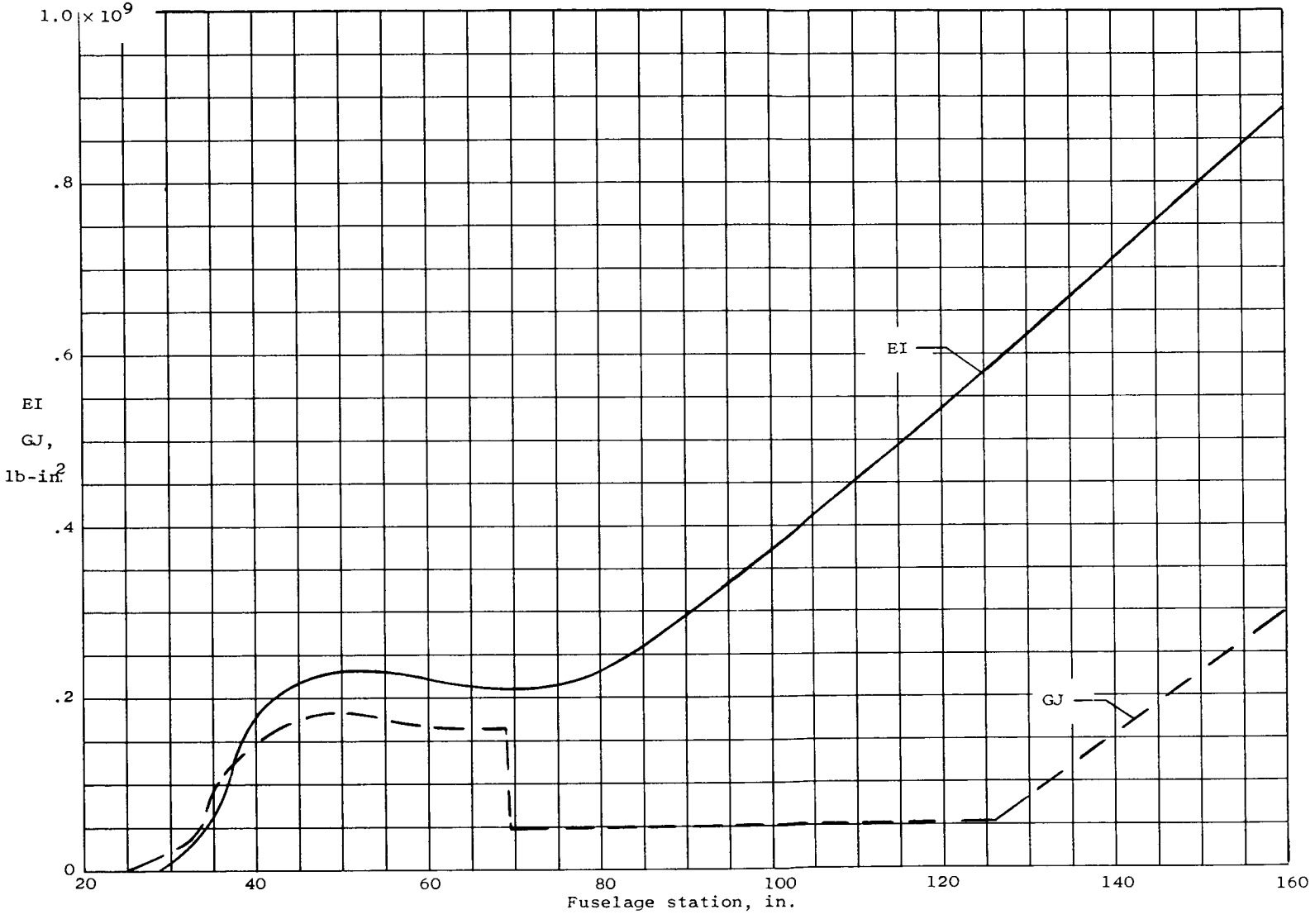

Figure 8.- Distributions of fuselage vertical bending and torsional stiffness.

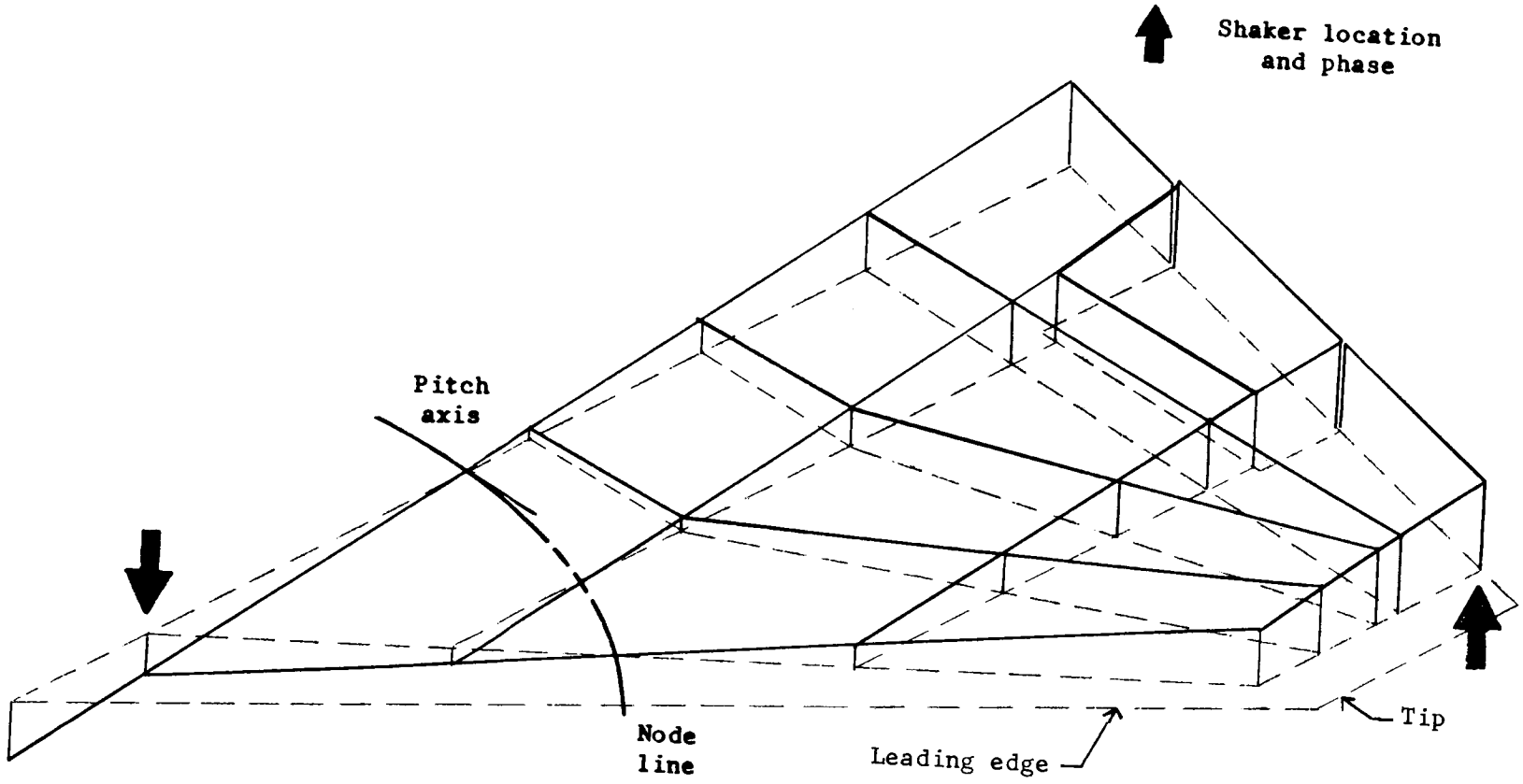

(a) First mode (pitch).

Figure 9.- Measured natural vibration modes for rigidly supported restrained canard with $\delta_t = 0^o$. Solid line indicates modal deflection; dashed line indicates static position.

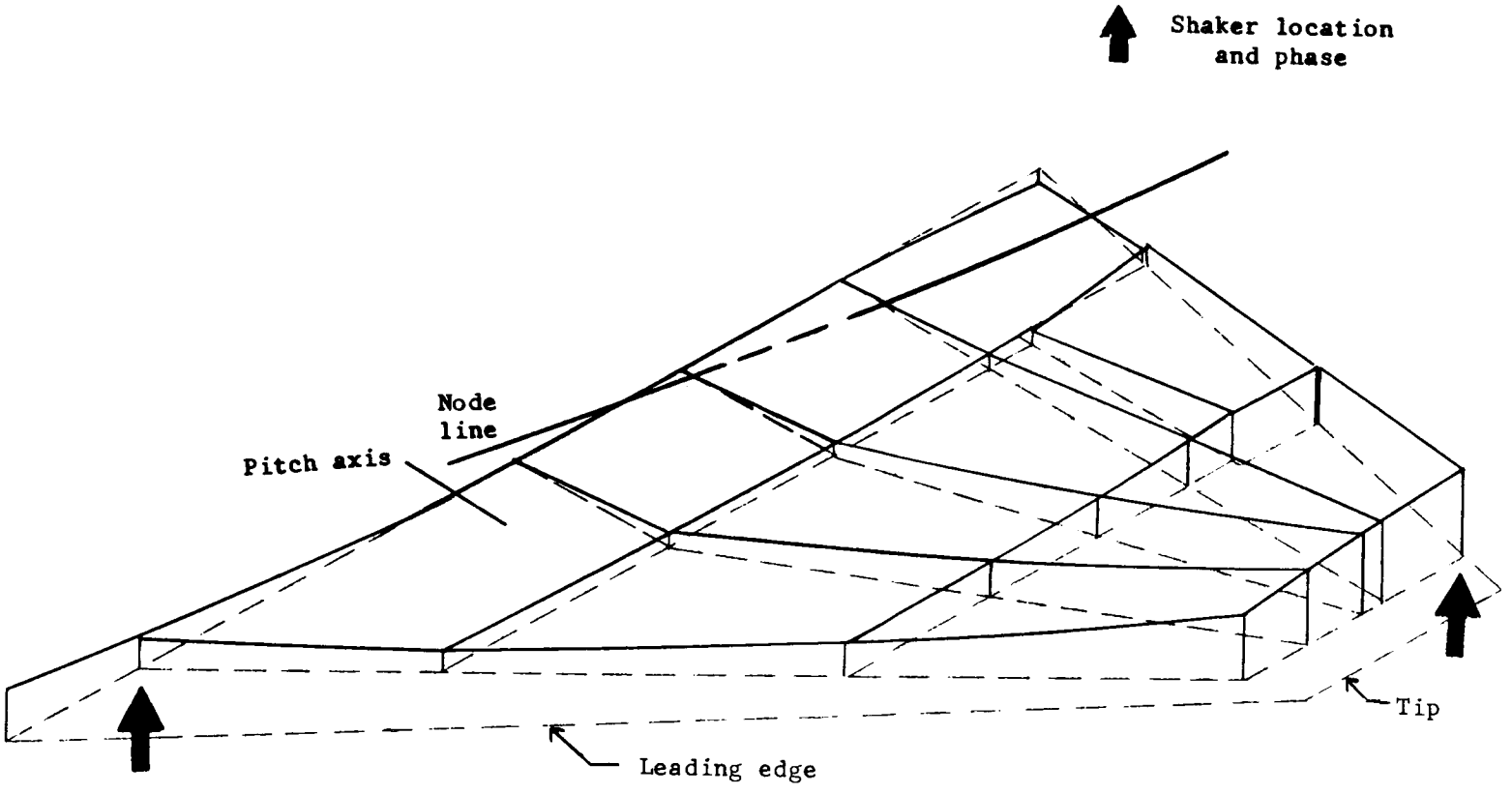

(b) Second mode (bending).

Figure 9.- Continued.

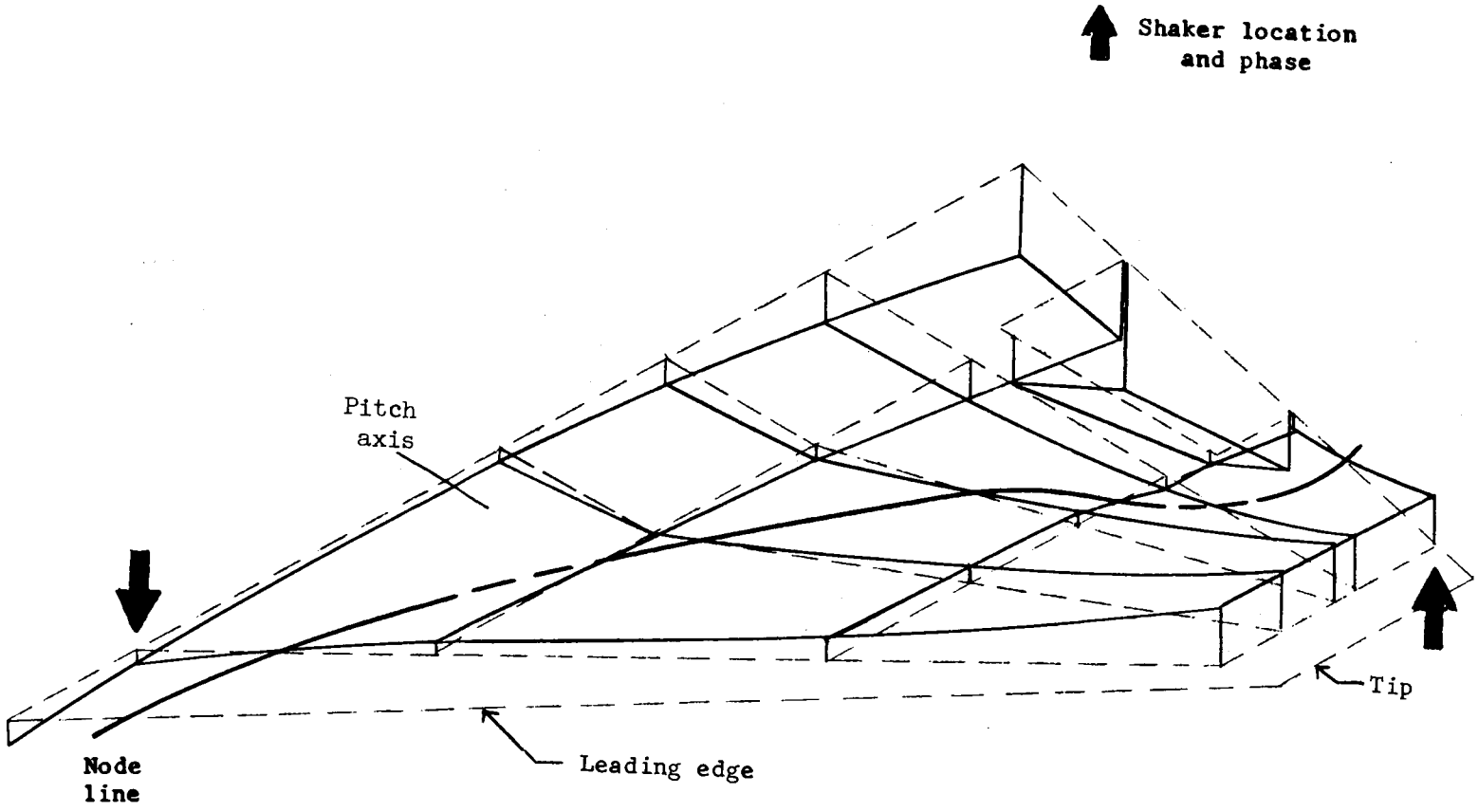

(c) Third mode.

Figure 9.- Continued.

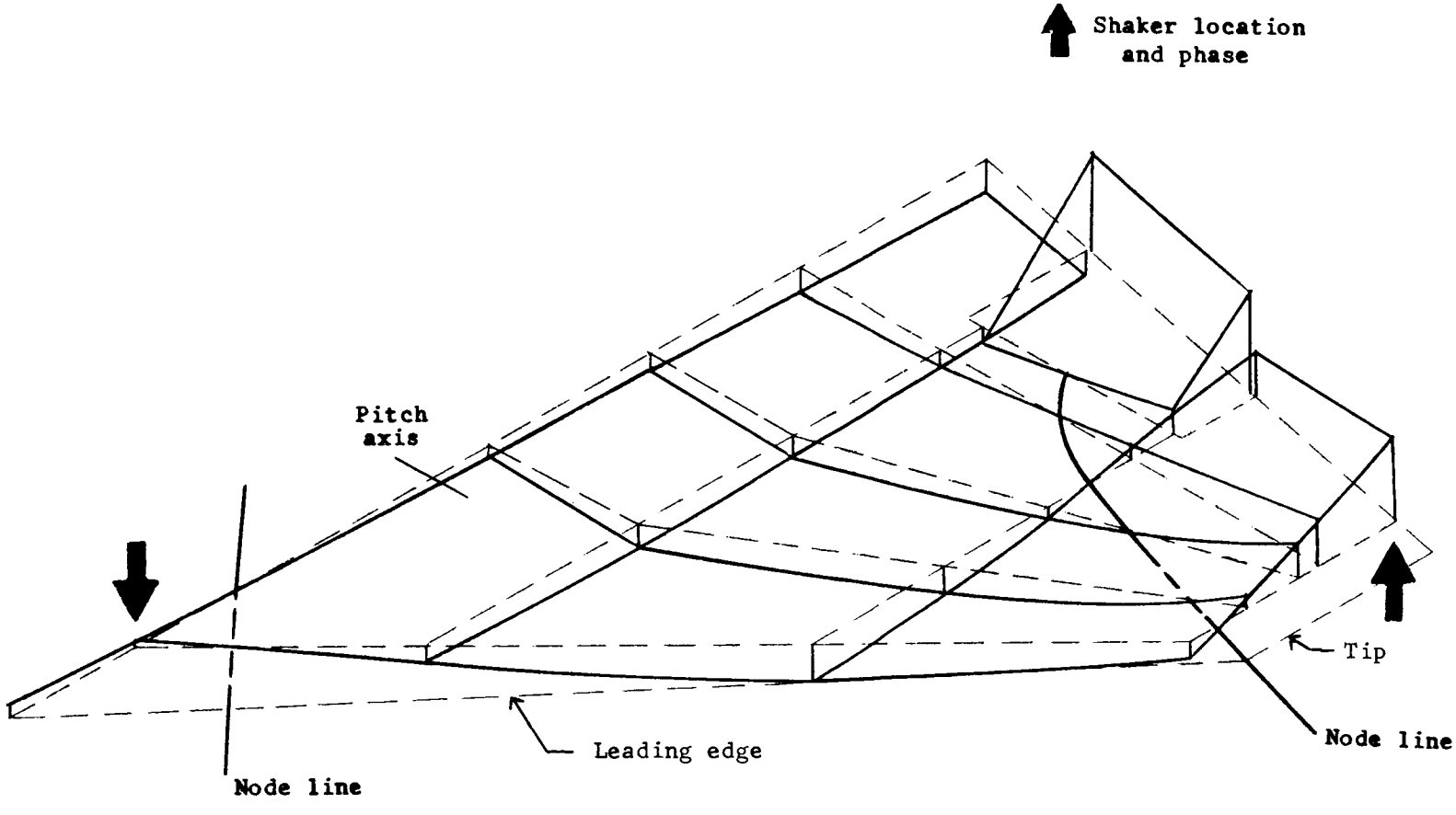

(d) Fourth mode.

Figure 9.- Concluded.

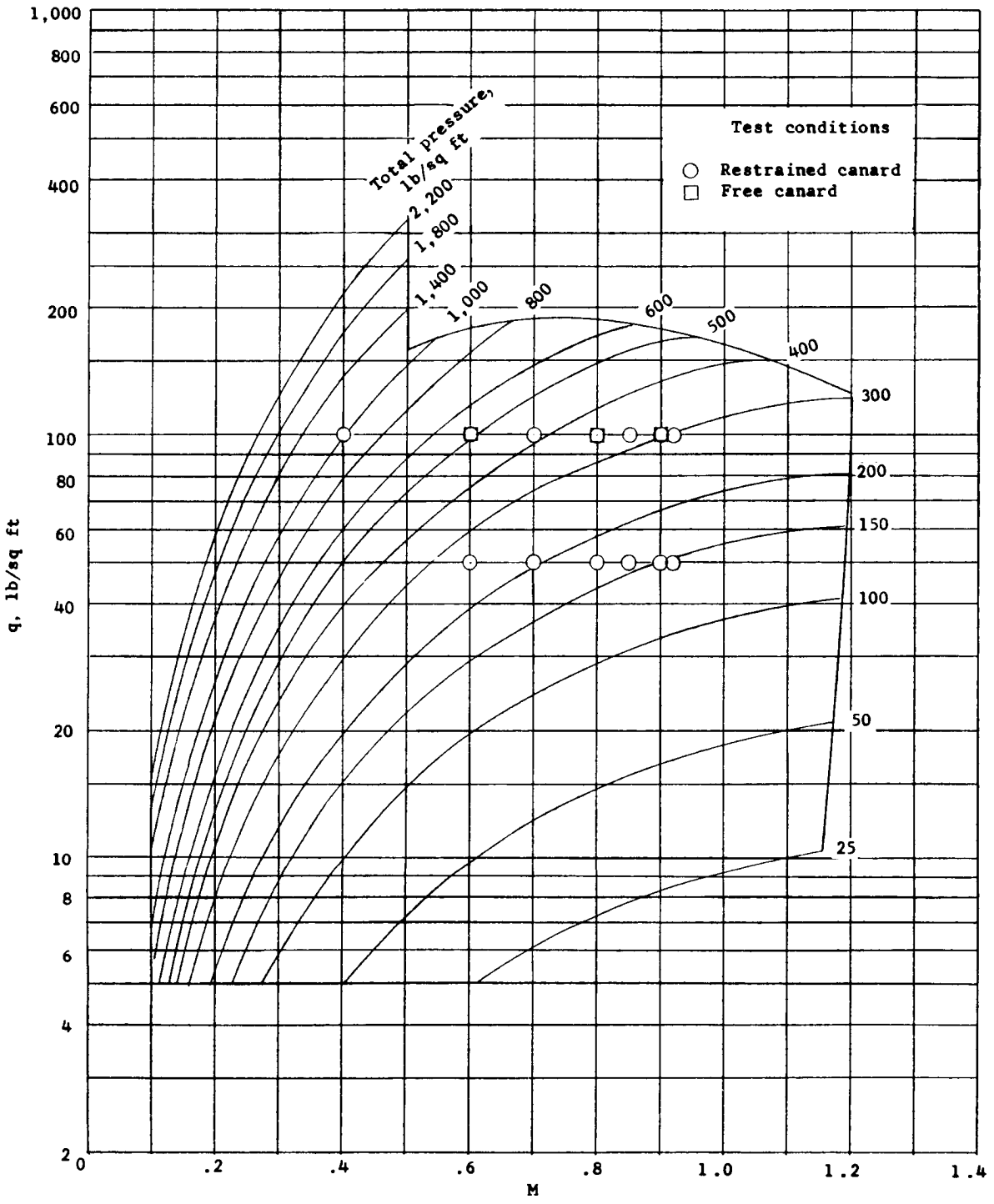

(a) All.

Figure 10.- Test conditions and tunnel characteristics.

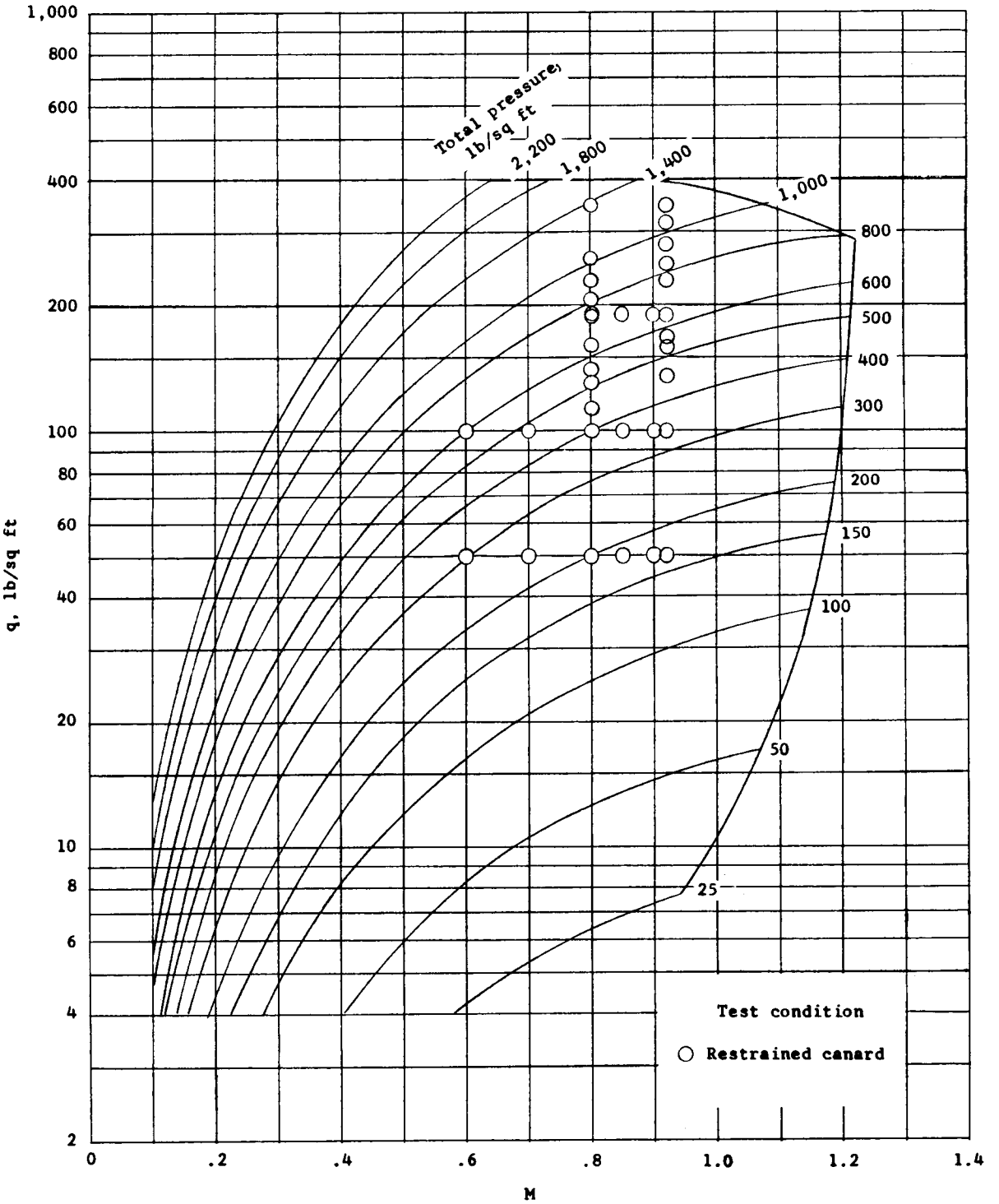

(b) Freon-12.

Figure 10.- Concluded.

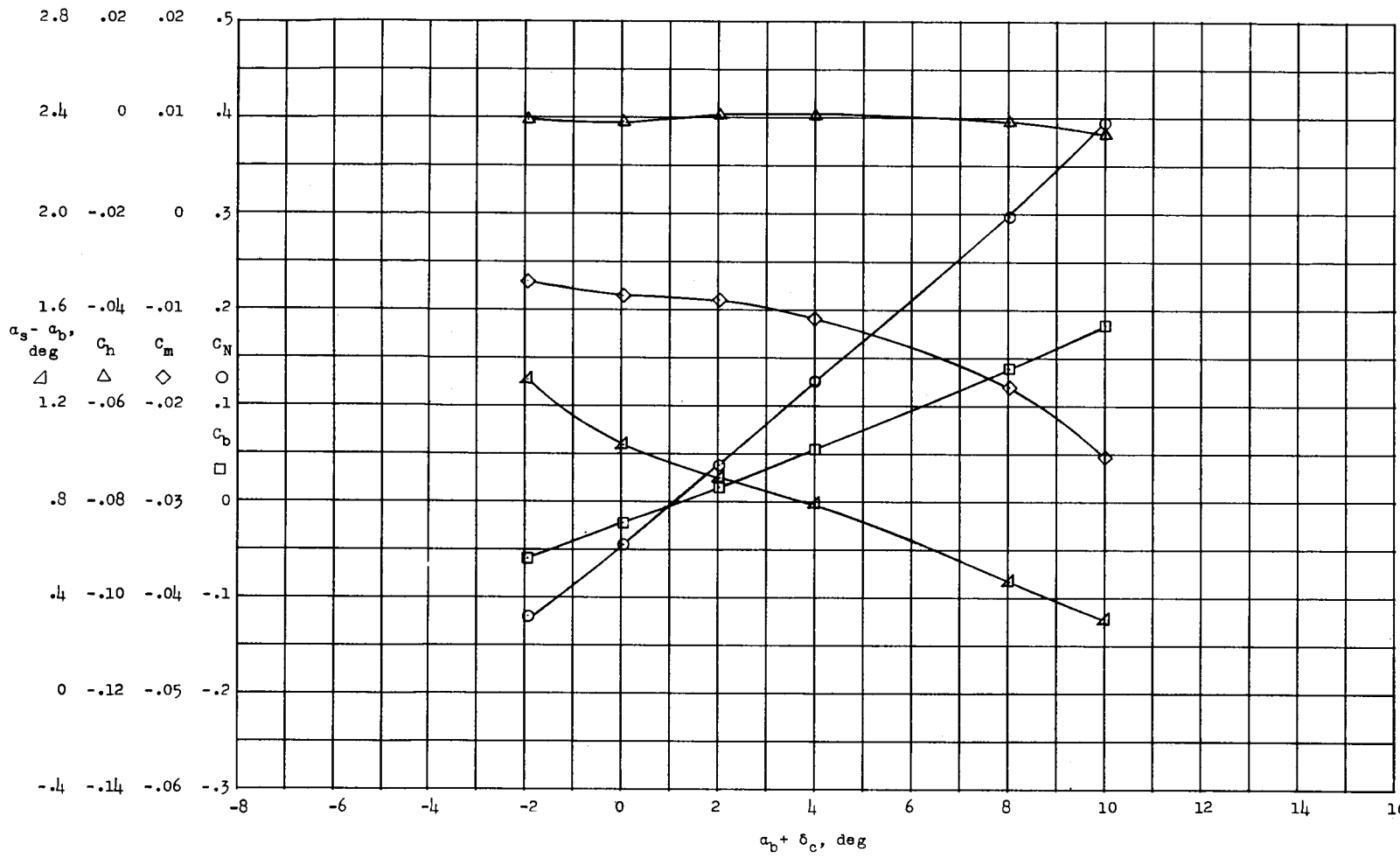

(a) $\delta_c = 0^\circ$

Figure 11.- Longitudinal aerodynamic characteristics of restrained canard in air at M = 0.40 and q = 100 lb/sq ft with $\delta_t = 0^\circ$.

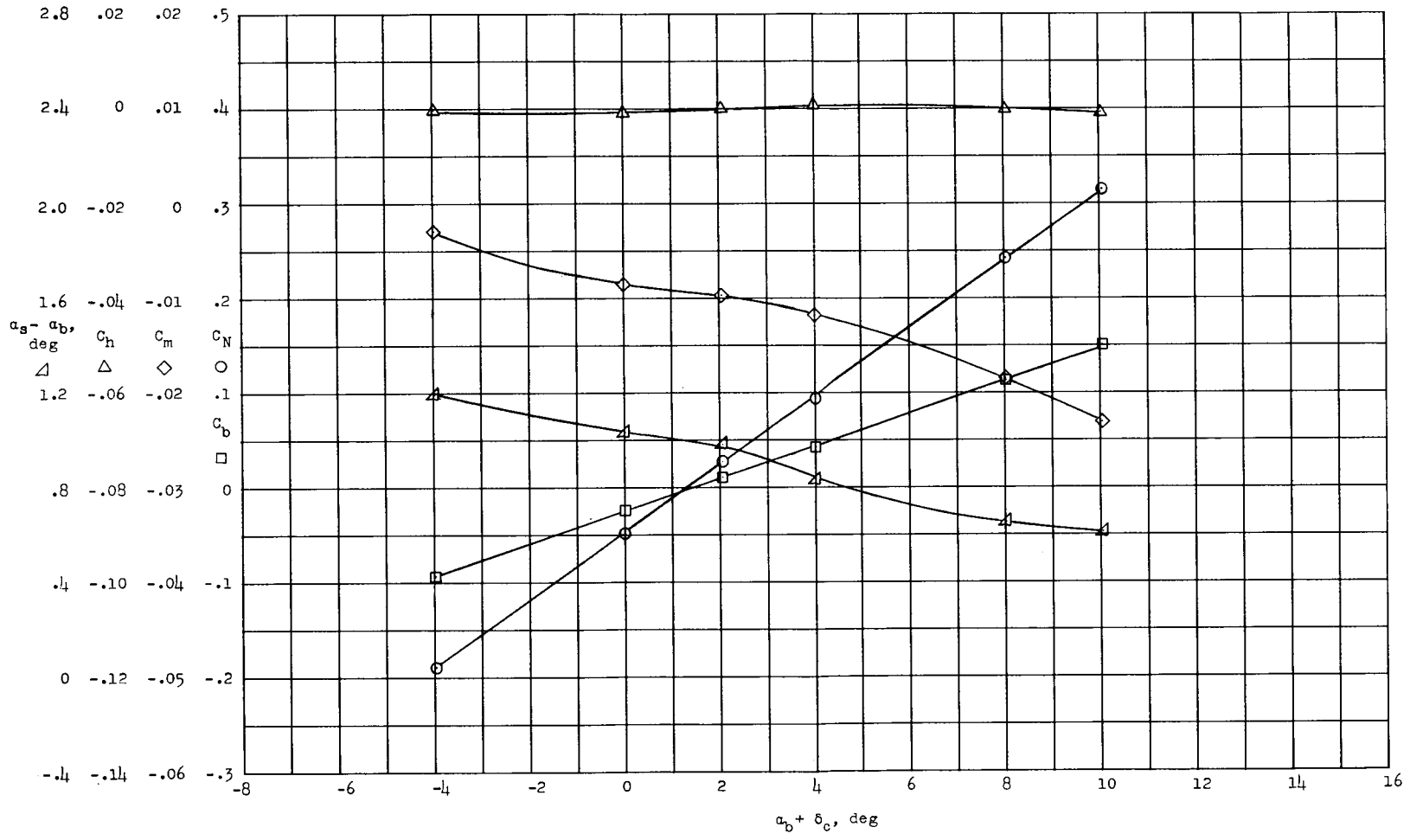

(b) $\alpha_b = 0^\circ$.

Figure 11.- Concluded.

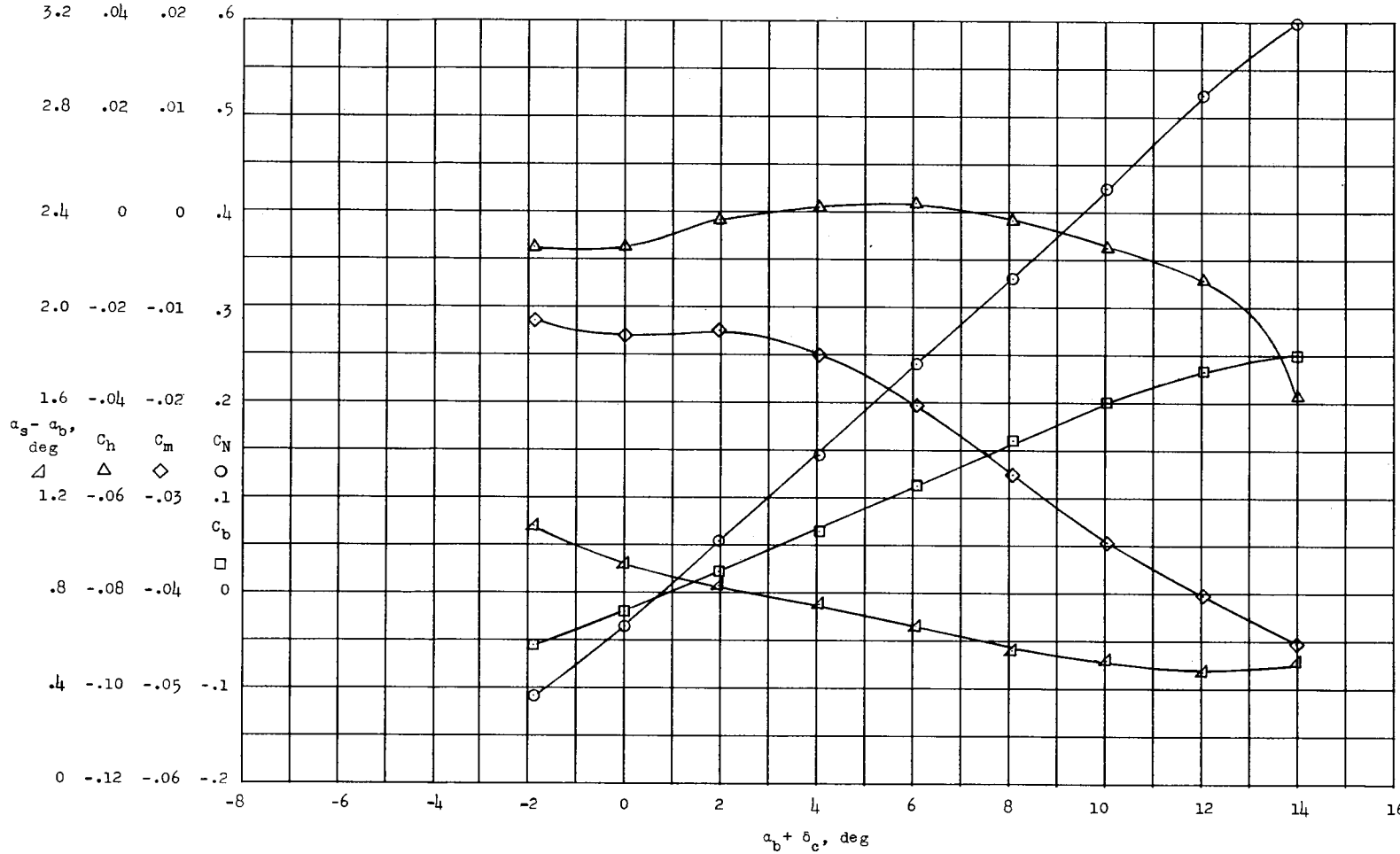

(a) $\delta_t = 0^\circ$; $\delta_c = 0^\circ$.

Figure 12.- Longitudinal aerodynamic characteristics of restrained canard in air at M = 0.60 and q = 50 lb/sq ft.

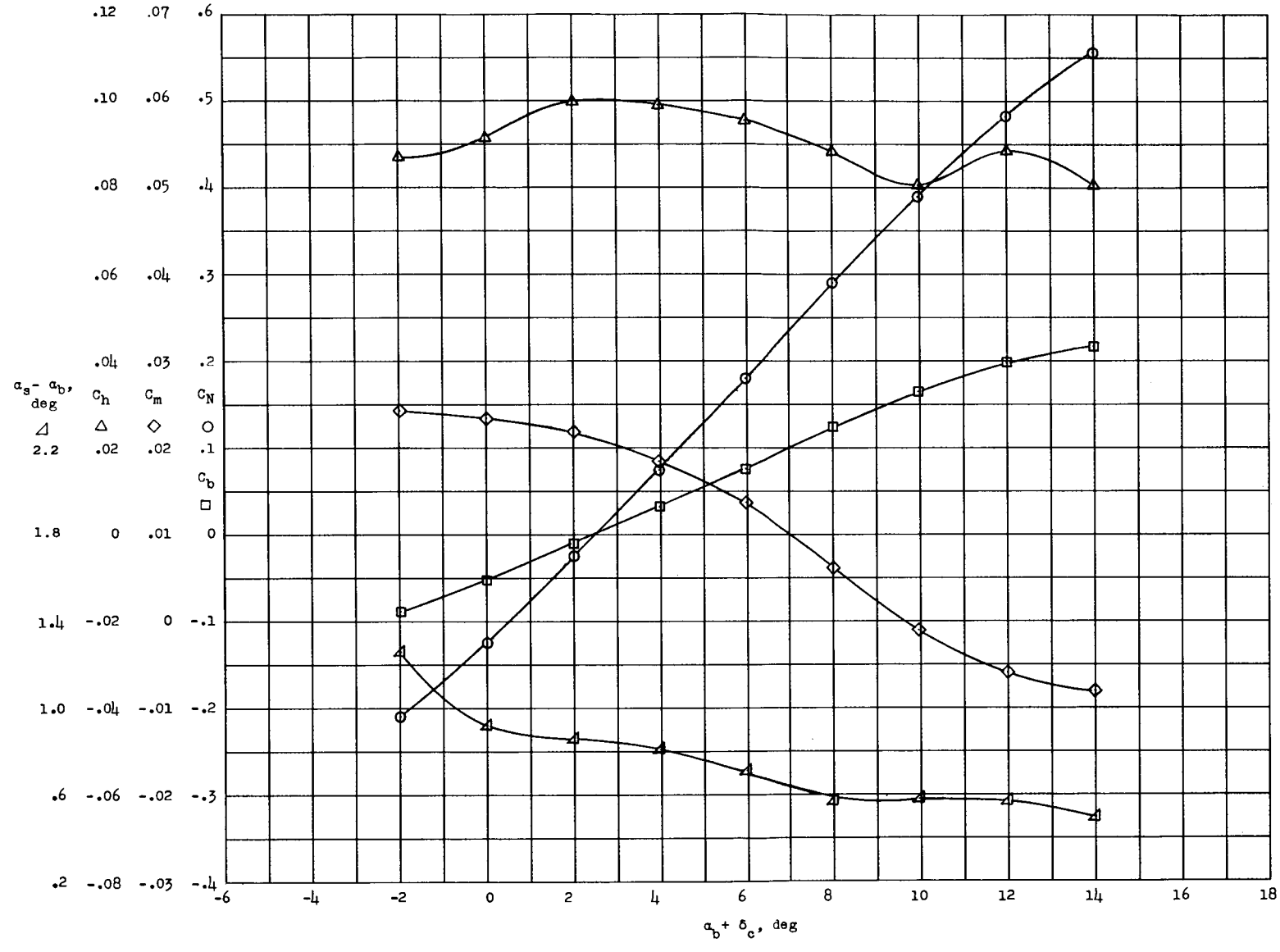

(b) $\delta_t = -12^\circ$; $\delta_c = 0^\circ$.

Figure 12.- Continued.

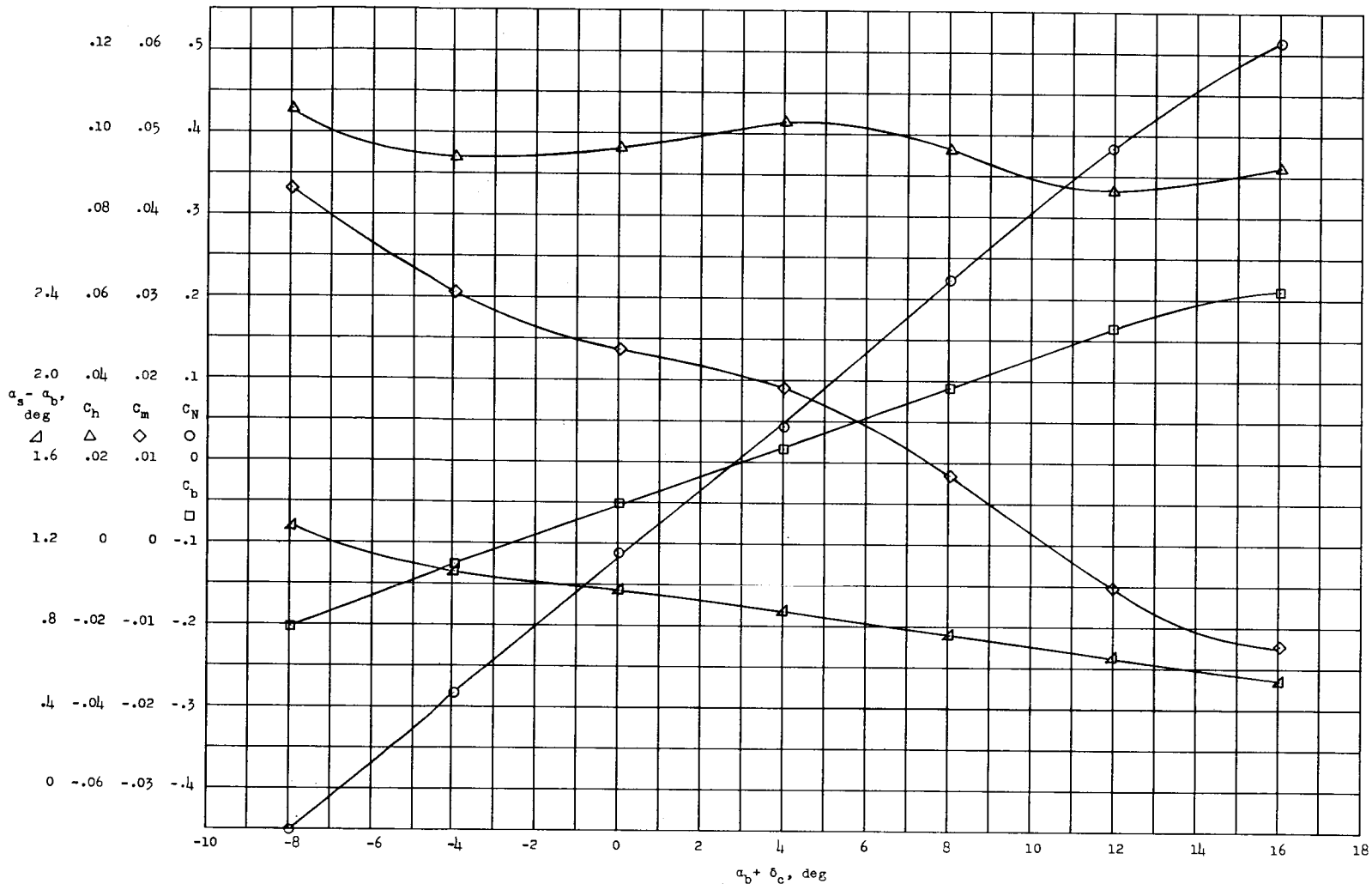

(c) $\delta_t = -12^\circ$; $\alpha_b = 0^\circ$.

Figure 12.- Concluded.

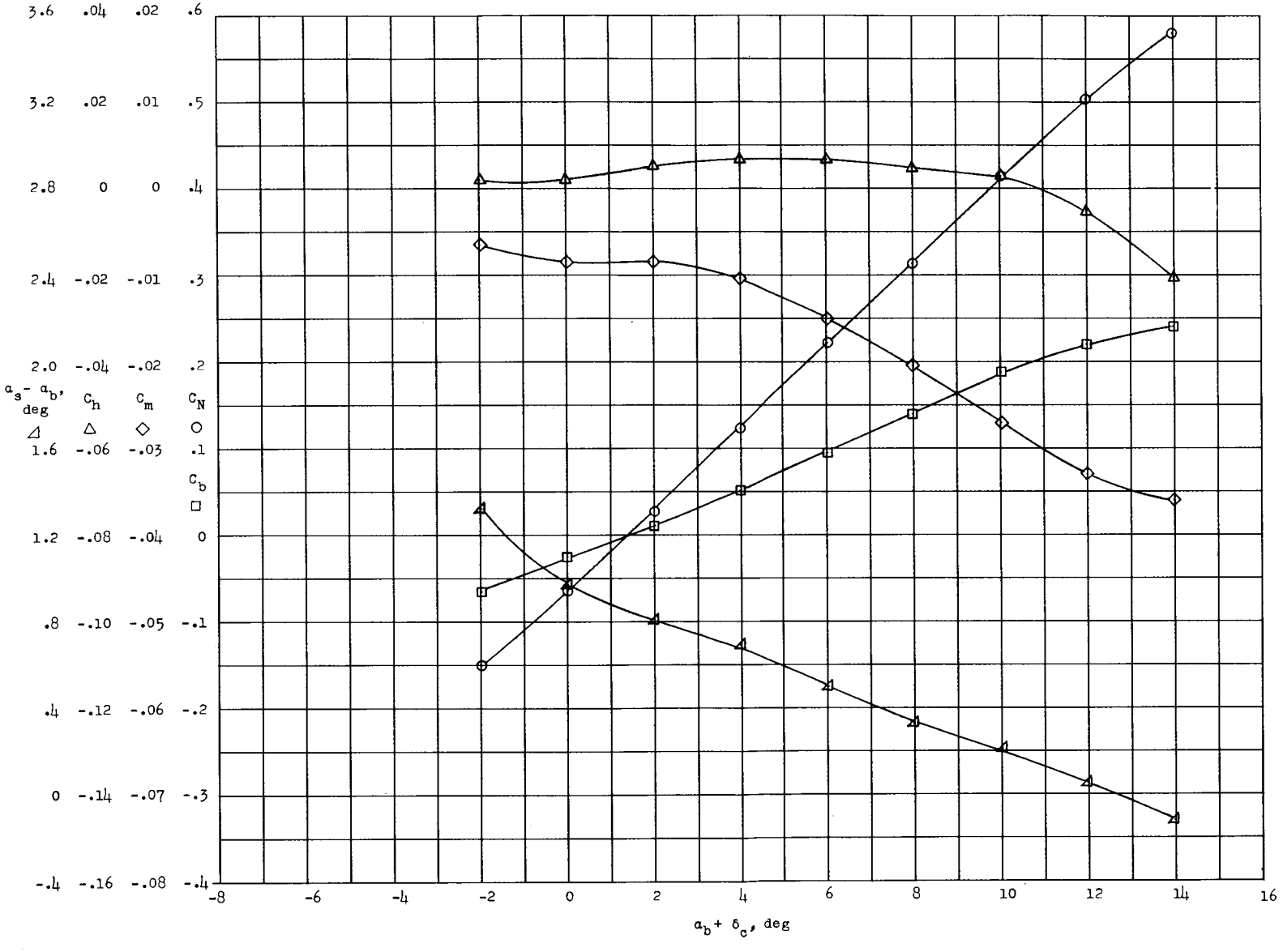

(a) $\delta_t = 0^o$; $\delta_c = 0^o$.

Figure 13.- Longitudinal aerodynamic characteristics of restrained canard in air at M = 0.60 and q = 100 lb/sq ft.

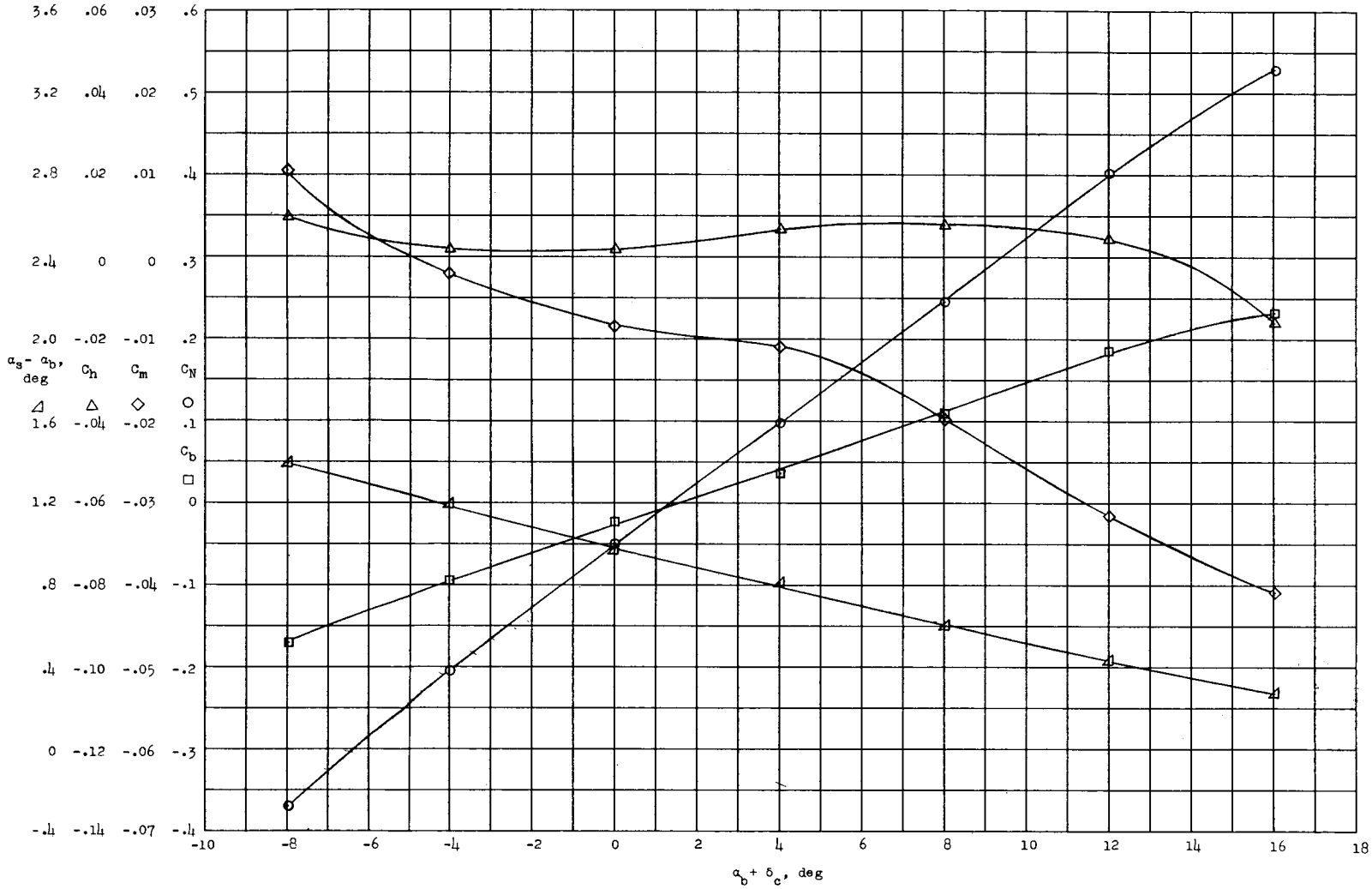

(b) $\delta_t = 0^o$; $\alpha_b = 0^o$.

Figure 13.- Continued.

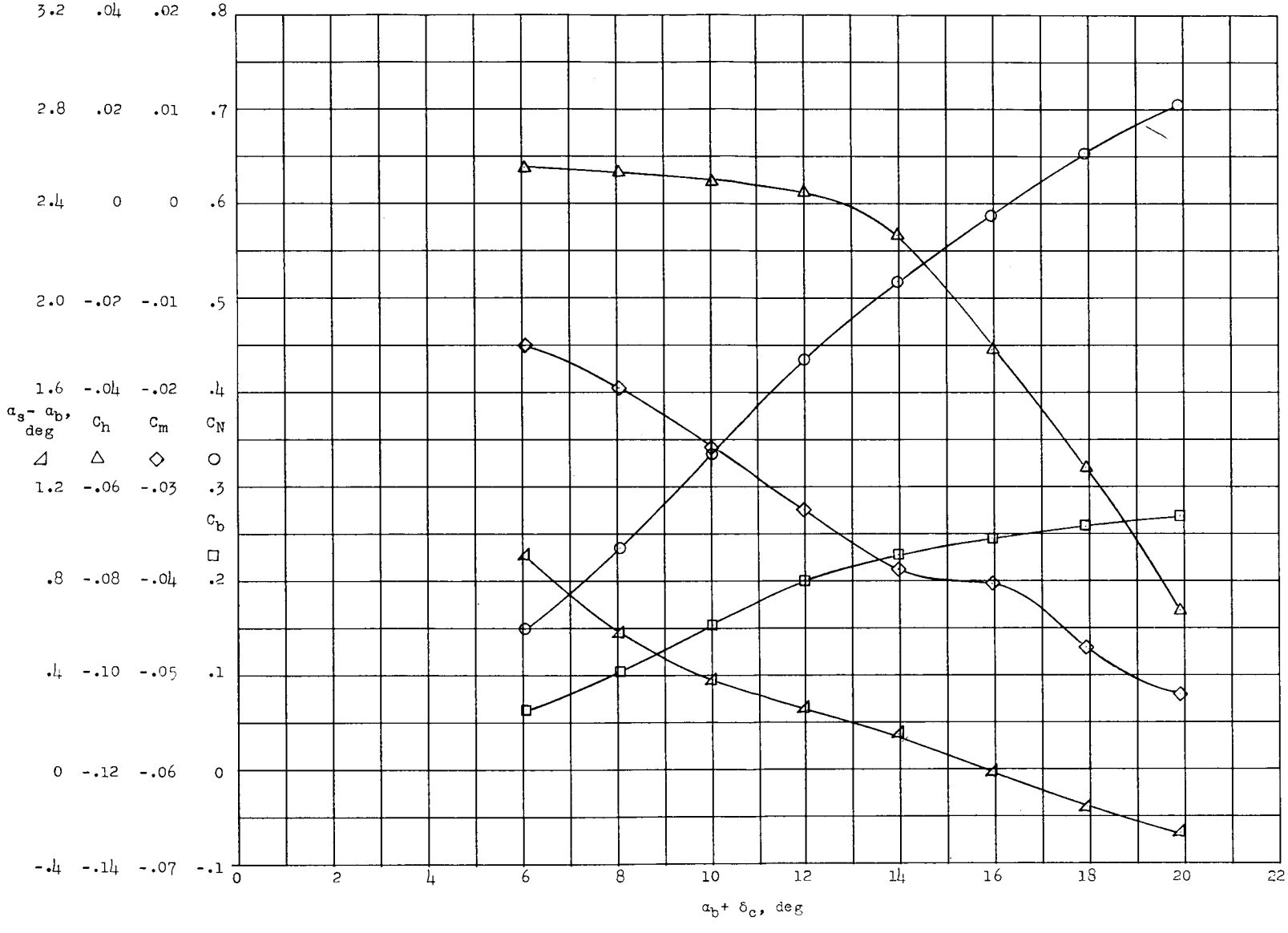

(c) $\delta_t = 0^\circ$; $\delta_c = 8^\circ$.

Figure 13.- Continued.

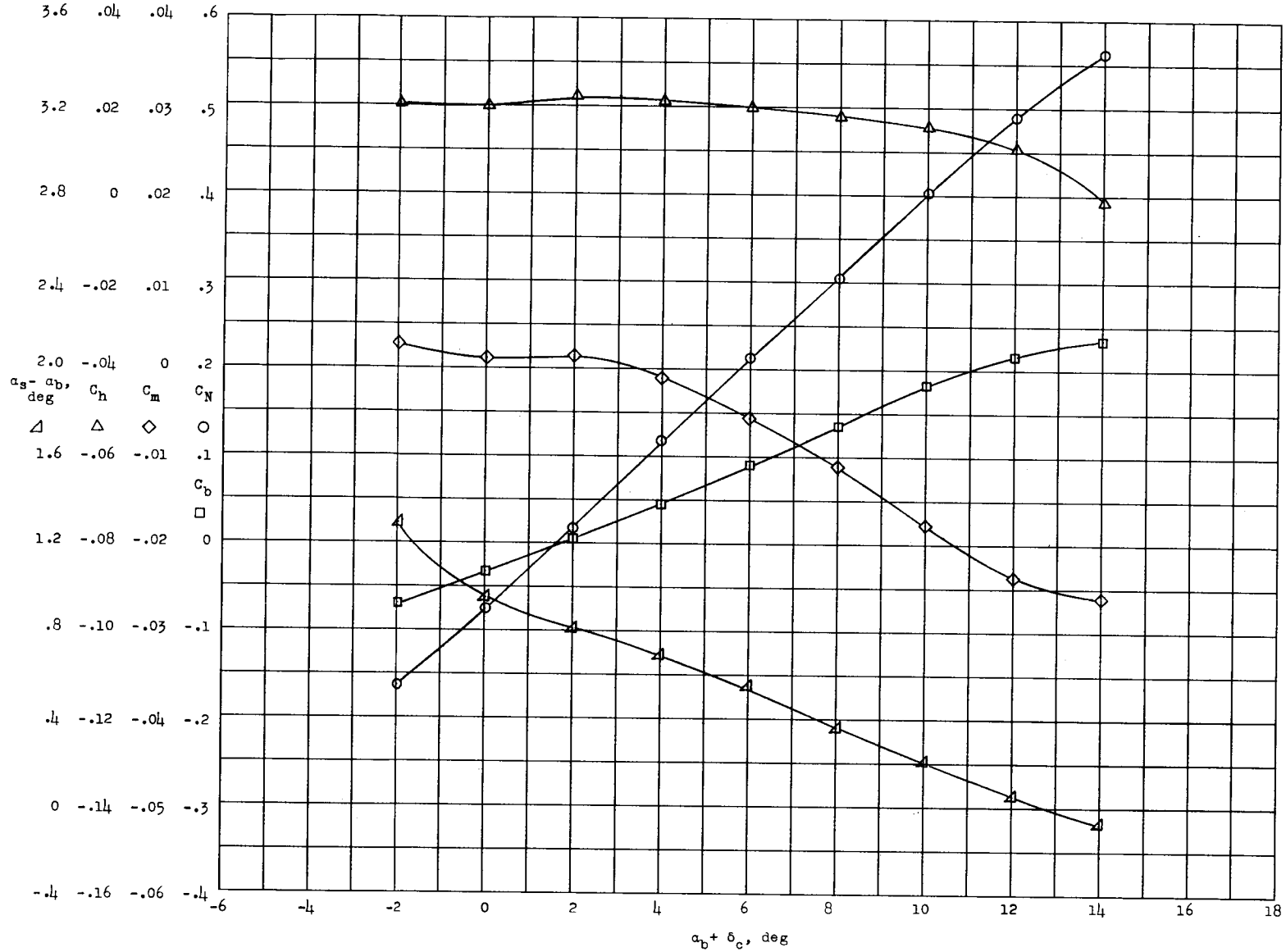

(d) $\delta_t = -4^\circ$; $\delta_c = 0^\circ$.

Figure 13.- Continued.

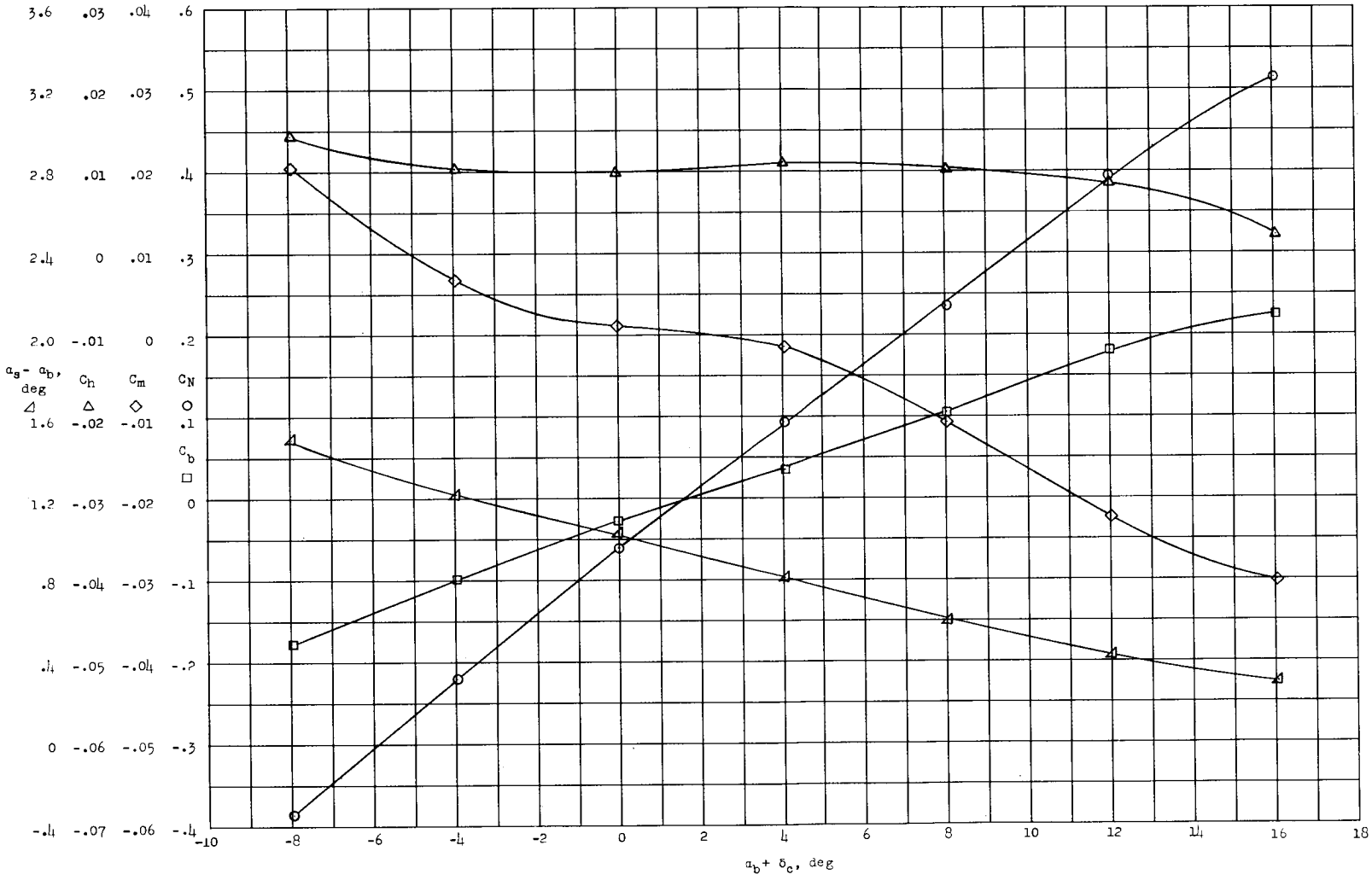

(e) $\delta_t = -4^\circ$; $\alpha_b = 0^\circ$.

Figure 13.- Continued.

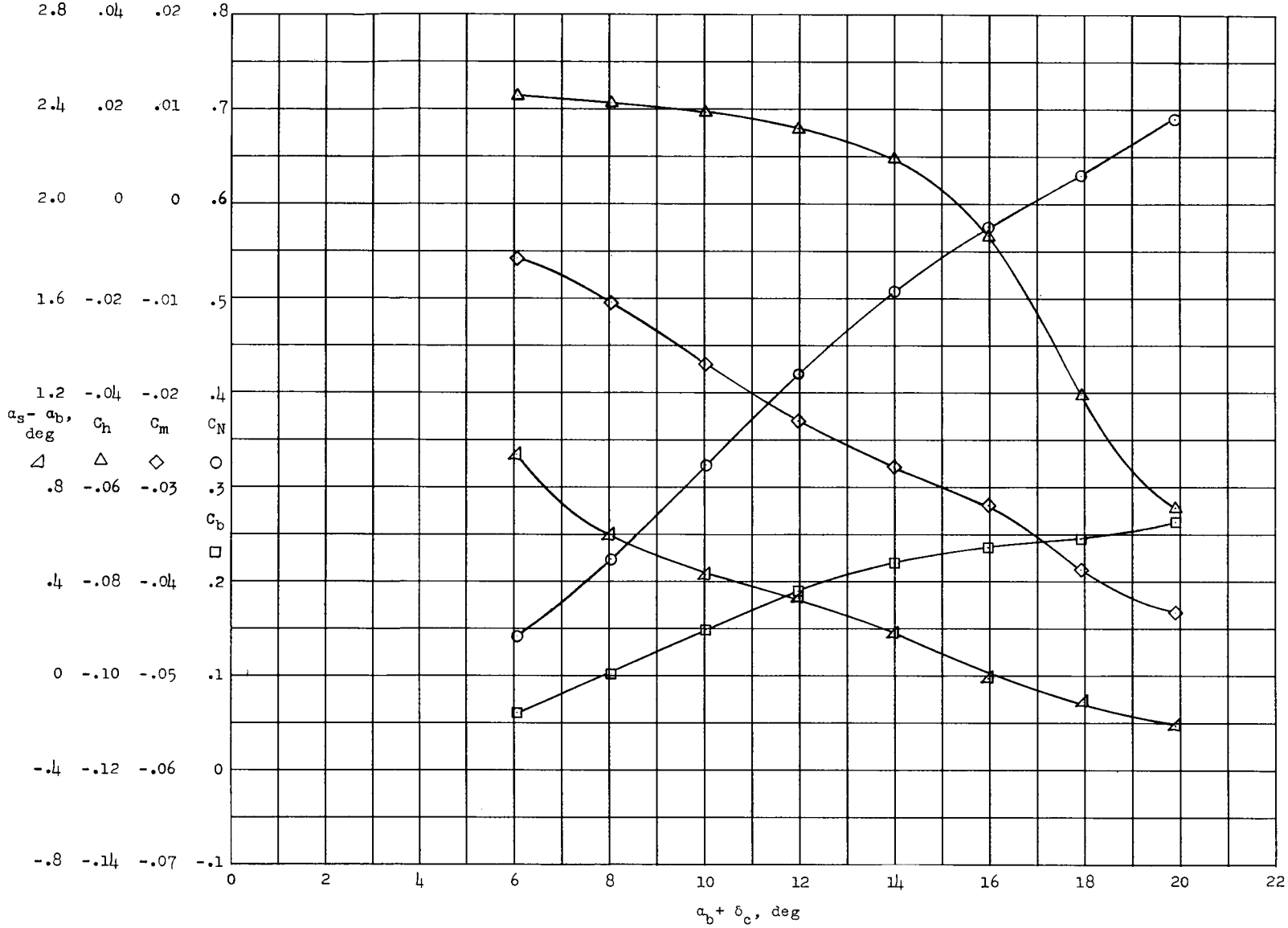

(f) $\delta_t = -4^\circ$; $\delta_c = 8^\circ$.

Figure 13.- Continued.

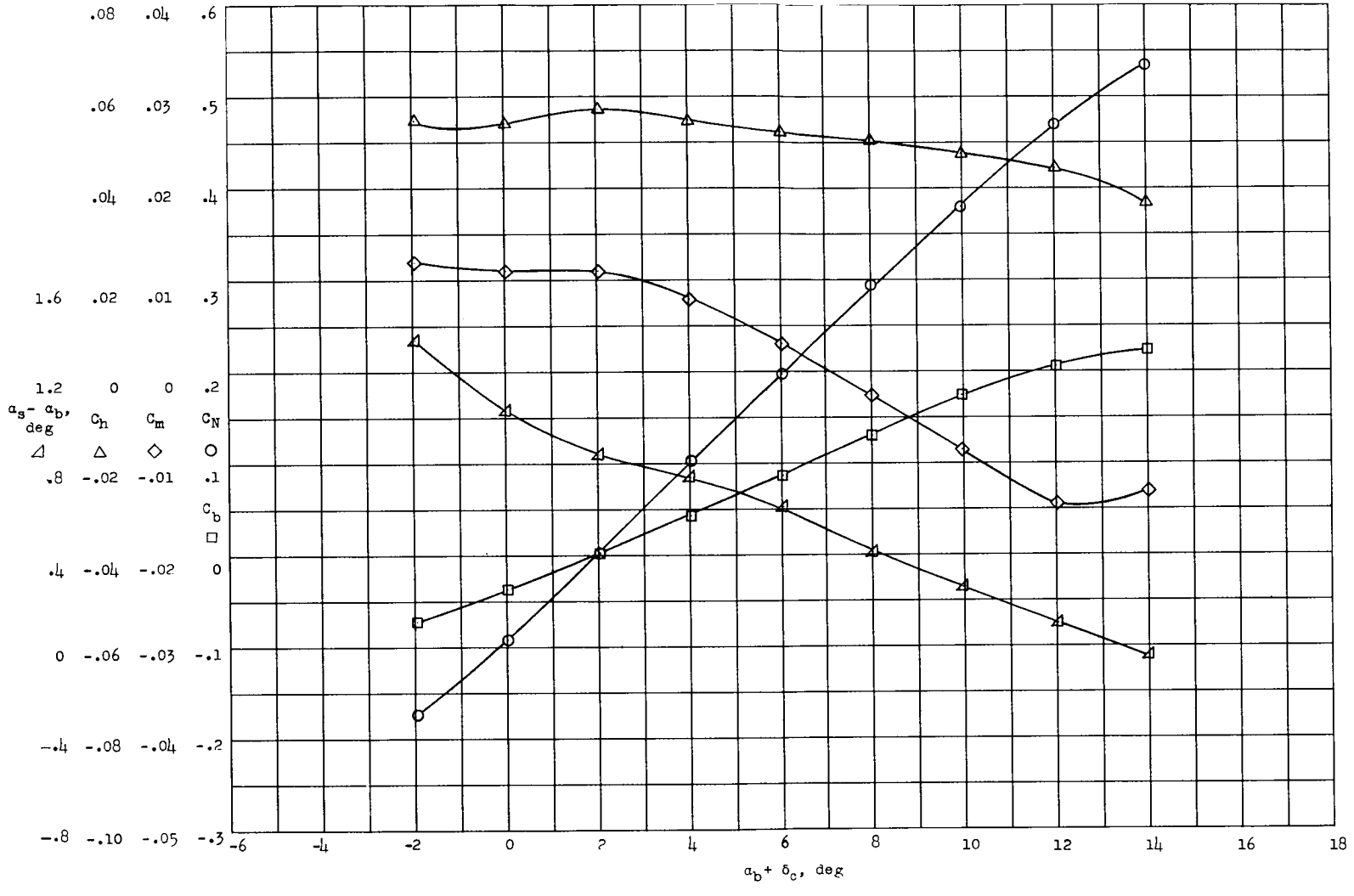

(g) $\delta_t = -8^\circ$; $\delta_c = 0^\circ$.

Figure 13.- Continued.

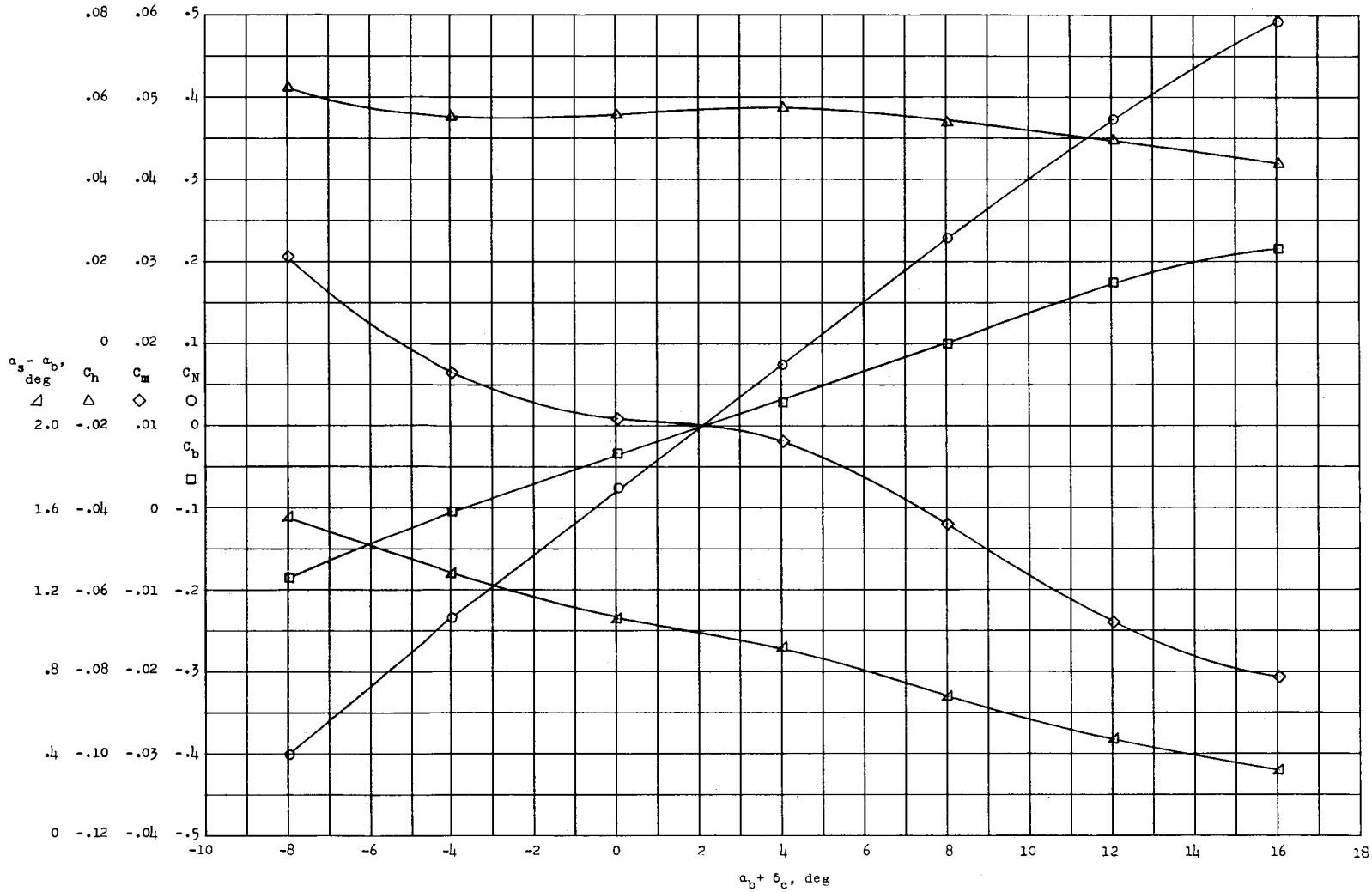

(h) $\delta_t = -8^\circ$; $\alpha_b = 0^\circ$.

Figure 13.- Continued.

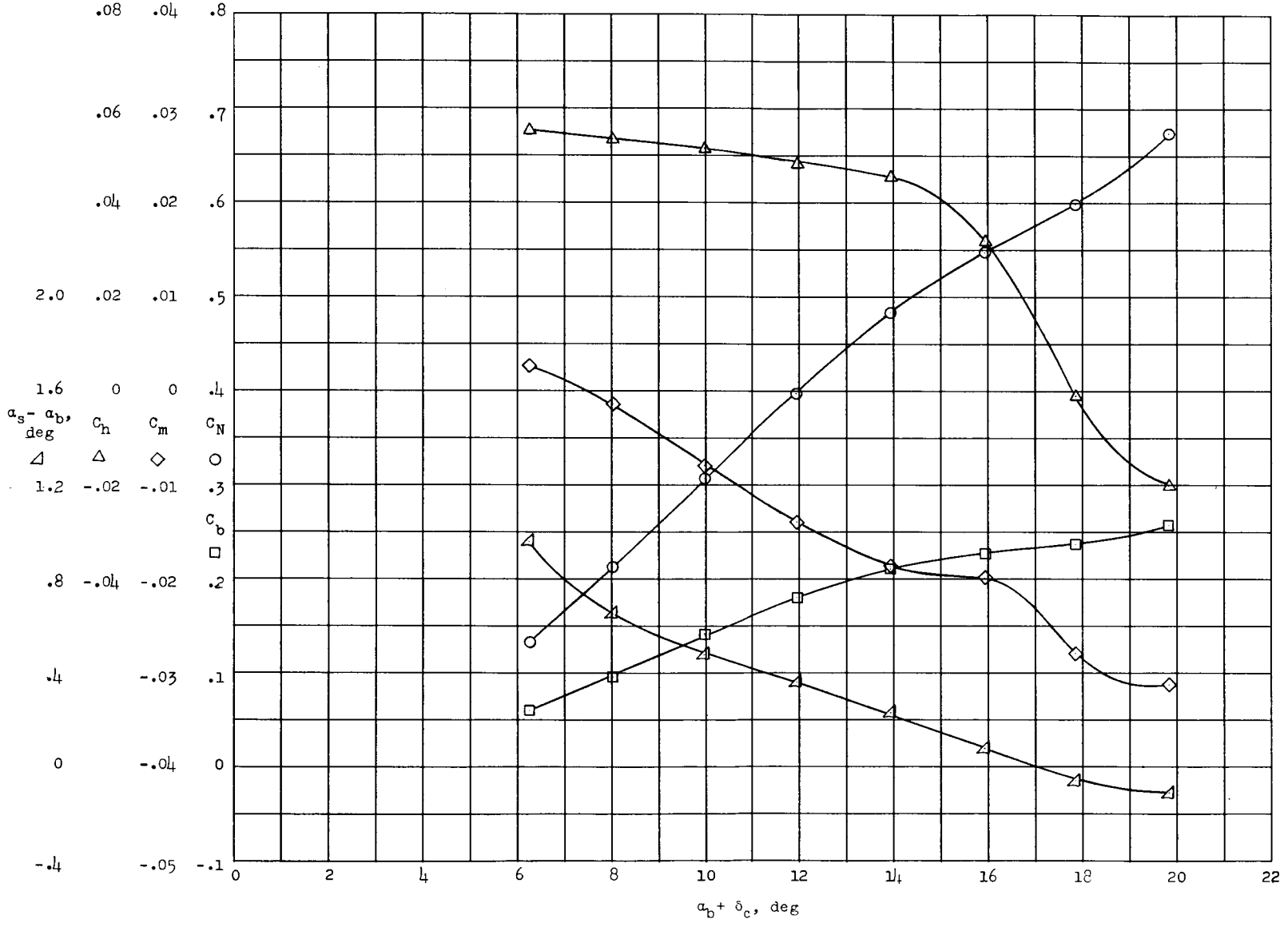

(i) $\delta_t = -8^\circ$; $\delta_c = 8^\circ$.

Figure 13.- Continued.

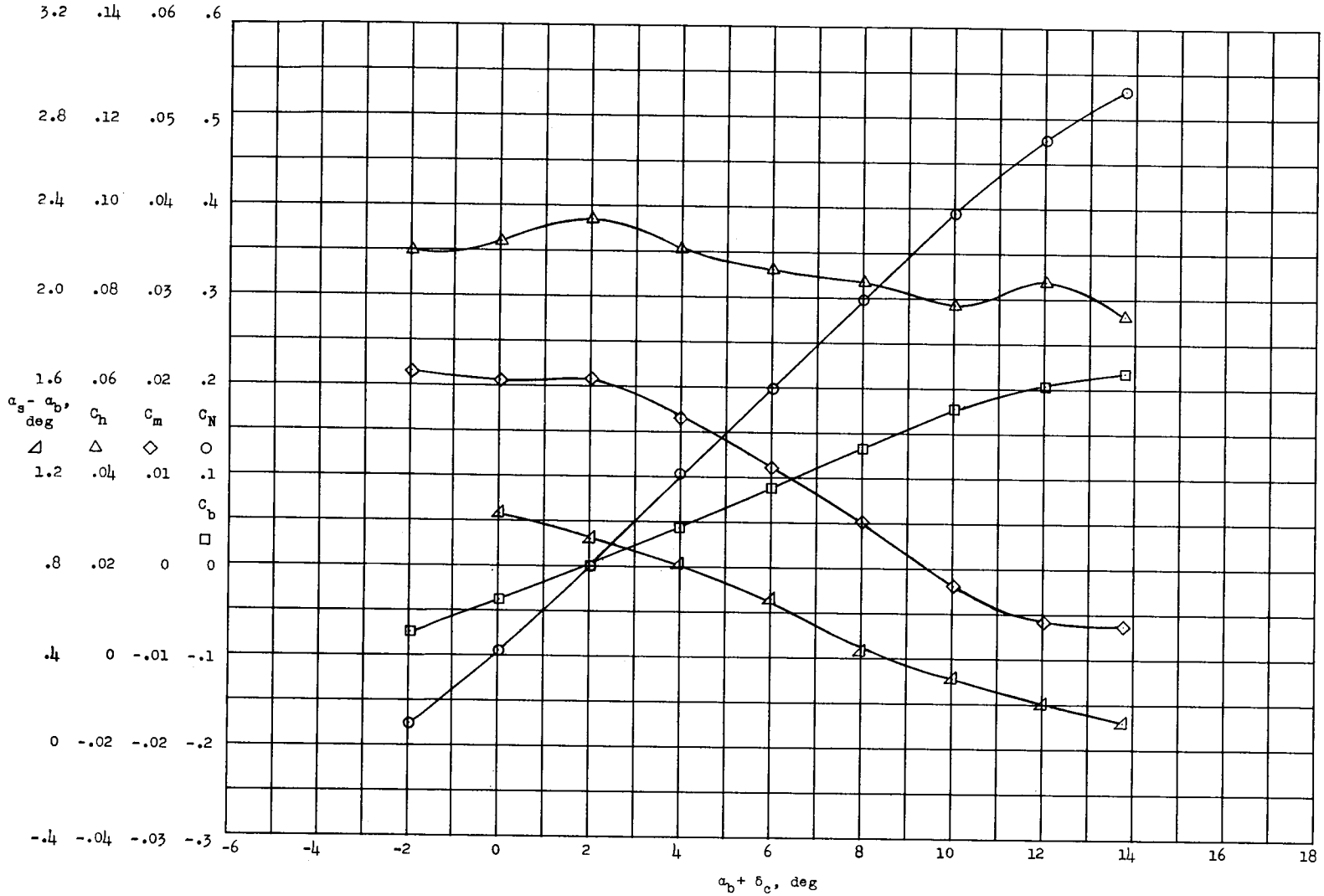

(j) $\delta_t = -12^\circ$; $\delta_c = 0^\circ$.

Figure 13.- Continued.

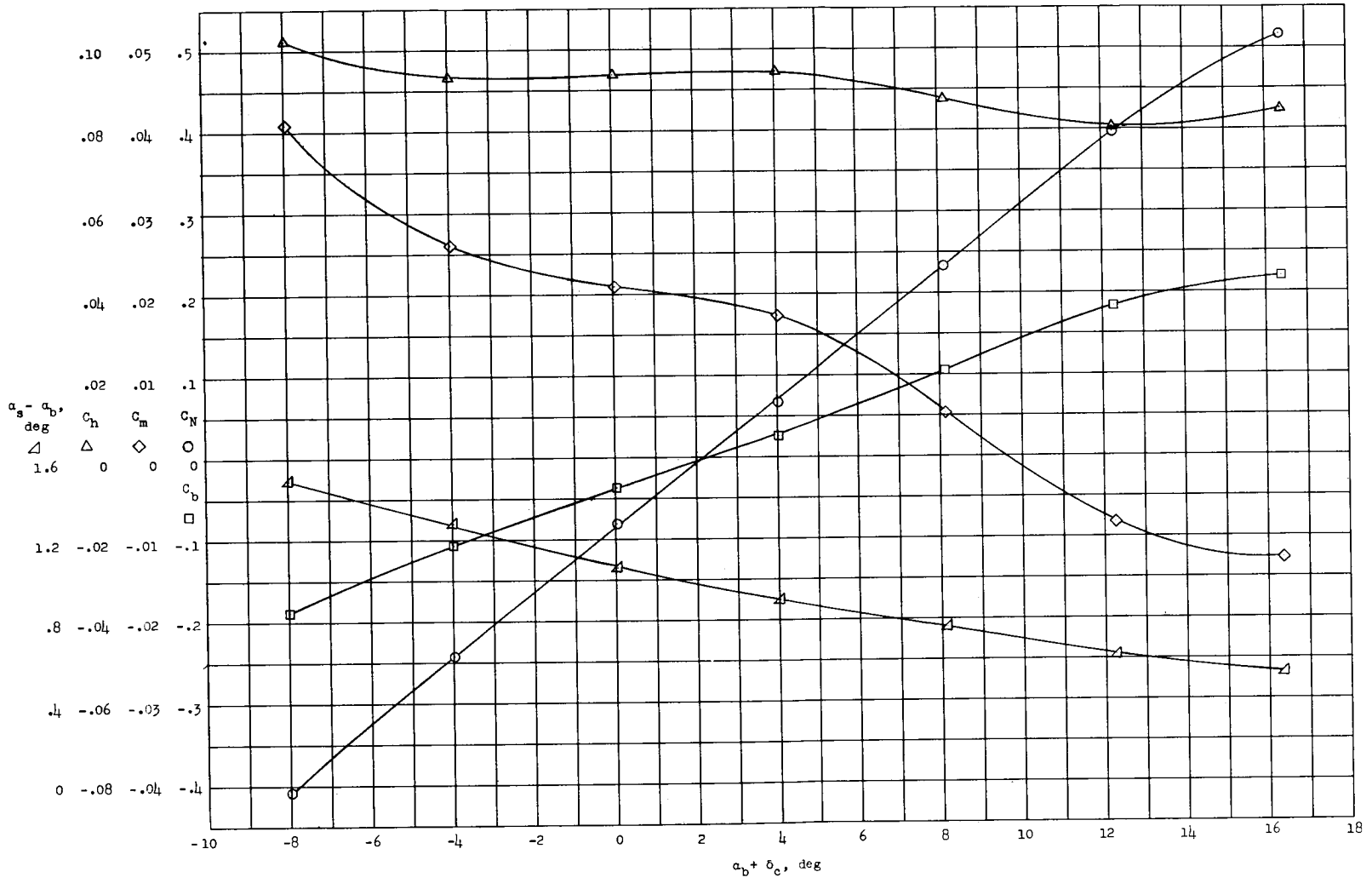

(k) $\delta_t = -12^\circ$; $\alpha_b = 0^\circ$.

Figure 13.- Concluded.

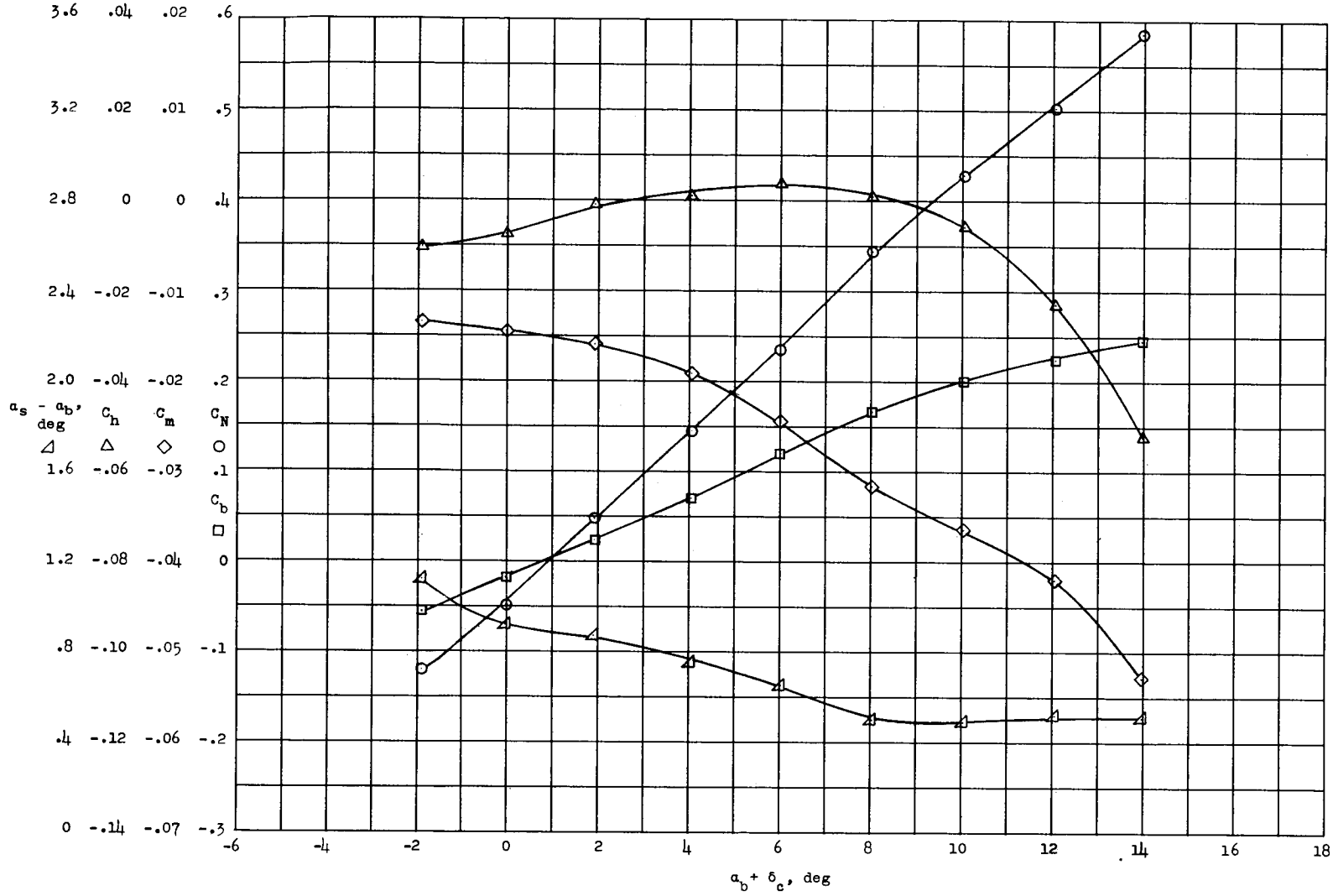

(a) $\delta_c = 0^\circ$.

Figure 14.- Longitudinal aerodynamic characteristics of restrained canard in air at M = 0.70 and q = 50 lb/sq ft with $\delta_t = 0^\circ$.

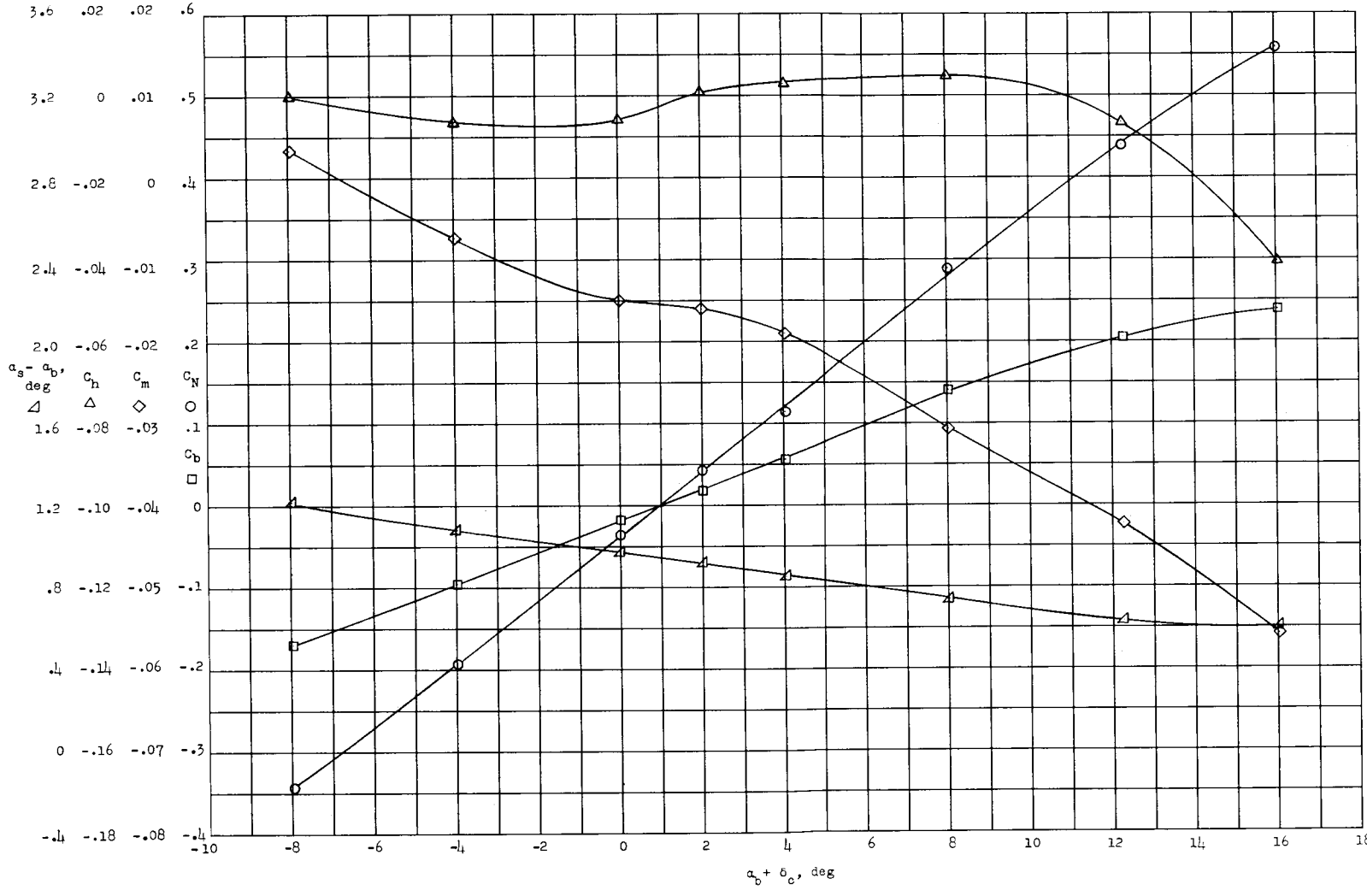

(b) $\alpha_b = 0^\circ$.

Figure 14.- Concluded.

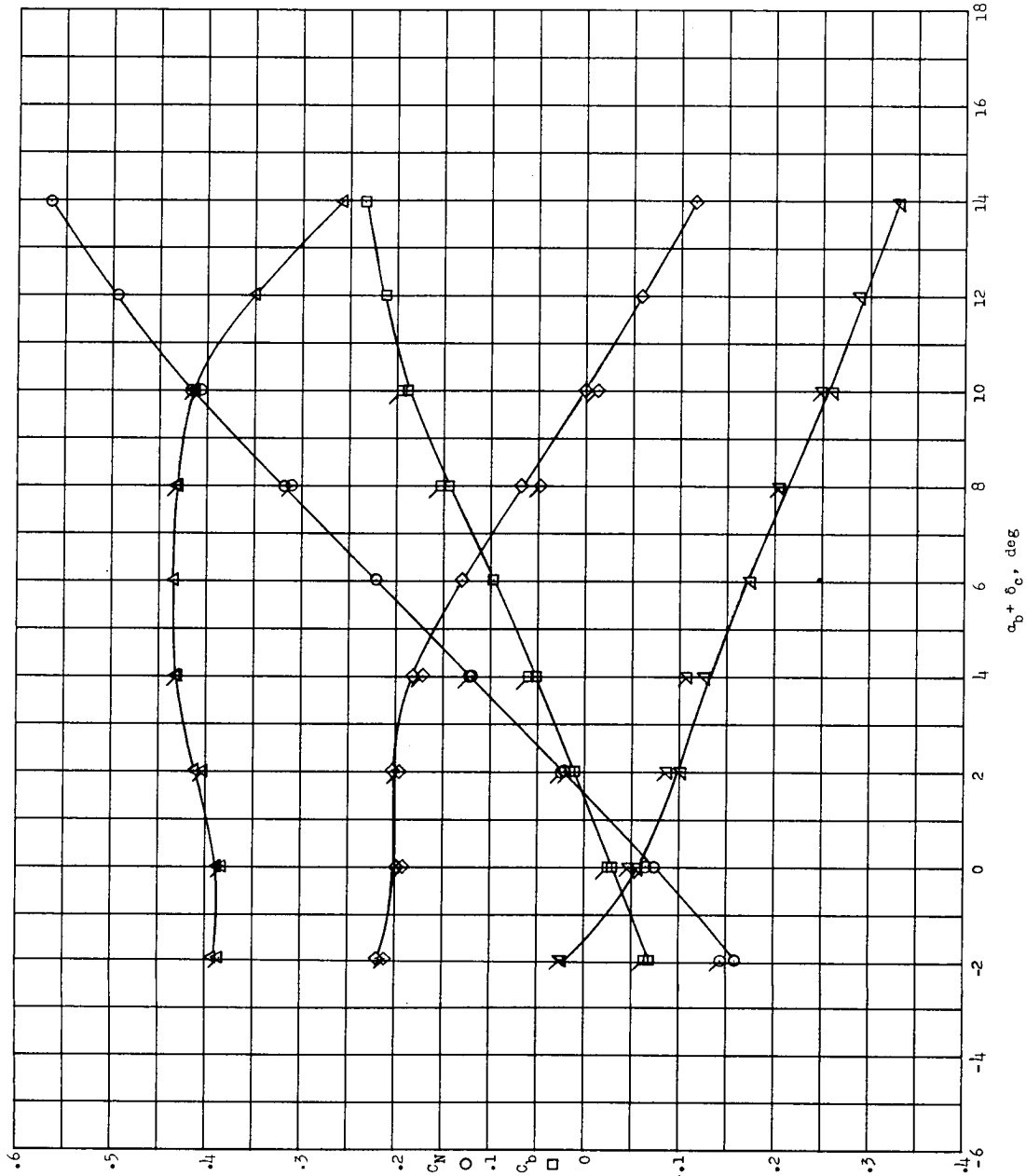

(a) $\delta_c = 0^\circ$.

Figure 15.- Longitudinal aerodynamic characteristics of restrained canard in air at M = 0.70 and q = 100 lb/sq ft with $\delta_t = 0^\circ$. Flagged symbols indicate points rerun to show repeatability.

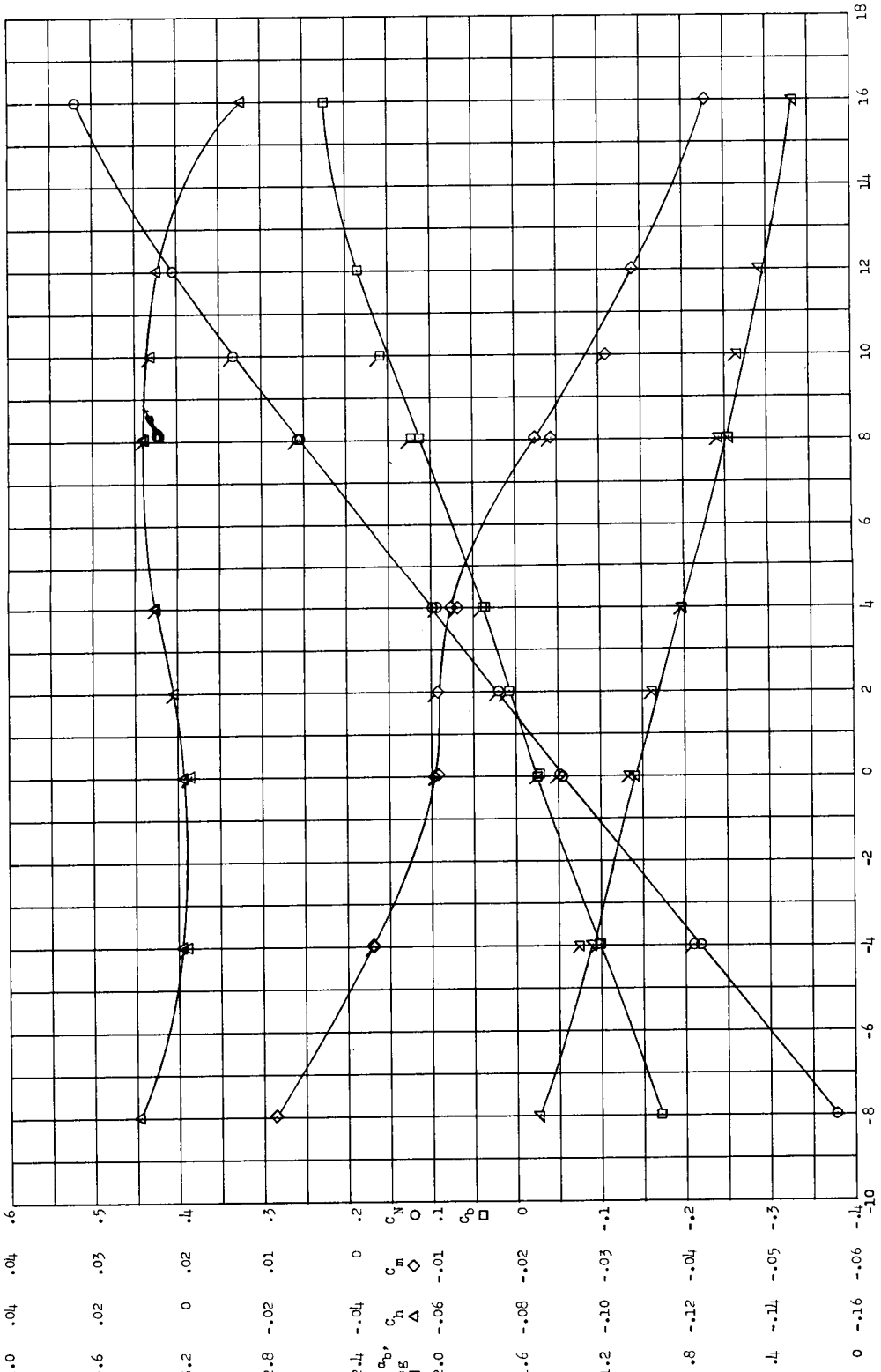

(b) $\alpha_b = 0^\circ$.

Figure 15.- Concluded.

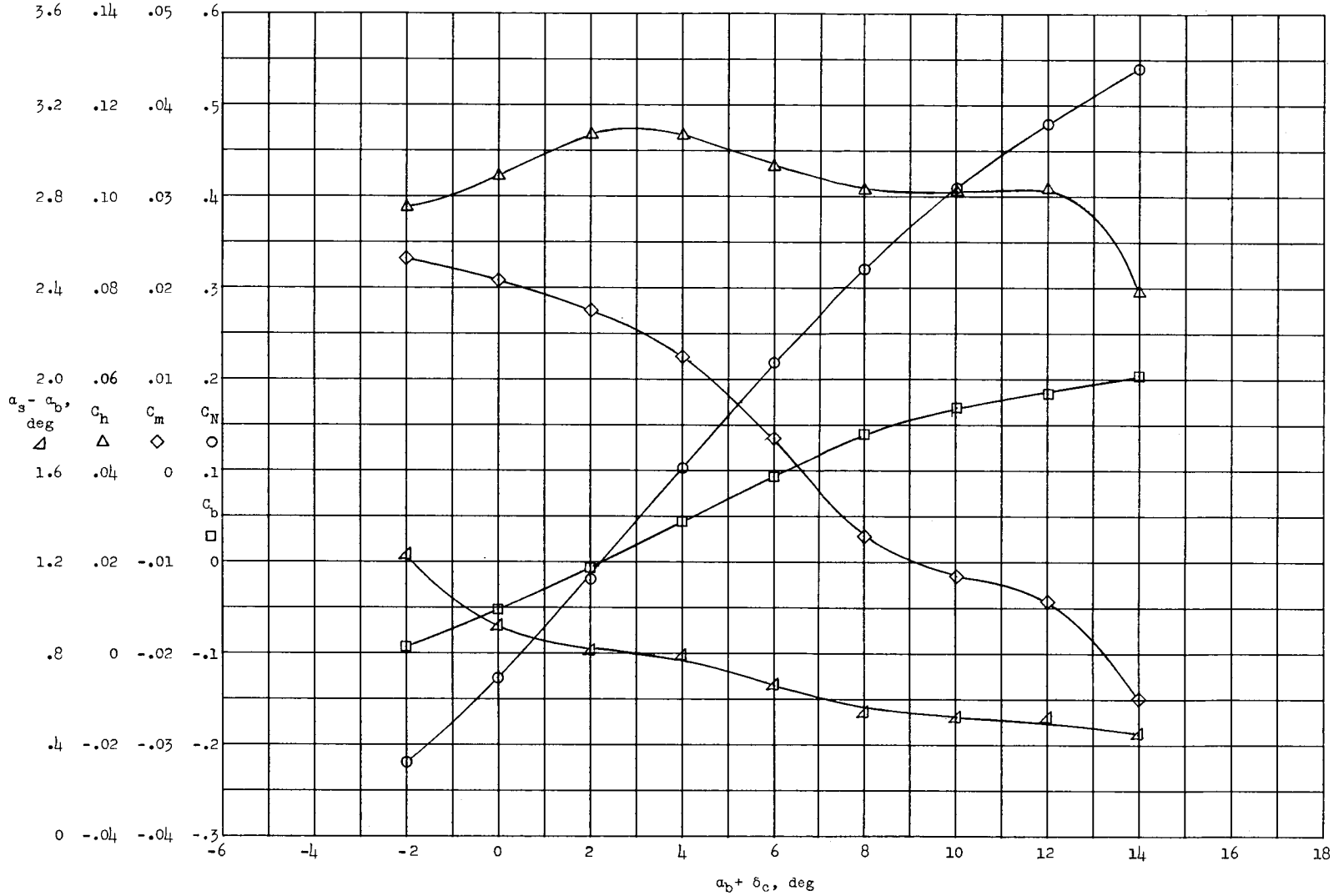

(b) $\delta_t = -12^\circ$; $\delta_c = 0^\circ$.

Figure 16.- Continued.

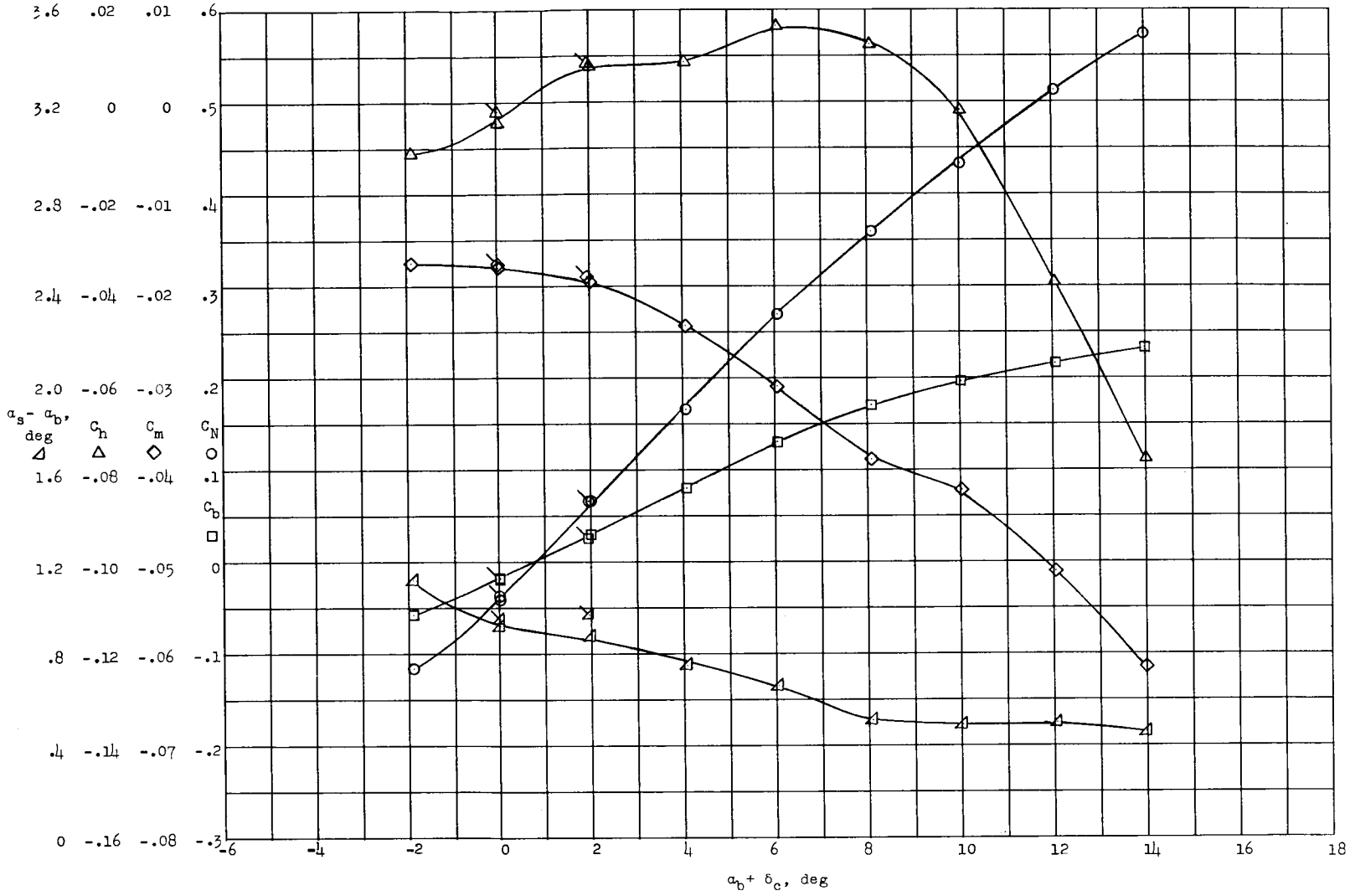

(a) $\delta_t = 0^\circ$; $\delta_c = 0^\circ$.

Figure 16.- Longitudinal aerodynamic characteristics of restrained canard in air at M = 0.80 and q = 50 lb/sq ft. Flagged symbols indicate points rerun to show repeatability.

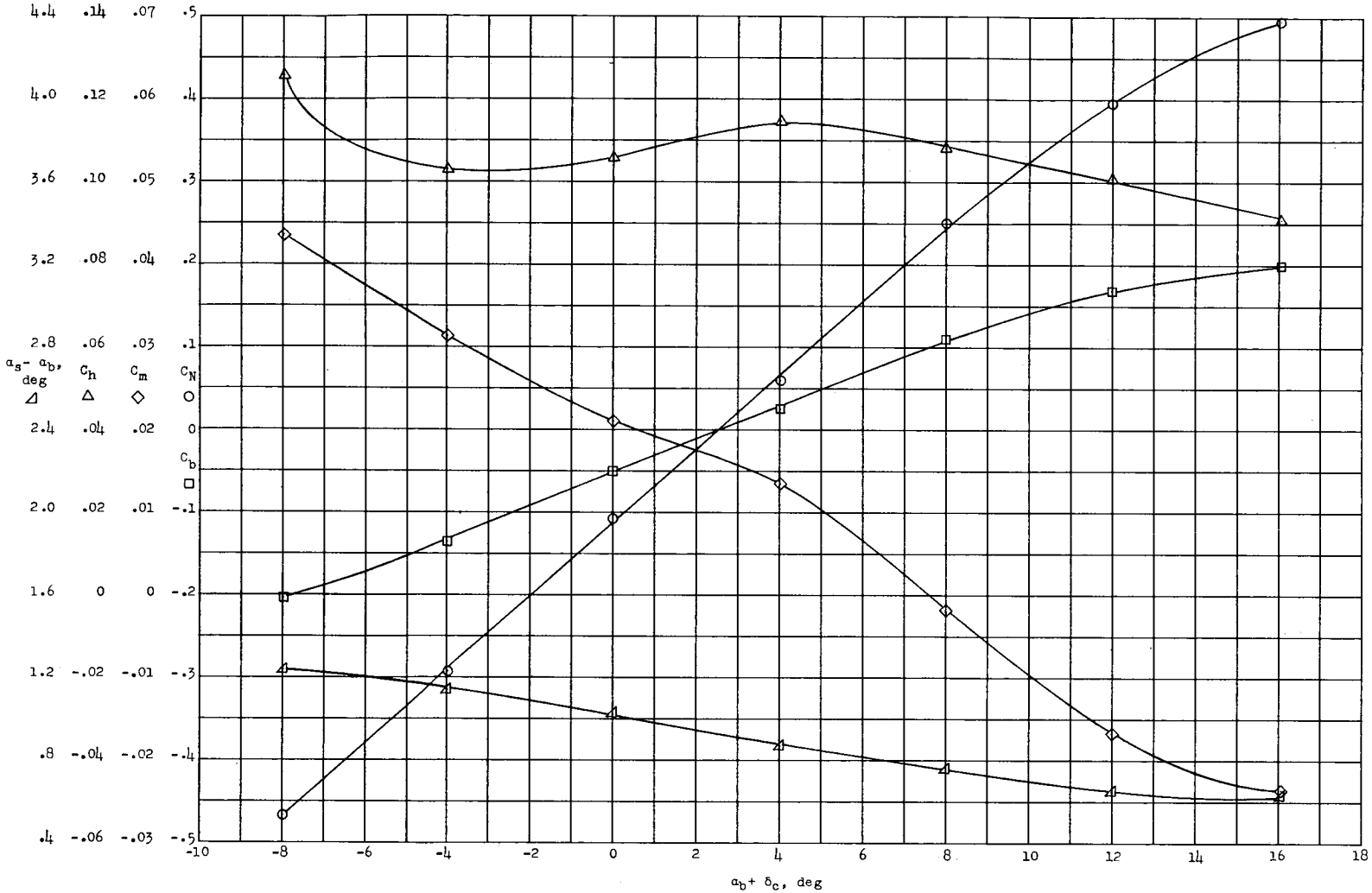

(c) $\delta_t = -12^\circ$; $\alpha_b = 0^\circ$.

Figure 16.- Concluded.

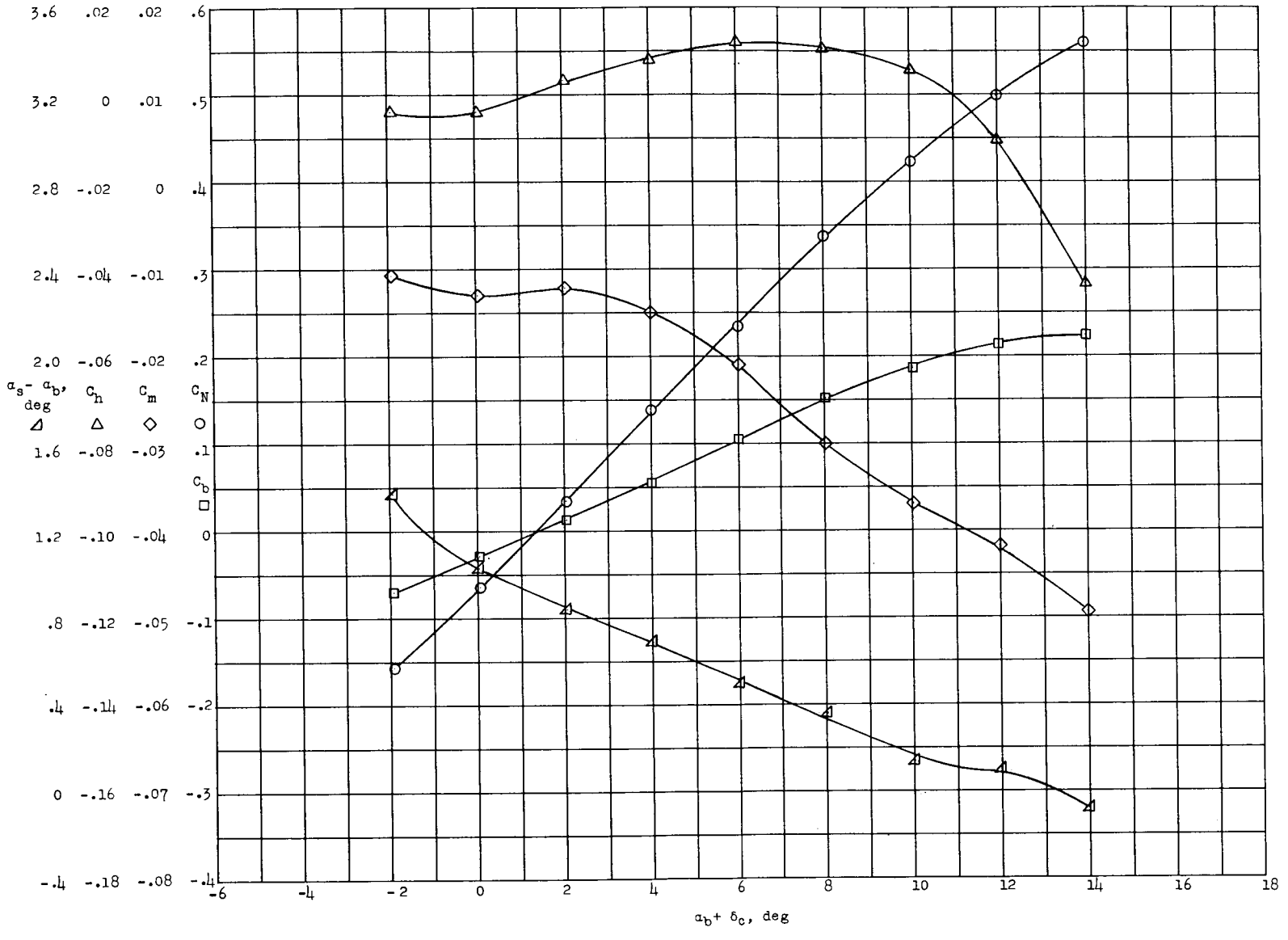

(a) $\delta_t = 0^\circ$; $\delta_c = 0^\circ$.

Figure 17.- Longitudinal aerodynamic characteristics of restrained canard in air at M = 0.80 and q = 100 lb/sq ft.

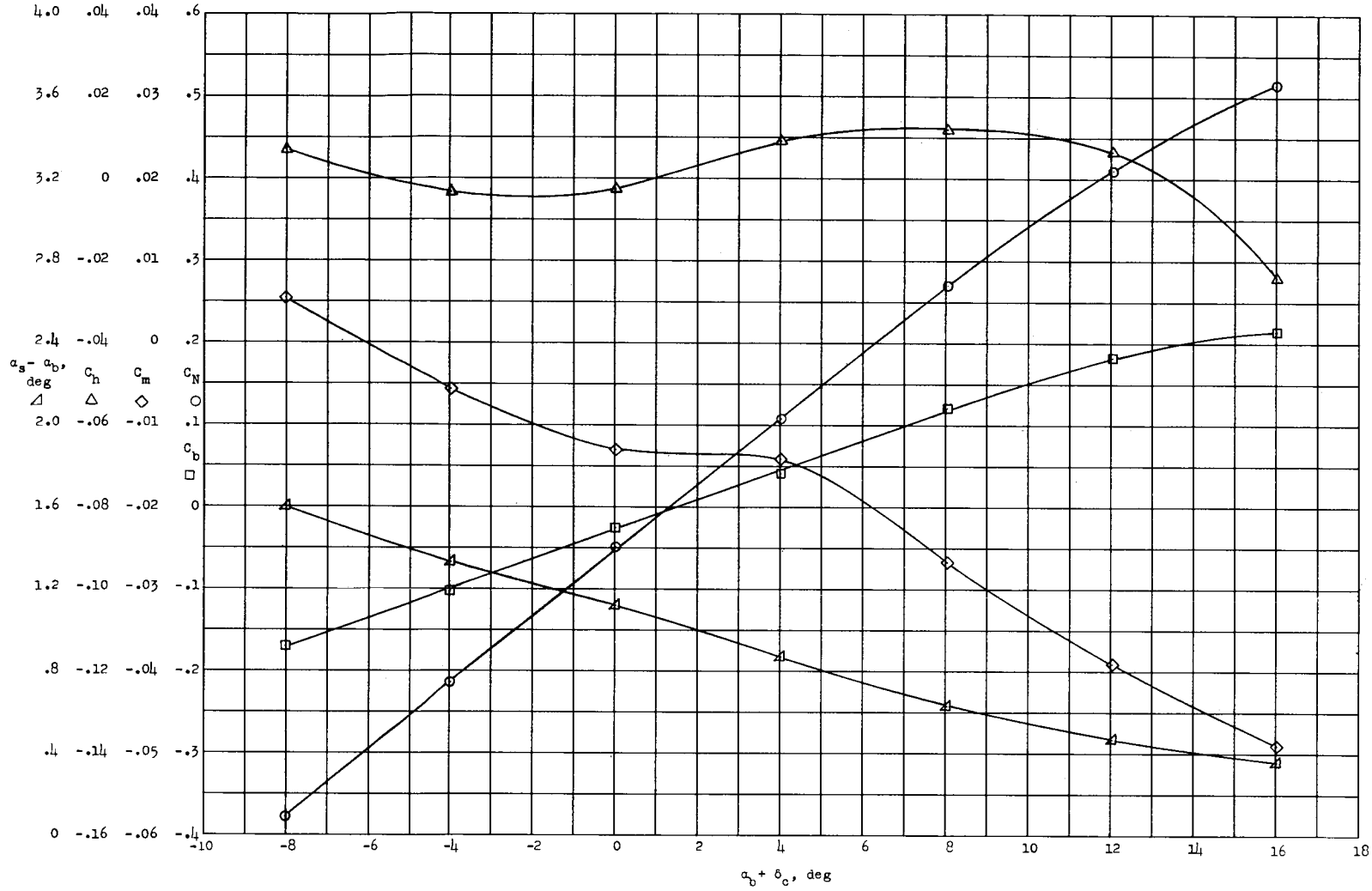

(b) $\delta_t = 0^\circ$; $\alpha_b = 0^\circ$.

Figure 17.- Continued.

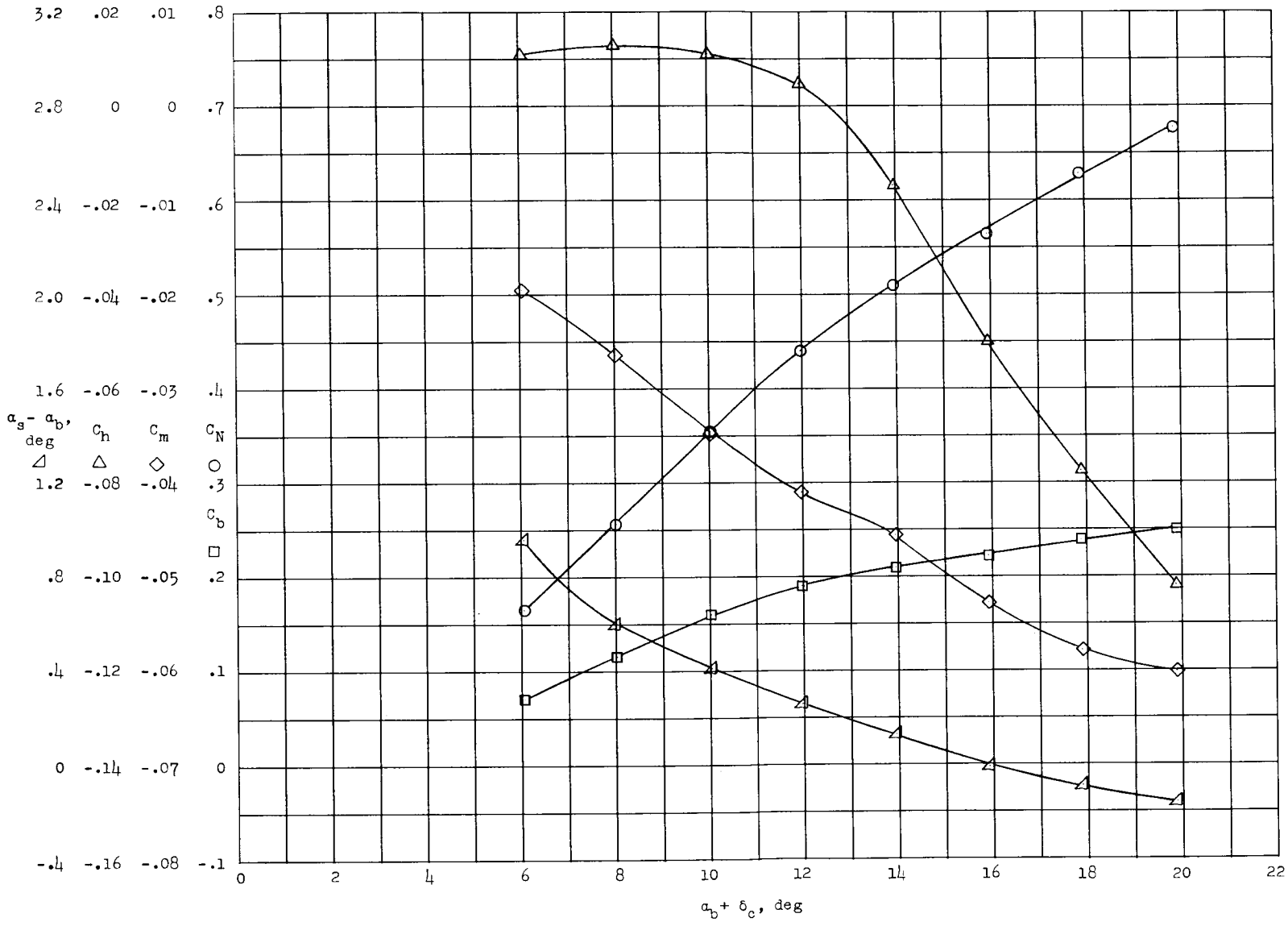

(c) $\delta_t = 0°$; $\delta_c = 8°$.

Figure 17.- Continued.

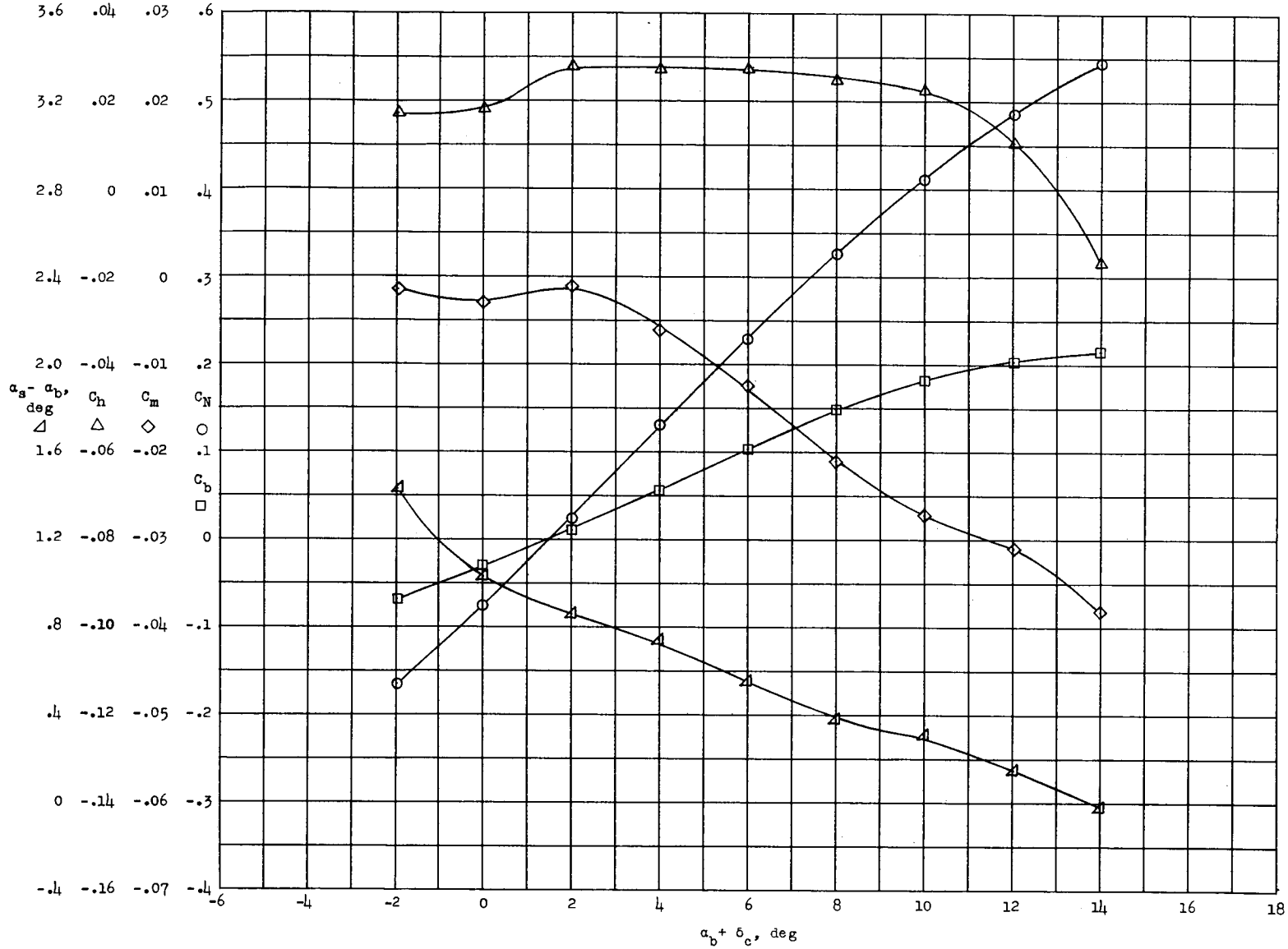

(d) $\delta_t = -4^\circ$; $\delta_c = 0^\circ$.

Figure 17.- Continued.

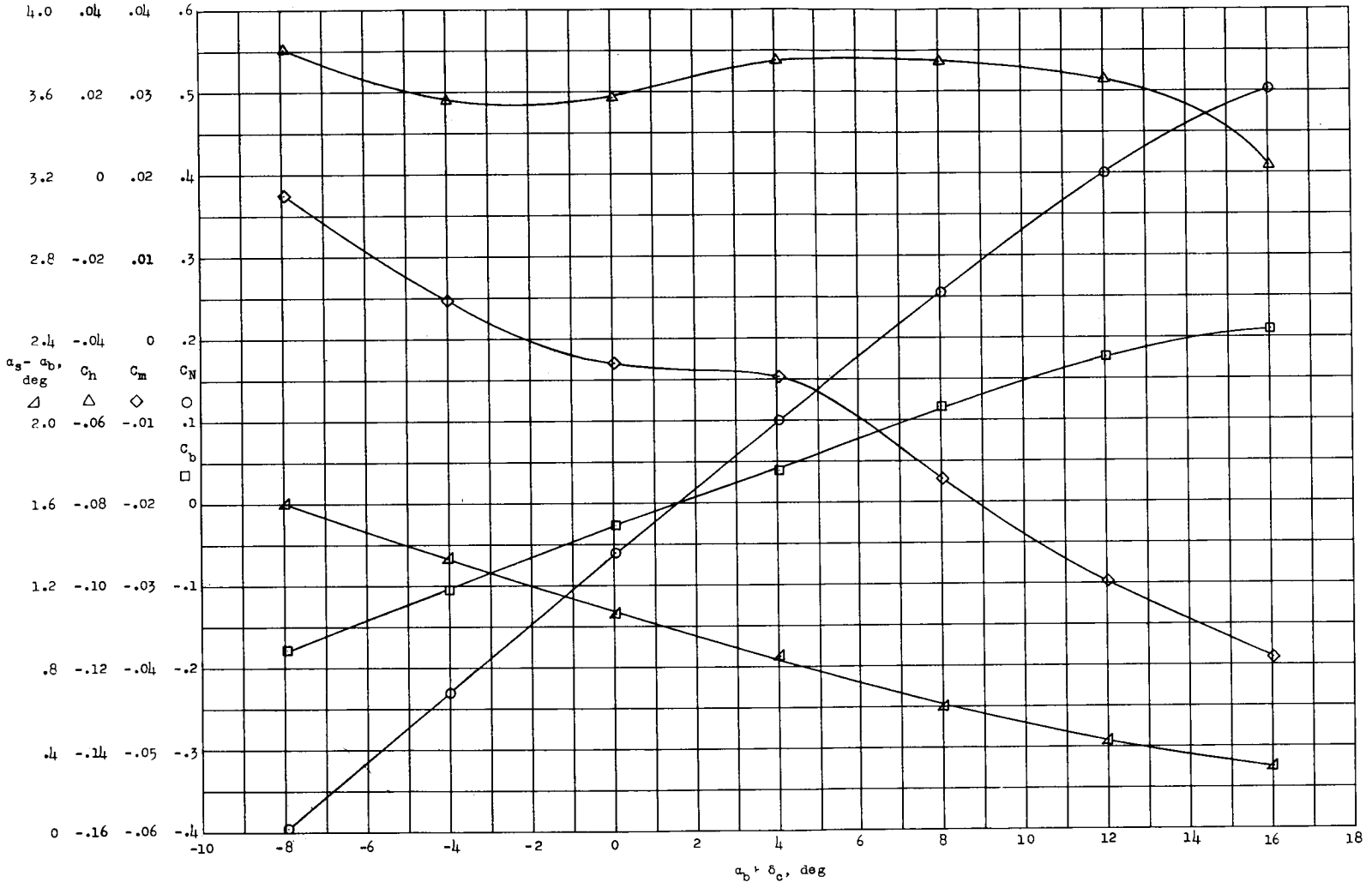

(e) $\delta_t = -4^\circ$; $\alpha_b = 0^\circ$.

Figure 17.- Continued.

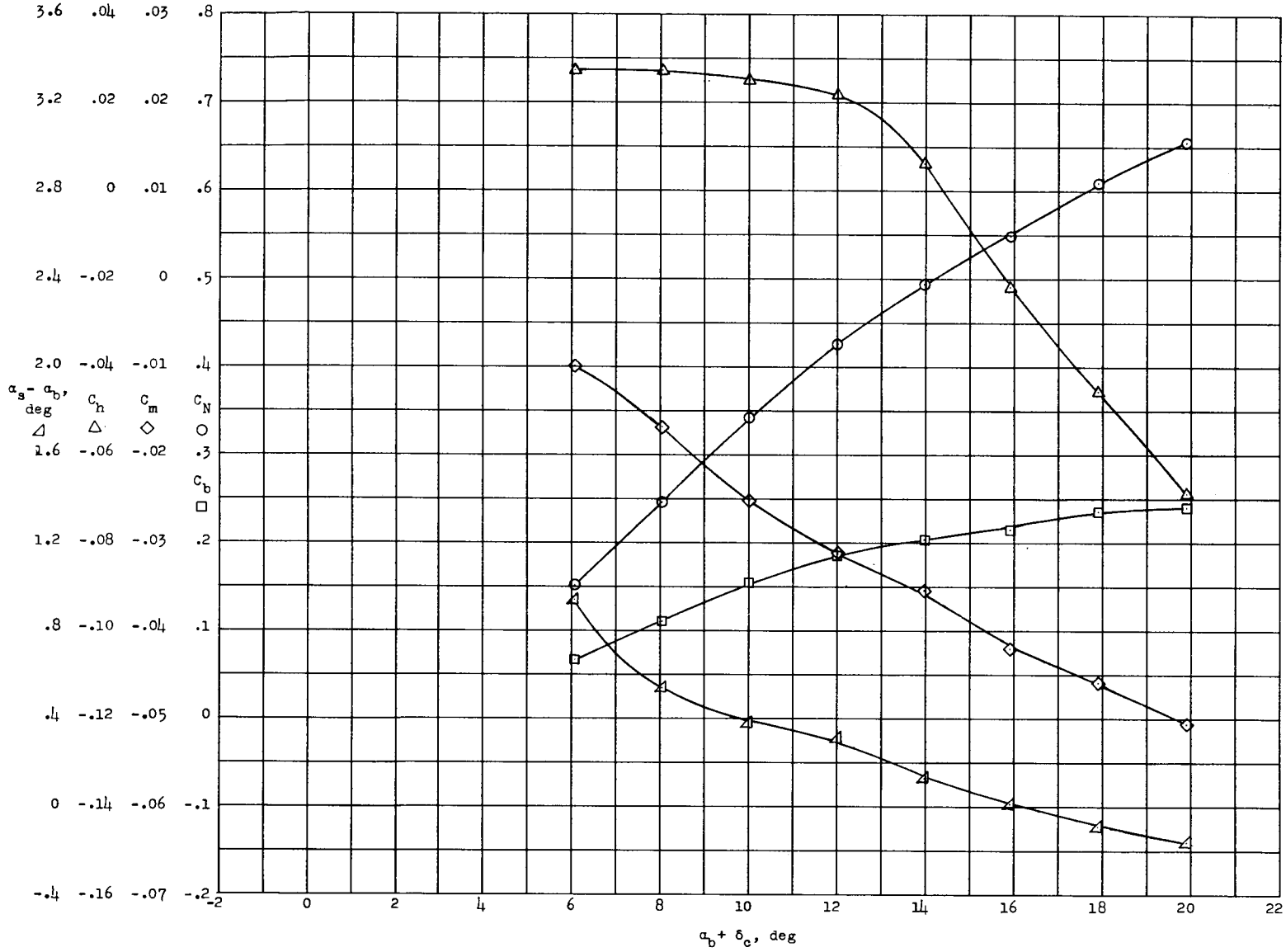

(f) $\delta_t = -4^\circ$; $\delta_c = 8^\circ$.

Figure 17.- Continued.

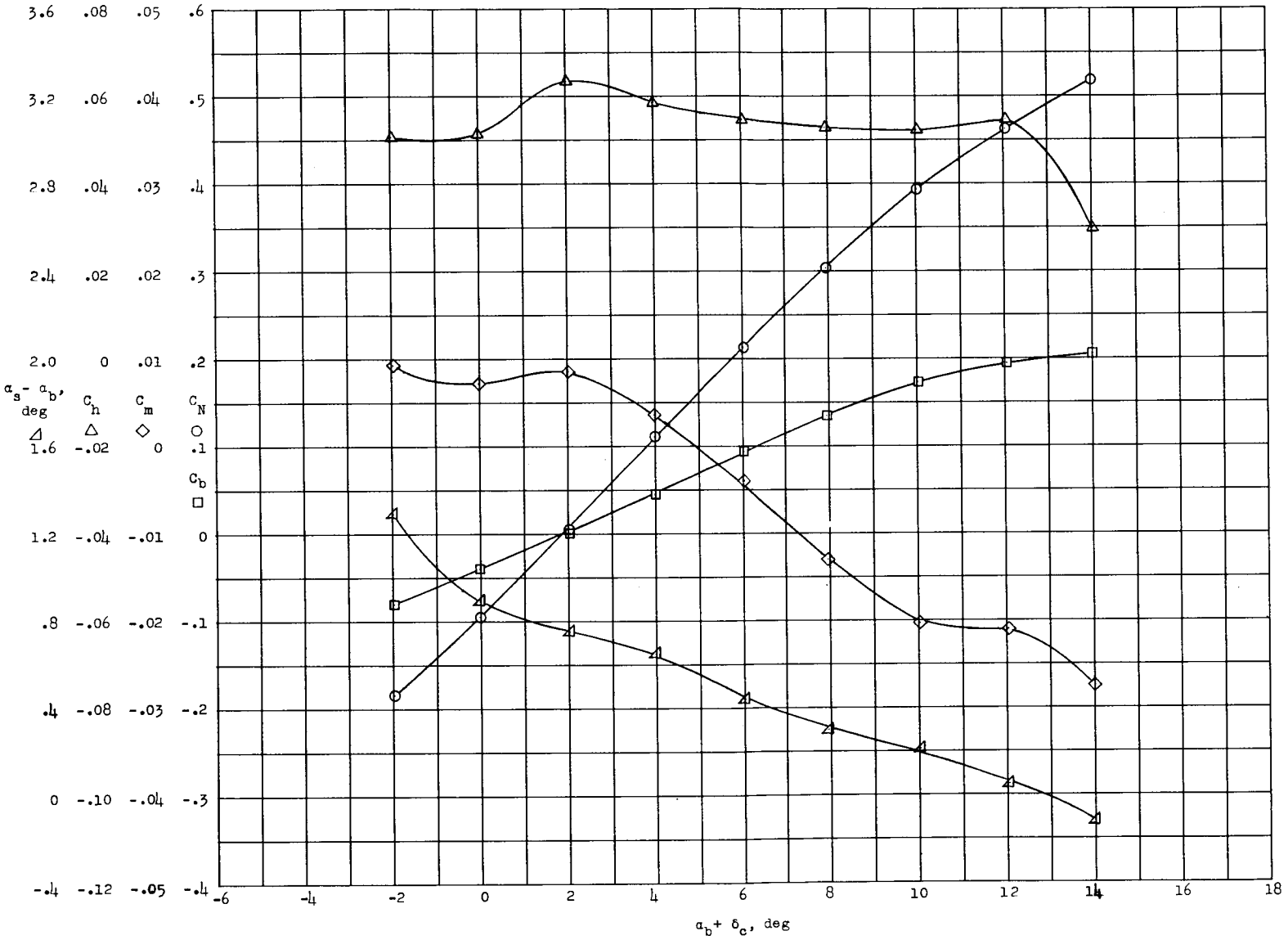

(g) $\delta_t = -8^\circ$; $\delta_c = 0^\circ$.

Figure 17.- Continued.

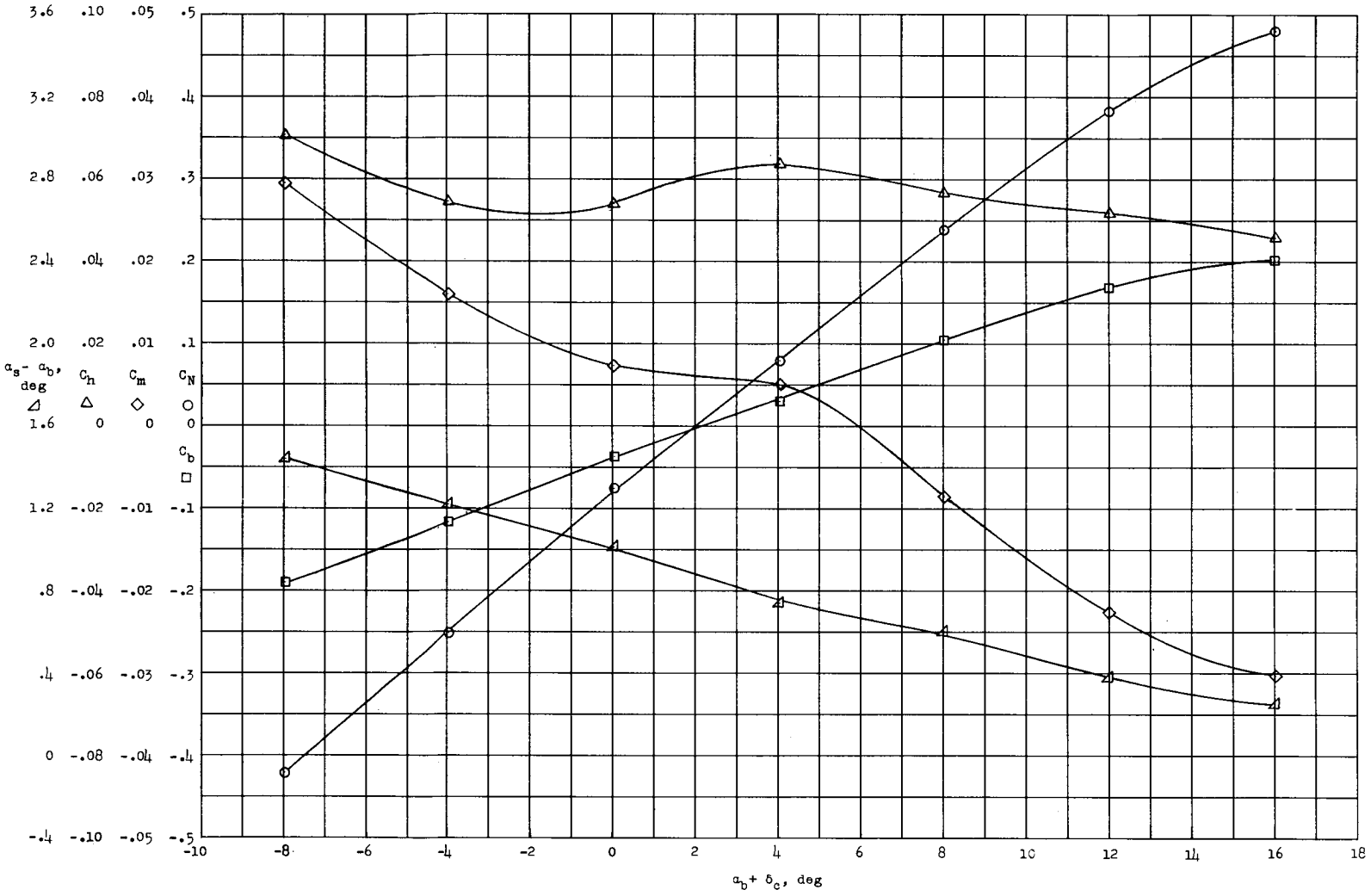

(h) $\delta_t = -8^o$; $\alpha_b = 0^o$.

Figure 17.- Continued.

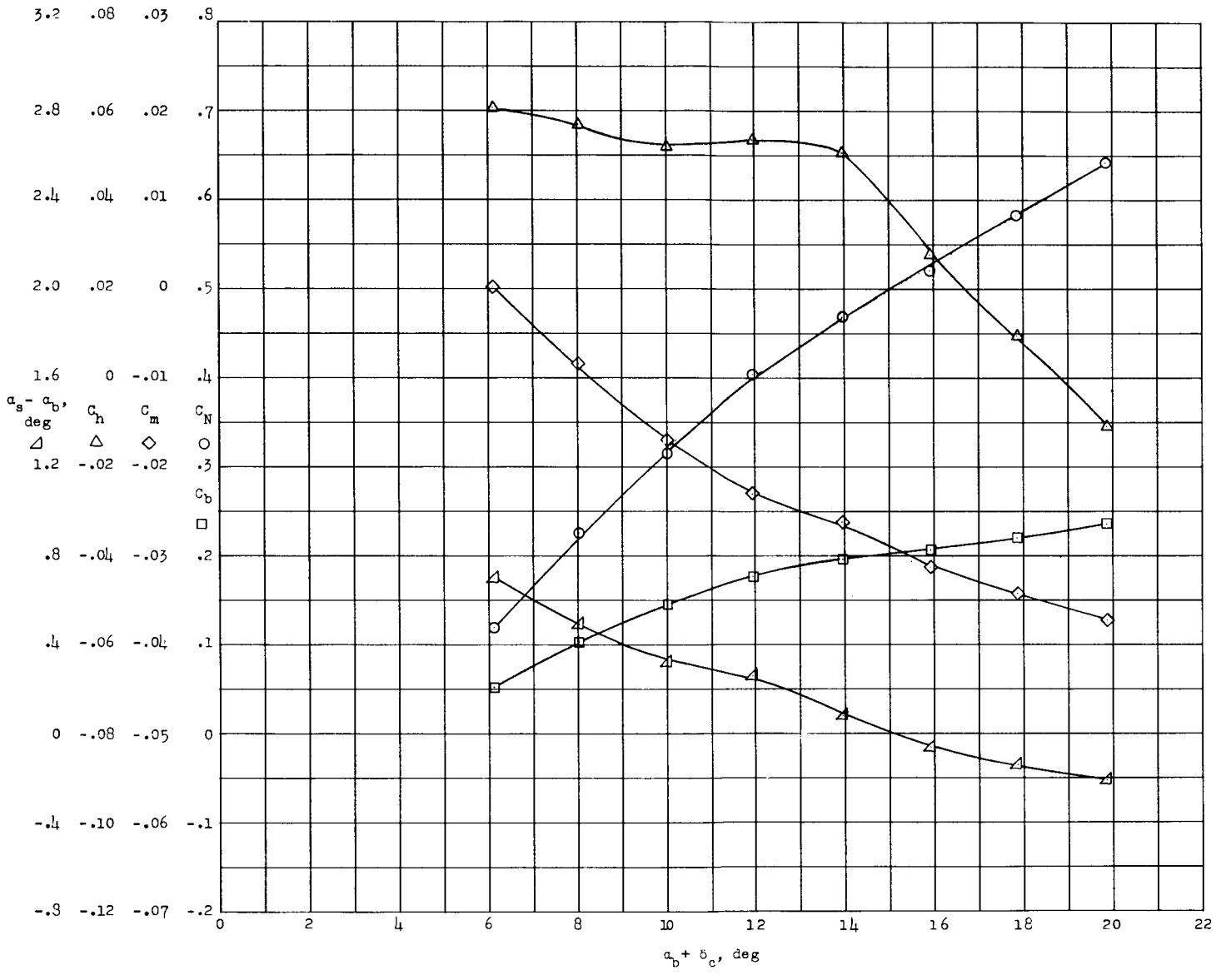

(i) $\delta_t = -8^\circ$; $\delta_c = 8^\circ$.

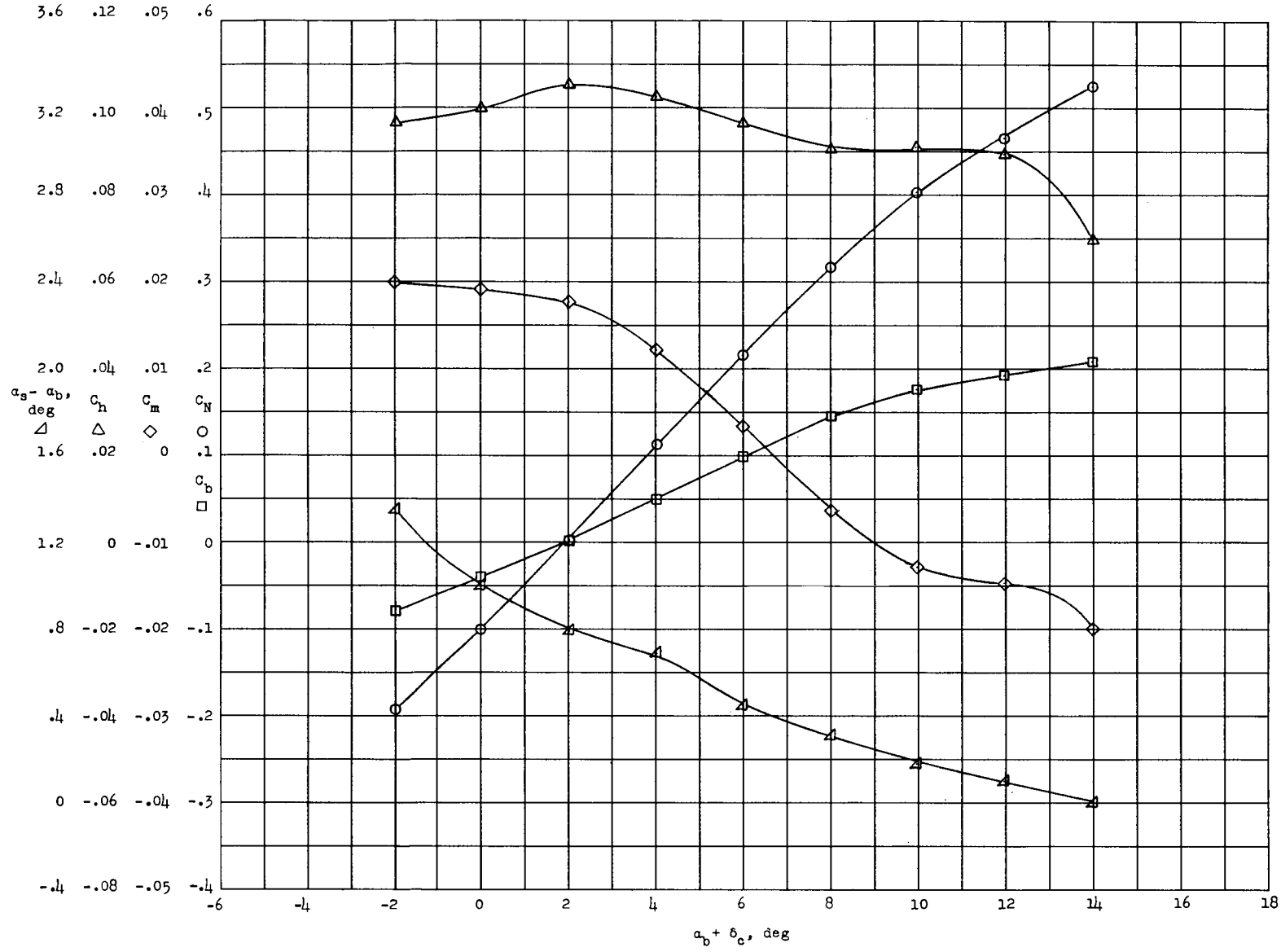

(j) $\delta_t = -12^\circ$; $\delta_c = 0^\circ$.

Figure 17.- Continued.

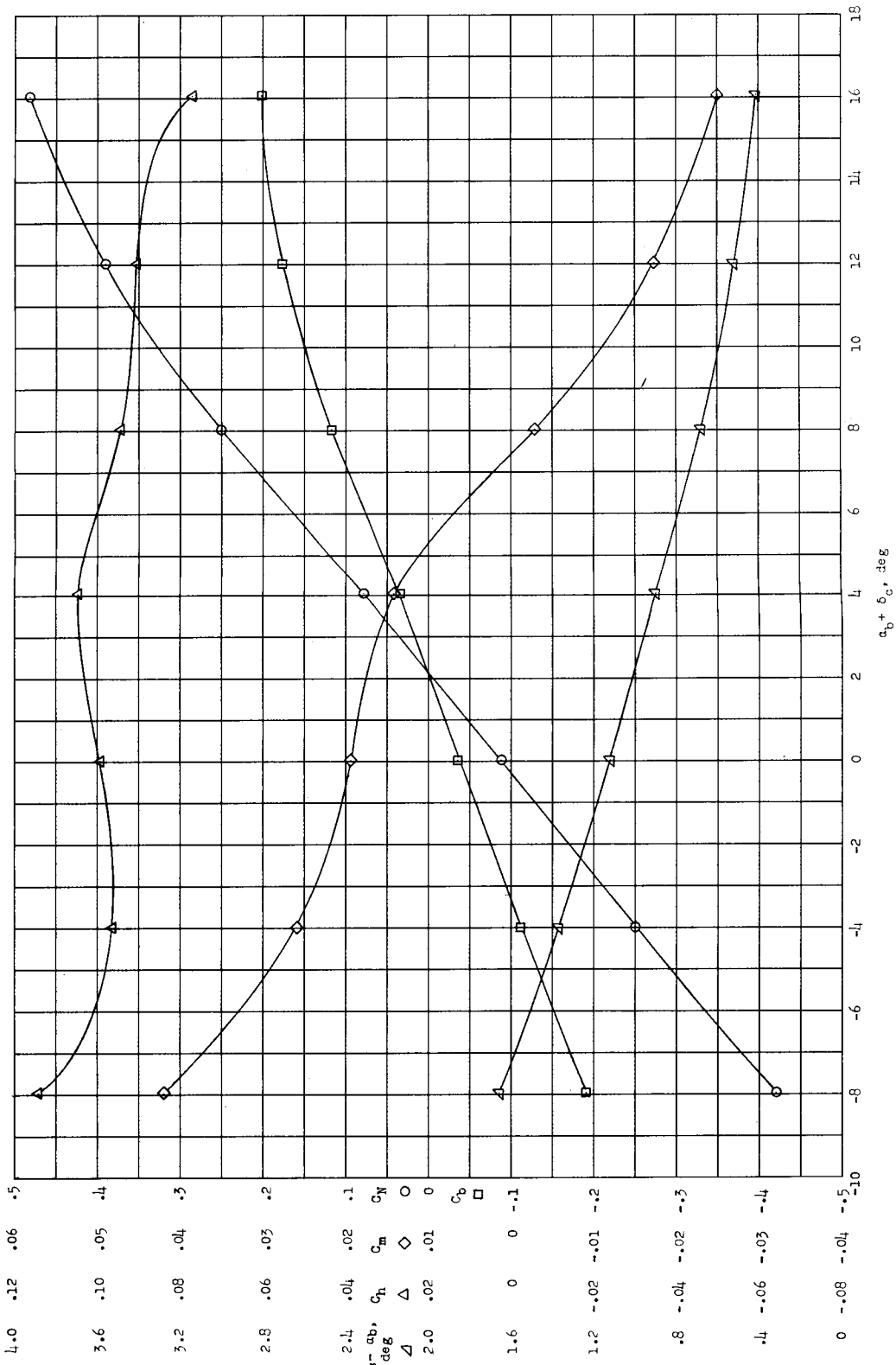

(k) $\delta_t = -12^\circ$; $\alpha_b = 0^\circ$.

Figure 17.- Continued.

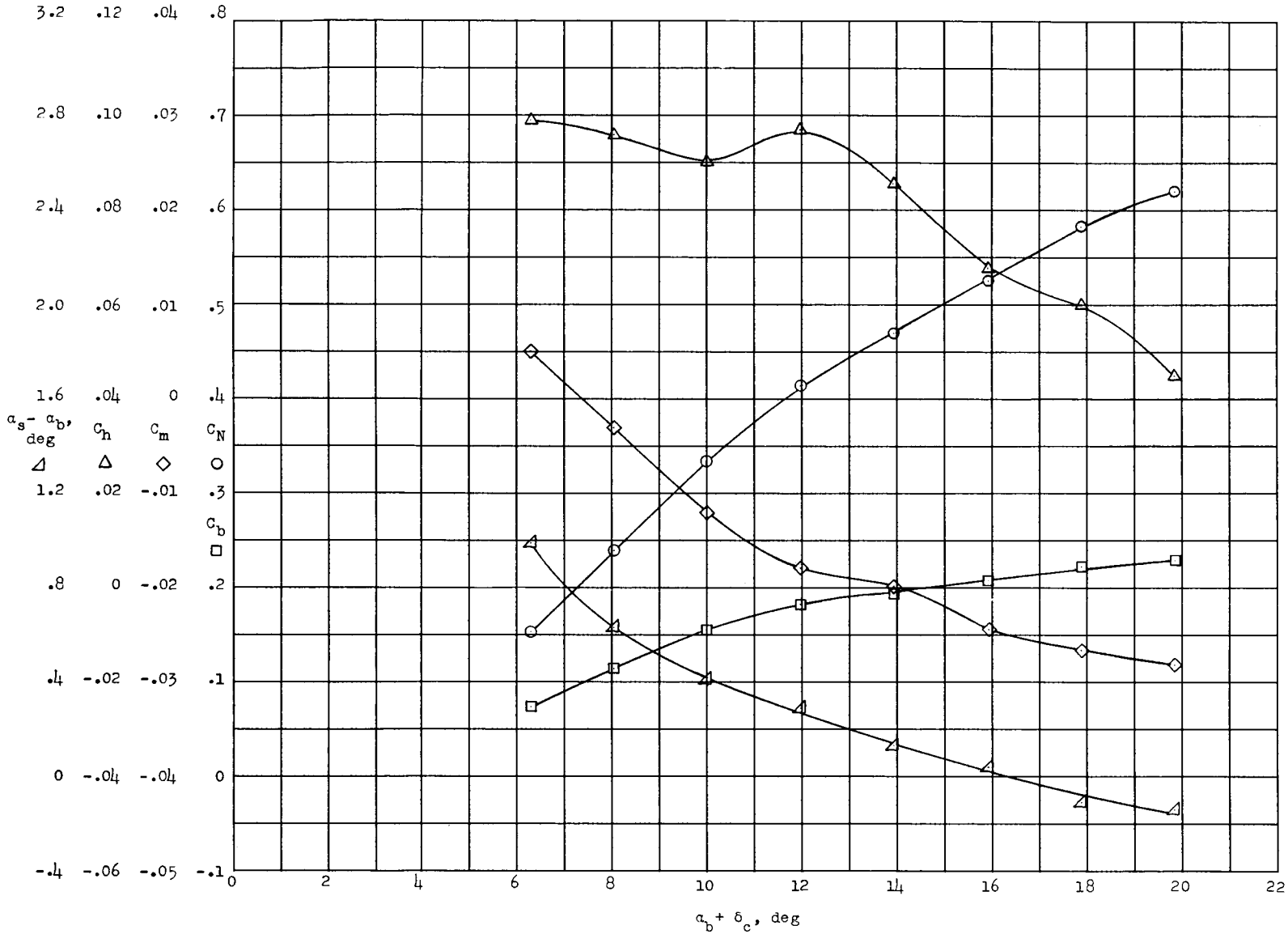

(*l*) $\delta_t = -12^\circ$; $\delta_c = 8^\circ$.

Figure 17.- Concluded.

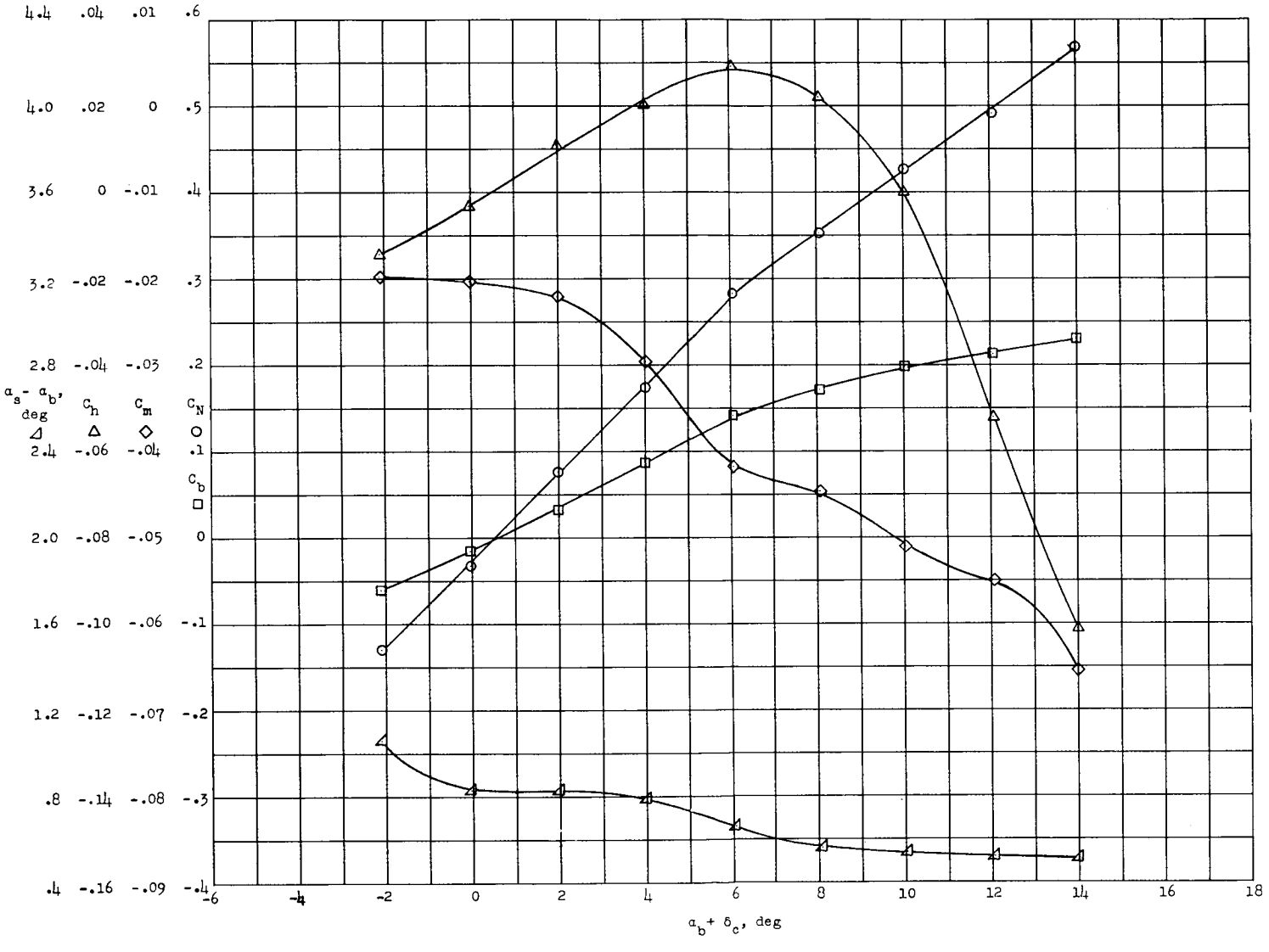

(a) $\delta_c = 0^\circ$.

Figure 18.- Longitudinal aerodynamic characteristics of restrained canard in air at M = 0.85 and q = 50 lb/sq ft with $\delta_t = 0^\circ$.

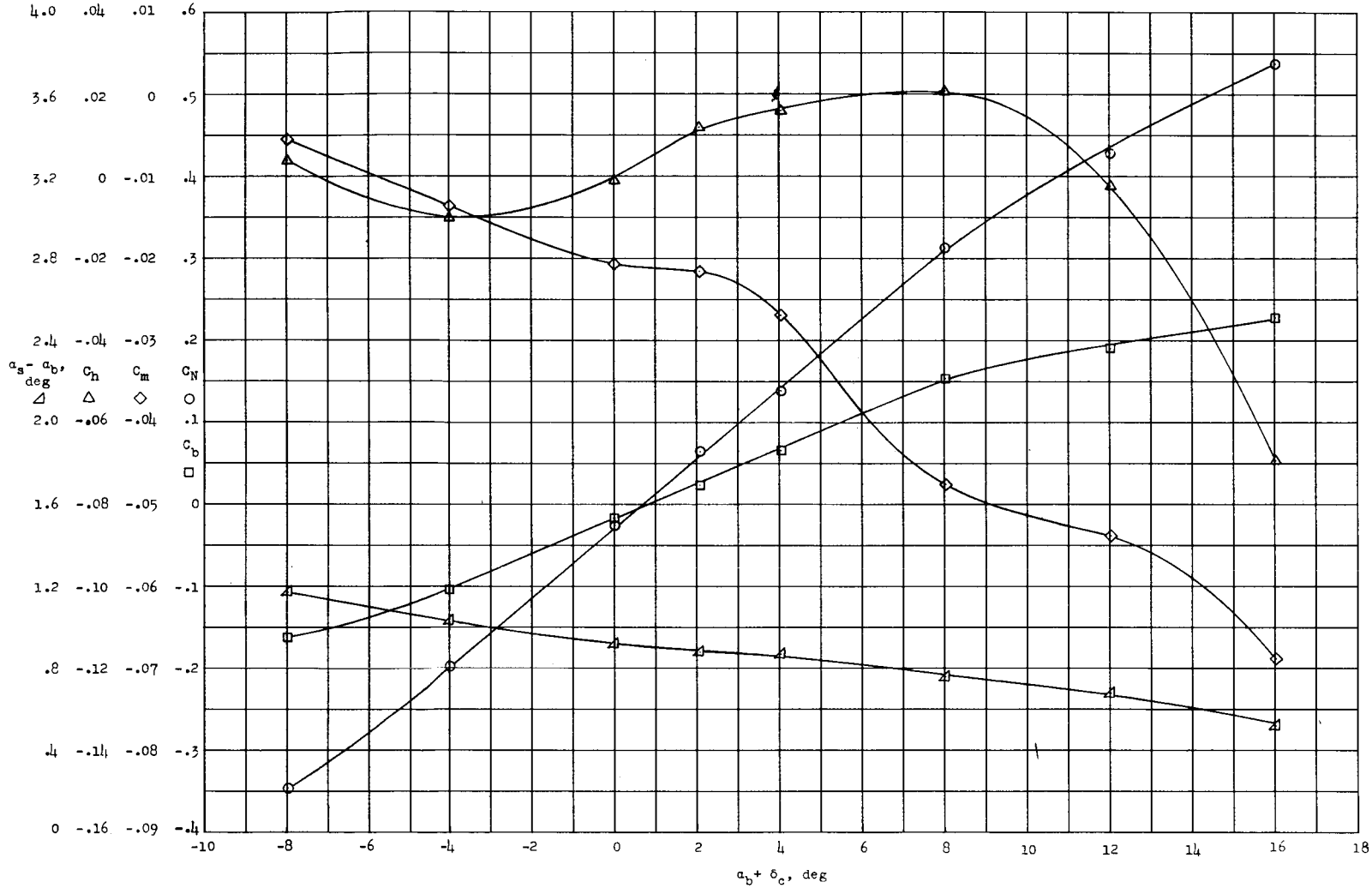

(b) $\alpha_b = 0^\circ$.

Figure 18.- Concluded.

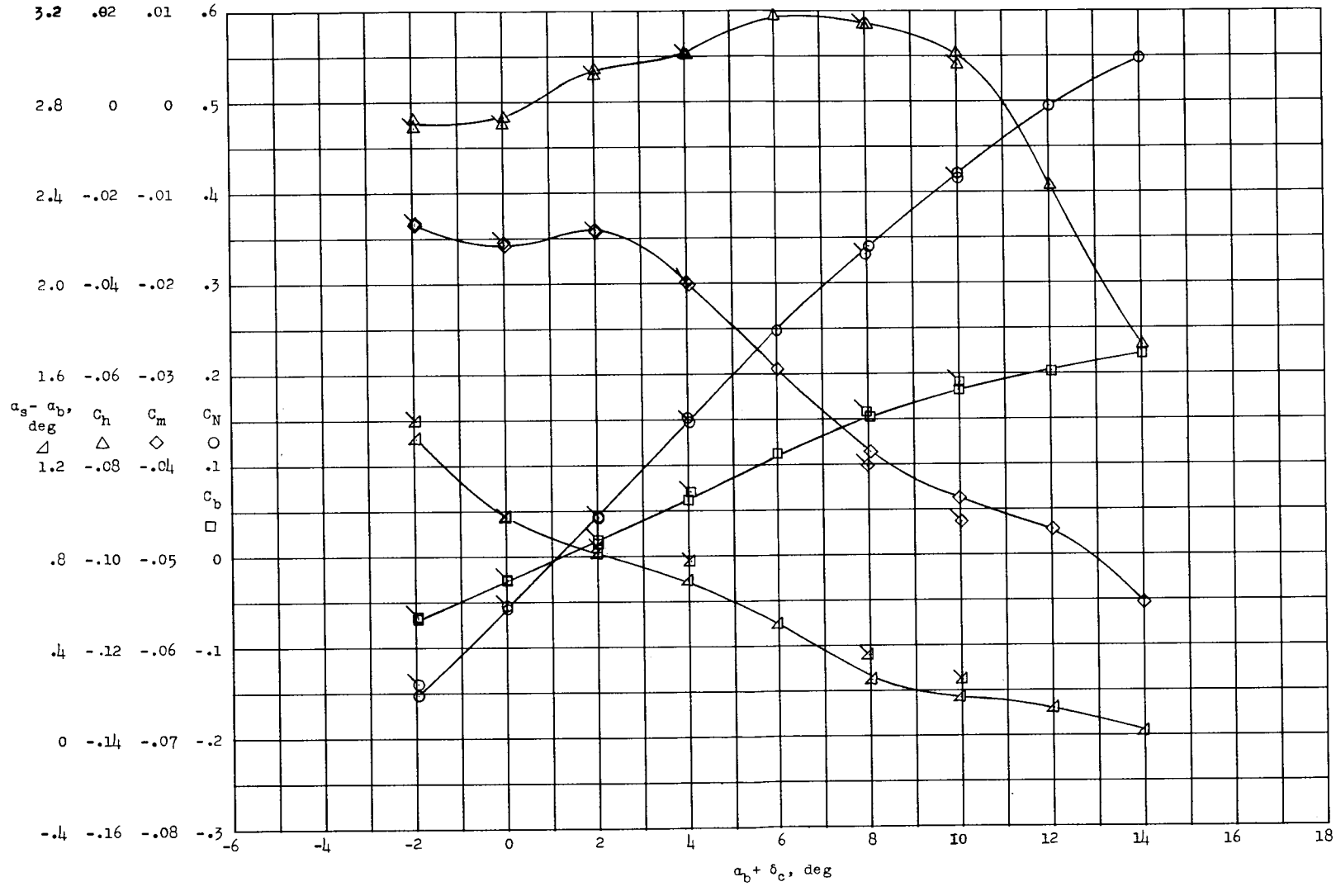

(a) $\delta_c = 0^o$.

Figure 19.- Longitudinal aerodynamic characteristics of restrained canard in air at M = 0.85 and q = 100 lb/sq ft with $\delta_t = 0^o$. Flagged symbols indicate points rerun to show repeatability.

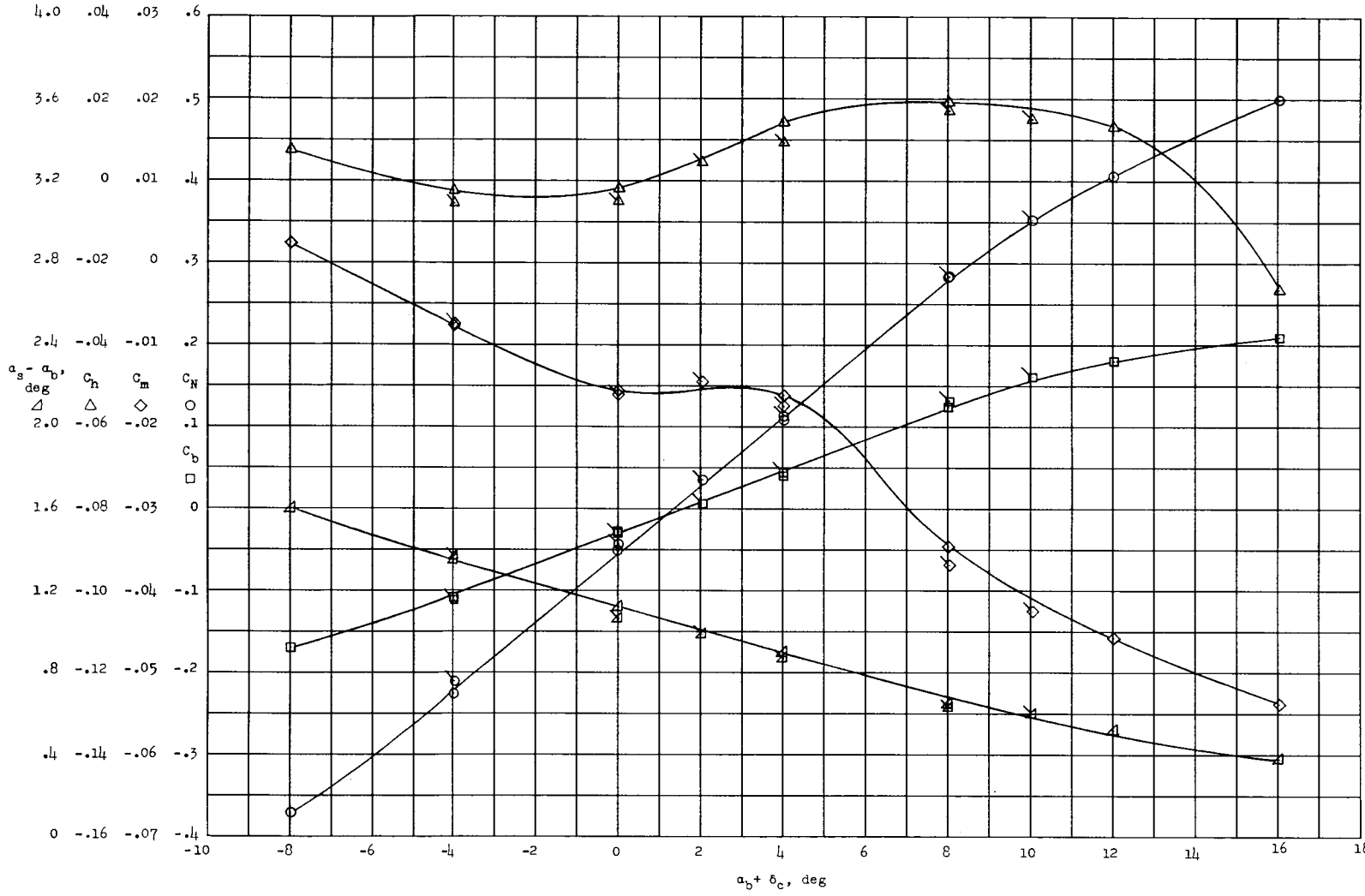

(b) $\alpha_b = 0^\circ$.

Figure 19.- Concluded.

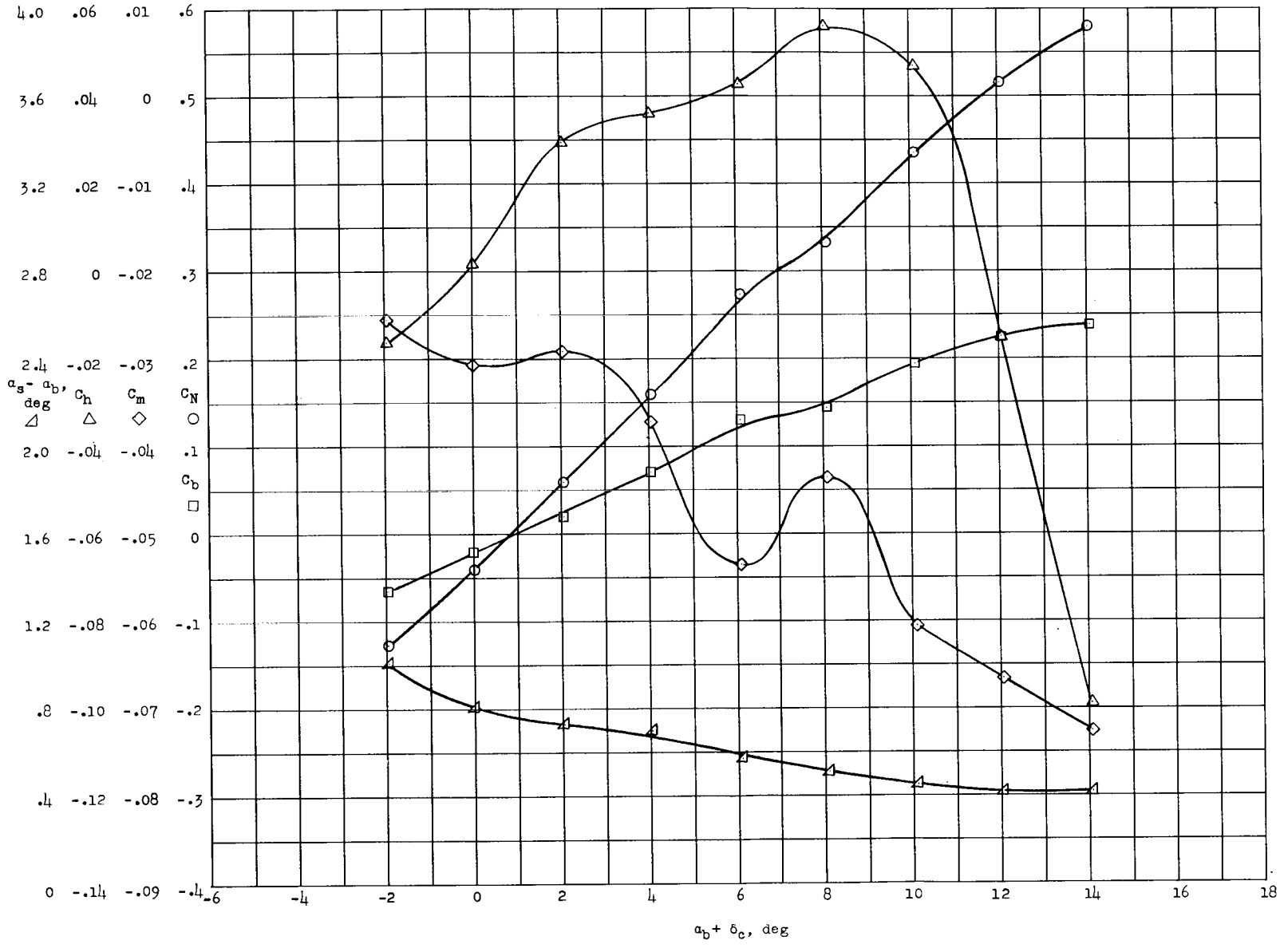

Figure 20.- Longitudinal aerodynamic characteristics of restrained canard in air at M = 0.90 and q = 50 lb/sq ft with $\delta_t = 0^o$ and $\delta_c = 0^o$.

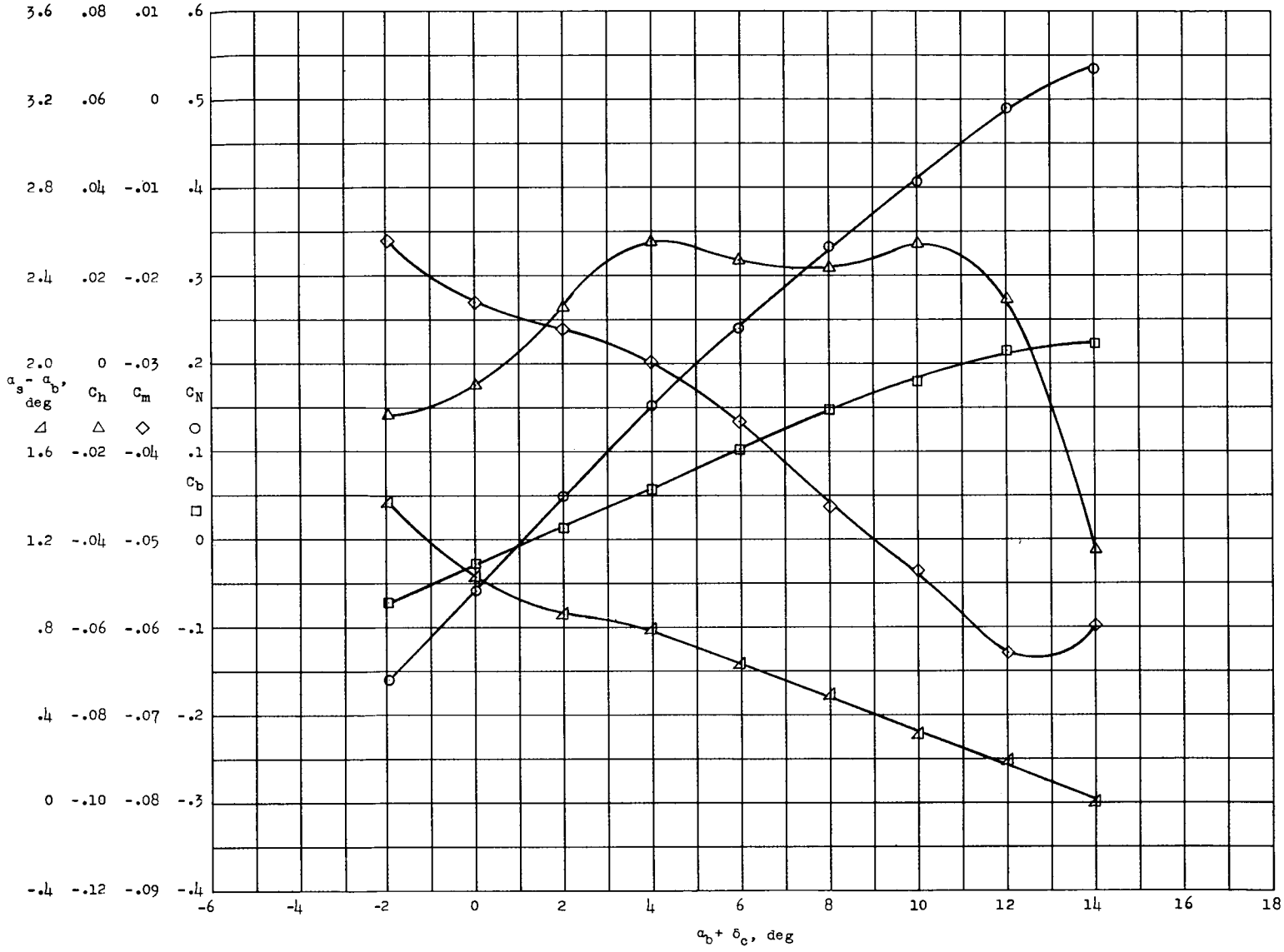

(a) $\delta_t = 0^o$; $\delta_c = 0^o$.

Figure 21.- Longitudinal aerodynamic characteristics of restrained canard in air at M = 0.90 and q = 100 lb/sq ft.

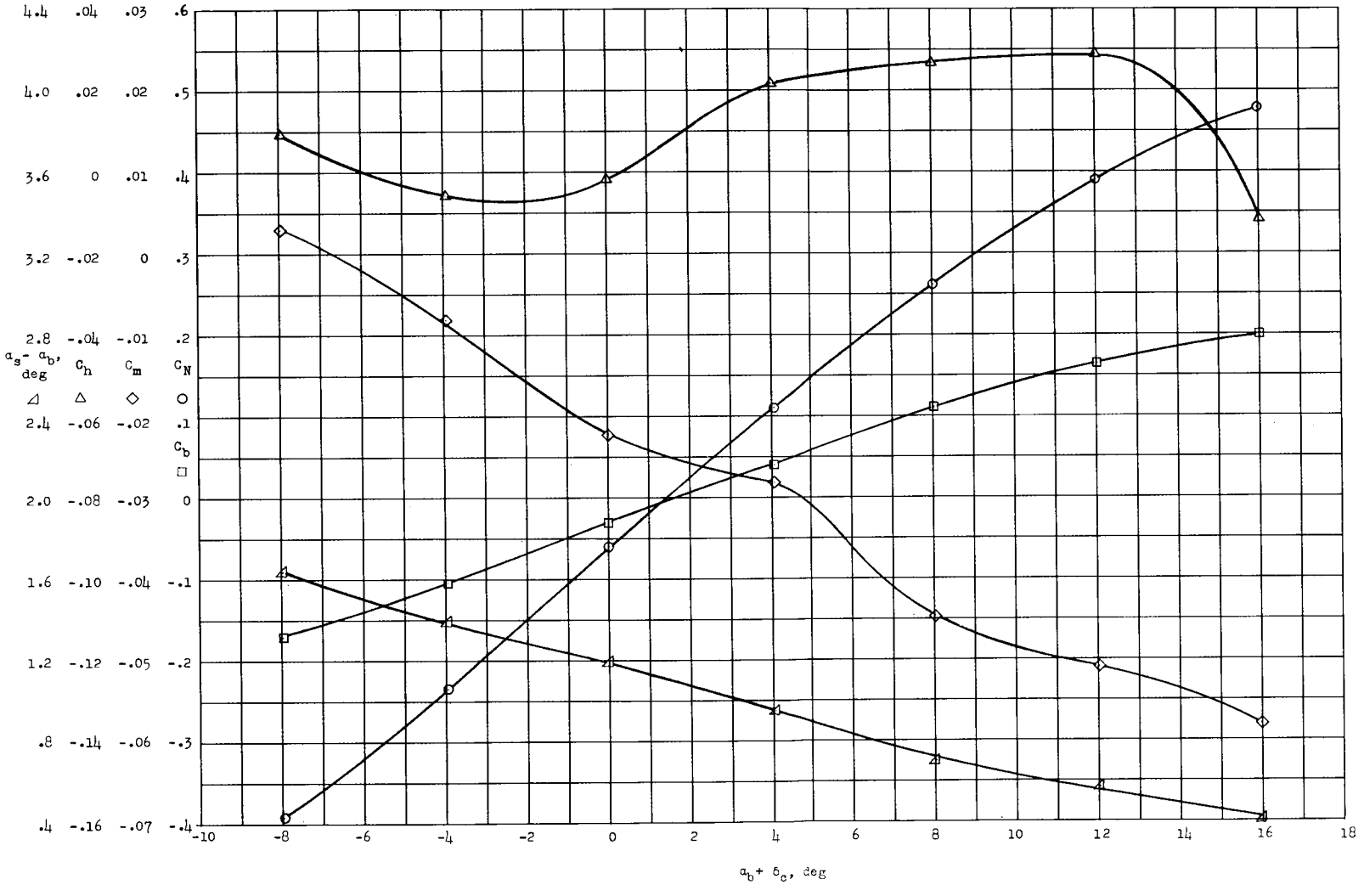

(b) $\delta_t = 0^\circ$; $\alpha_b = 0^\circ$.

Figure 21.- Continued.

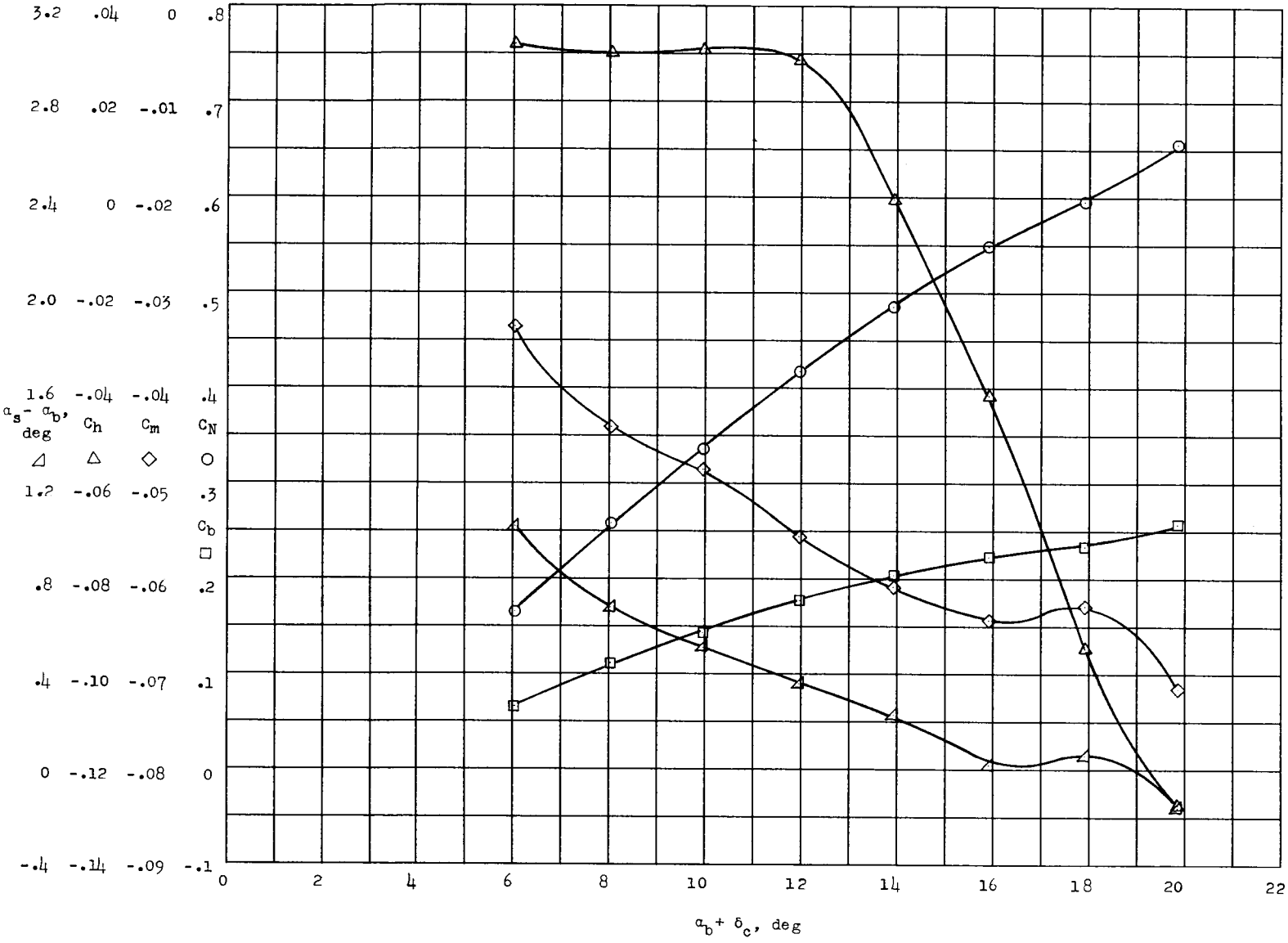

(c) $\delta_t = 0^\circ$; $\delta_c = 8^\circ$.

Figure 21.- Continued.

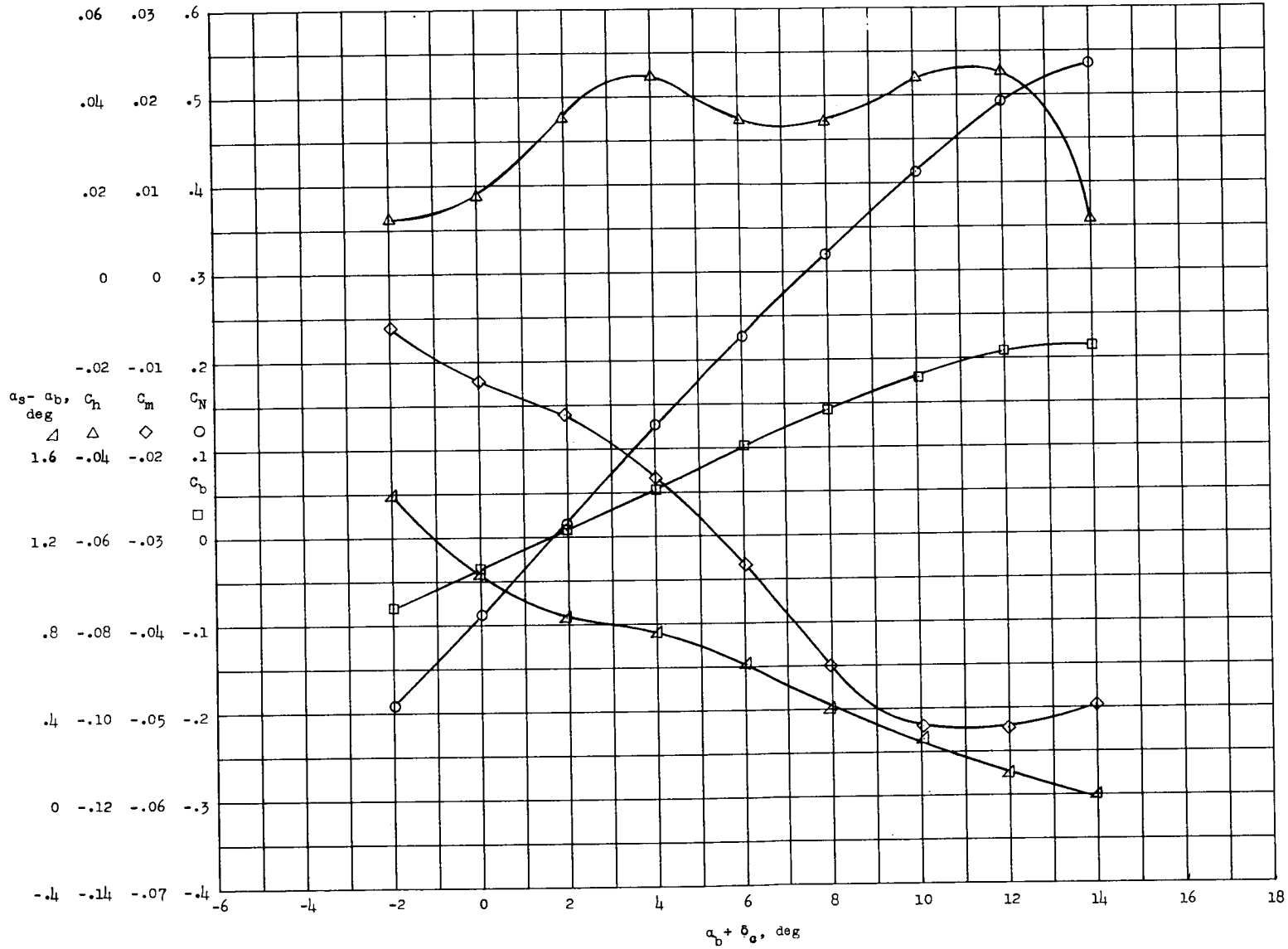

(d) $\delta_t = -4^\circ$; $\delta_c = 0^\circ$.

Figure 21.- Continued.

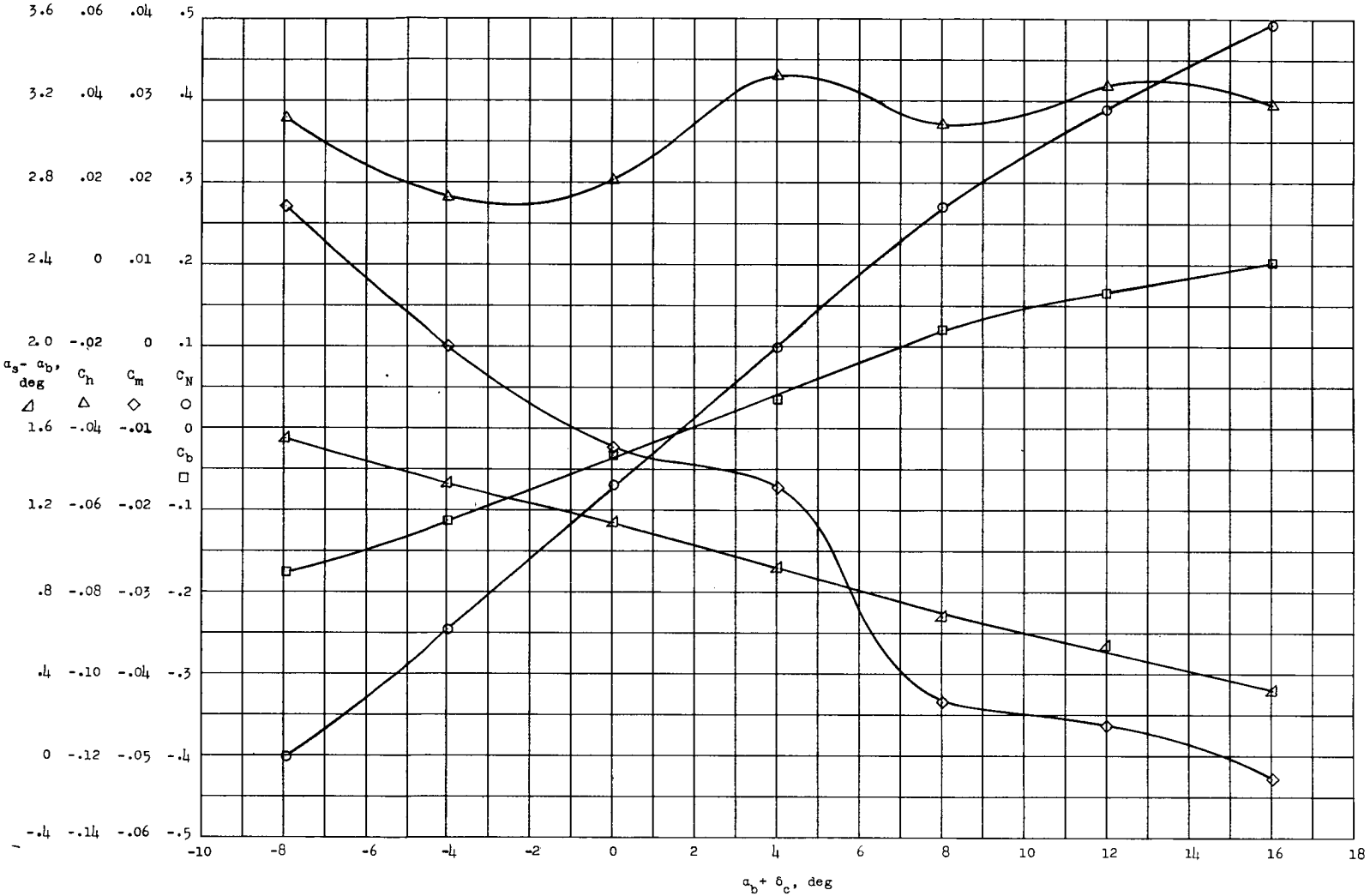

(e) $\delta_t = -4^o$; $\alpha_b = 0^o$.

Figure 21.- Continued.

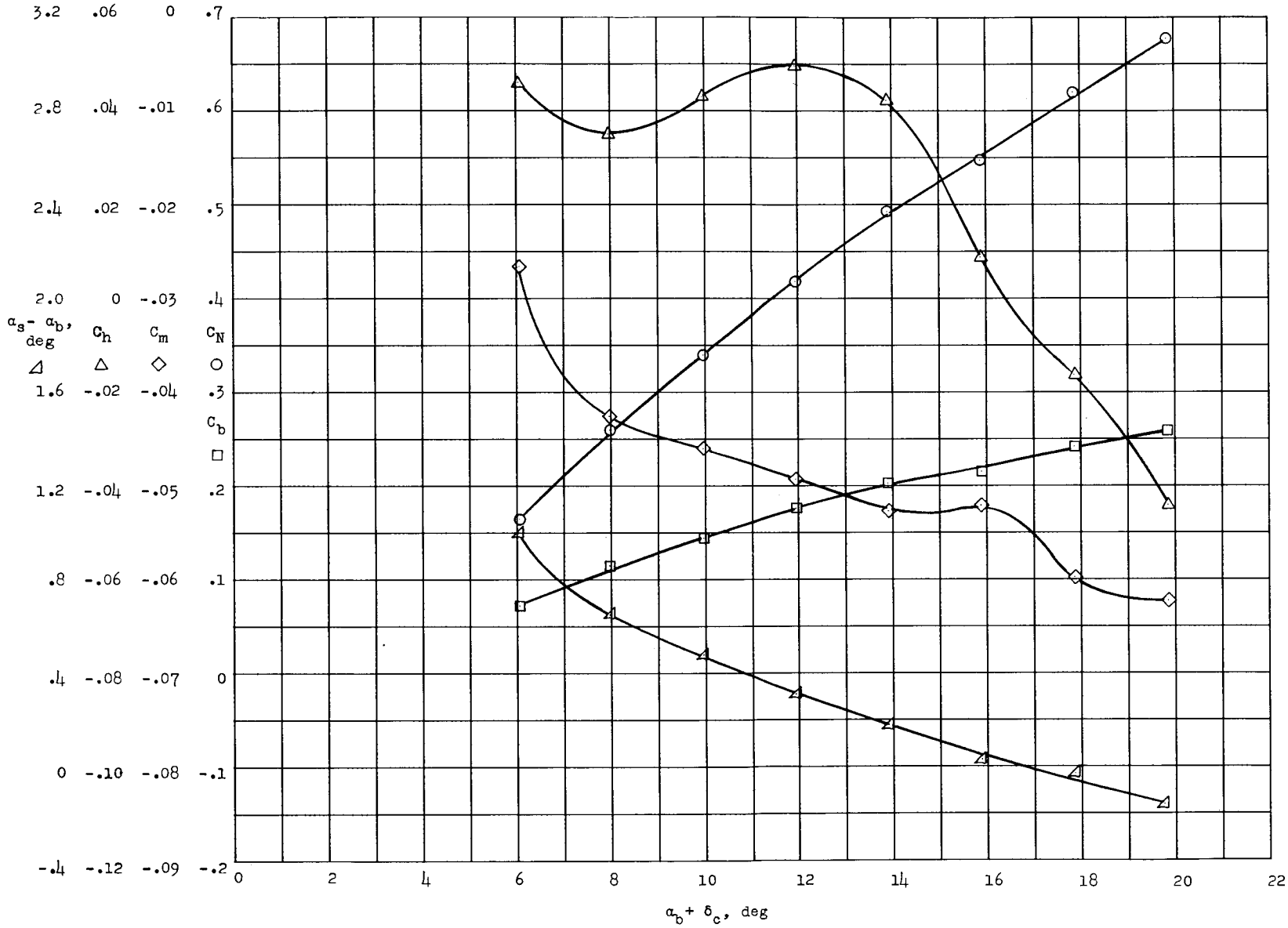

(f) $\delta_t = -4^\circ$; $\delta_c = 8^\circ$.

Figure 21.- Continued.

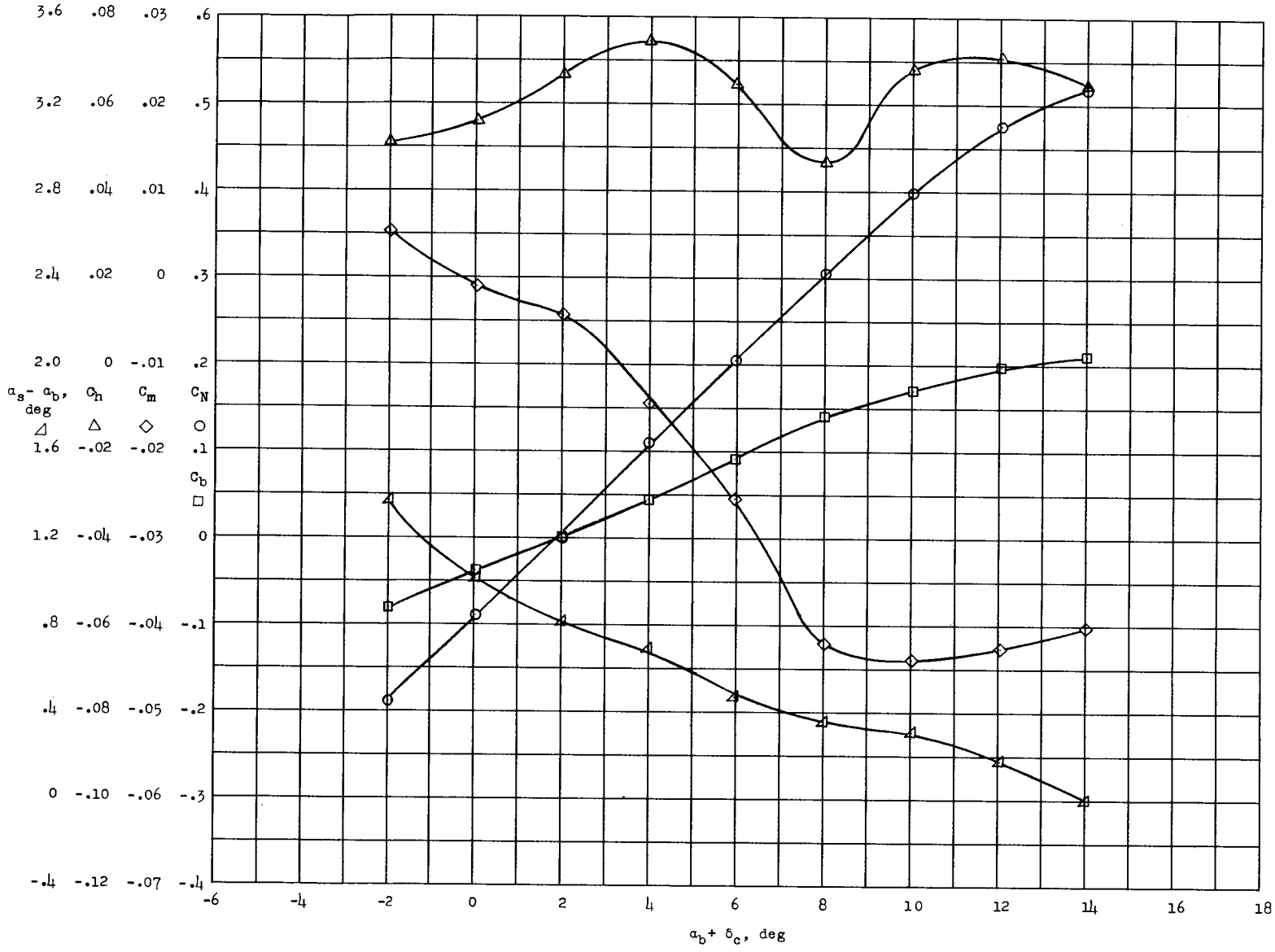

(g) $\delta_t = -8^\circ$; $\delta_c = 0^\circ$.

Figure 21.- Continued.

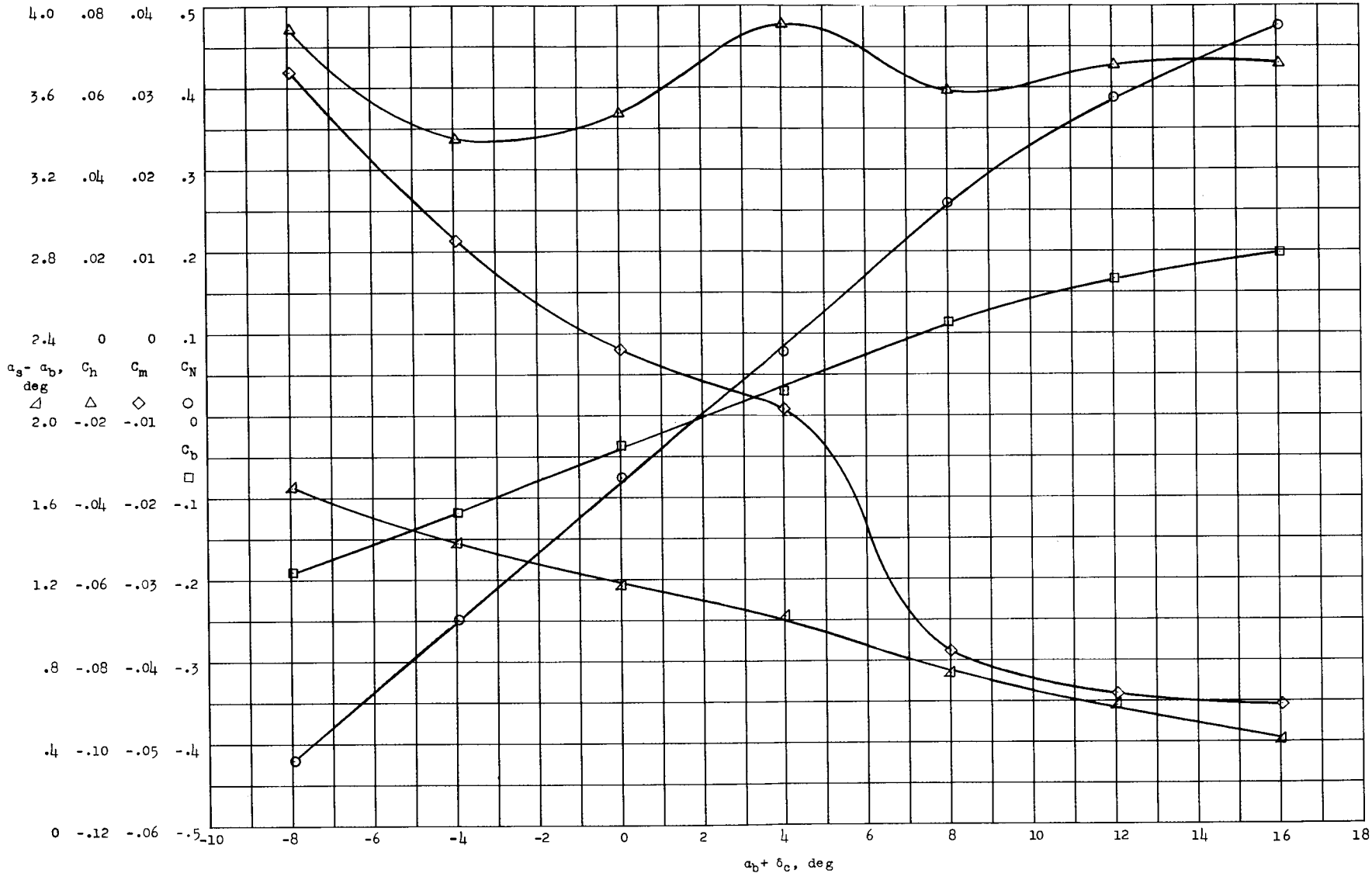

(h) $\delta_t = -8^\circ$; $\alpha_b = 0^\circ$.

Figure 21.- Continued.

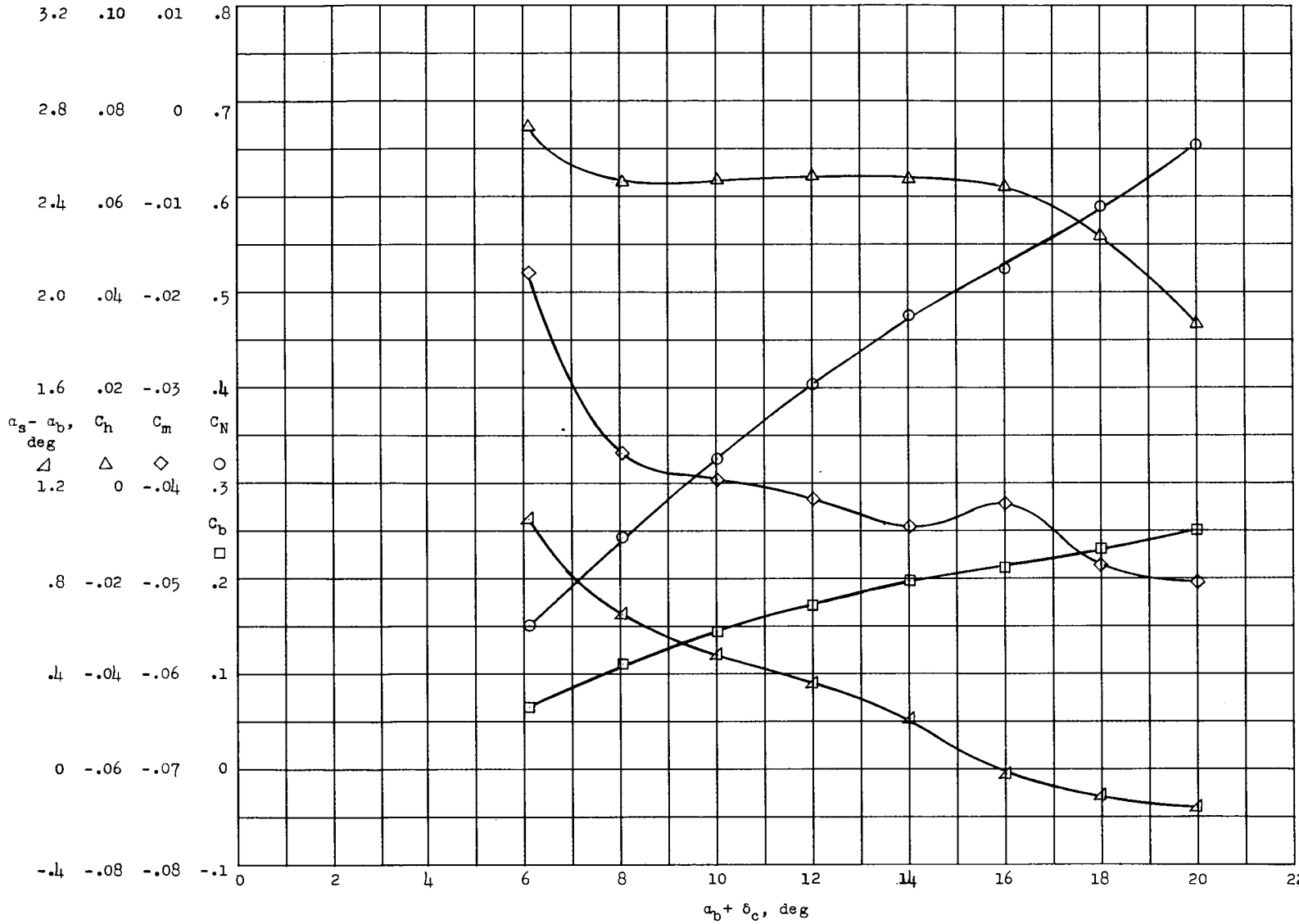

(i) $\delta_t = -8^\circ$; $\delta_c = 8^\circ$.

Figure 21.- Continued.

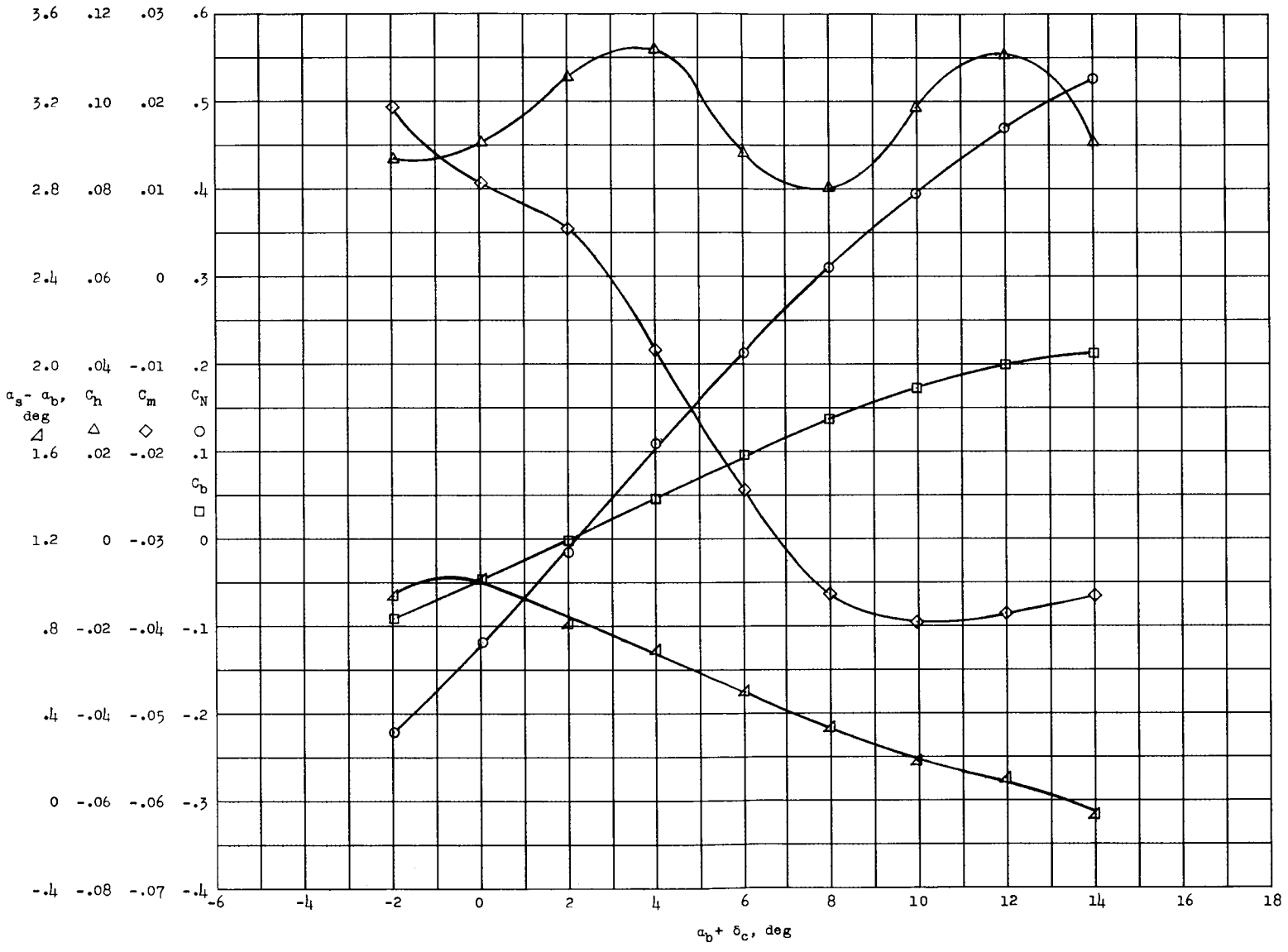

(j) $\delta_t = -12^\circ$; $\delta_c = 0^\circ$.

Figure 21.- Continued.

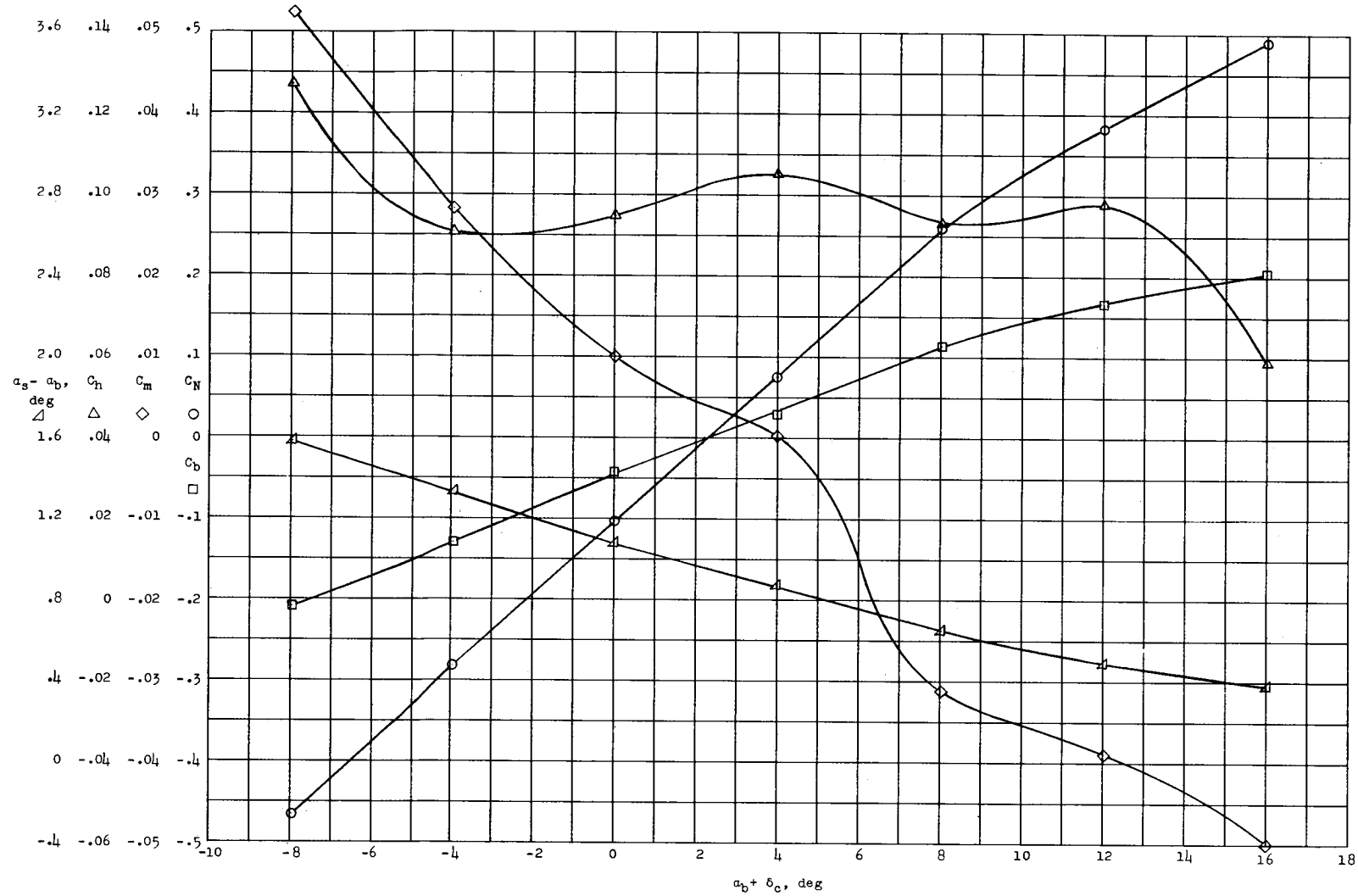

(k) $\delta_t = -12^\circ$; $\alpha_b = 0^\circ$.

Figure 21.- Continued.

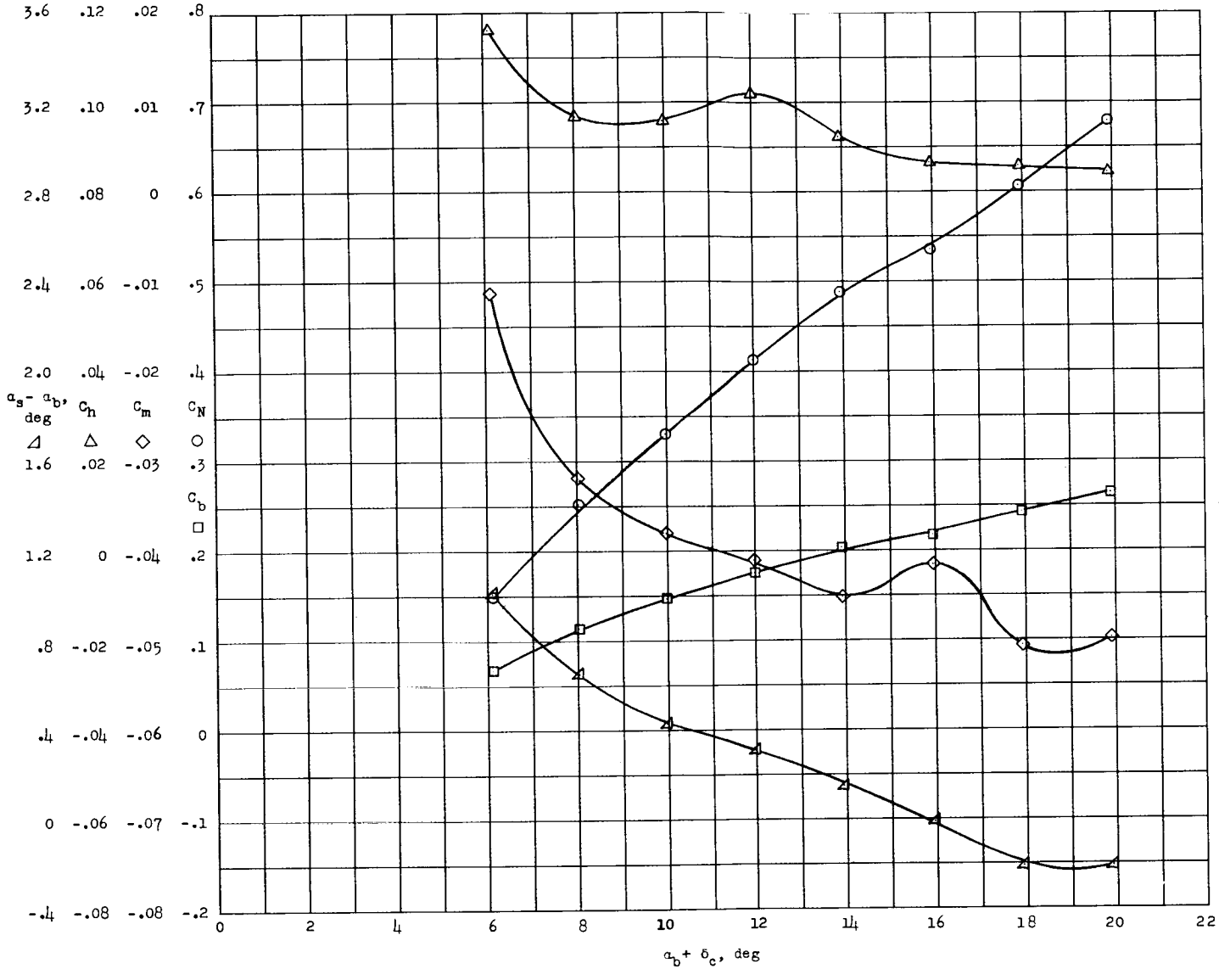

(*l*) $\delta_t = -12^\circ$; $\delta_c = 8^\circ$.

Figure 21.- Concluded.

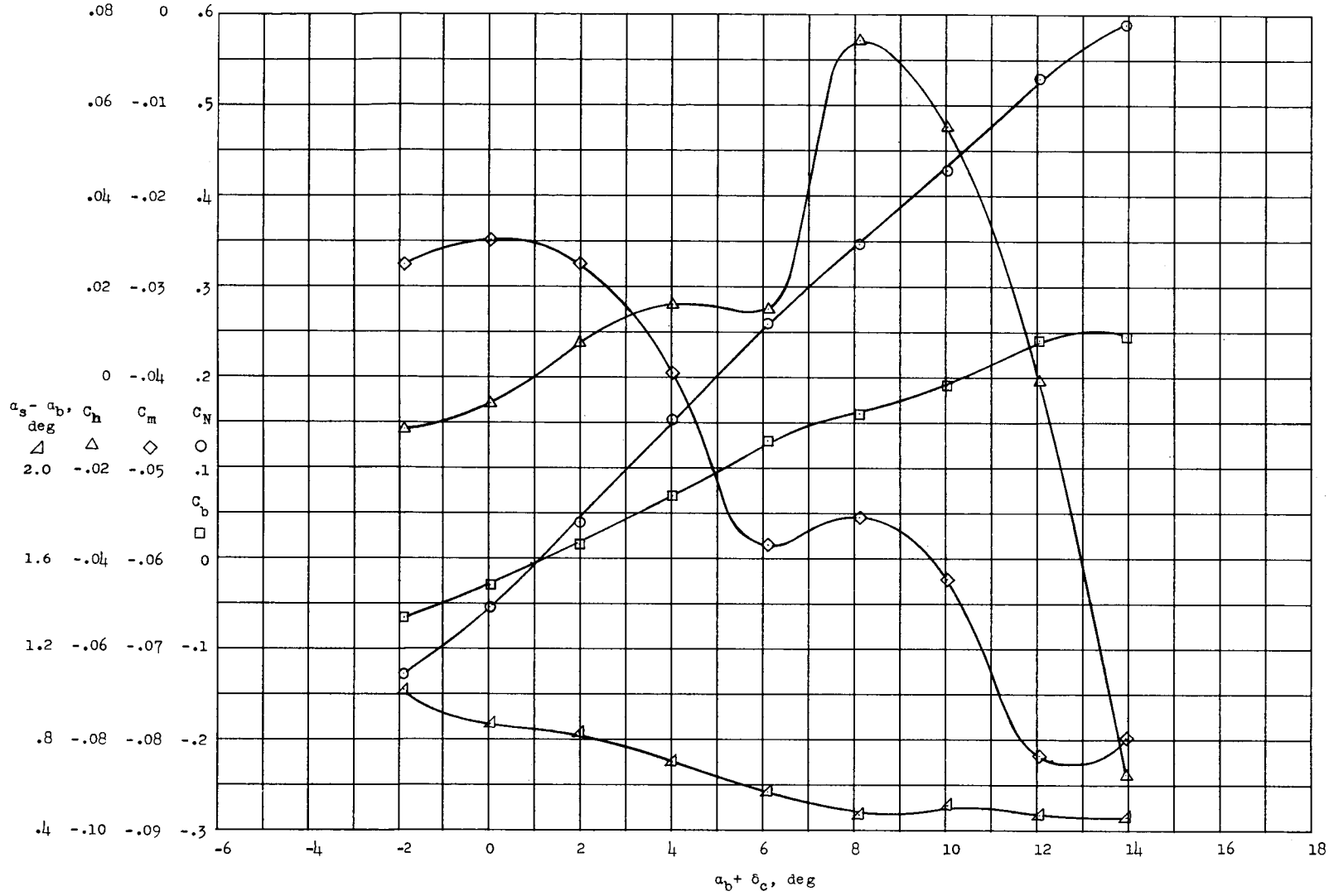

(a) $\delta_c = 0^\circ$.

Figure 22.- Longitudinal aerodynamic characteristics of restrained canard in air at M = 0.92 and q = 50 lb/sq ft with $\delta_t = 0^\circ$.

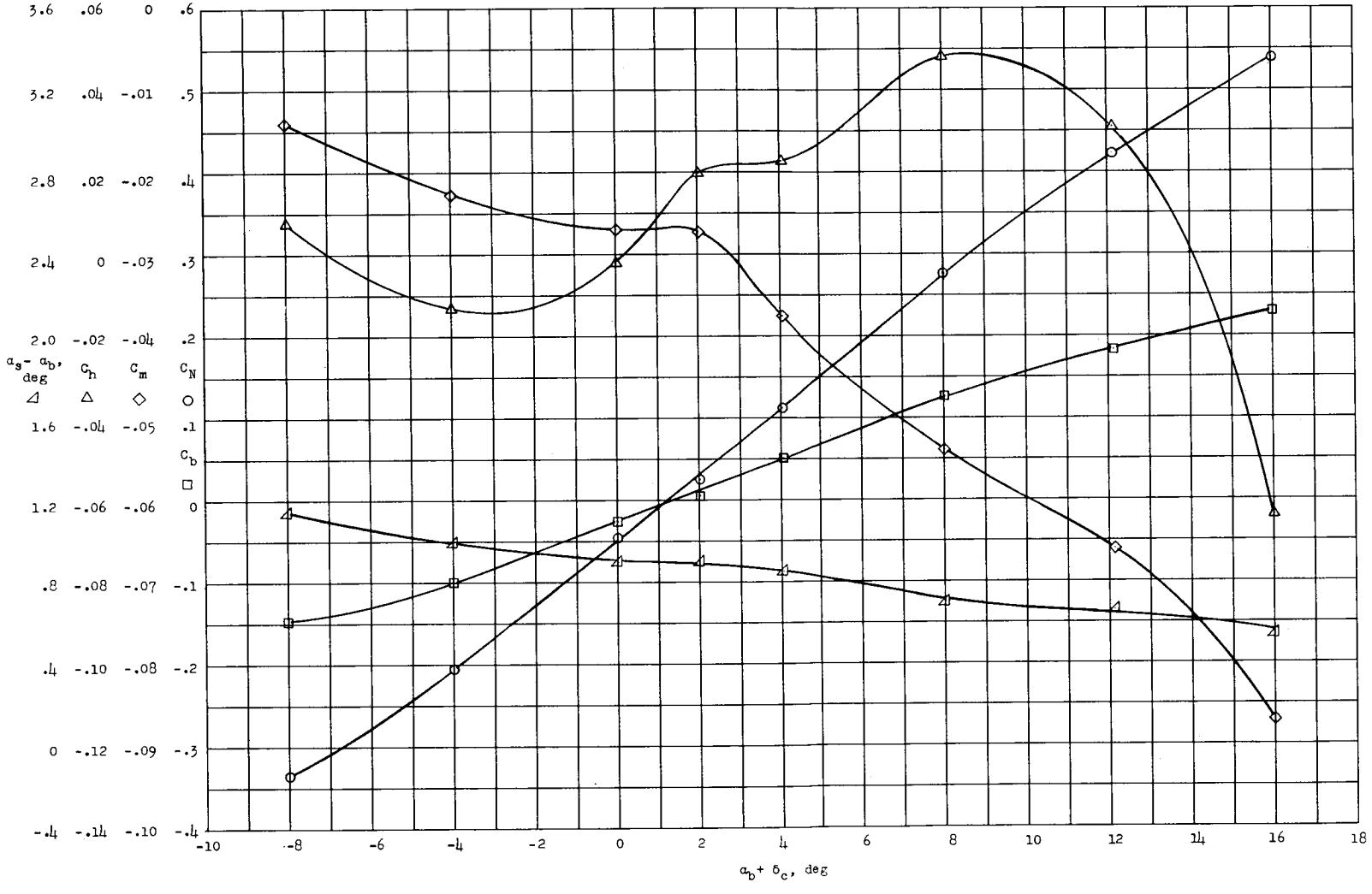

(b) $\alpha_b = 0^\circ$.

Figure 22.- Concluded.

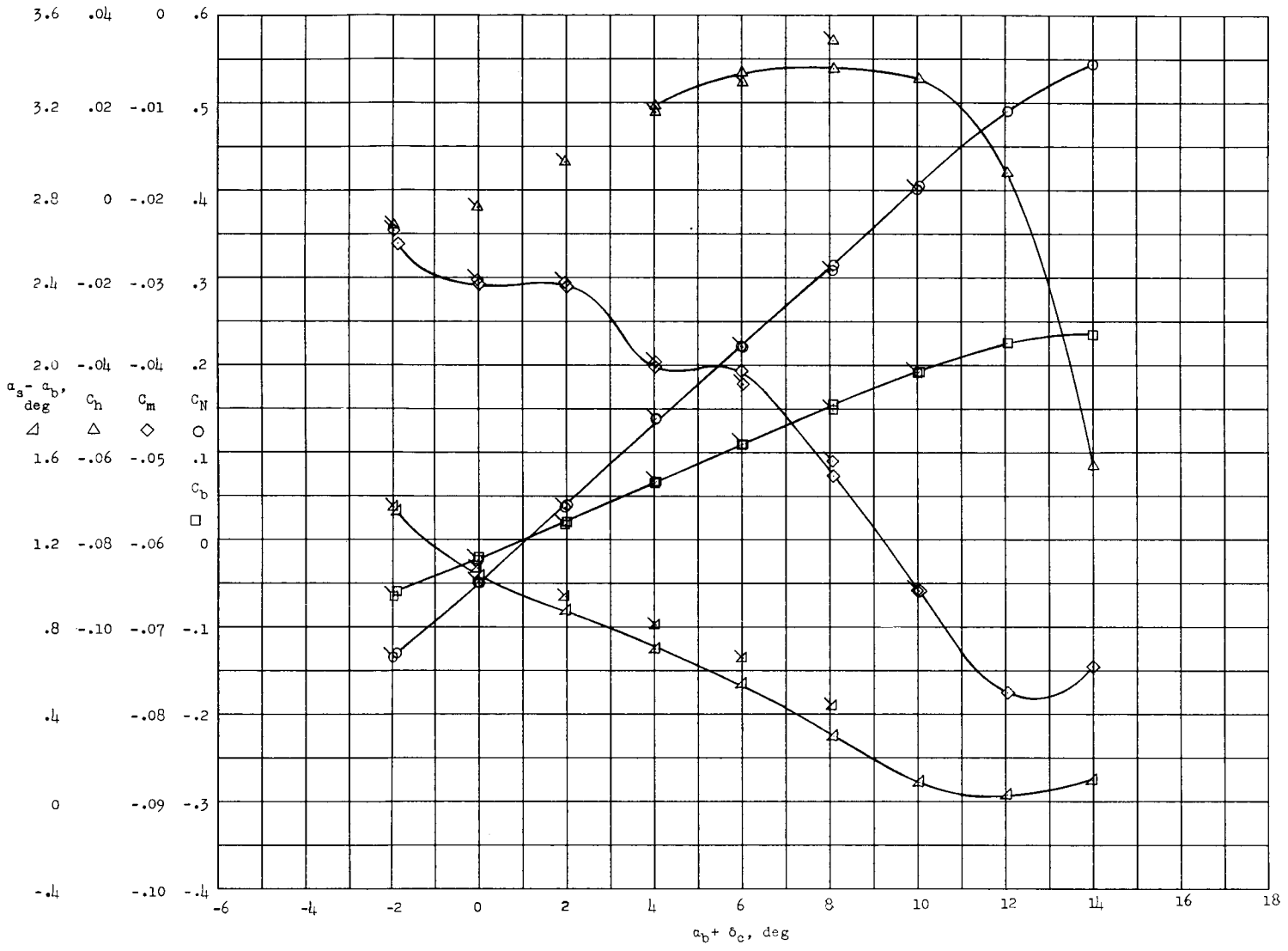

(a) $\delta_c = 0^o$.

Figure 23.- Longitudinal aerodynamic characteristics of restrained canard in air at M = 0.92 and q = 100 lb/sq ft with $\delta_t = 0^o$. Flagged symbols indicate points rerun to show repeatability.

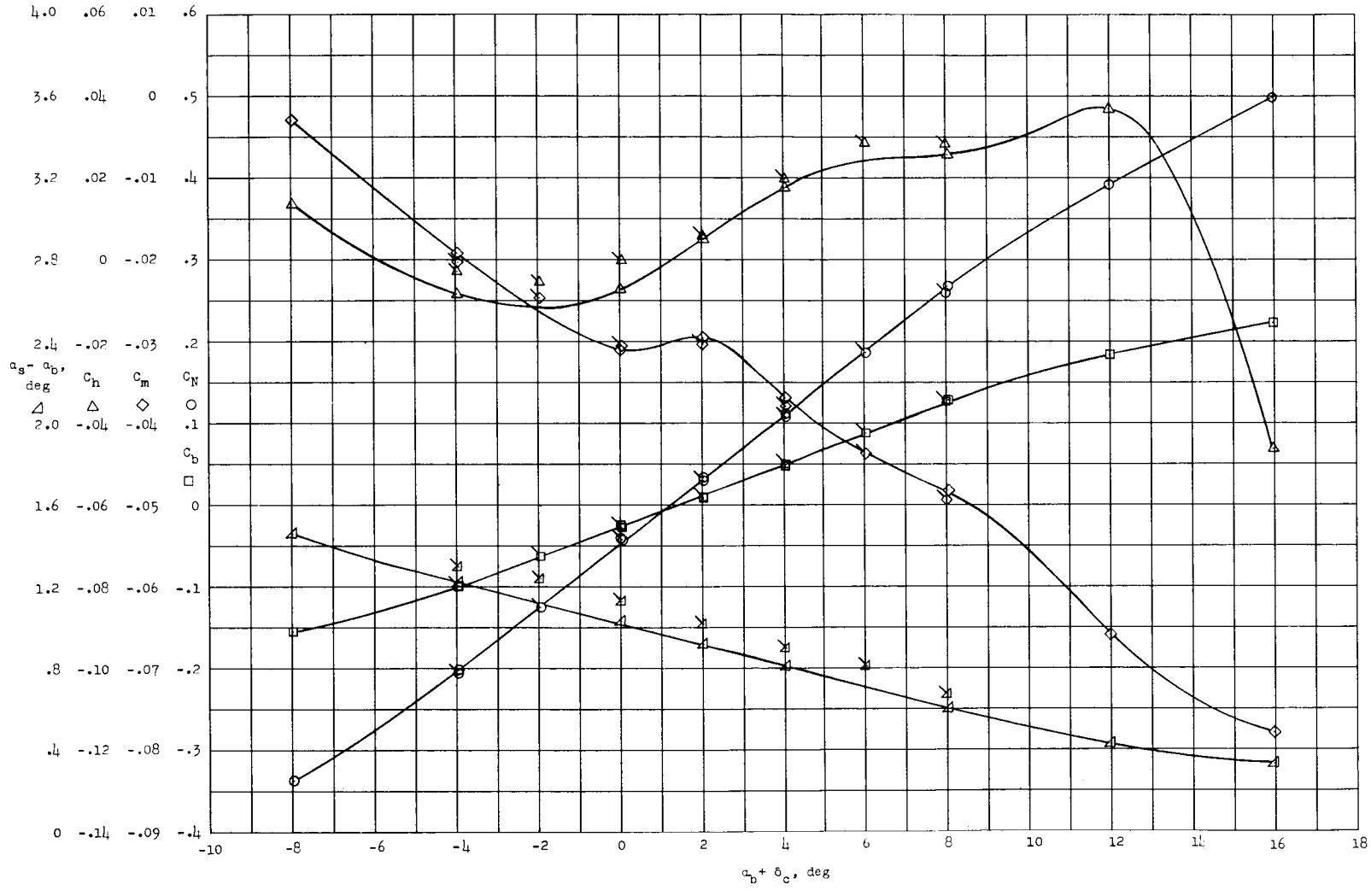

(b) $\alpha_b = 0^\circ$.

Figure 23.- Continued.

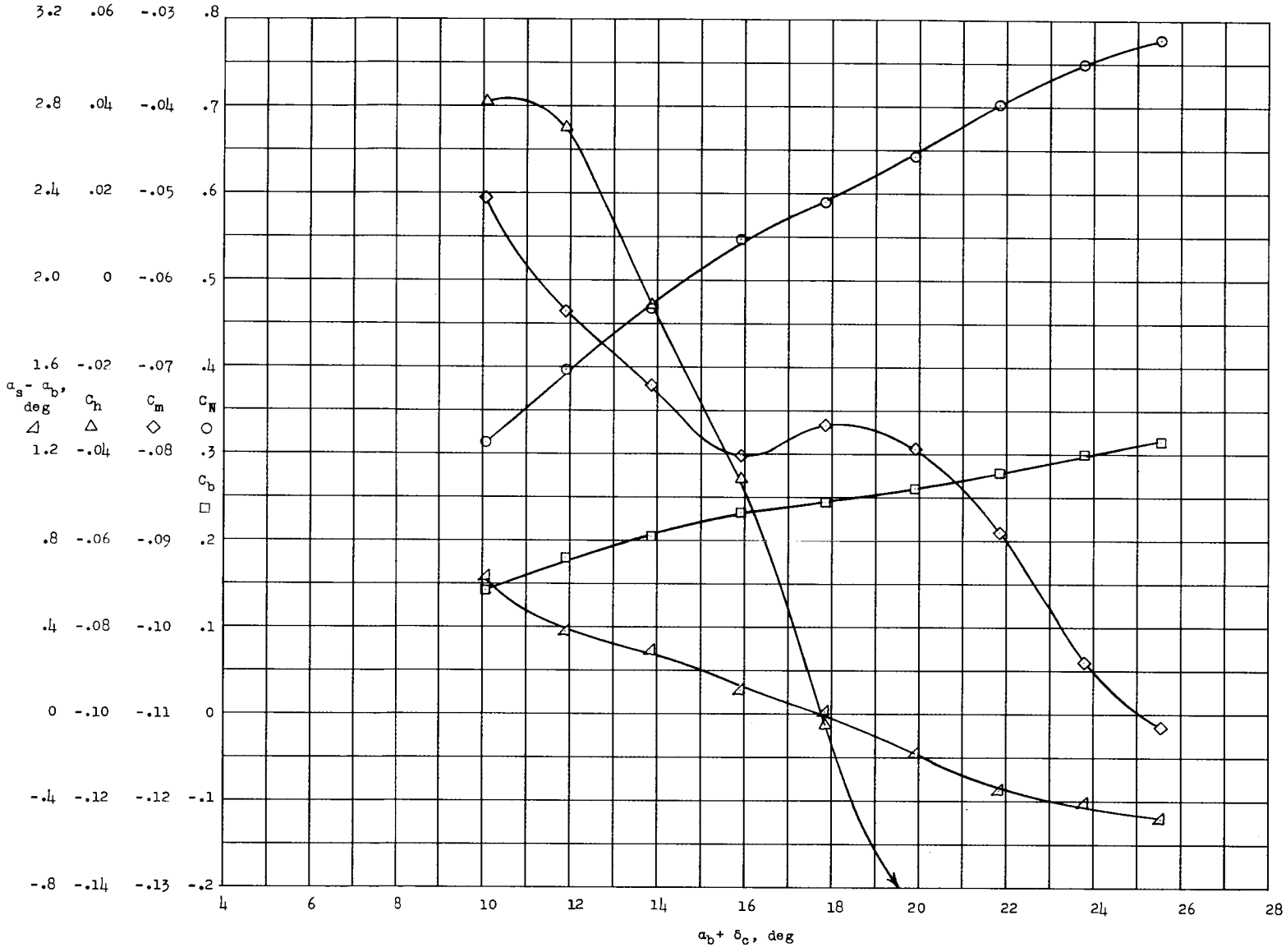

(c) $\delta_c = 12^\circ$.

Figure 23.- Concluded.

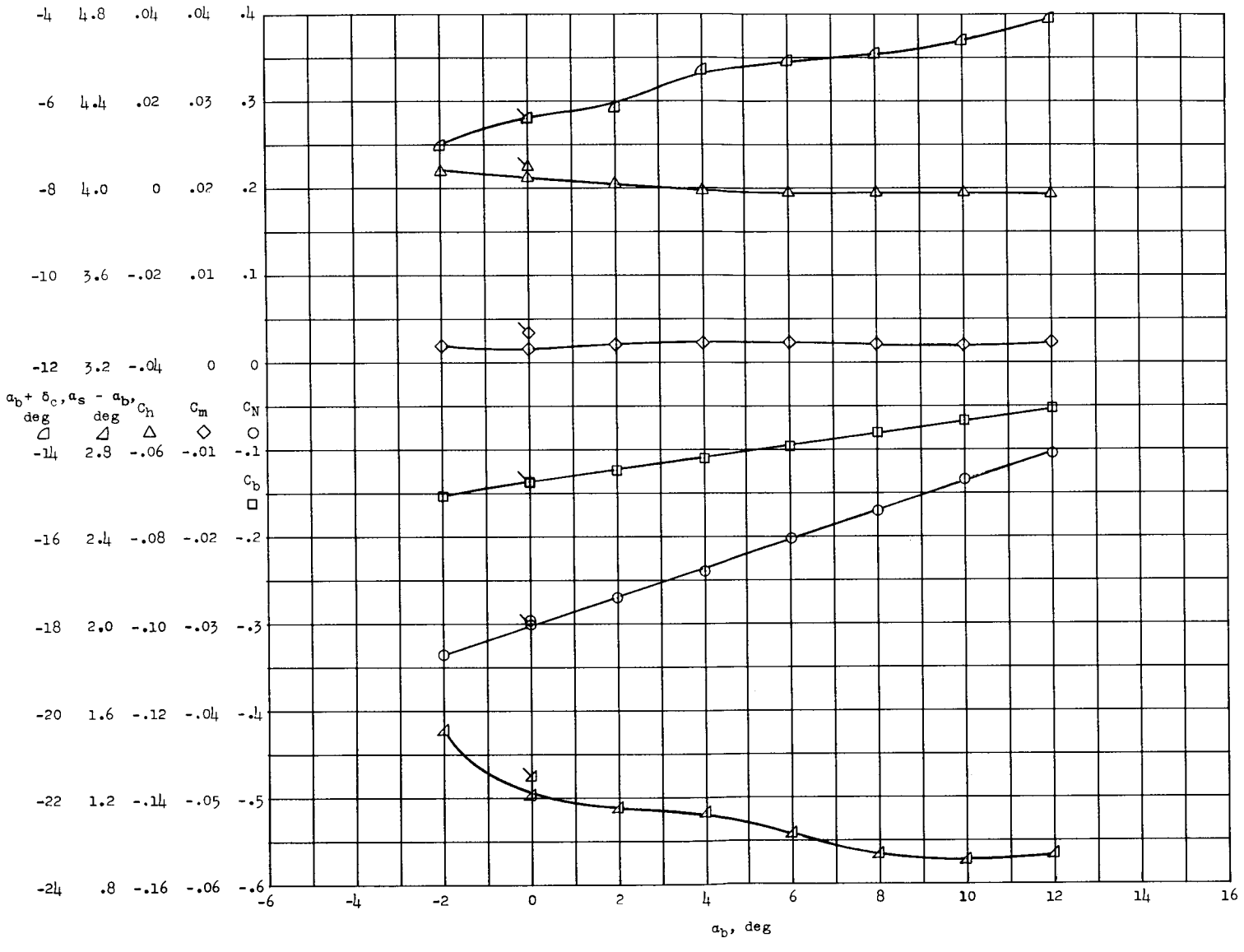

(a) $\delta_t = 0^o$. Flagged symbols indicate points reproduced from figure 13(b).

Figure 24.- Longitudinal aerodynamic characteristics of free canard in air at M = 0.60 and q = 100 lb/sq ft.

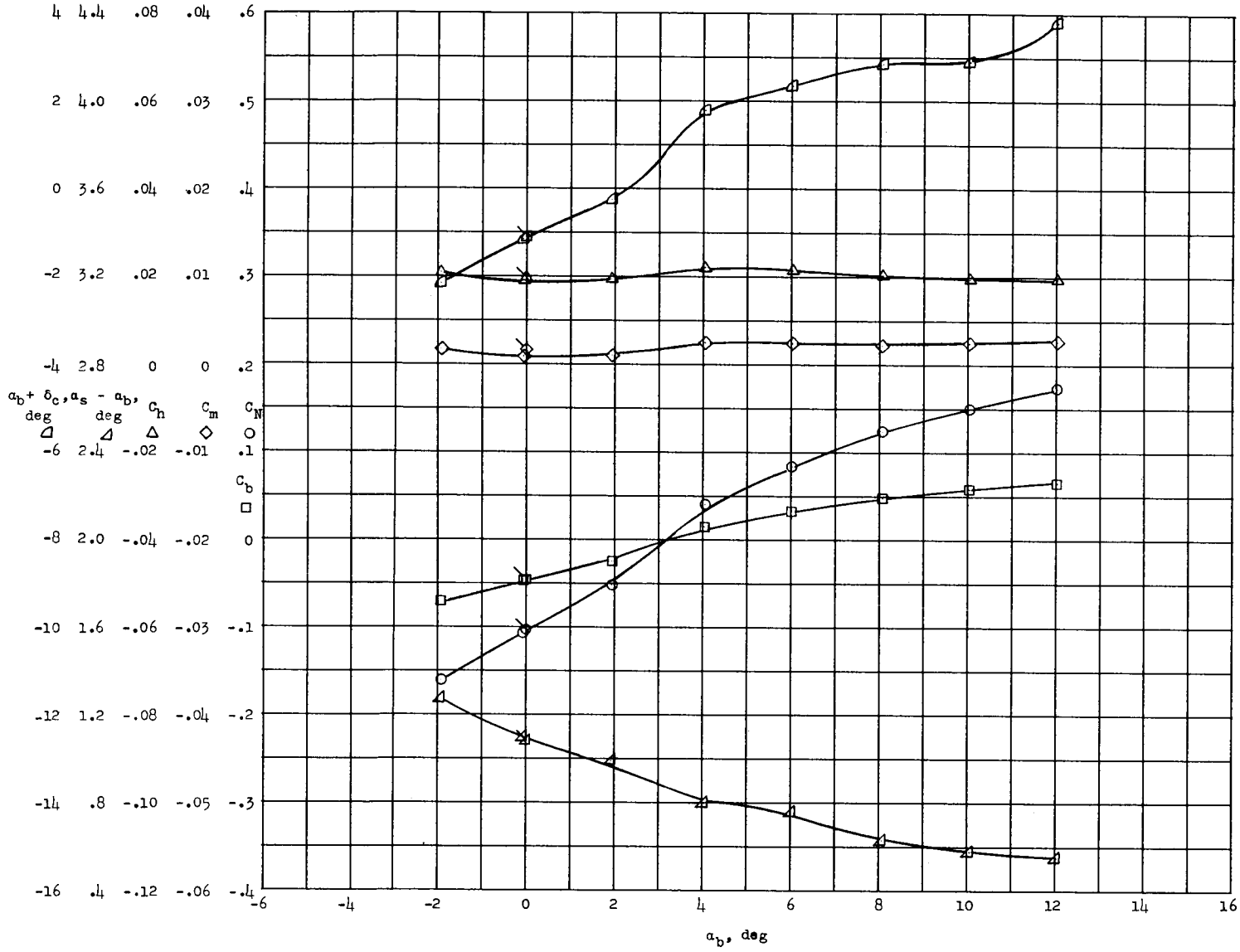

(b) $\delta_t = -4^\circ$. Flagged symbols indicate points reproduced from figure 13(e).

Figure 24.- Continued.

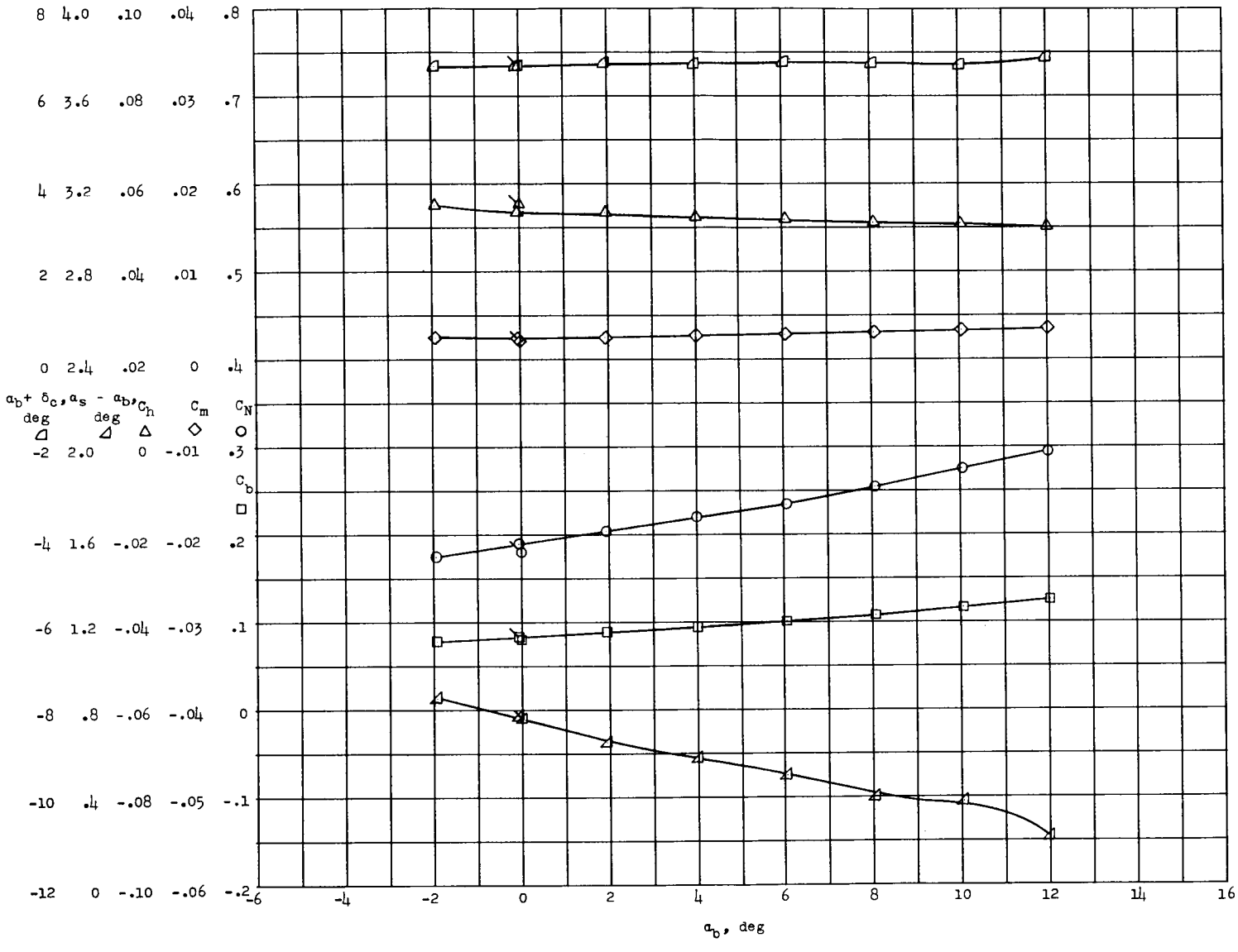

(c) $\delta_t = -8^o$. Flagged symbols indicate points reproduced from figure 13(h).

Figure 24.- Continued.

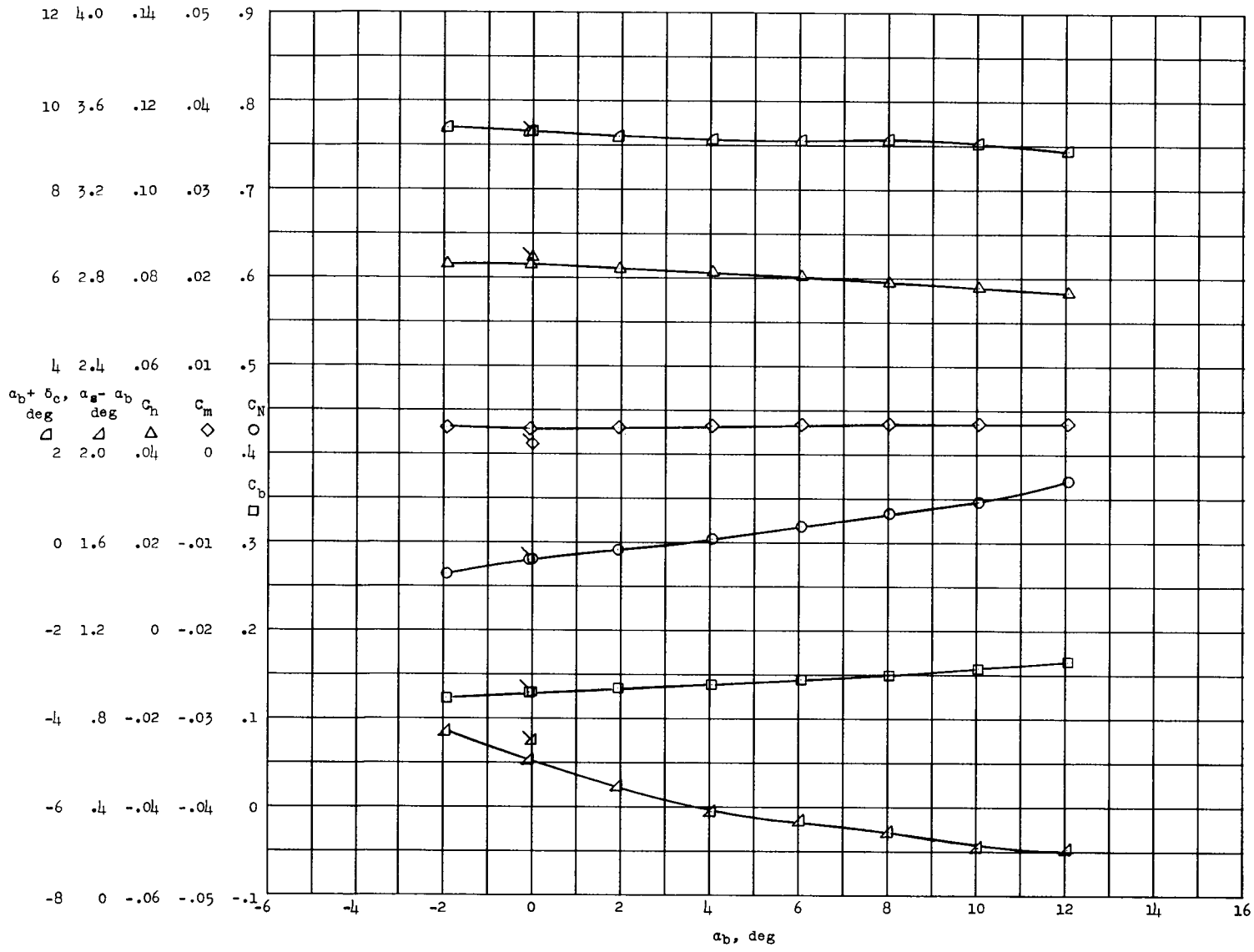

(d) $\delta_t = -12^\circ$. Flagged symbols indicate points reproduced from figure 13(k).

Figure 24.- Concluded.

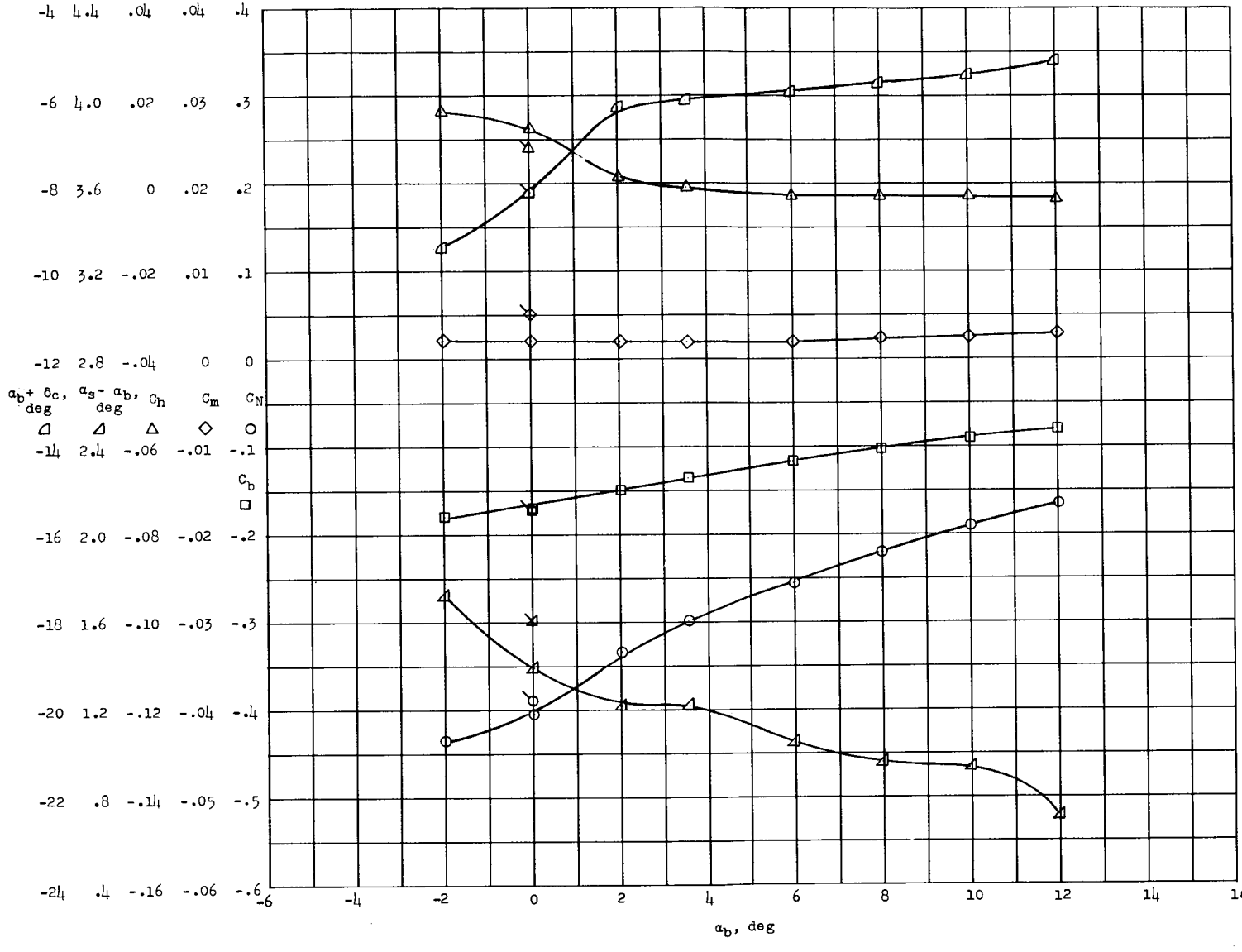

(a) $\delta_t = 0^\circ$. Flagged symbols indicate points reproduced from figure 17(b).

Figure 25.- Longitudinal aerodynamic characteristics of free canard in air at M = 0.80 and q = 100 lb/sq ft.

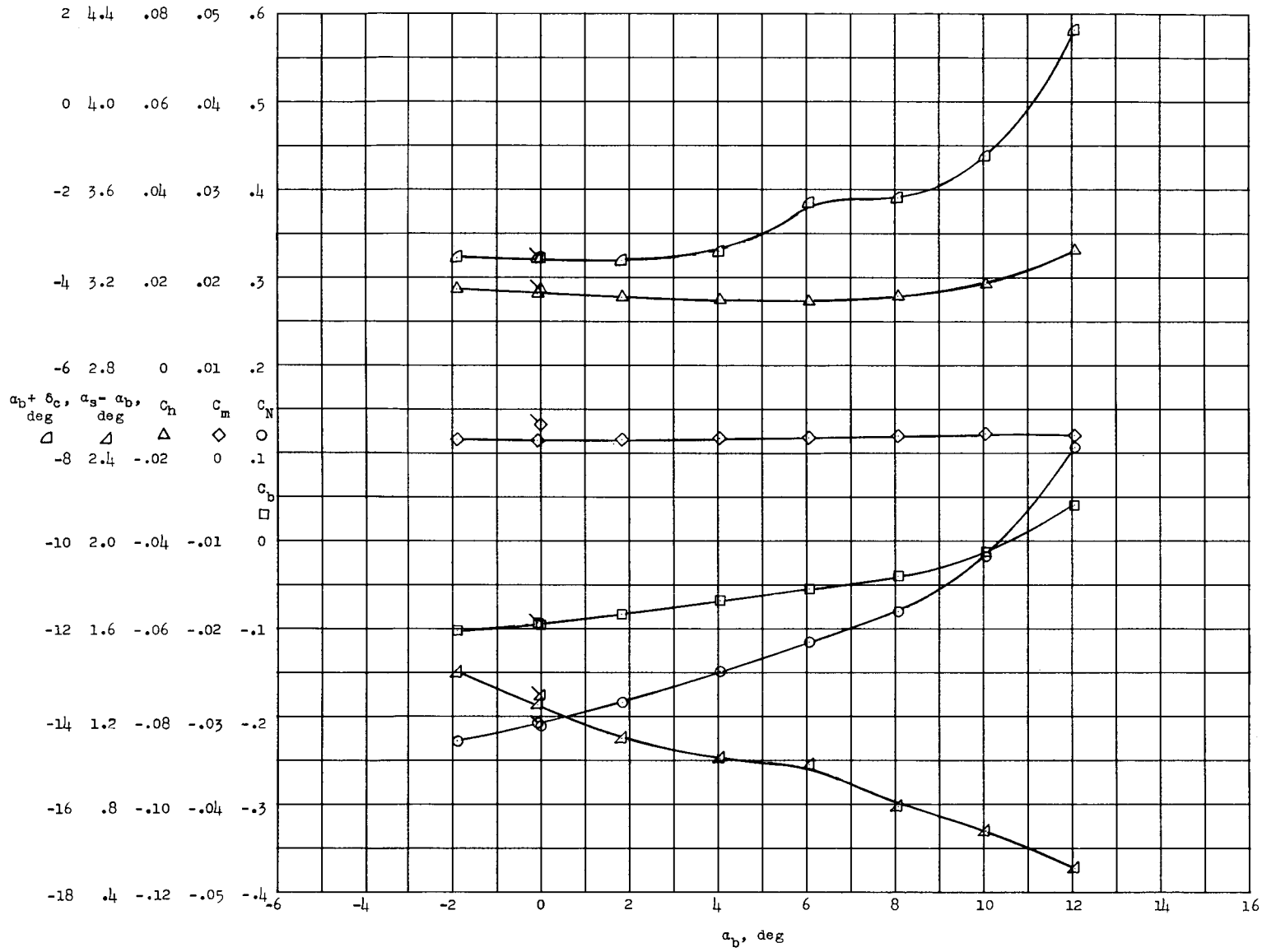

(b) $\delta_t = -4^\circ$. Flagged symbols indicate points reproduced from figure 17(e).

Figure 25.- Continued.

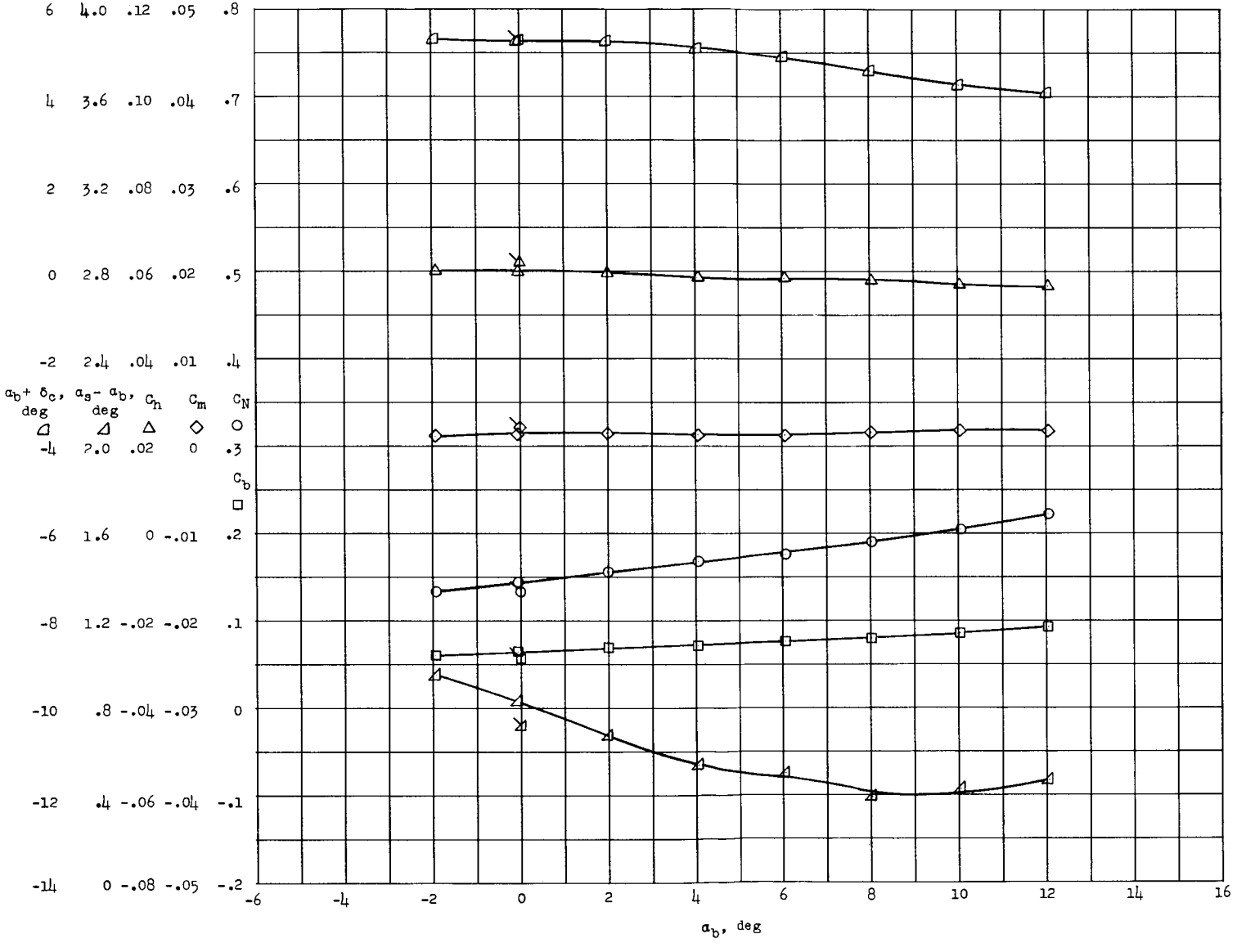

(c) $\delta_t = -8^\circ$. Flagged symbols indicate points reproduced from figure 17(h).

Figure 25.- Continued.

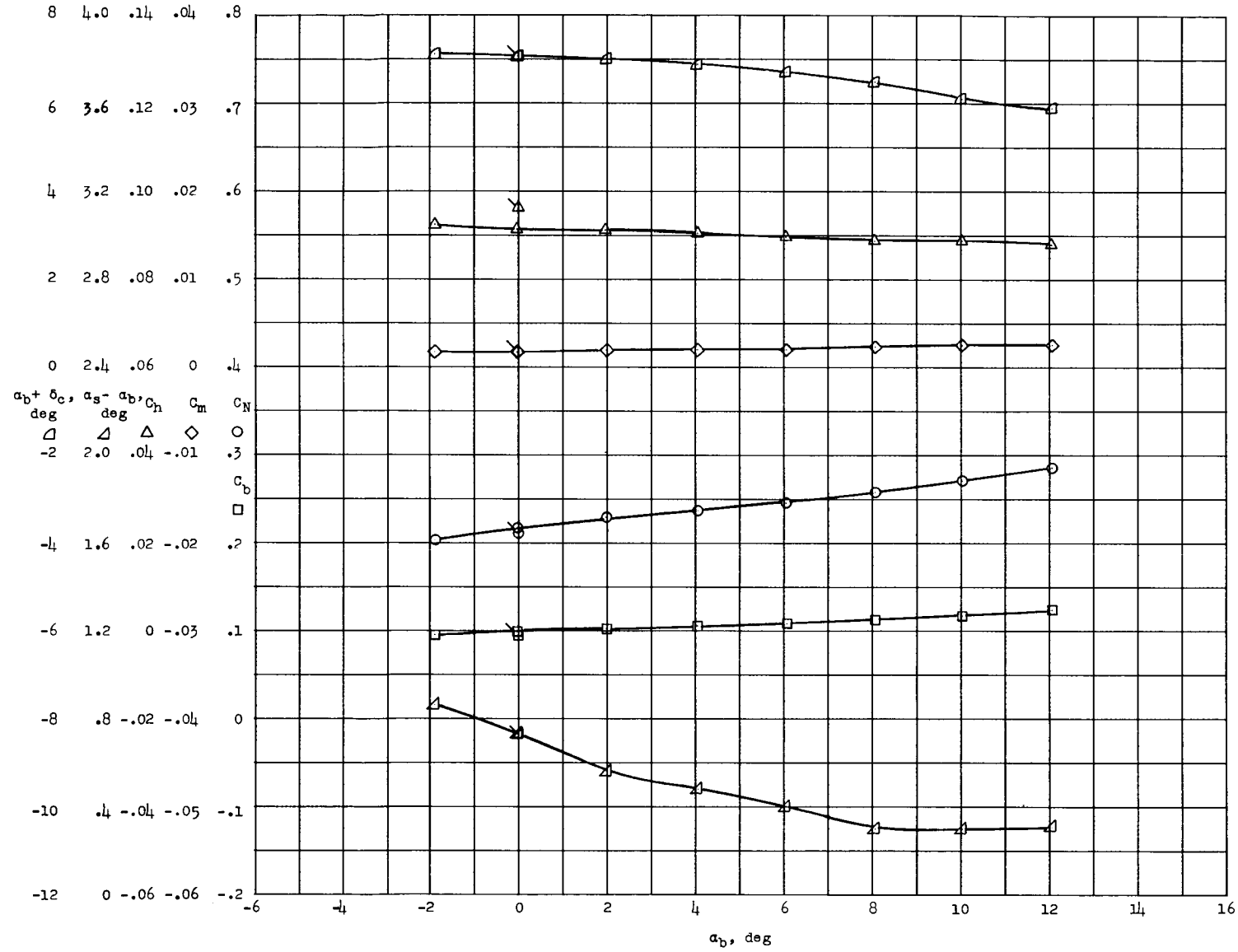

(d) $\delta_t = -12^\circ$. Flagged symbols indicate points reproduced from figure 17(k).

Figure 25.- Concluded.

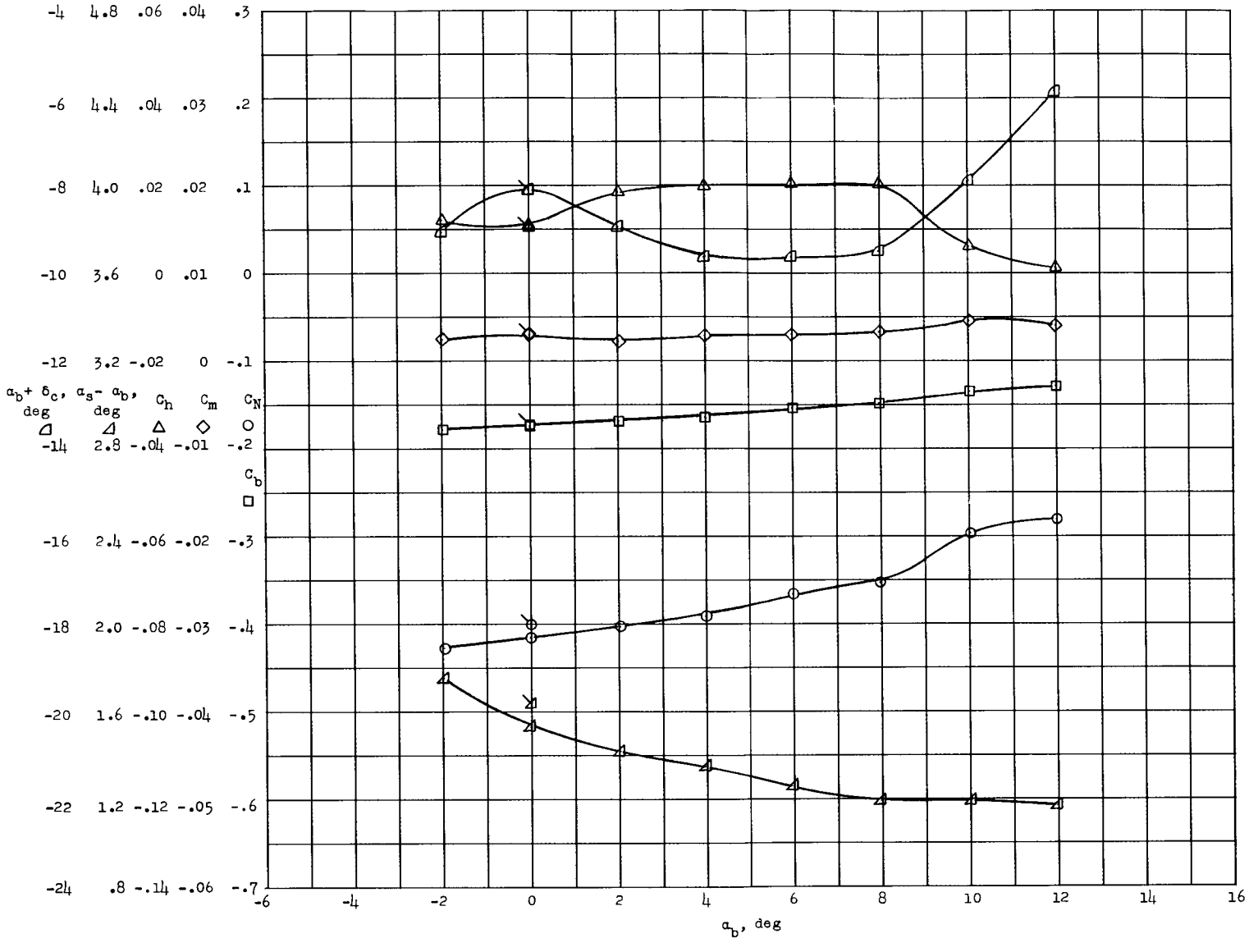

(a) $\delta_t = 0^o$. Flagged symbols indicate points reproduced from figure 21(b).

Figure 26.- Longitudinal aerodynamic characteristics of free canard in air at M = 0.90 and q = 100 lb/sq ft.

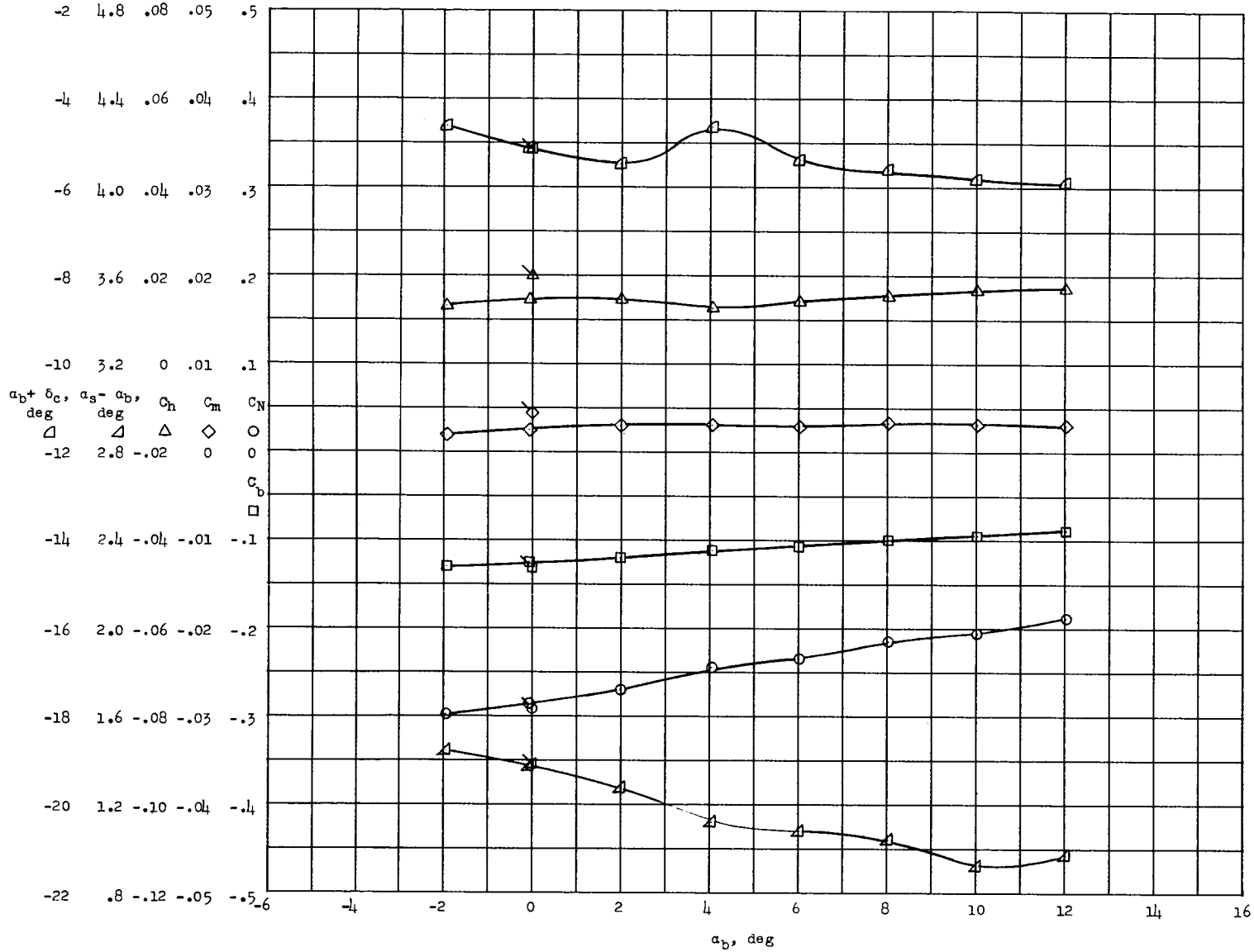

(b) $\delta_t = -4^o$. Flagged symbols indicate points reproduced from figure 21(e).

Figure 26.- Continued.

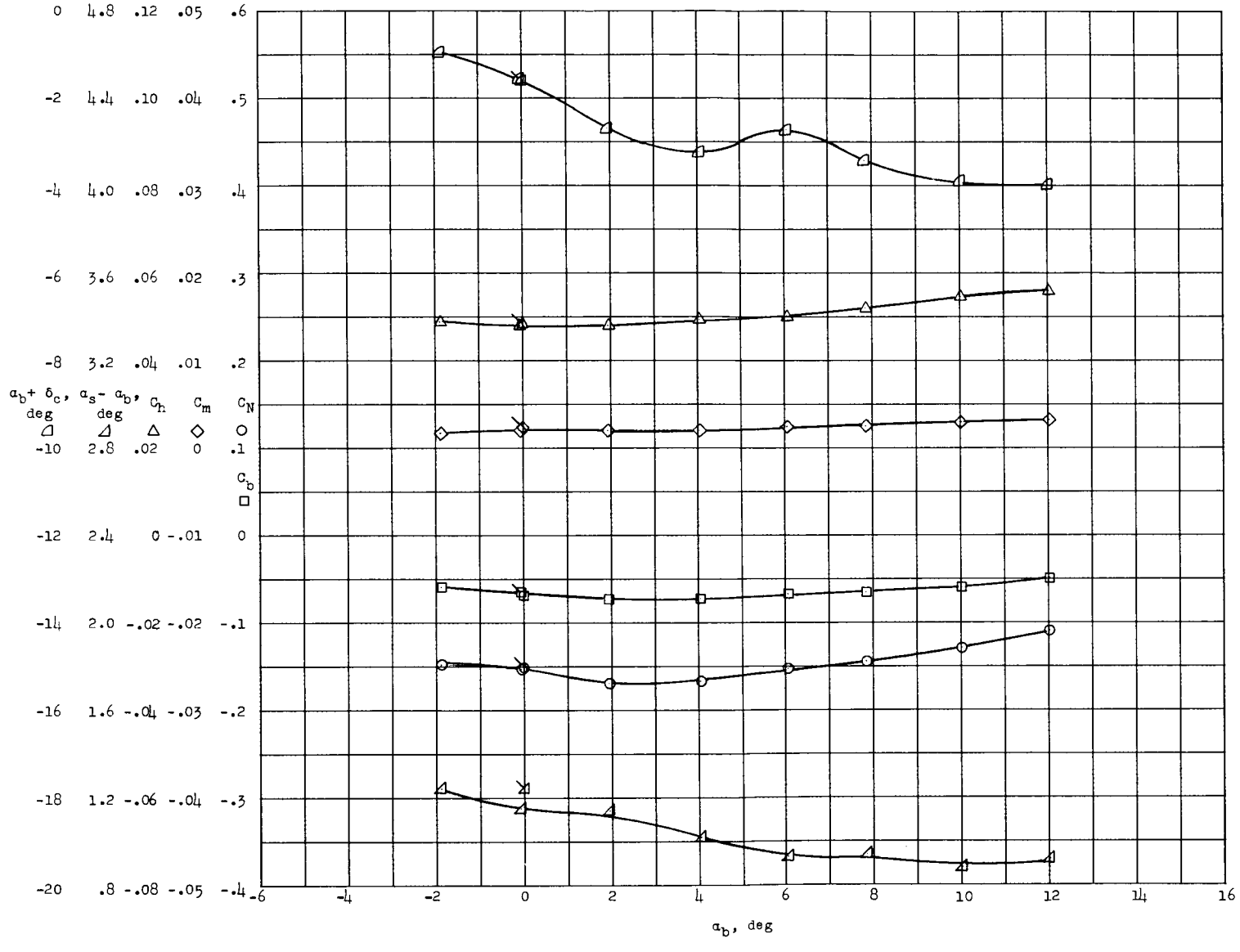

(c) $\delta_t = -8^\circ$. Flagged symbols indicate points reproduced from figure 21(h).

Figure 26.- Continued.

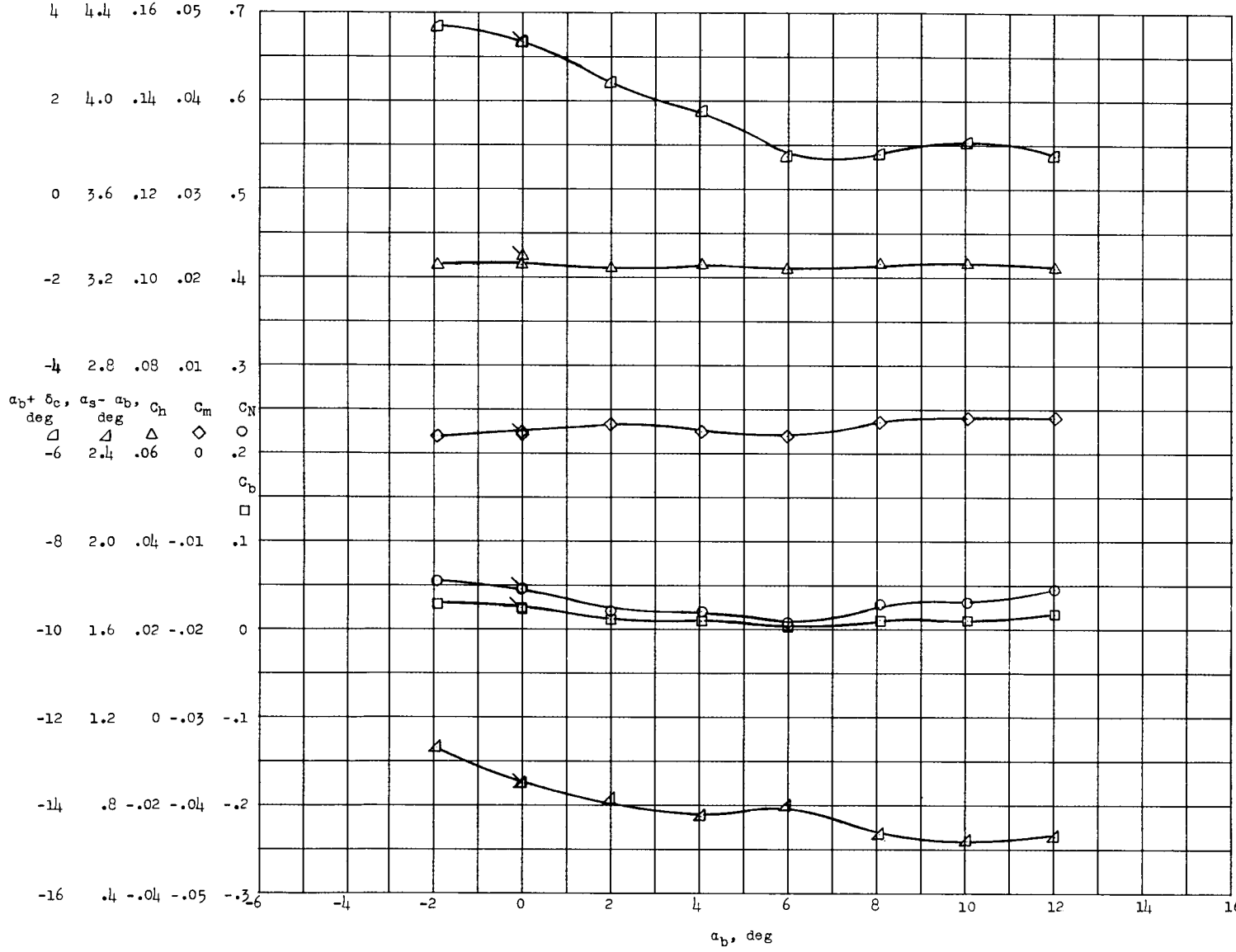

(d) $\delta_t = -12^\circ$. Flagged symbols indicate points reproduced from figure 21(k).

Figure 26.- Concluded.

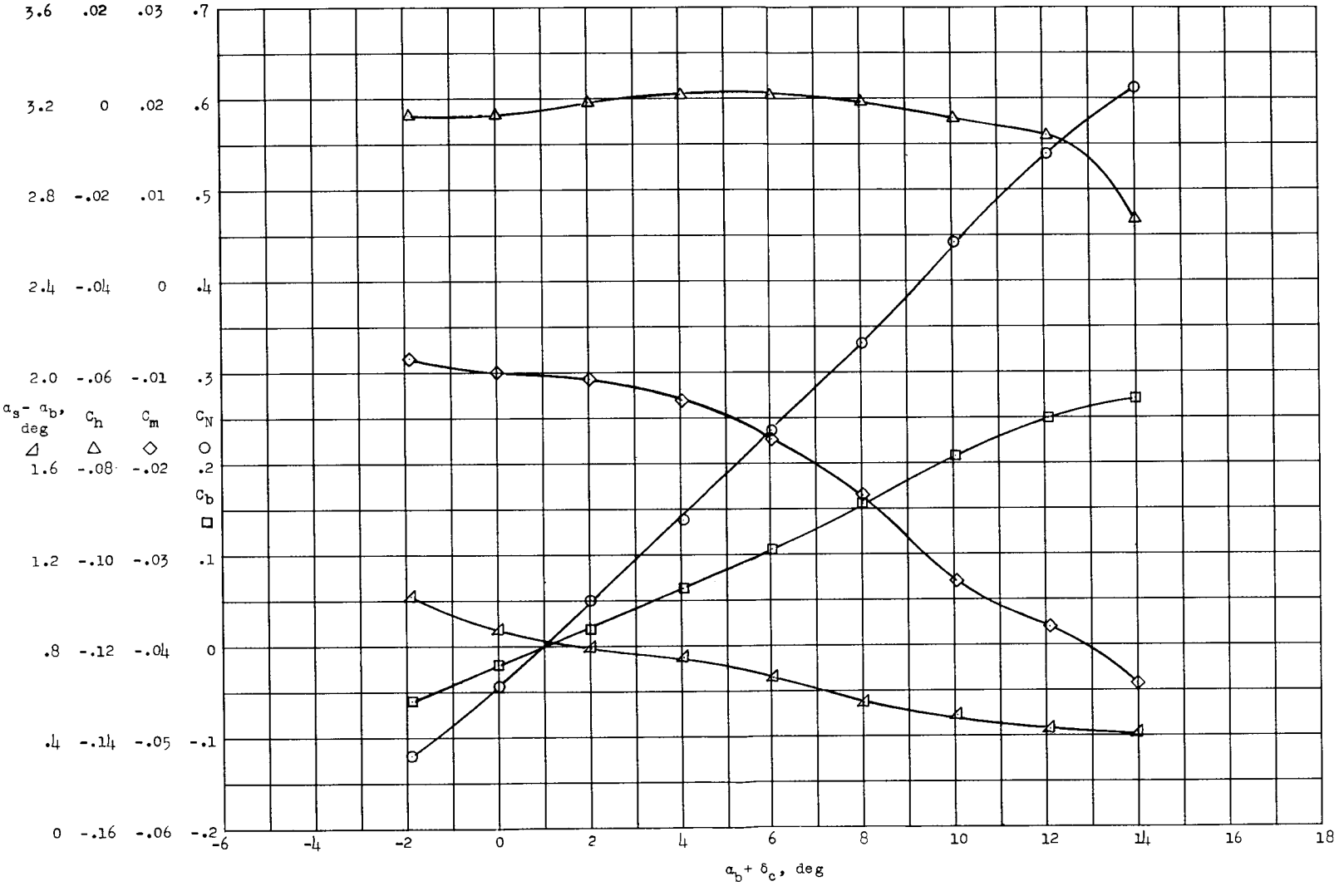

Figure 27.- Longitudinal aerodynamic characteristics of restrained canard in Freon-12 at M = 0.60 and q = 50 lb/sq ft with $\delta_t = 0^o$ and $\delta_c = 0^o$.

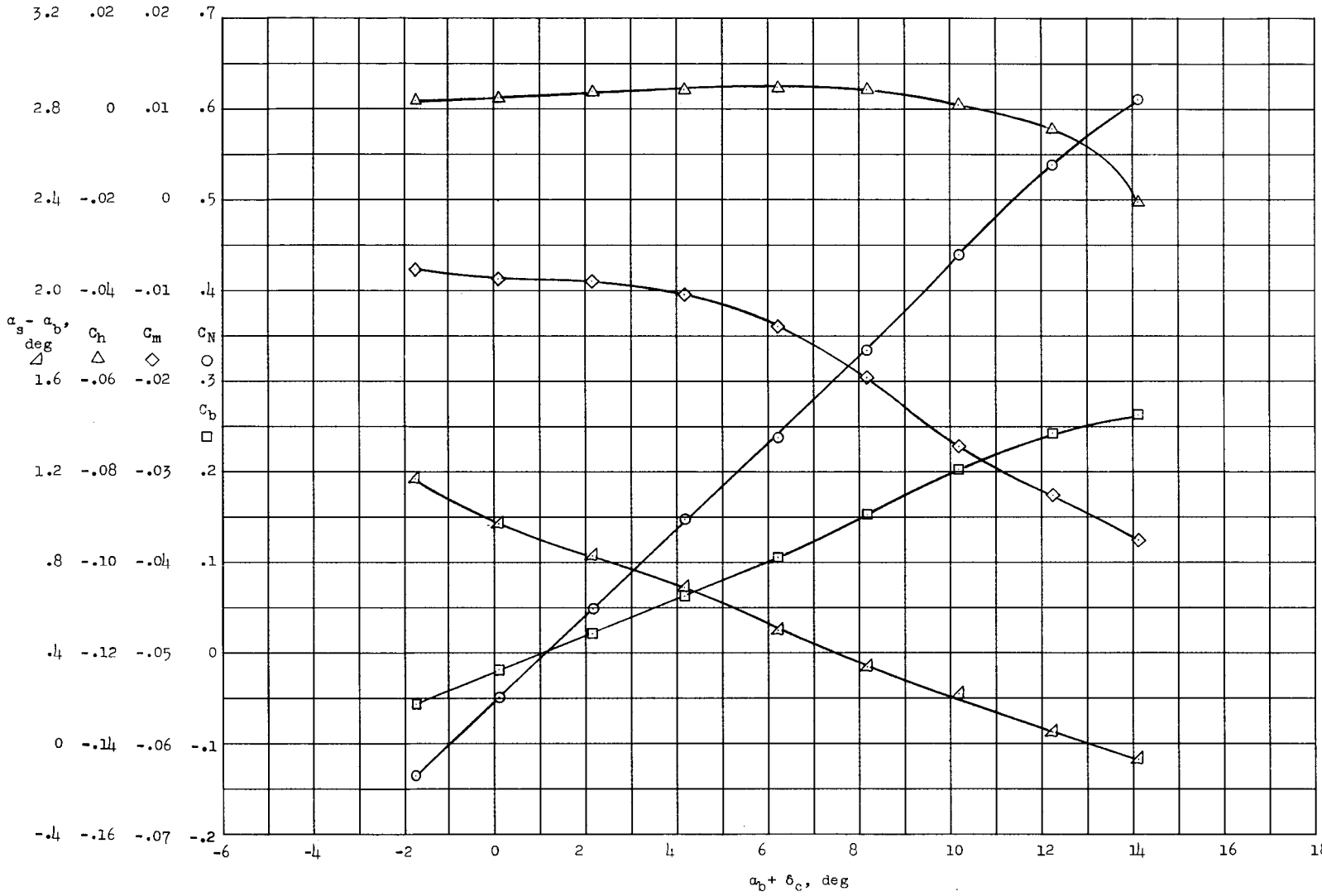

(a) $\delta_c = 0^\circ$.

Figure 28.- Longitudinal aerodynamic characteristics of restrained canard in Freon-12 at M = 0.60 and q = 100 lb/sq ft with $\delta_t = 0^\circ$.

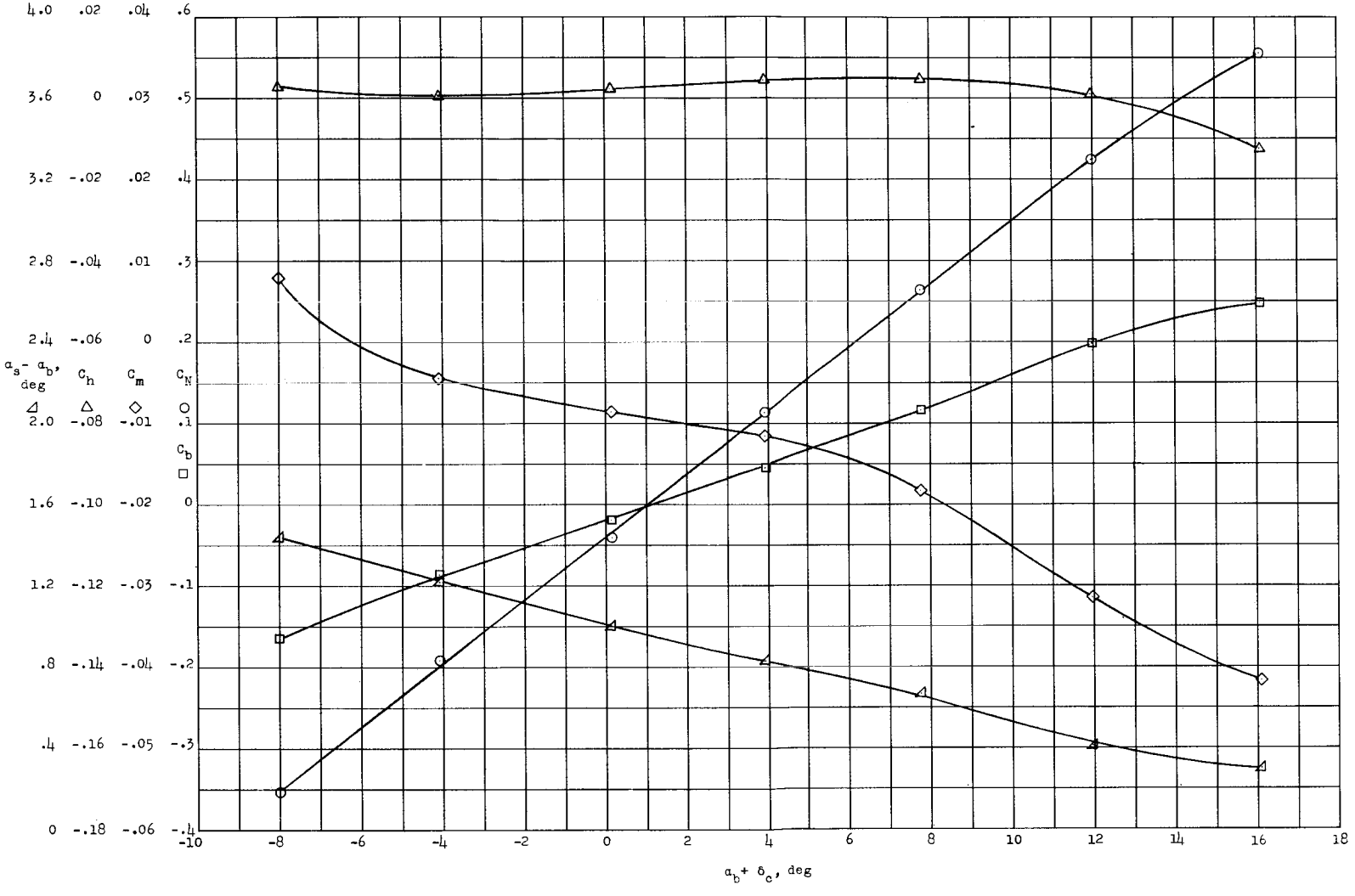

(b) $\alpha_b = 0^\circ$.

Figure 28.- Concluded.

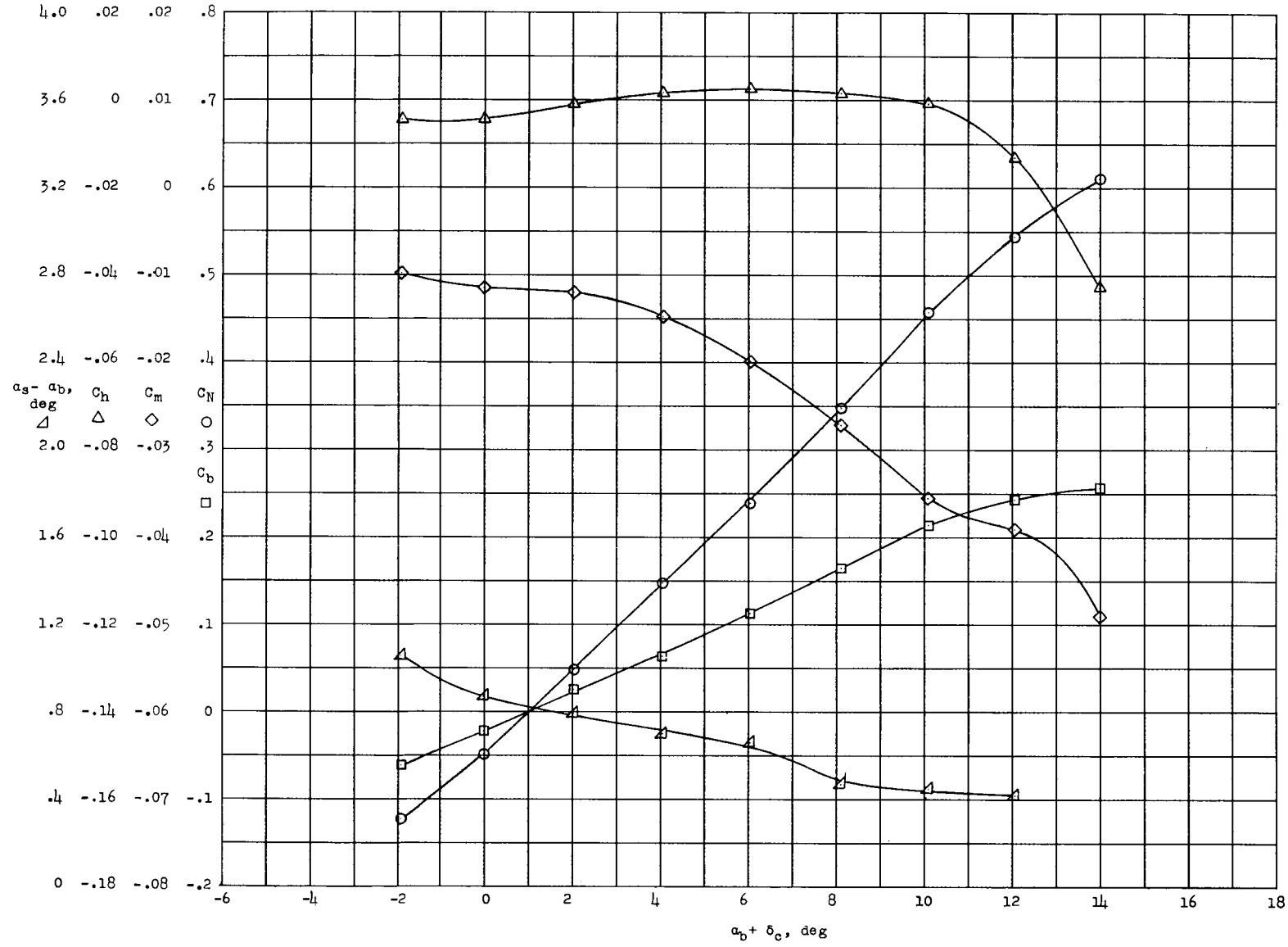

(a) $\delta_c = 0^\circ$.

Figure 29.- Longitudinal aerodynamic characteristics of restrained canard in Freon-12 at M = 0.70 and q = 50 lb/sq ft with $\delta_t = 0^\circ$.

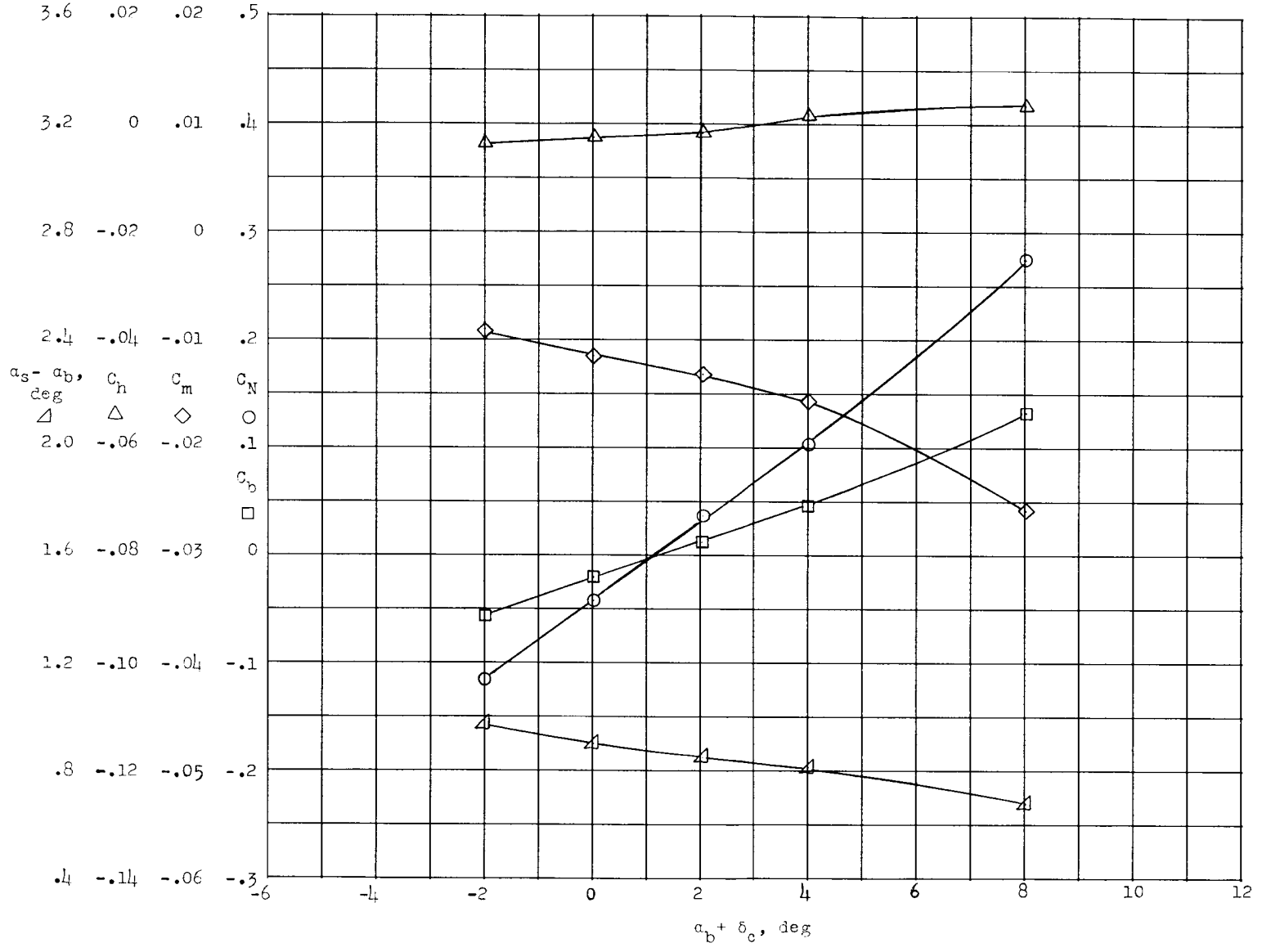

(b) $\alpha_b = 0^\circ$.

Figure 29.- Concluded.

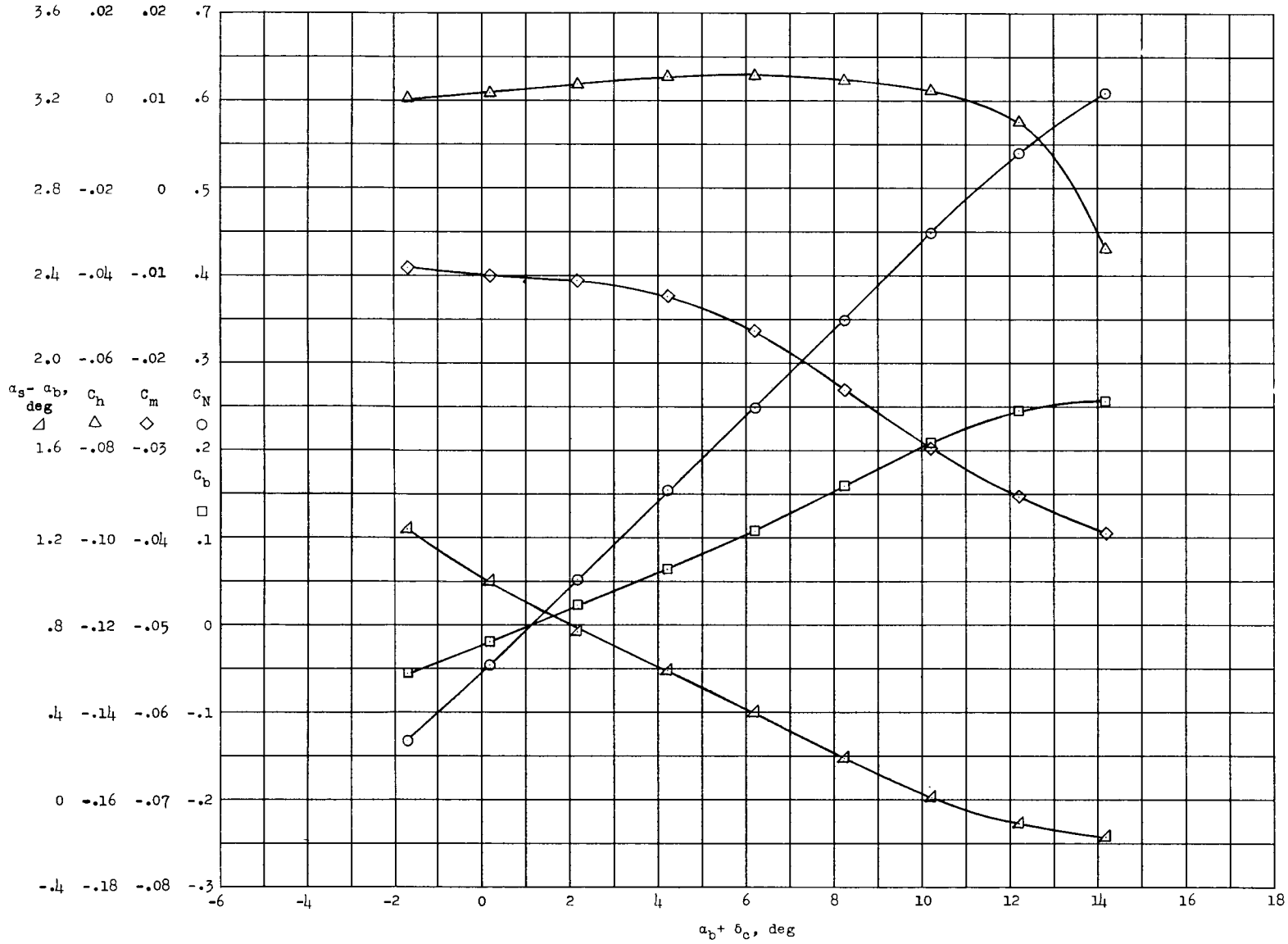

(a) $\delta_c = 0^\circ$.

Figure 30.- Longitudinal aerodynamic characteristics of restrained canard in Freon-12 at M = 0.70 and q = 100 lb/sq ft with $\delta_t = 0^\circ$.

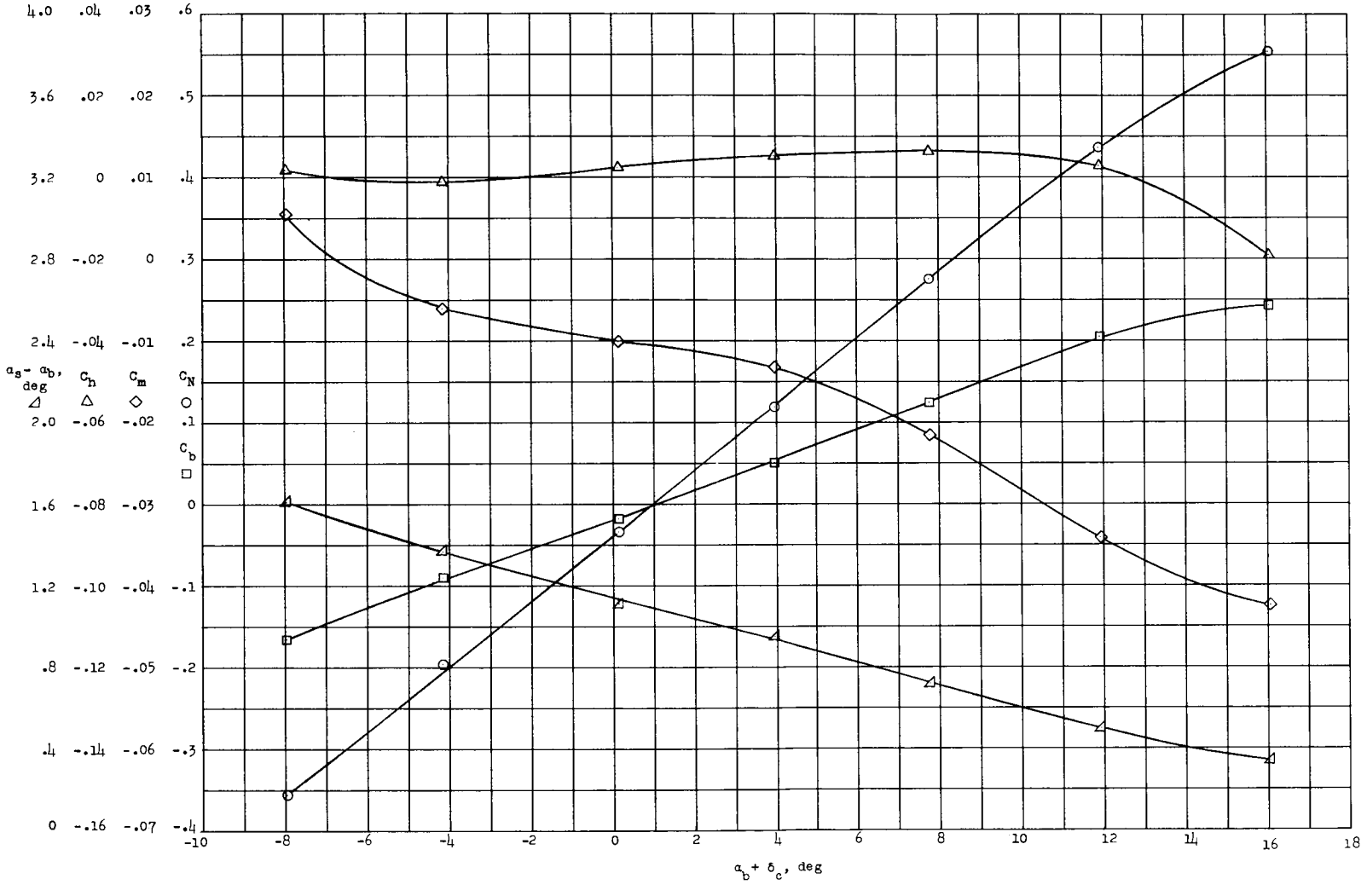

(b) $\alpha_b = 0^\circ$.

Figure 30.- Concluded.

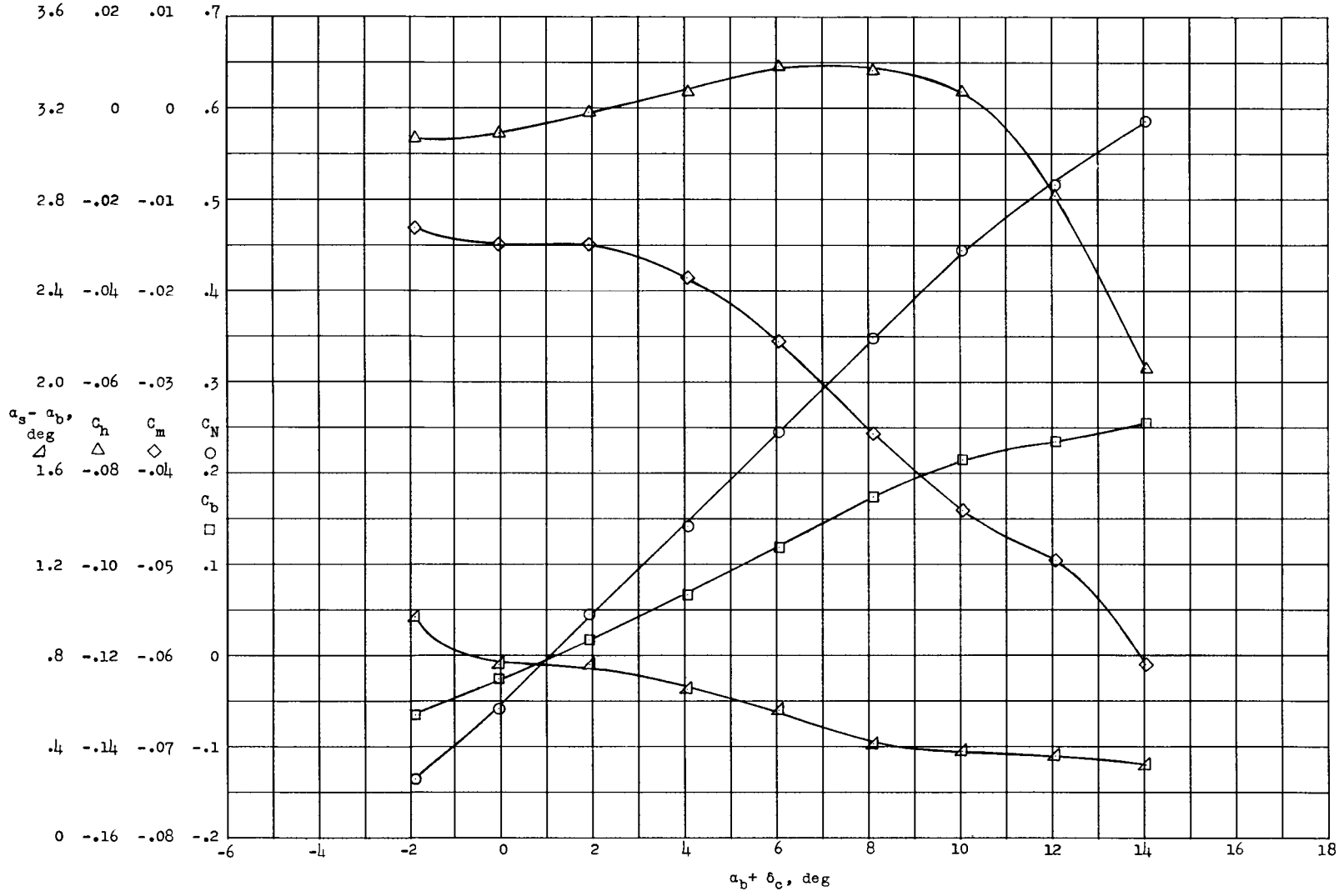

Figure 31.- Longitudinal aerodynamic characteristics of restrained canard in Freon-12 at M = 0.80 and q = 50 lb/sq ft with $\delta_t = 0^\circ$ and $\delta_c = 0^\circ$.

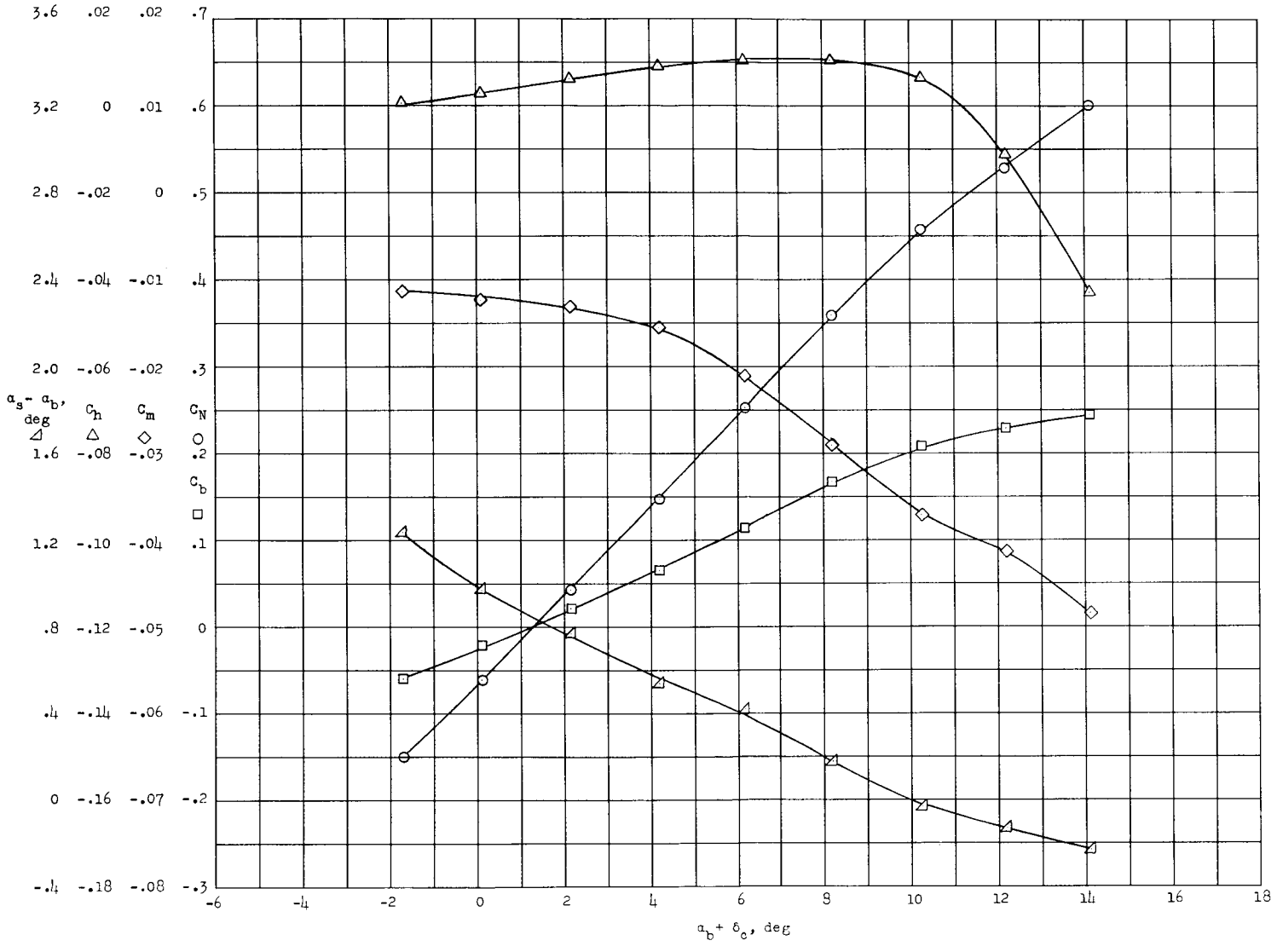

(a) $\delta_c = 0^o$.

Figure 32.- Longitudinal aerodynamic characteristics of restrained canard in Freon-12 at M = 0.80 and q = 100 lb/sq ft with $\delta_t = 0^o$.

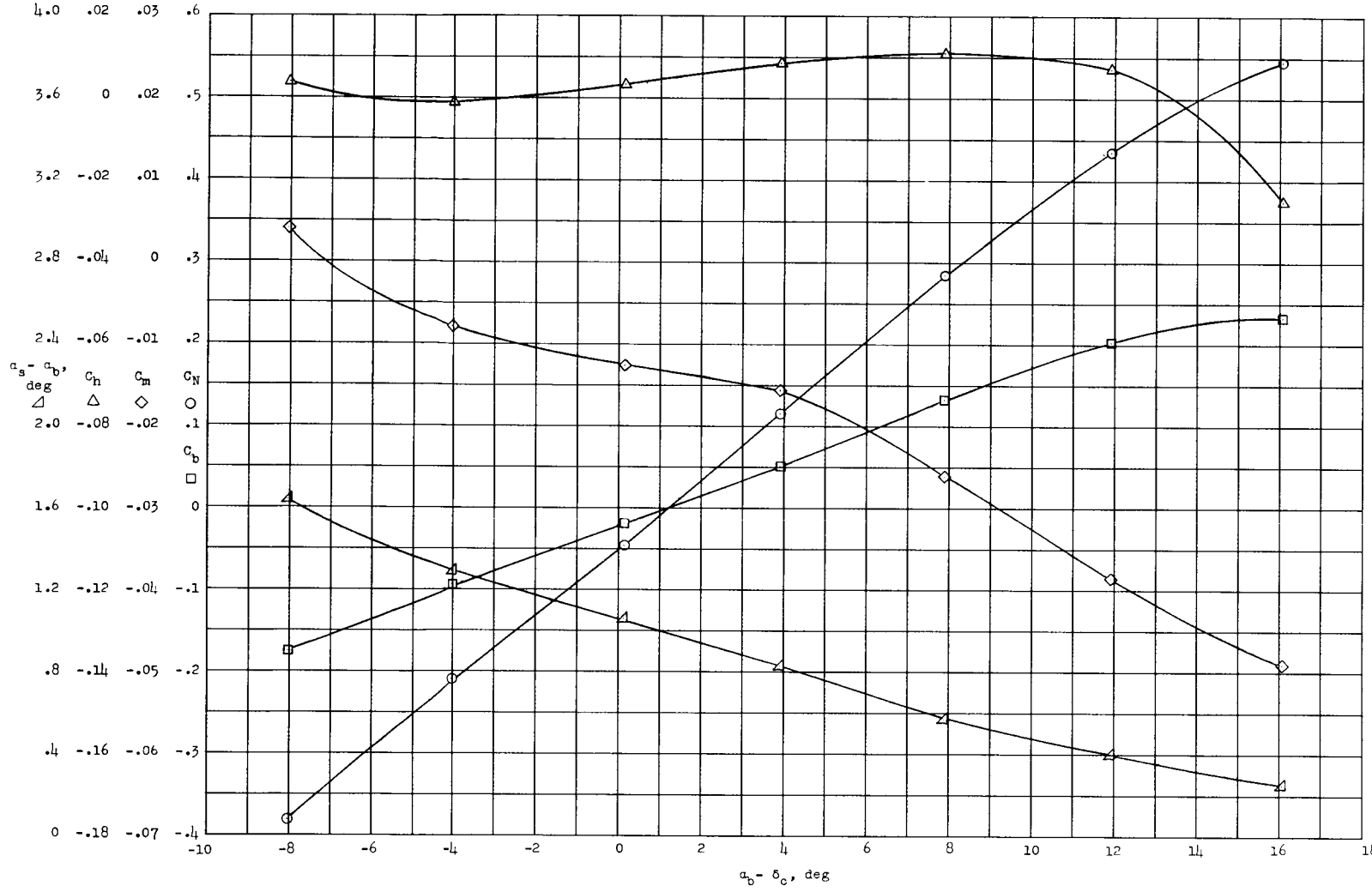

(b) $\alpha_b = 0^\circ$.

Figure 32.- Concluded.

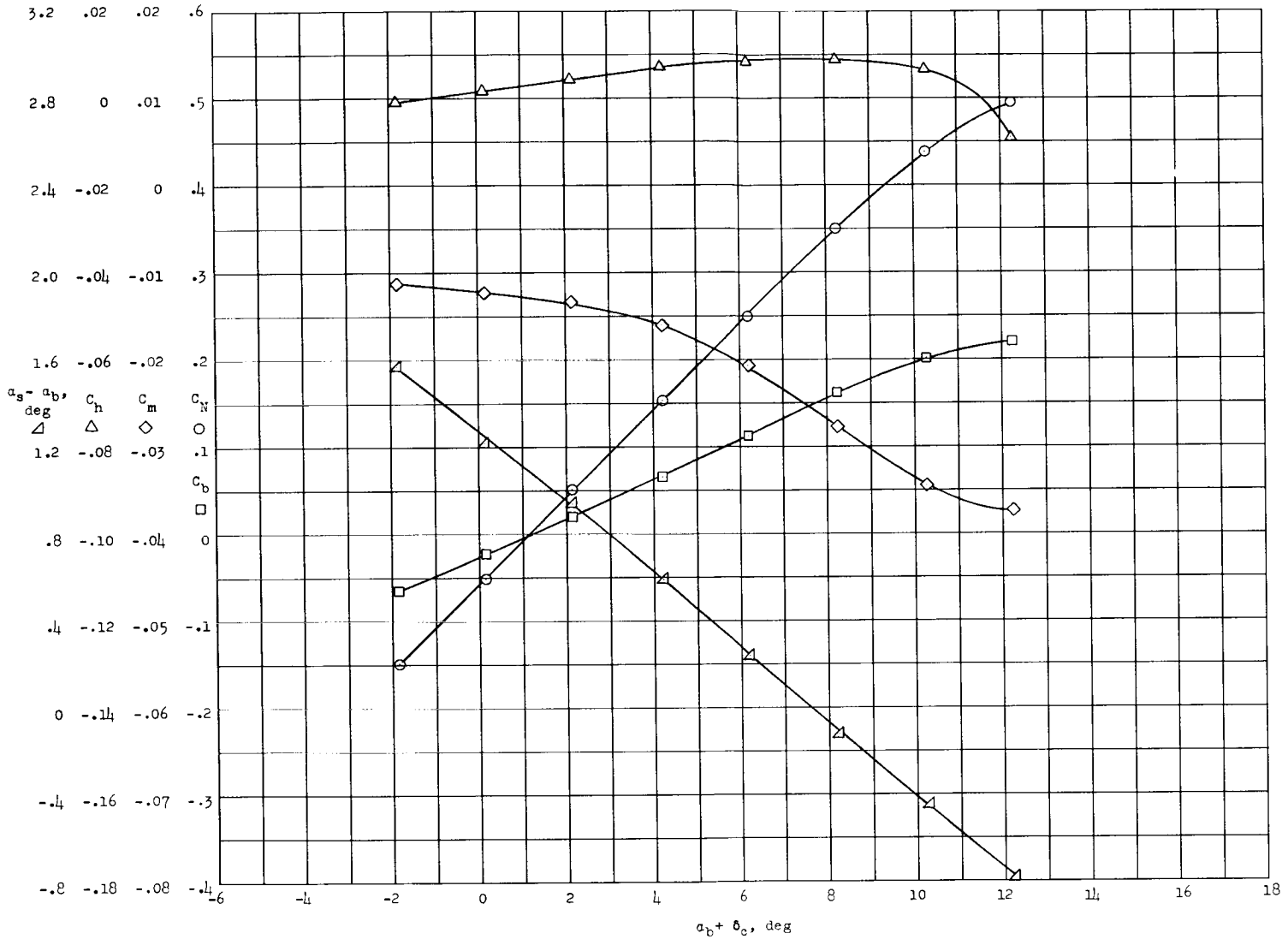

(a) $\delta_c = 0^\circ$.

Figure 33.- Longitudinal aerodynamic characteristics of restrained canard in Freon-12 at M = 0.80 and q = 190 lb/sq ft with $\delta_t = 0^\circ$.

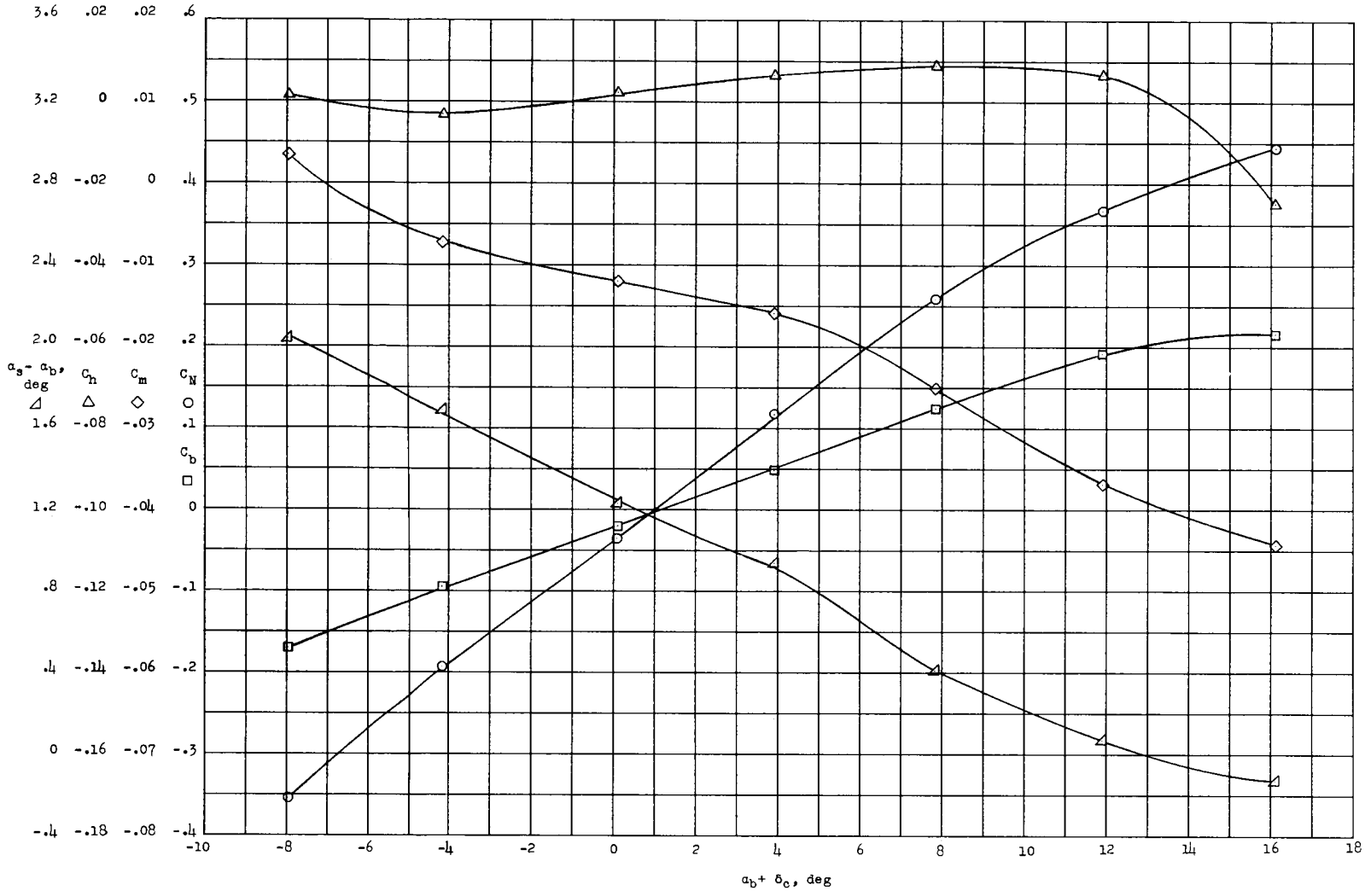

(b) $\alpha_b = 0^\circ$.

Figure 33.- Concluded.

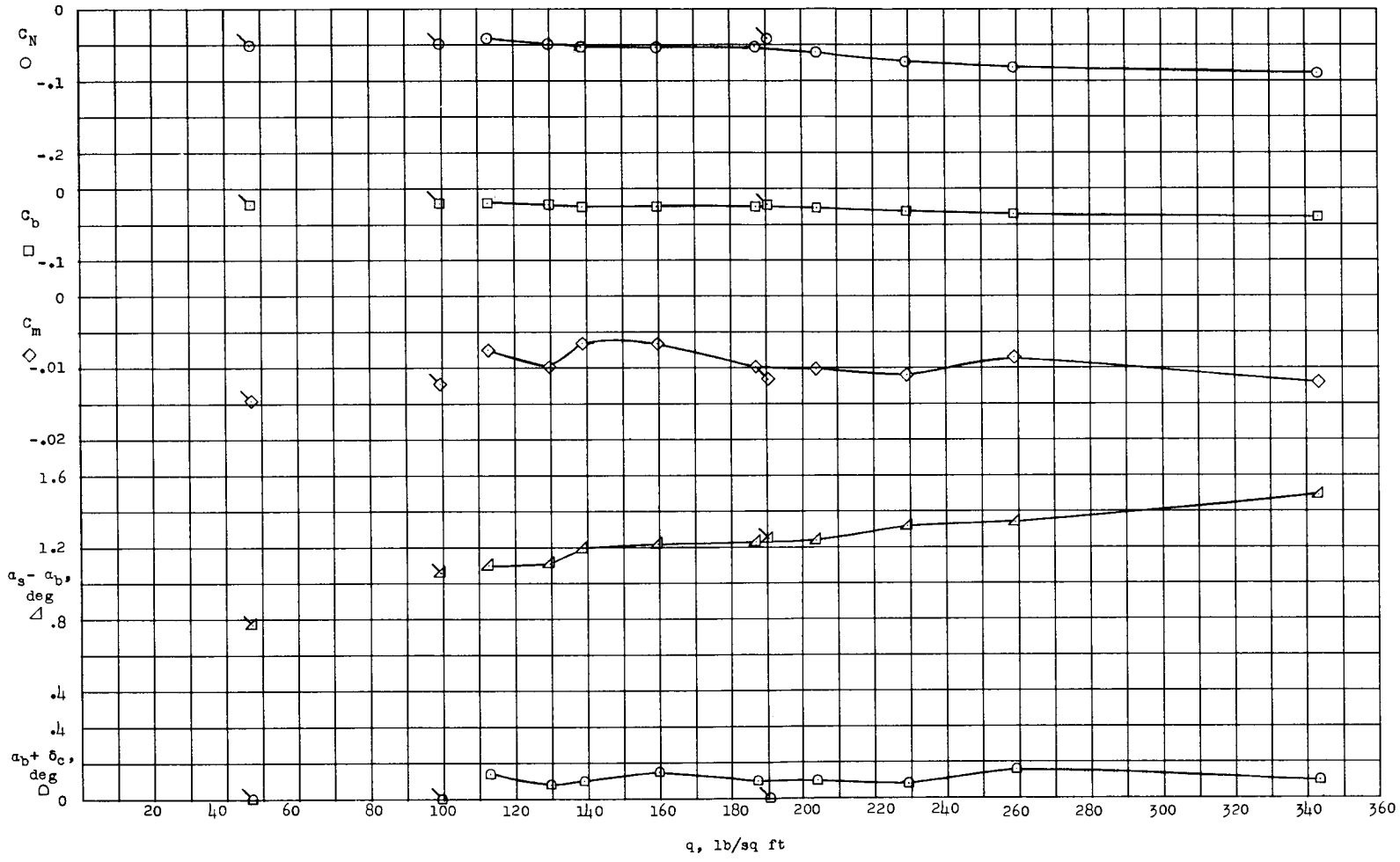

(a) $\delta_c \approx 0^\circ$. Flagged symbols indicate points reproduced from figures 31, 32(b), and 33(b).

Figure 34.- Longitudinal aerodynamic characteristics of restrained canard in Freon-12 at M = 0.80 with $\delta_t \approx 0^\circ$ and $\alpha_b = 0^\circ$.

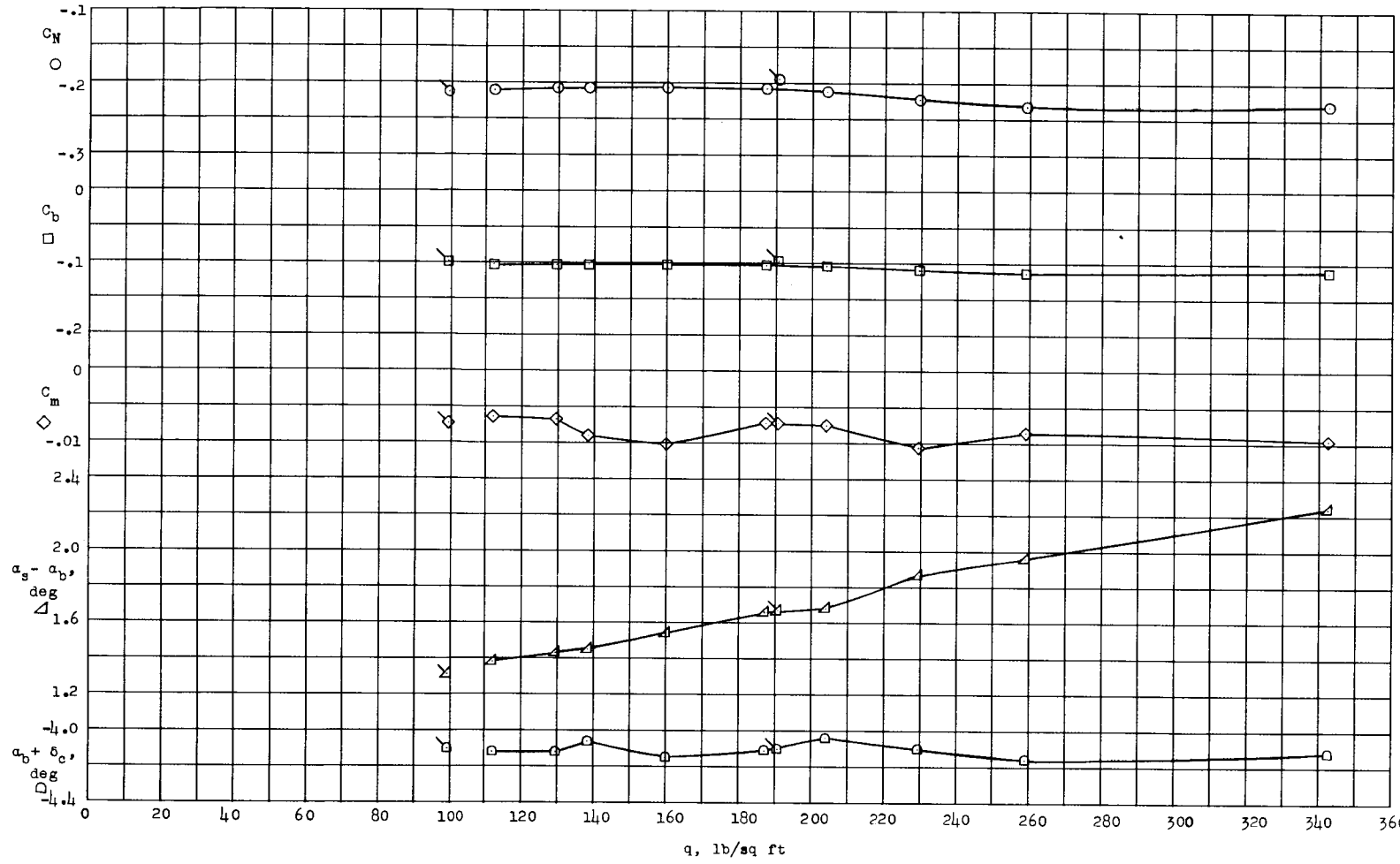

(b) $\delta_c \approx -4^\circ$. Flagged symbols indicate points reproduced from figures 32(b) and 33(b).

Figure 34.- Concluded.

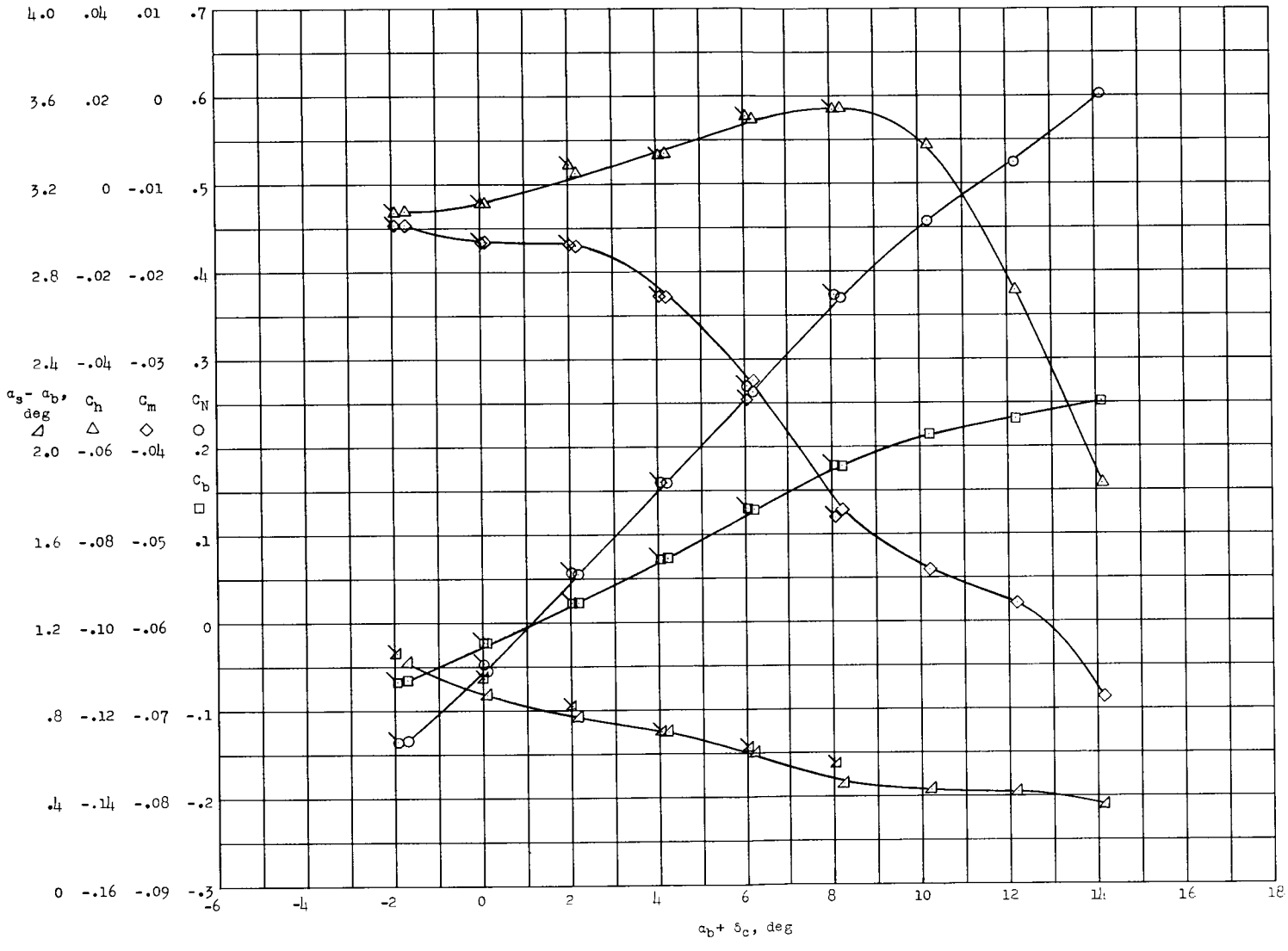

(a) $\delta_c = 0^\circ$. Flagged symbols indicate points rerun to show repeatability.

Figure 35.- Longitudinal aerodynamic characteristics of restrained canard in Freon-12 at M = 0.85 and q = 50 lb/sq ft with $\delta_t = 0^\circ$.

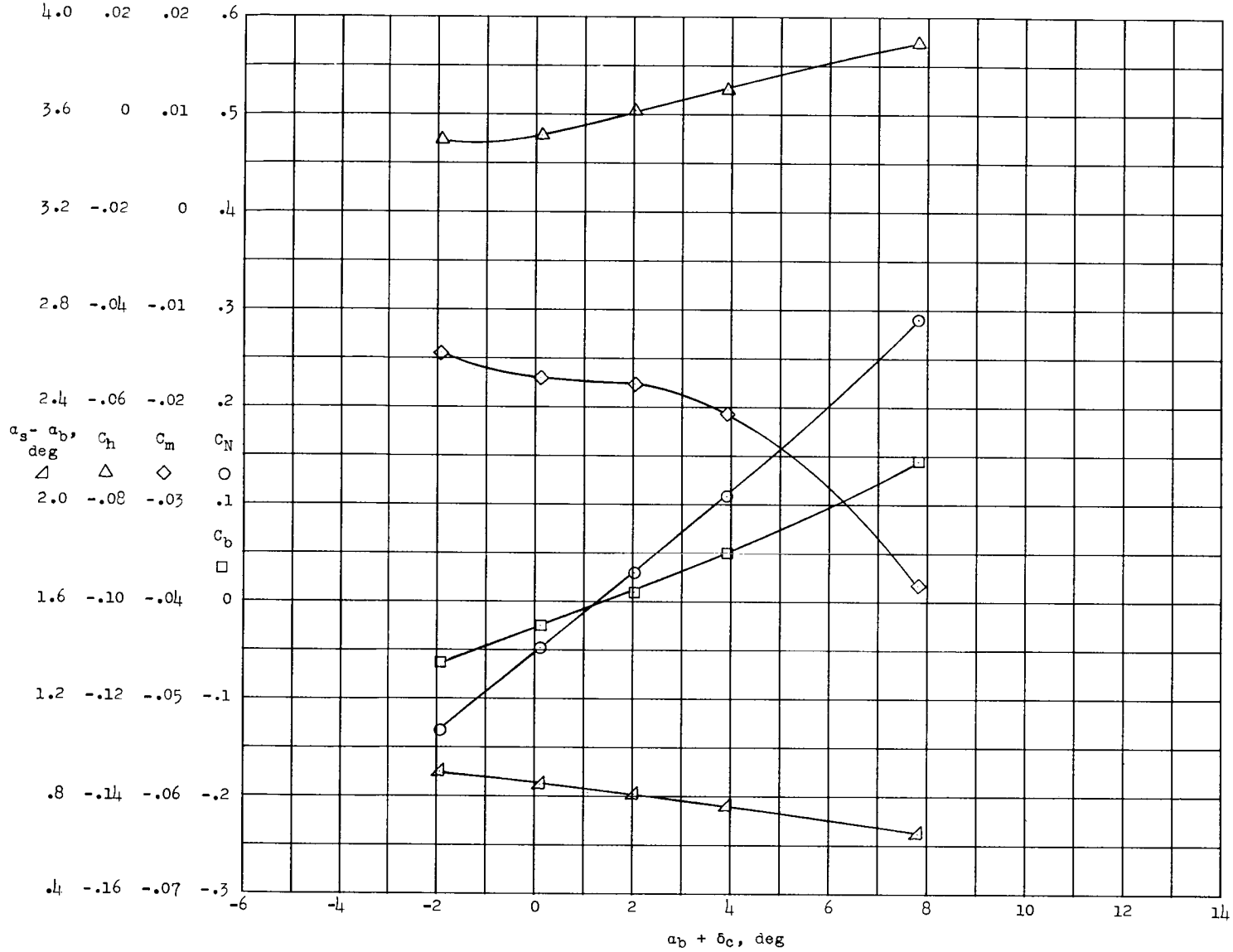

(b) $\alpha_b = 0^\circ$.

Figure 35.- Concluded.

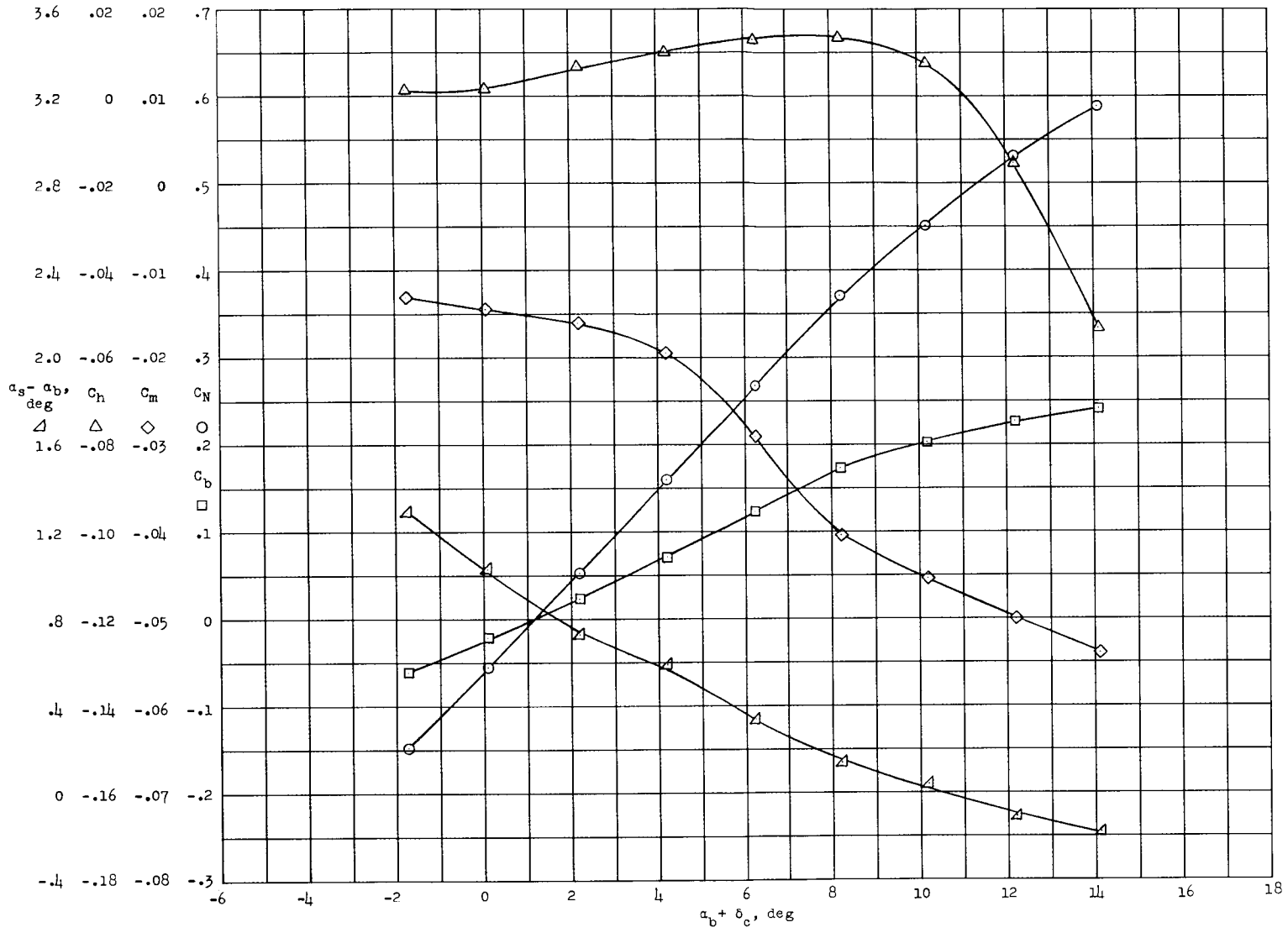

(a) $\delta_c = 0^\circ$.

Figure 36.- Longitudinal aerodynamic characteristics of restrained canard in Freon-12 at M = 0.85 and q = 100 lb/sq ft with $\delta_t = 0^\circ$.

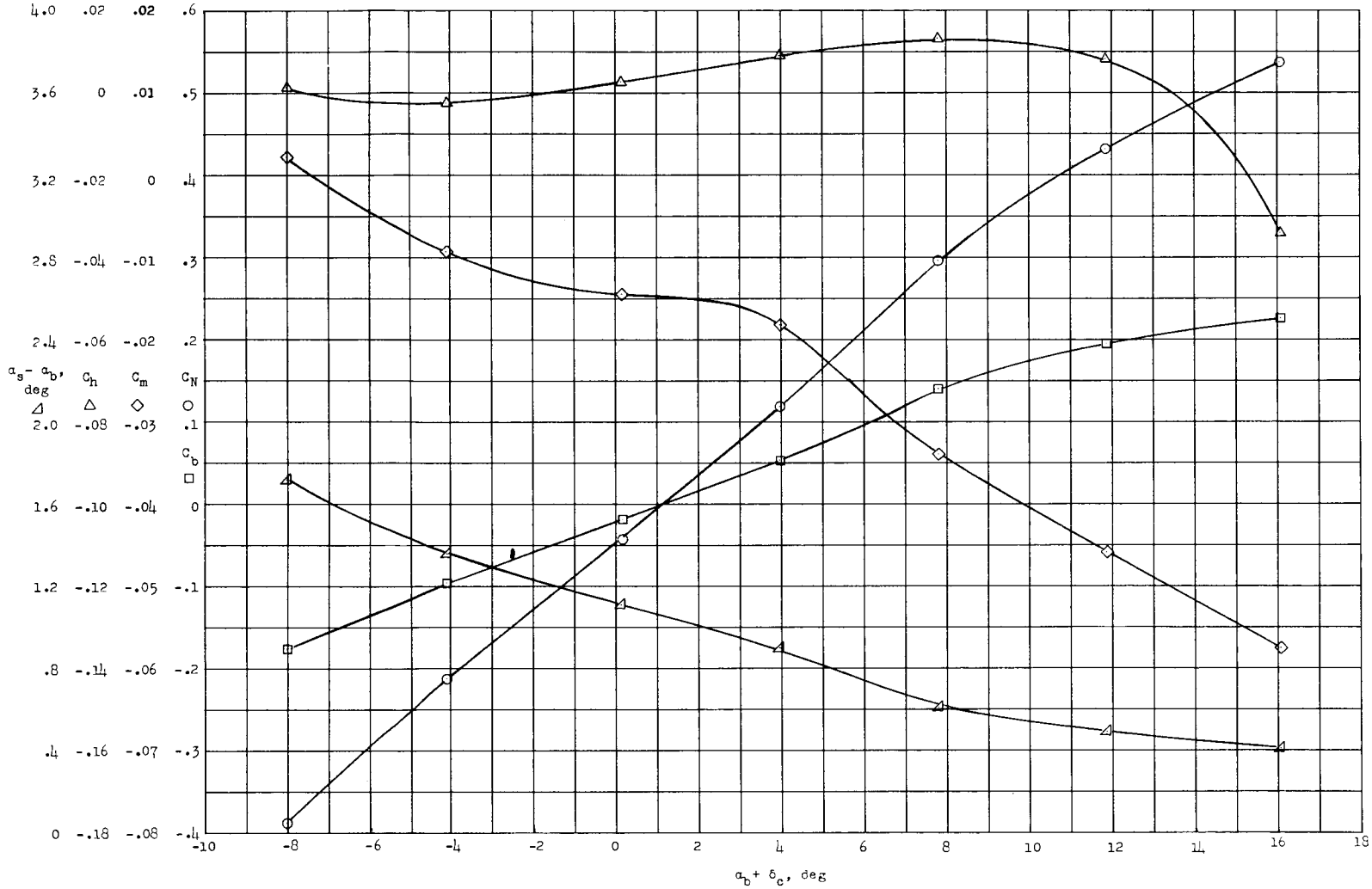

(b) $\alpha_b = 0^\circ$.

Figure 36.- Concluded.

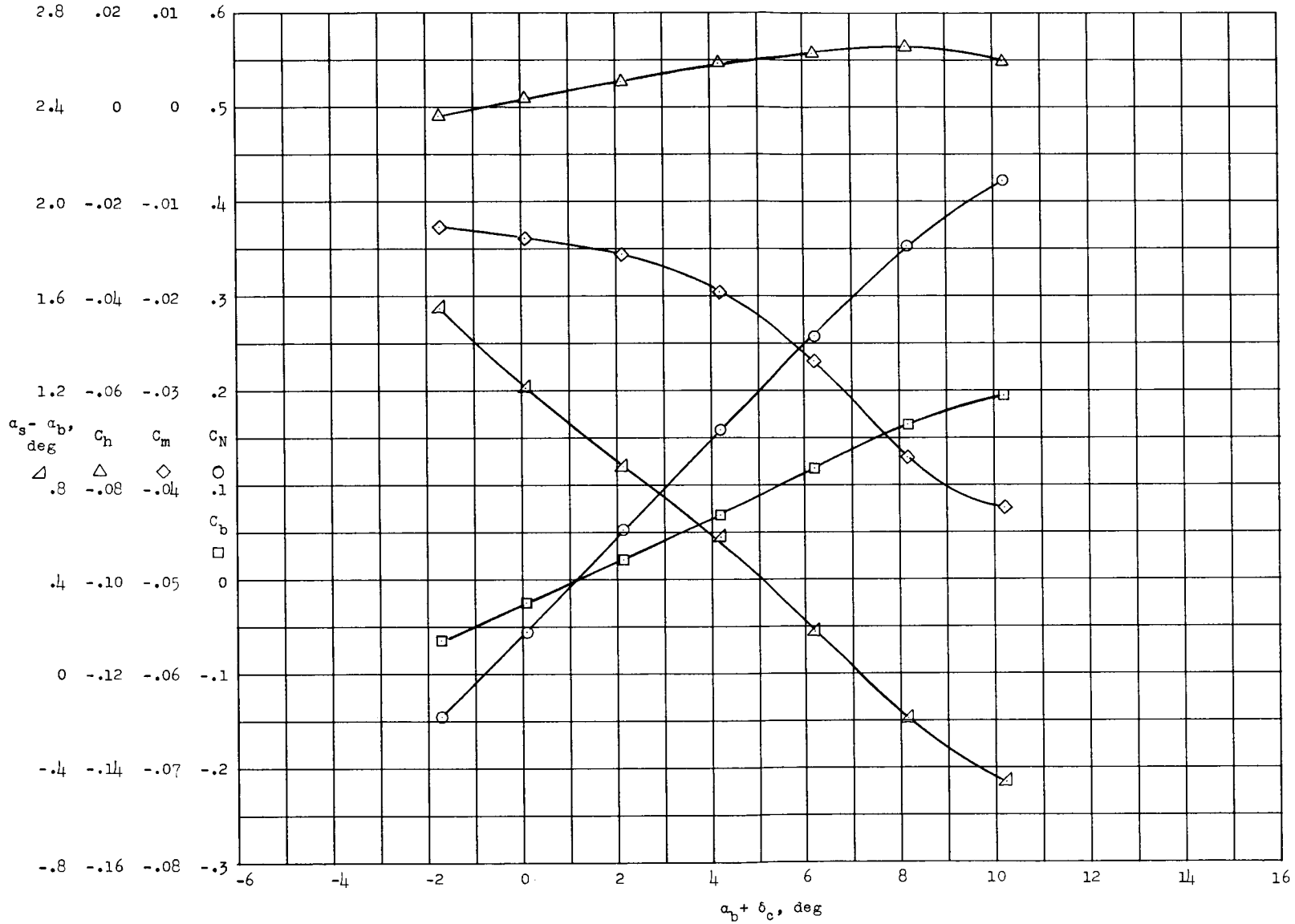

(a) $\delta_c = 0°$.

Figure 37.- Longitudinal aerodynamic characteristics of restrained canard in Freon-12 at M = 0.85 and q = 190 lb/sq ft

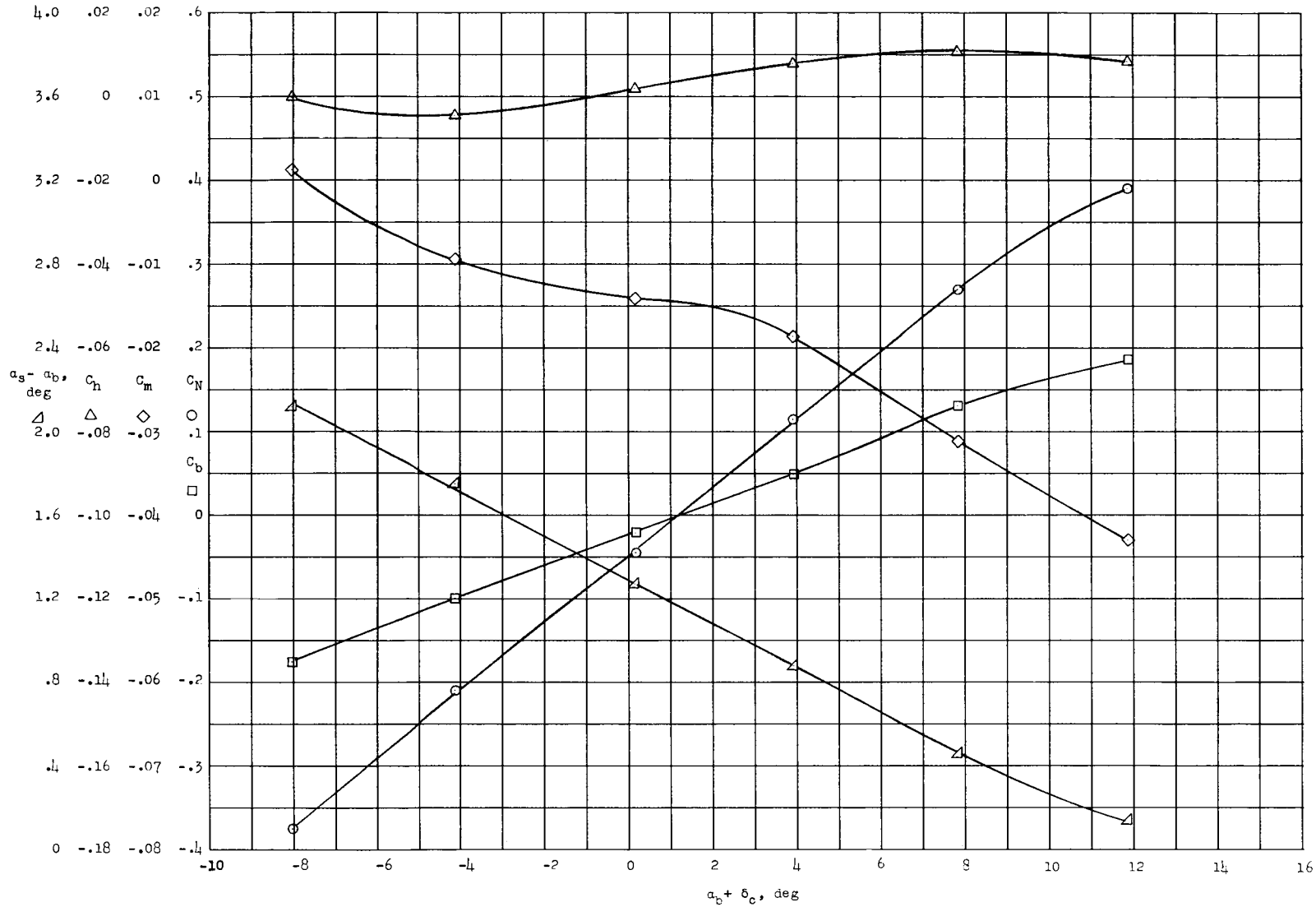

(b) $\alpha_b = 0^\circ$.

Figure 37.- Concluded.

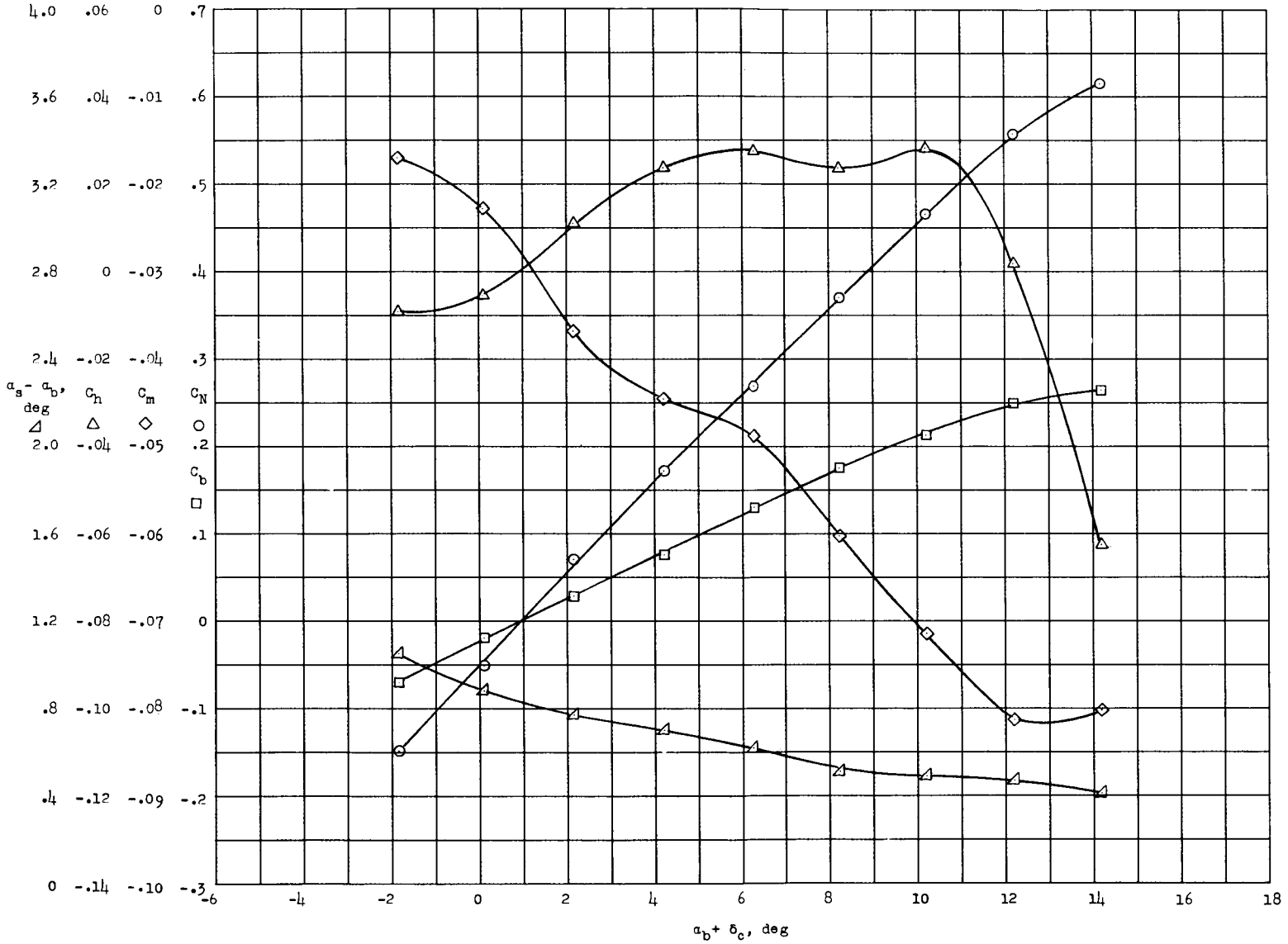

(a) $\delta_c = 0^\circ$.

Figure 38.- Longitudinal aerodynamic characteristics of restrained canard in Freon-12 at M = 0.90 and q = 50 lb/sq ft with $\delta_t = 0^\circ$.

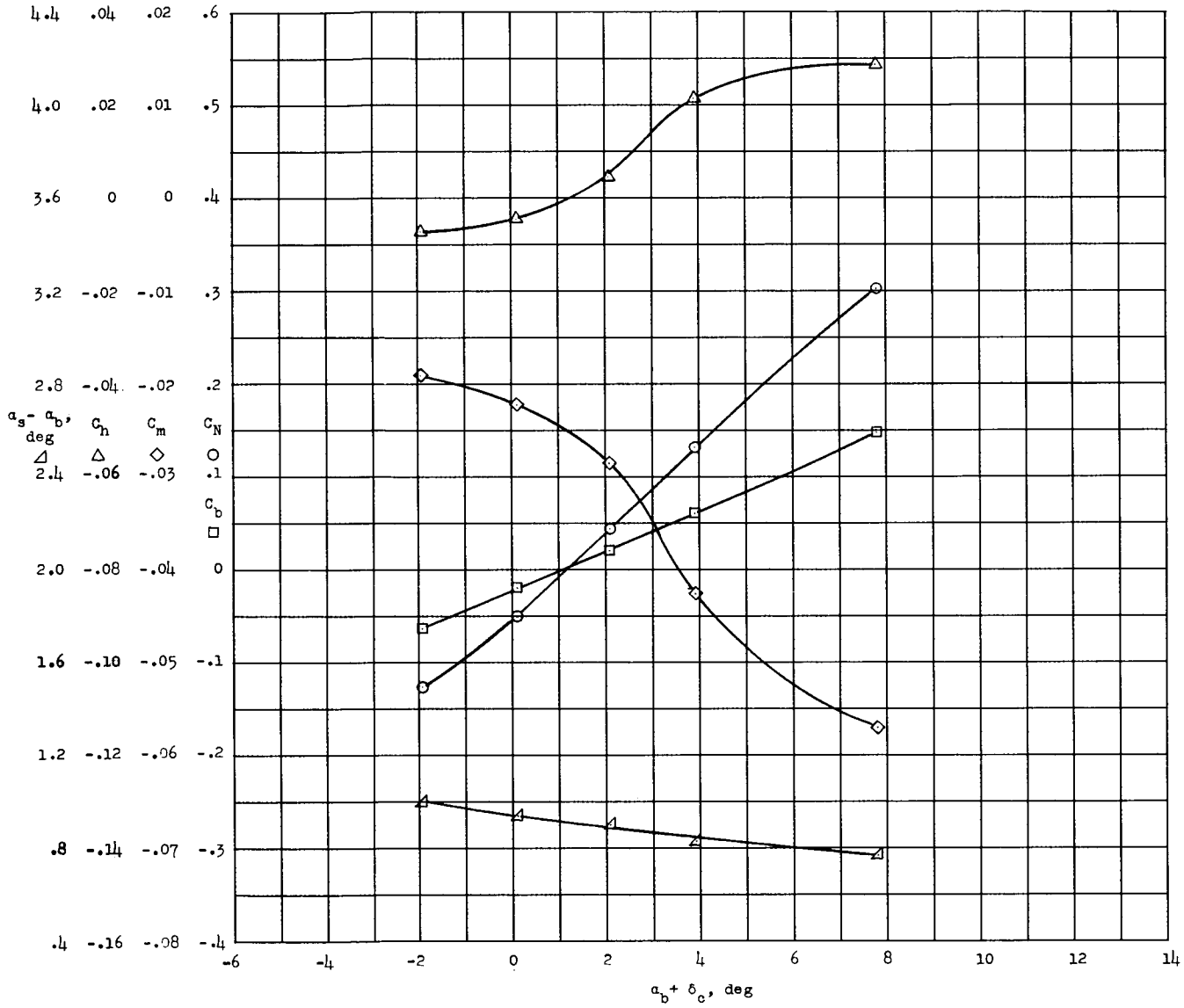

(b) $\alpha_b = 0^\circ$.

Figure 38.- Concluded.

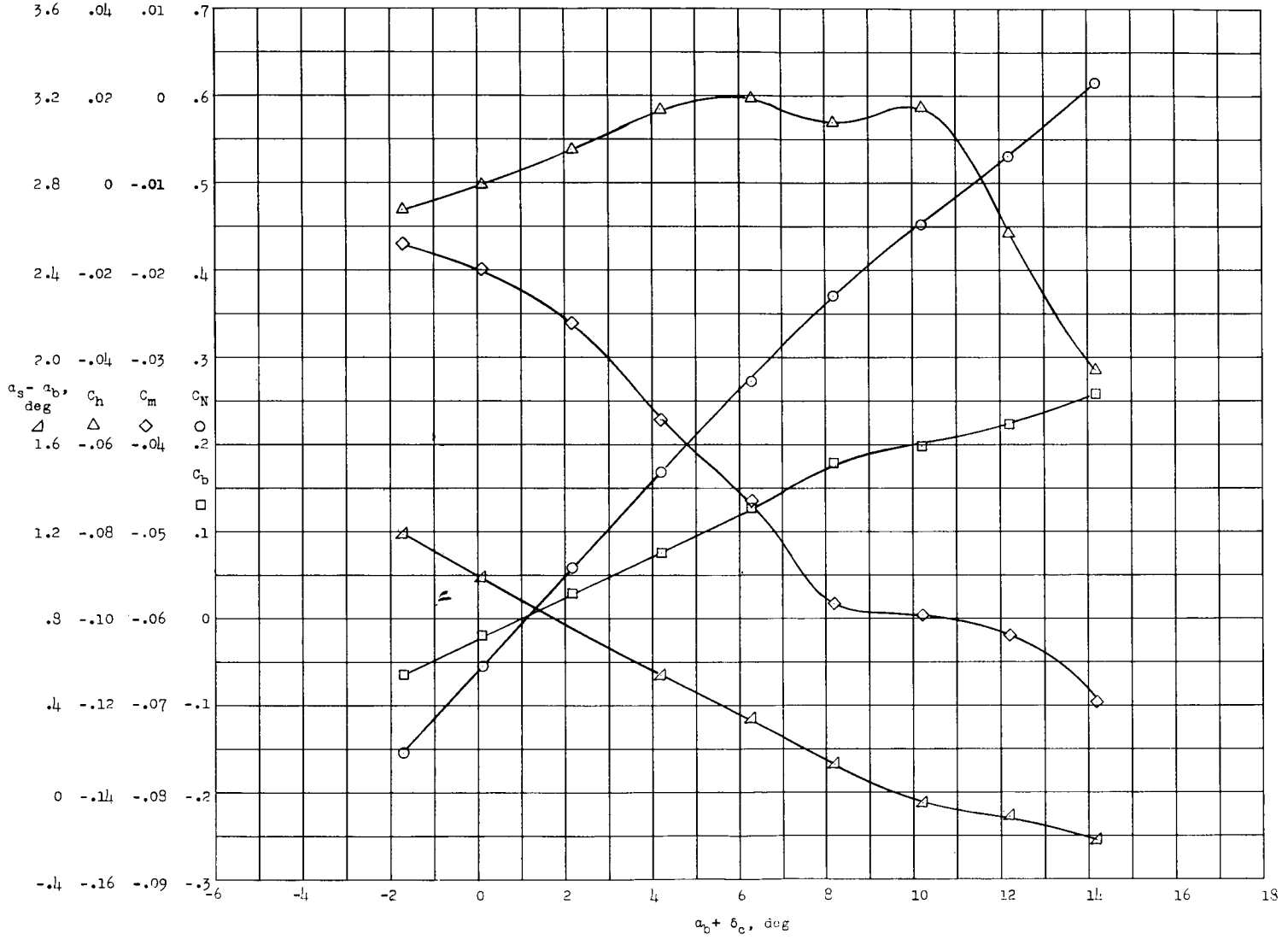

(a) $\delta_c = 0^o$.

Figure 39.- Longitudinal aerodynamic characteristics of restrained canard in Freon-12 at M = 0.90 and q = 100 lb/sq ft with $\delta_t = 0^o$.

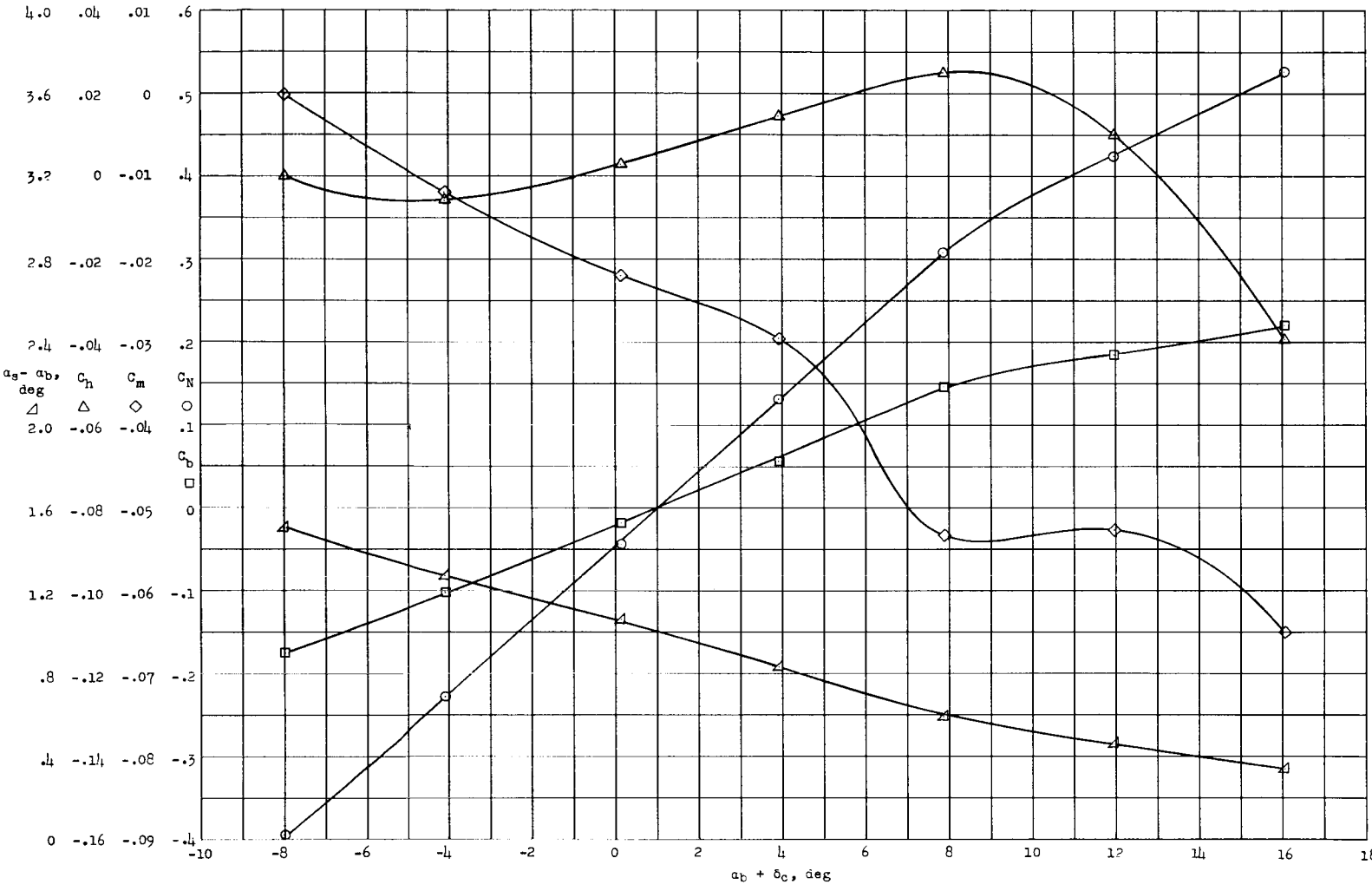

(b) $\alpha_b = 0^\circ$.

Figure 39.- Concluded.

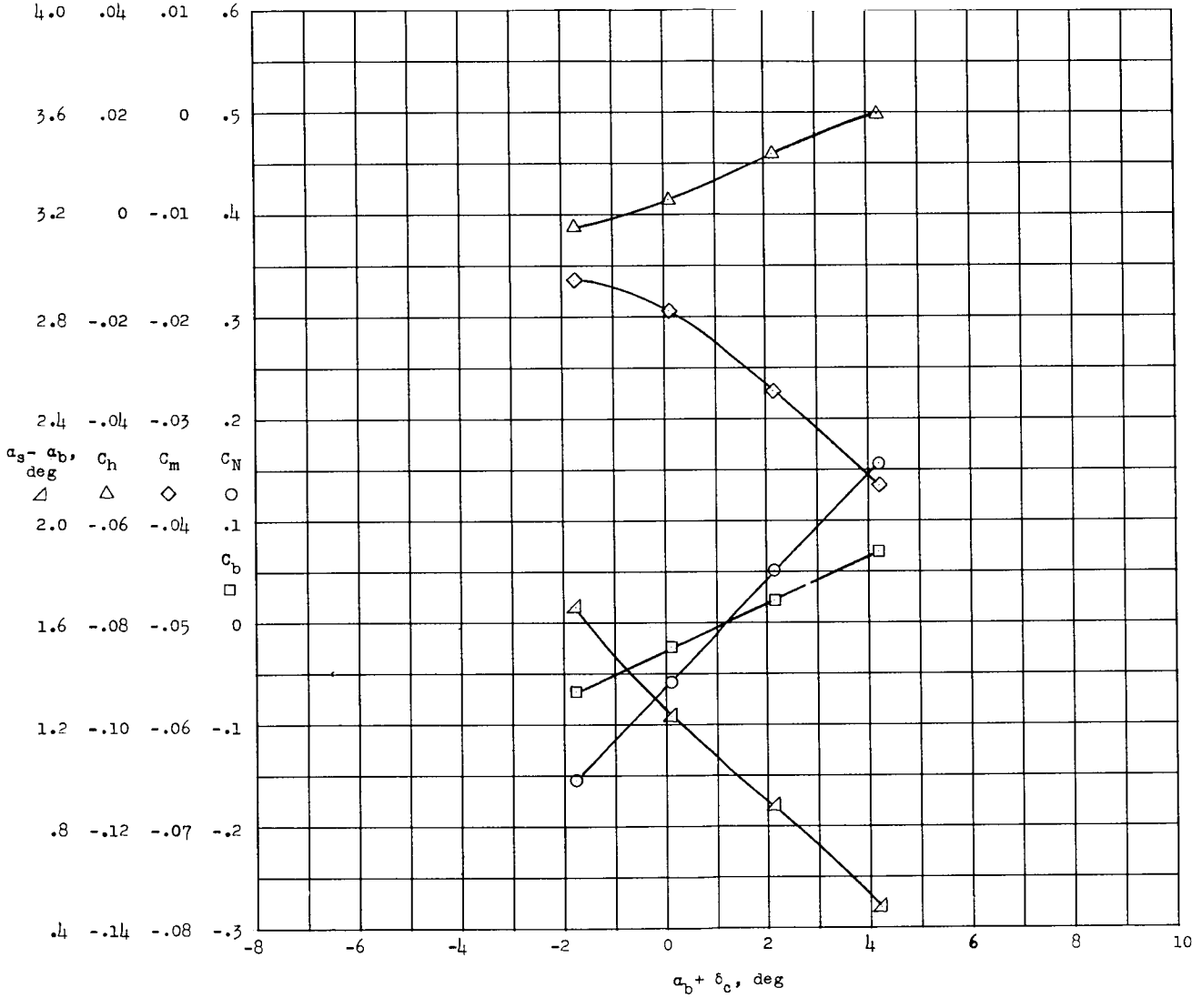

(a) $\delta_c = 0^\circ$.

Figure 40.- Longitudinal aerodynamic characteristics of restrained canard in Freon-12 at M = 0.90 and q = 190 lb/sq ft with $\delta_t = 0^\circ$.

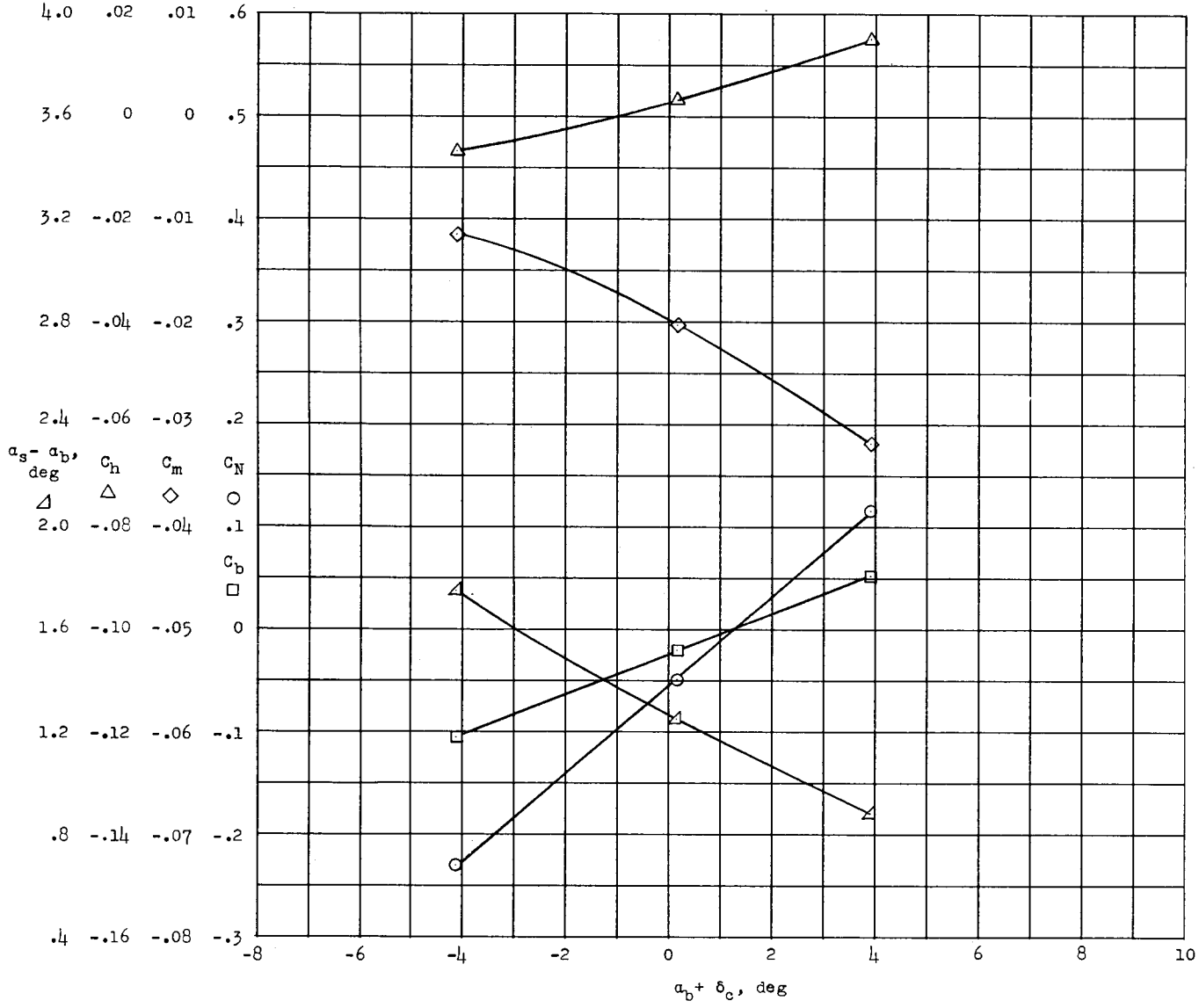

(b) $\alpha_b = 0^\circ$.

Figure 40.- Concluded.

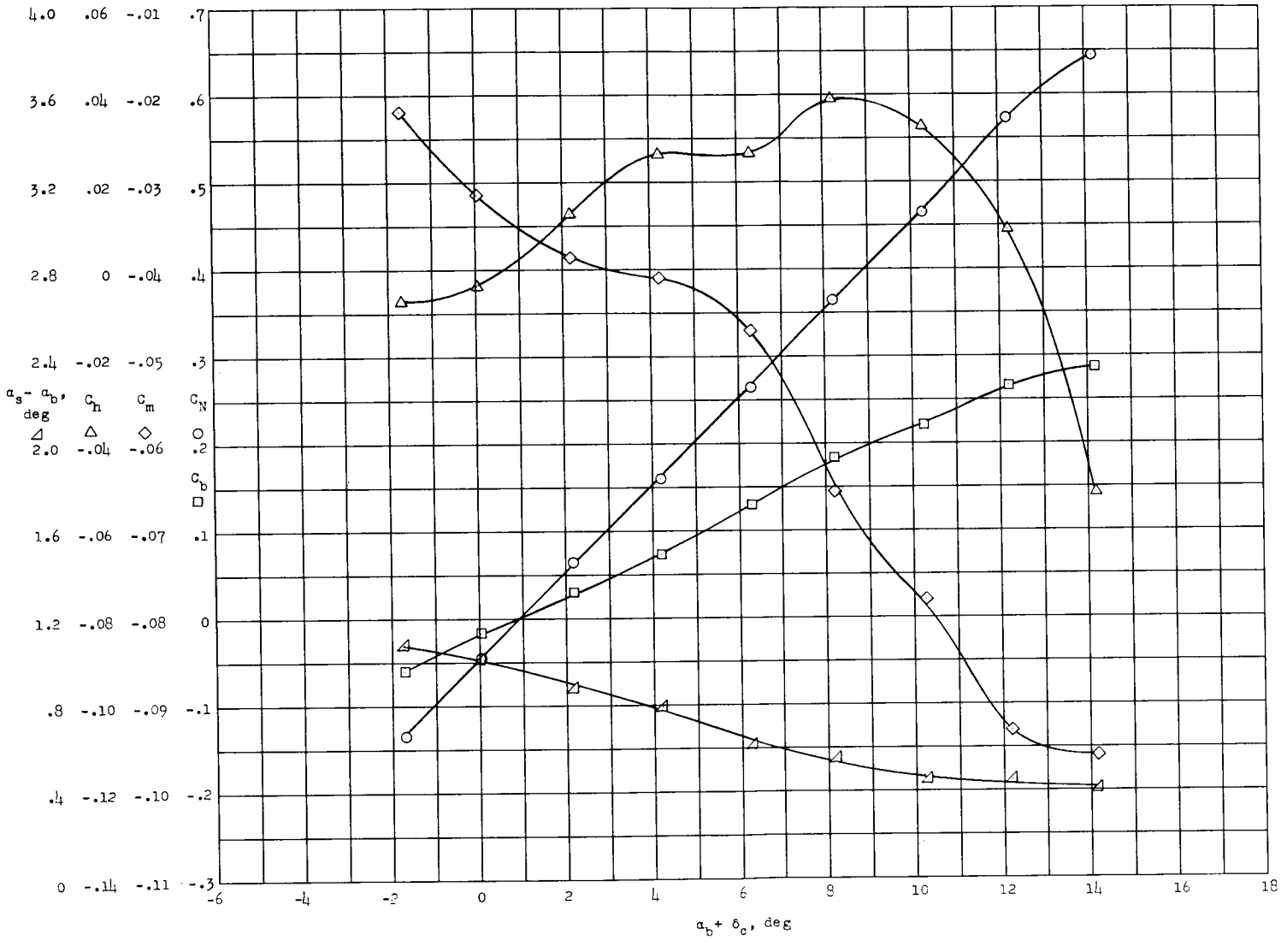

(a) $\delta_c = 0^o$.

Figure 41.- Longitudinal aerodynamic characteristics of restrained canard in Freon-12 at M = 0.92 and q = 50 lb/sq ft with $\delta_t = 0^o$.

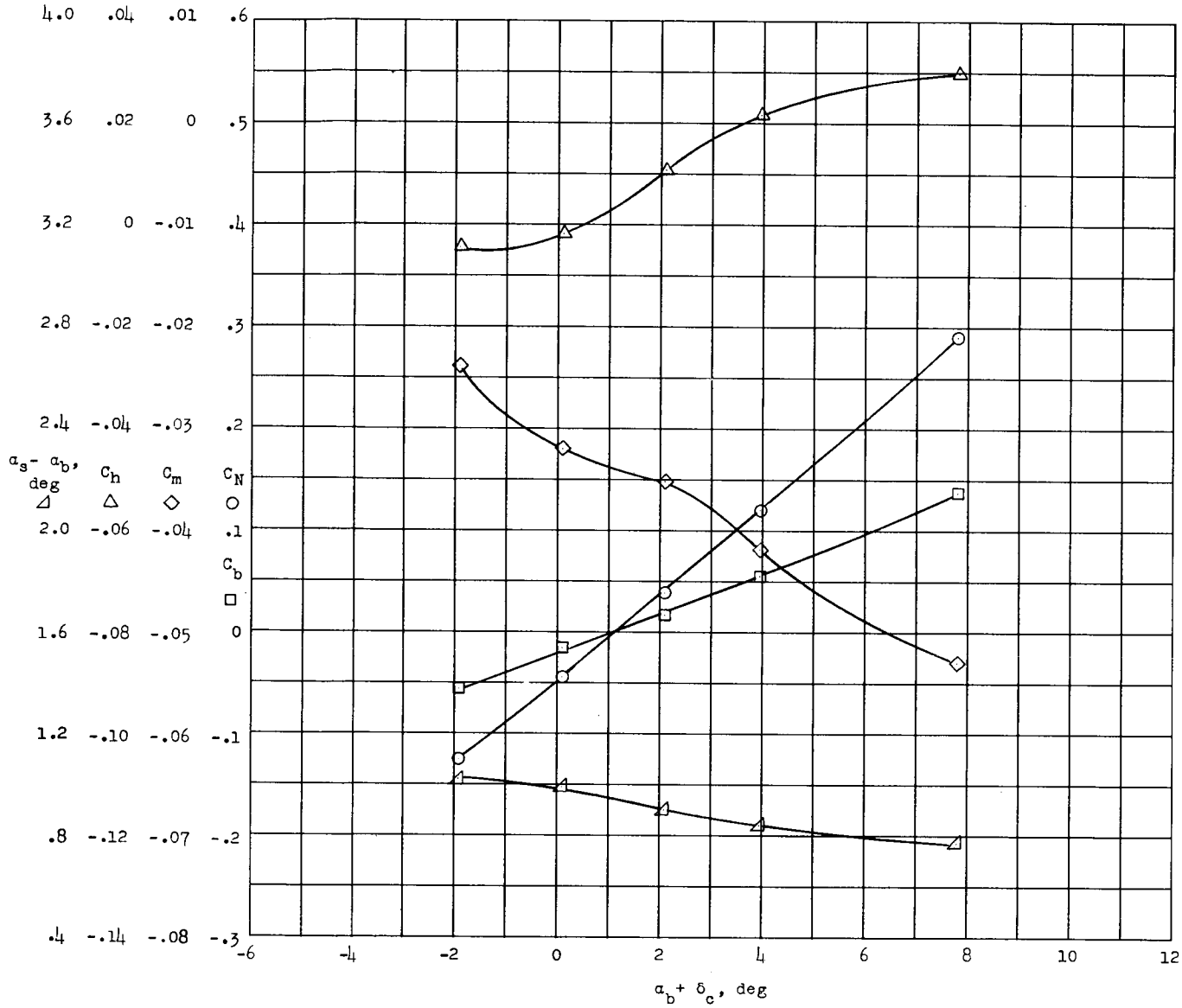

(b) $\alpha_b = 0°$.

Figure 41.- Concluded.

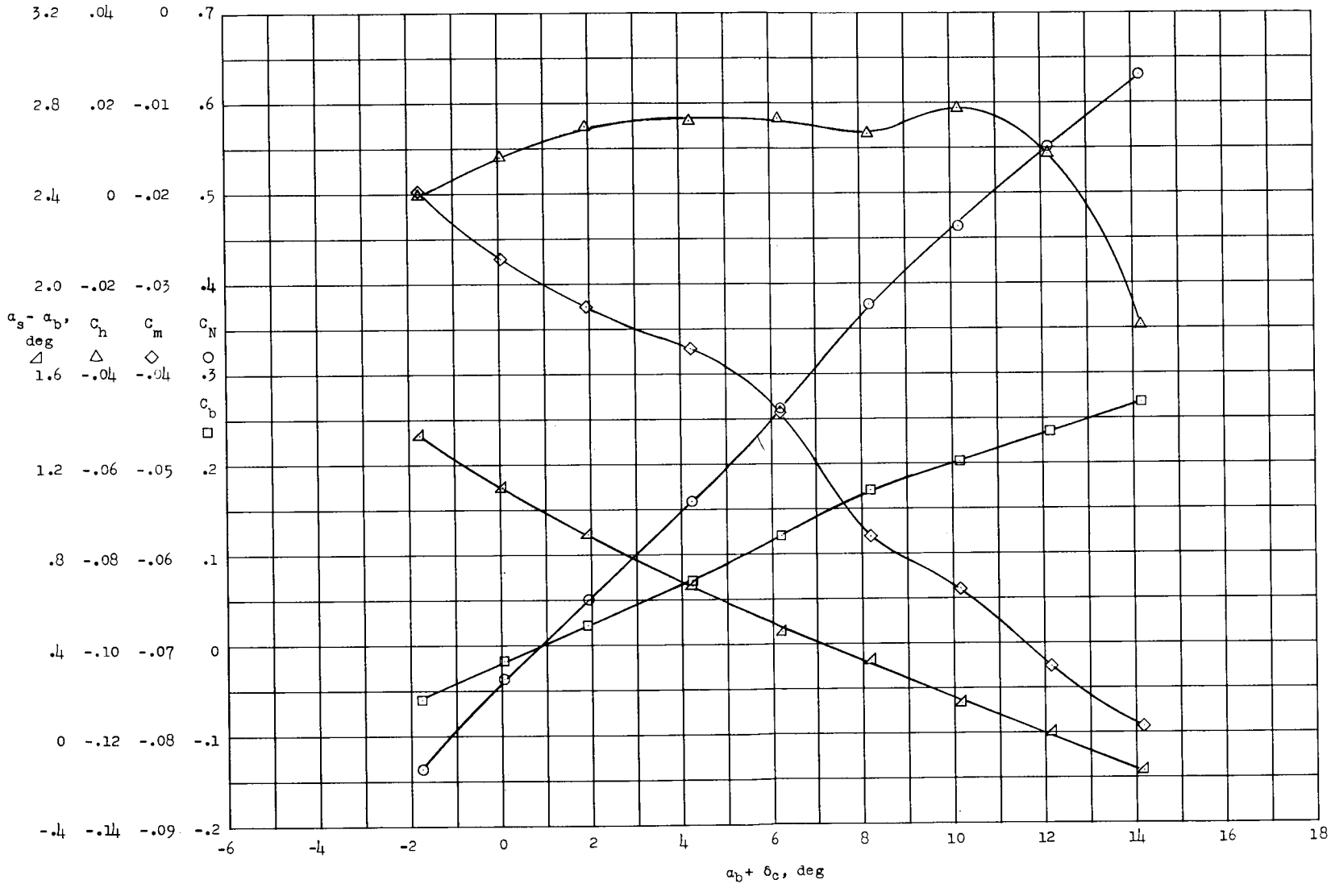

(a) $\delta_c = 0^o$.

Figure 42.- Longitudinal aerodynamic characteristics of restrained canard in Freon-12 at M = 0.92 and q = 100 lb/sq ft with $\delta_t = 0^o$.

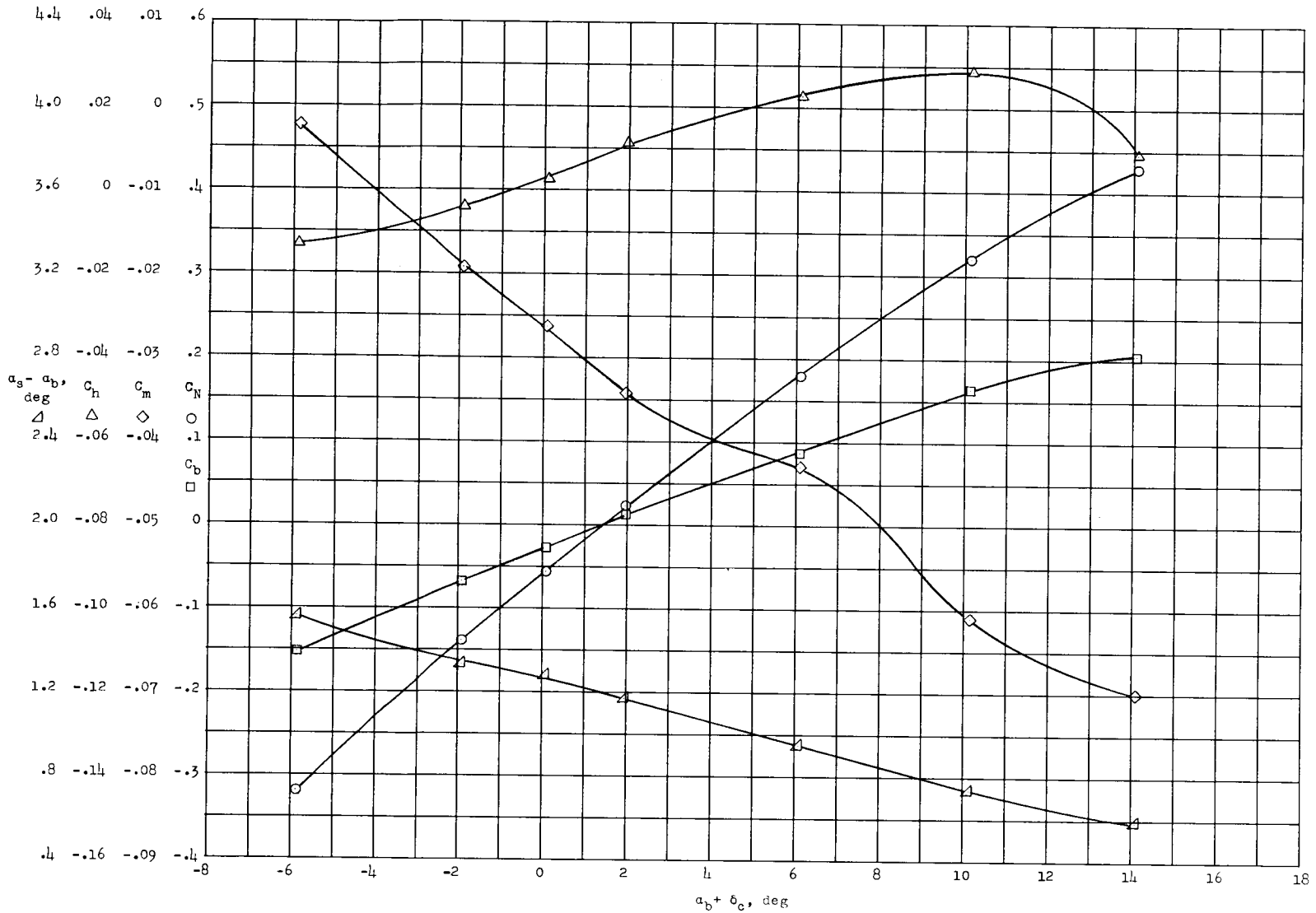

(b) $\alpha_b = -2^\circ$.

Figure 42.- Continued.

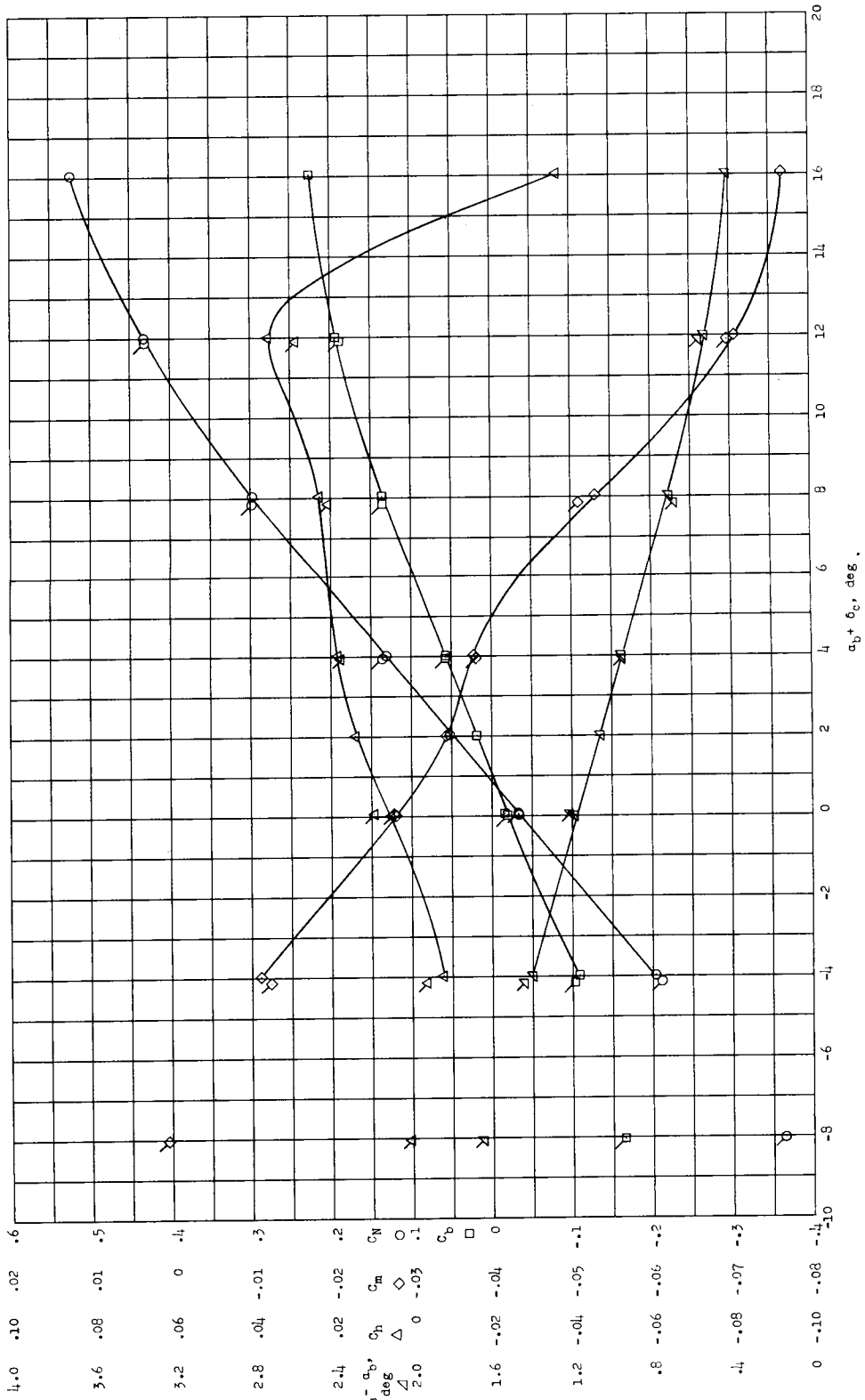

(c) $\alpha_b = 0^\circ$. Flagged symbols indicate points rerun to show repeatability.

Figure 42.- Continued.

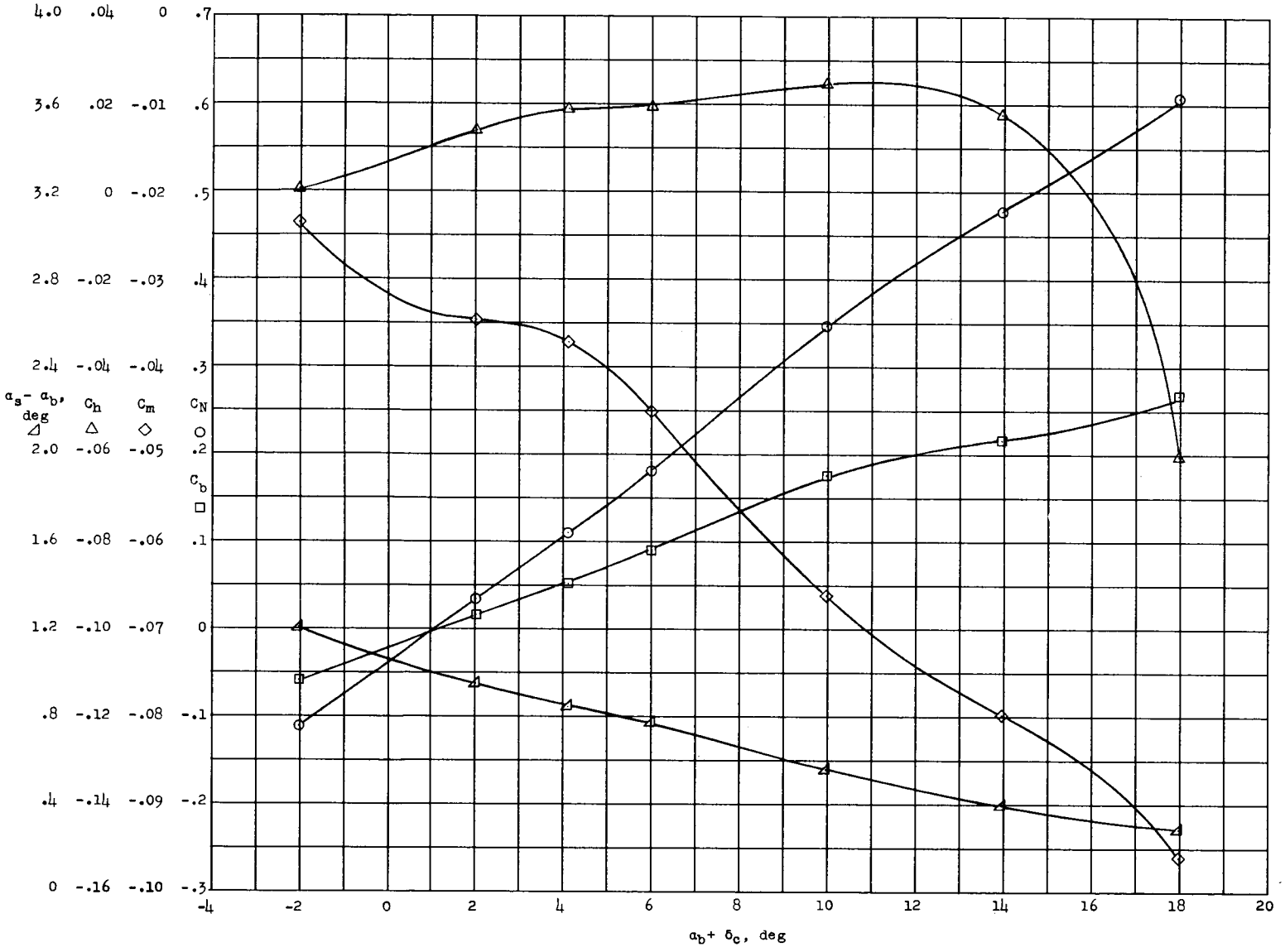

(d) $\alpha_b = 2^\circ$.

Figure 42.- Continued.

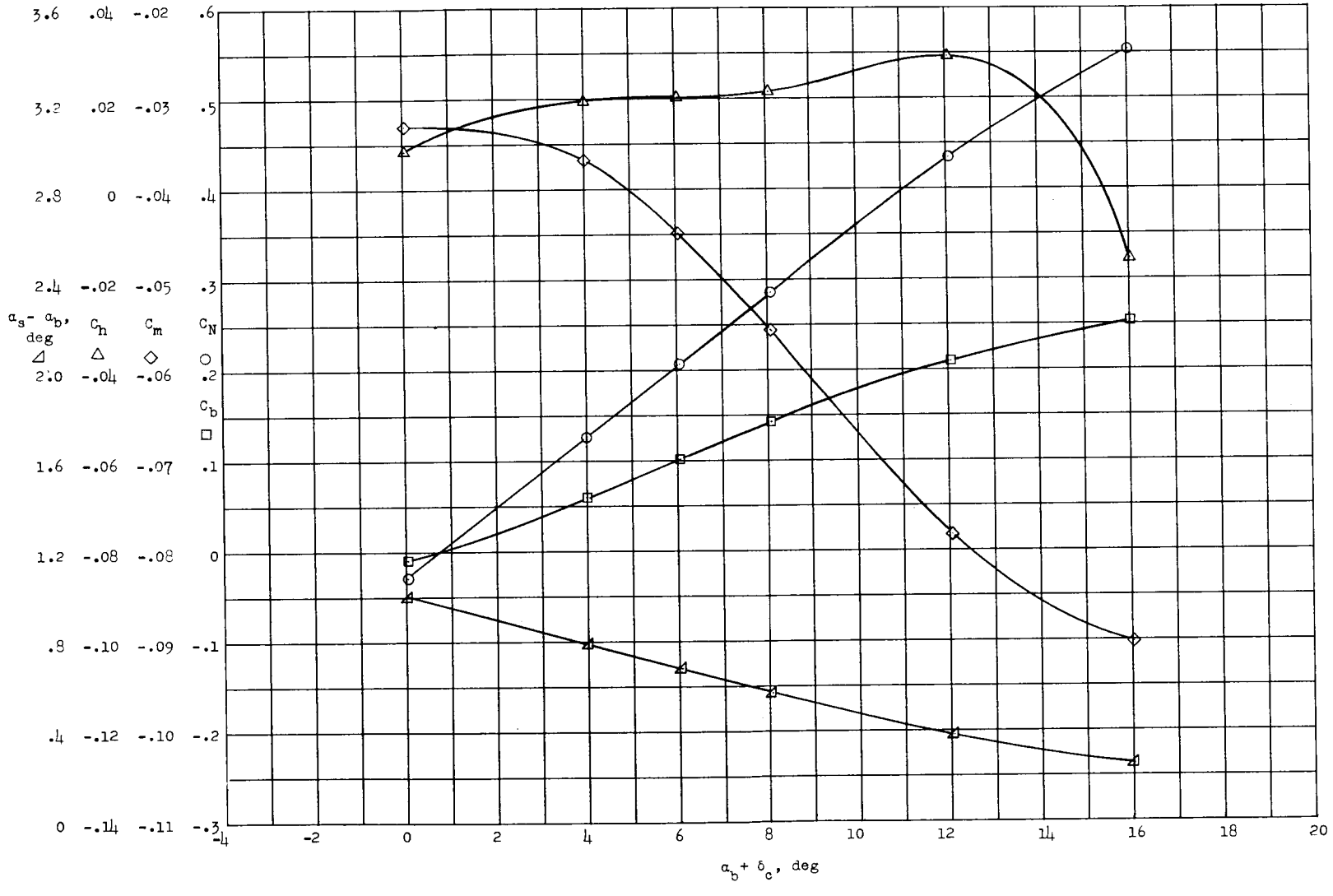

(e) $\alpha_b = 4^\circ$.

Figure 42.- Continued.

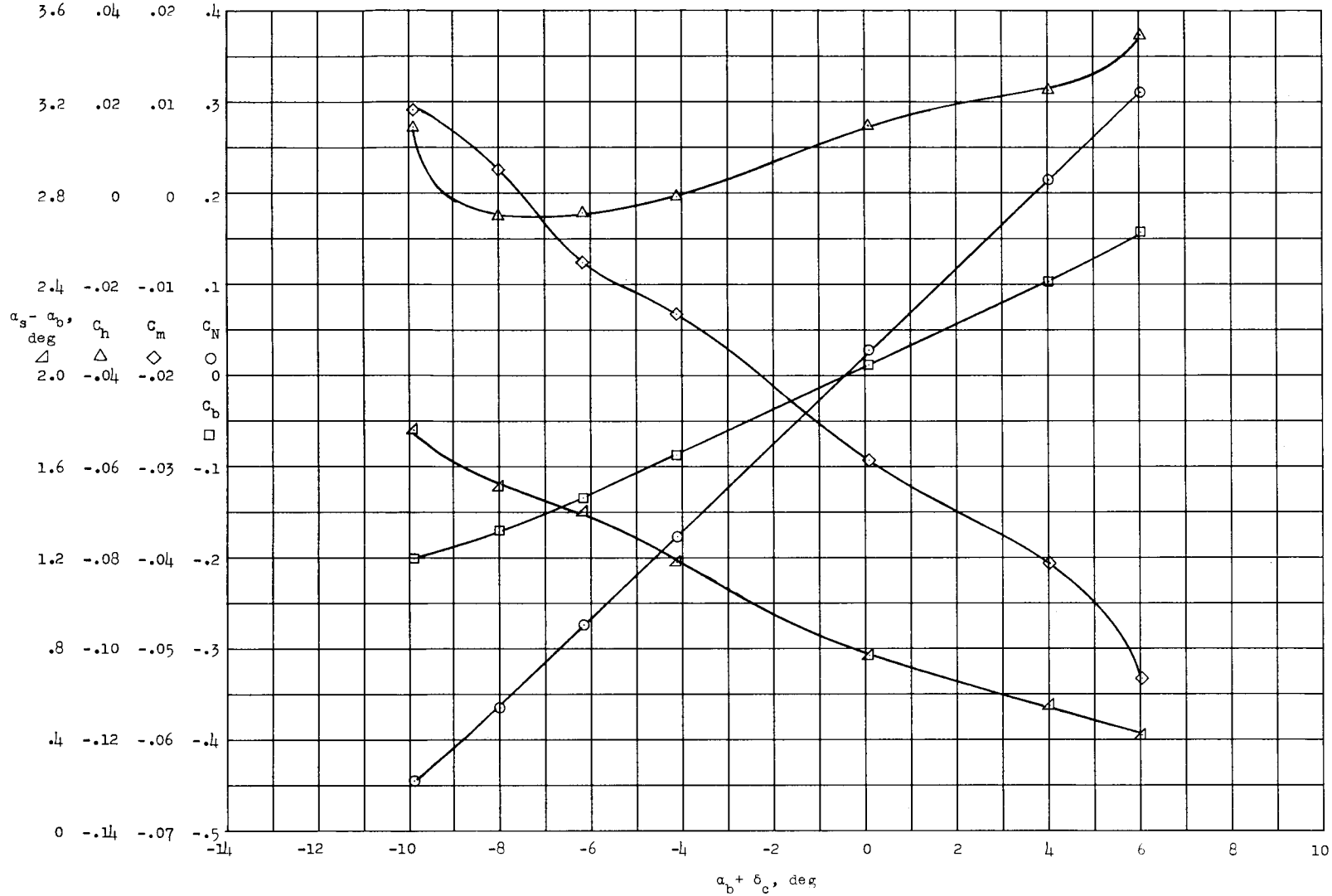

(f) $\delta_c = -8^\circ$.

Figure 42.- Concluded.

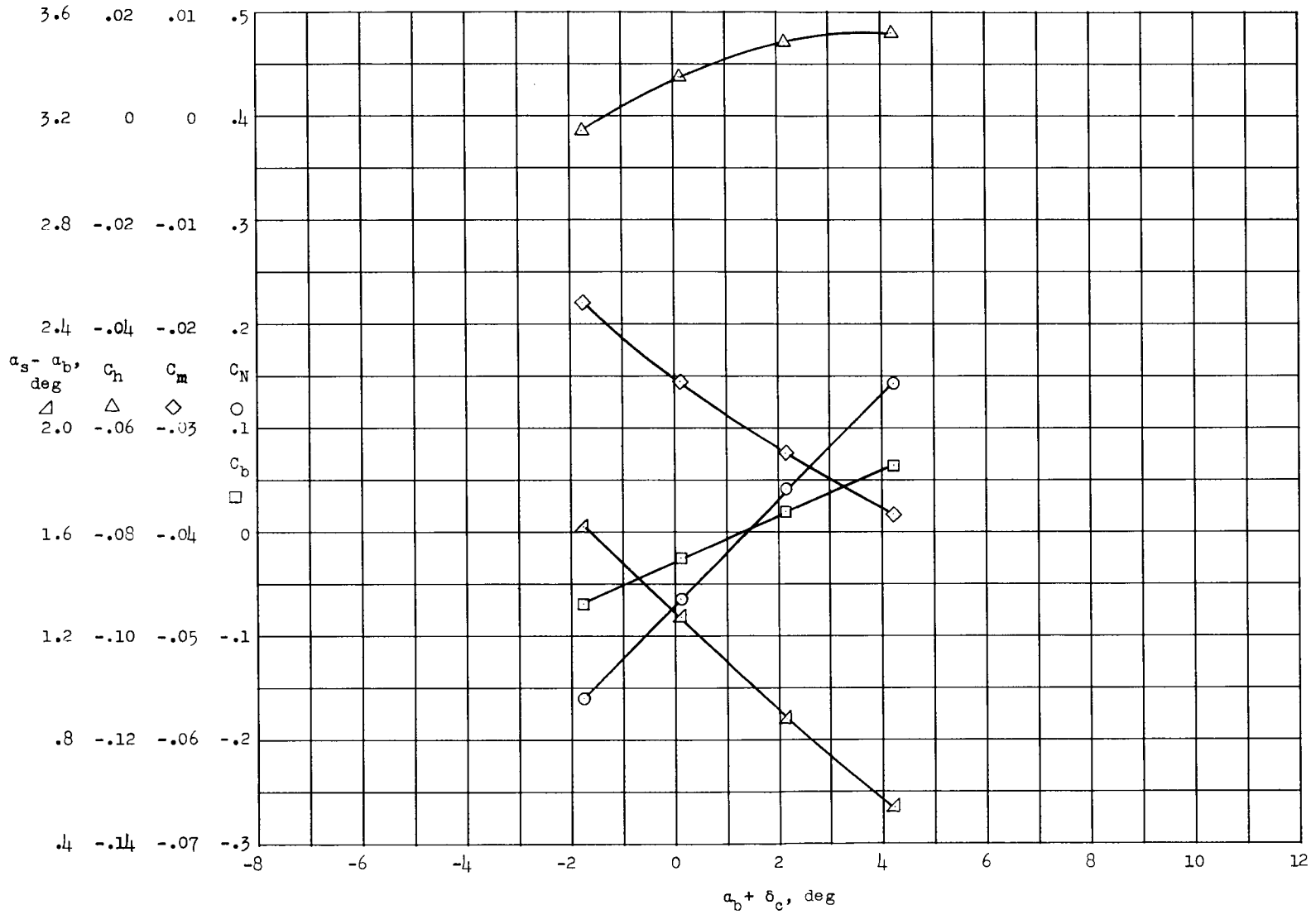

(a) $\delta_c = 0^\circ$.

Figure 43.- Longitudinal aerodynamic characteristics of restrained canard in Freon-12 at M = 0.92 and q = 190 lb/sq ft with $\delta_t = 0^\circ$.

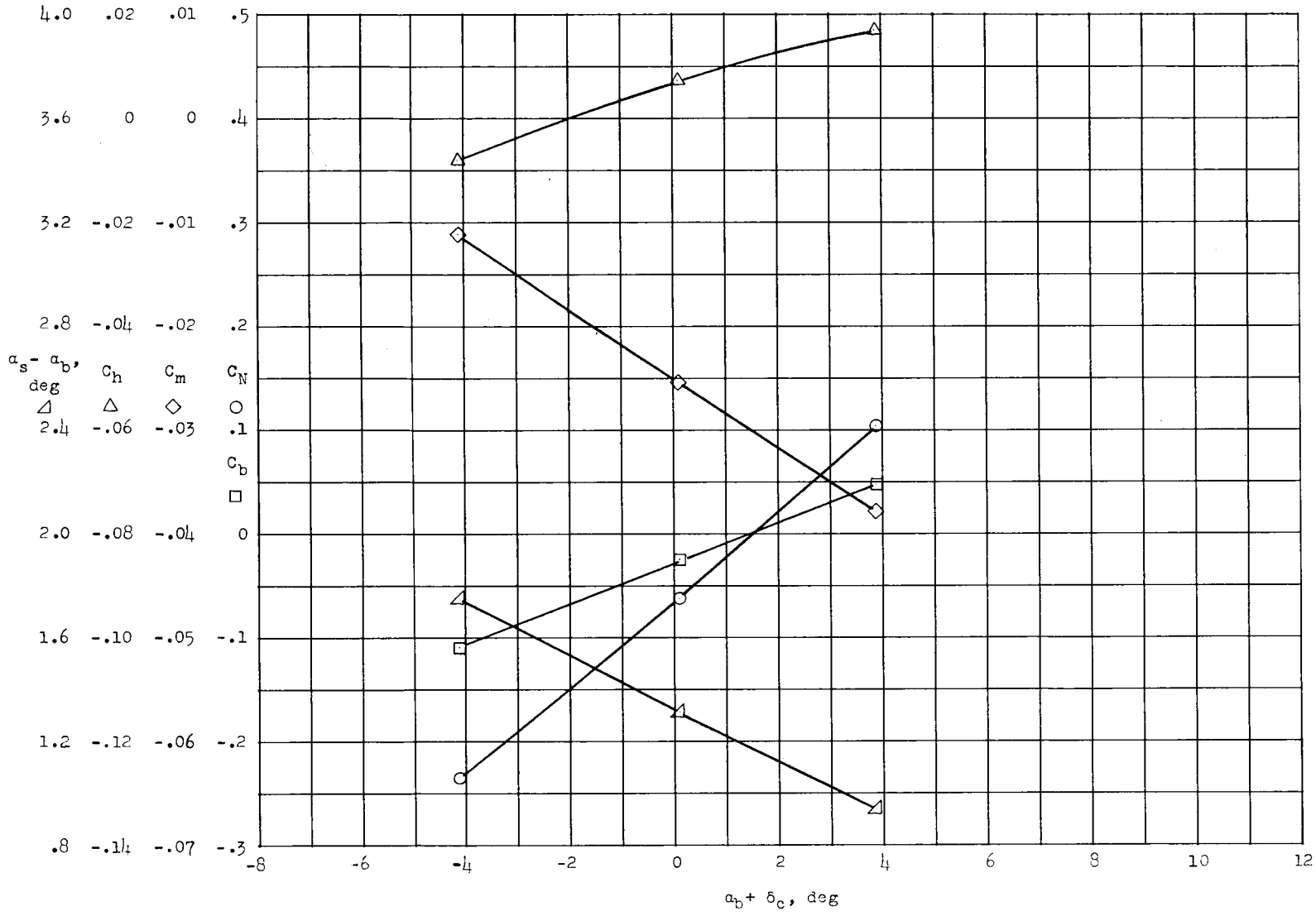

(b) $\alpha_b = 0°$.

Figure 43.- Concluded.

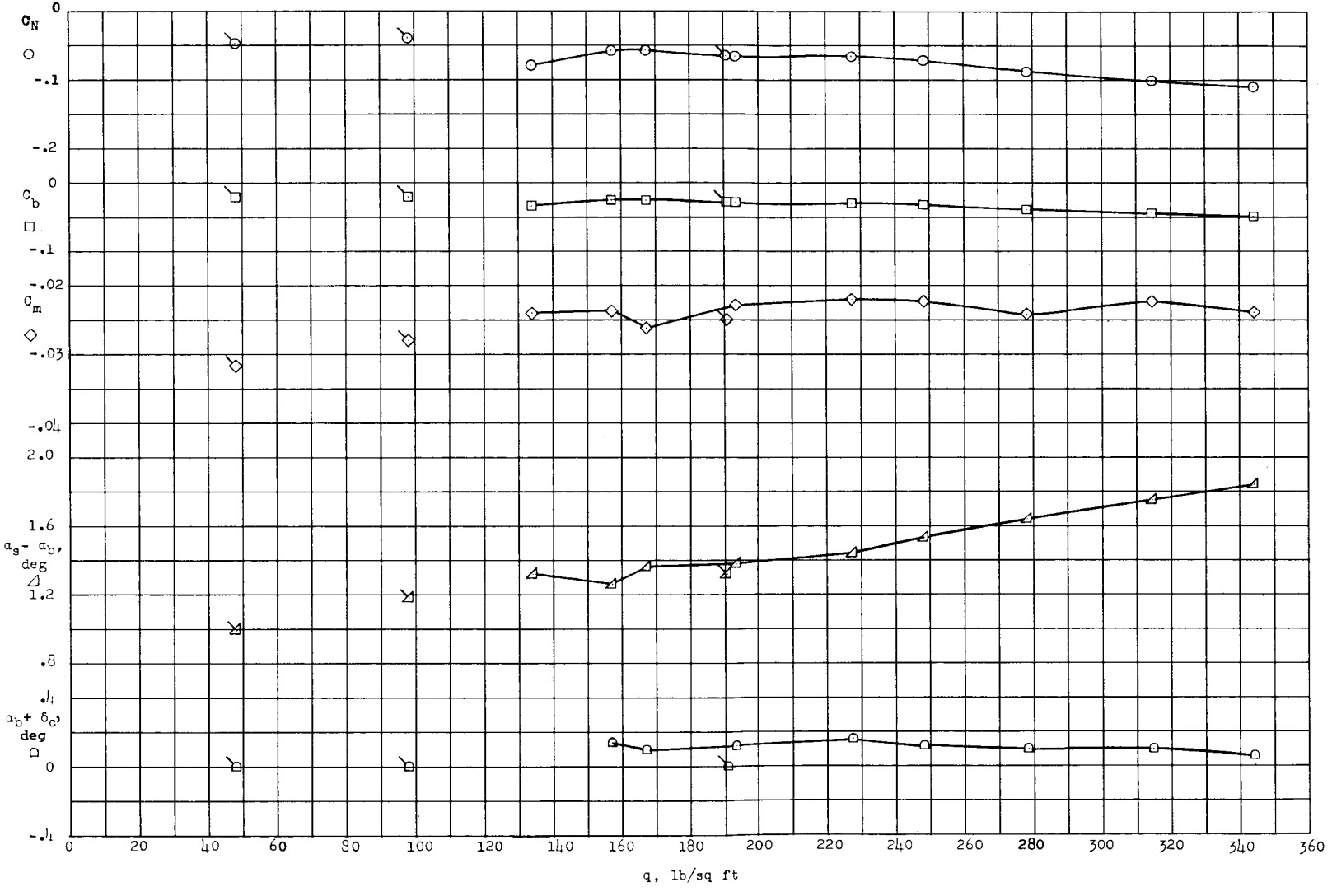

Figure 44.- Longitudinal aerodynamic characteristics of restrained canard in Freon-12 at $M = 0.92$ with $\delta_t \approx 0^\circ$, $\delta_c \approx 0^\circ$, and $\alpha_b = 0^\circ$. Flagged symbols indicate points reproduced from figures 41(b), 42(c), and 43(b).

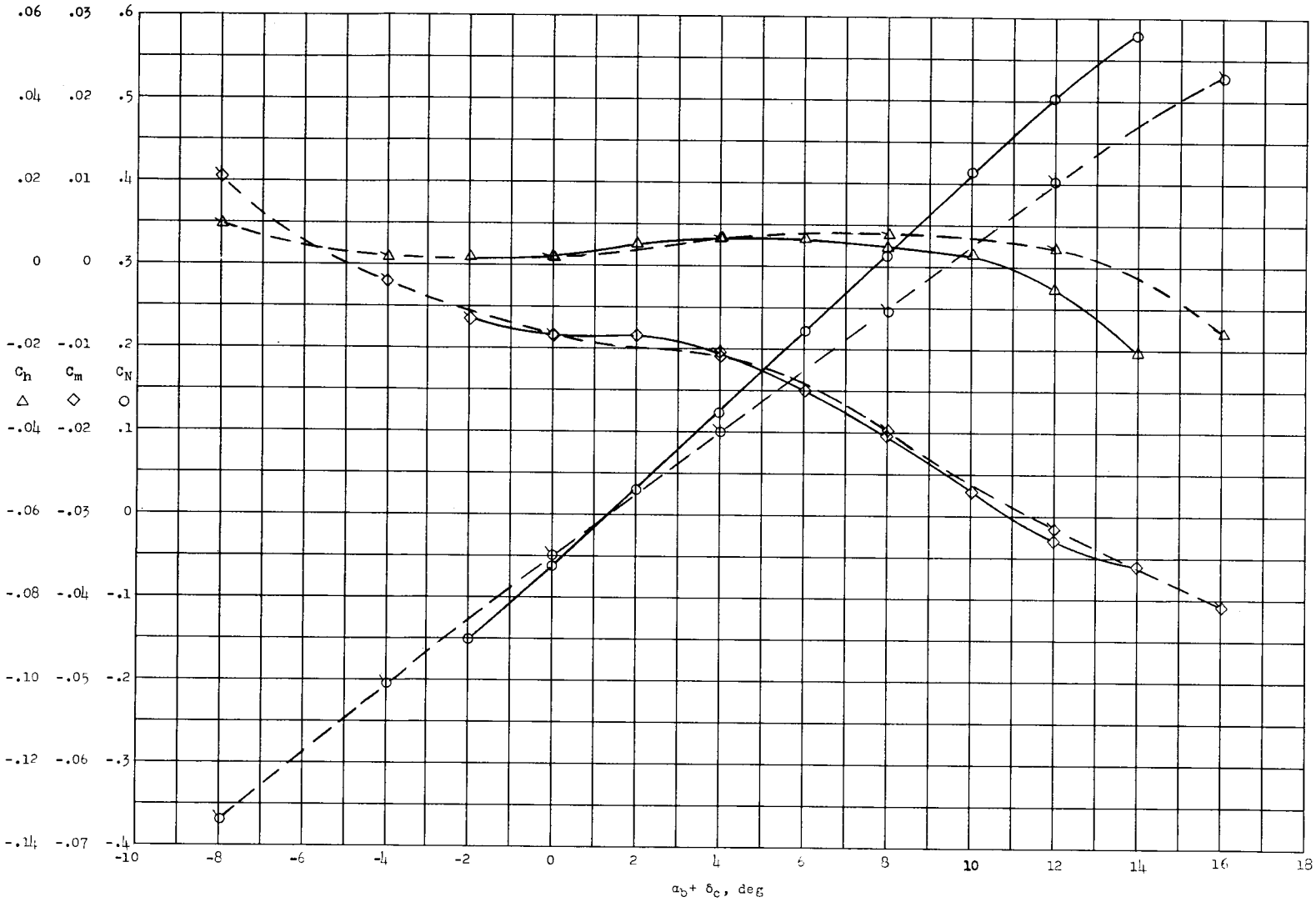

(a) M = 0.60.

Figure 45.- Comparison of test results obtained with $\delta_c = 0^o$ (plain symbols) and with $\alpha_b = 0^o$ (flagged symbols). Tests of restrained canard in air at q = 100 lb/sq ft with $\delta_t = 0^o$.

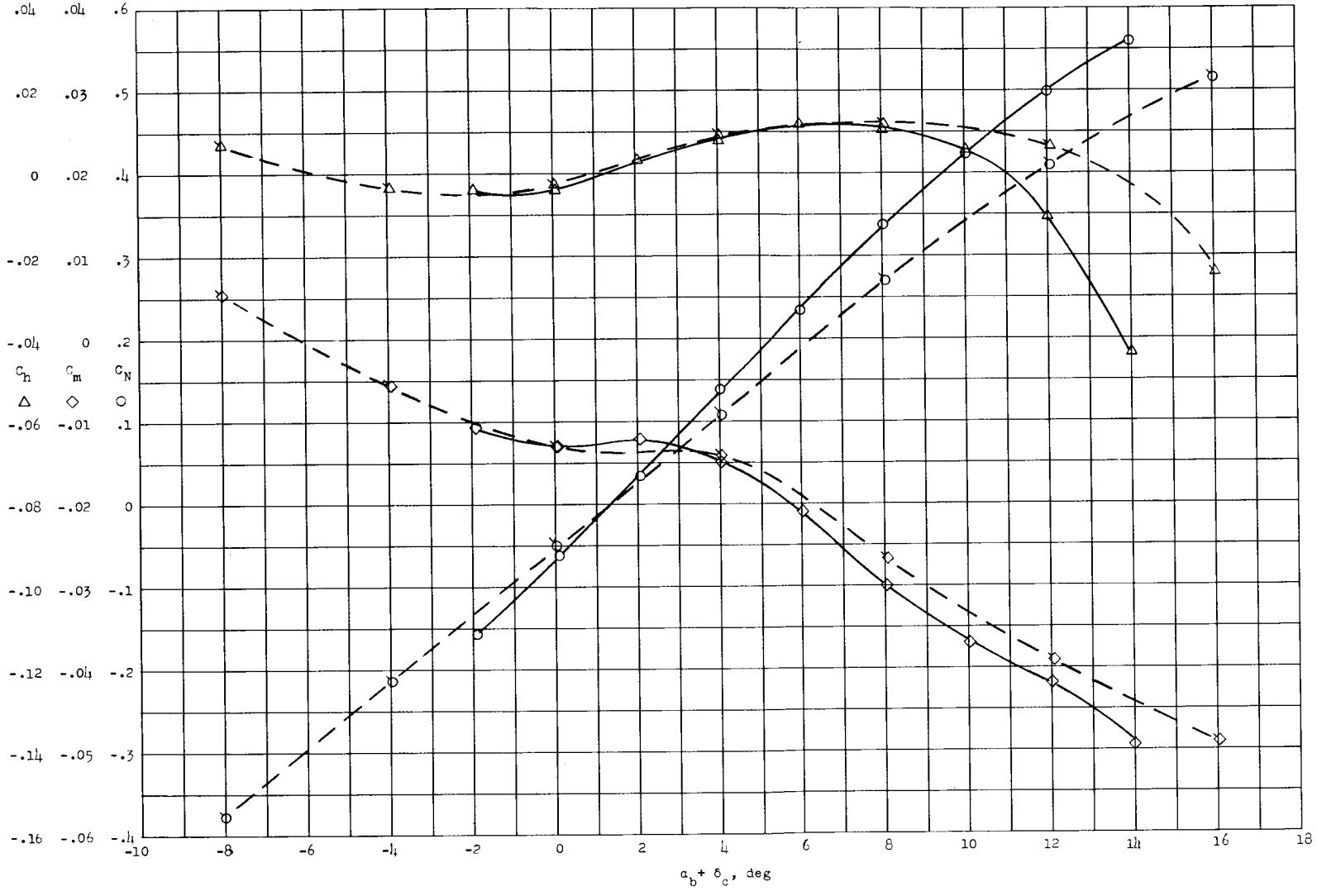

(b) M = 0.80.

Figure 45.- Continued.

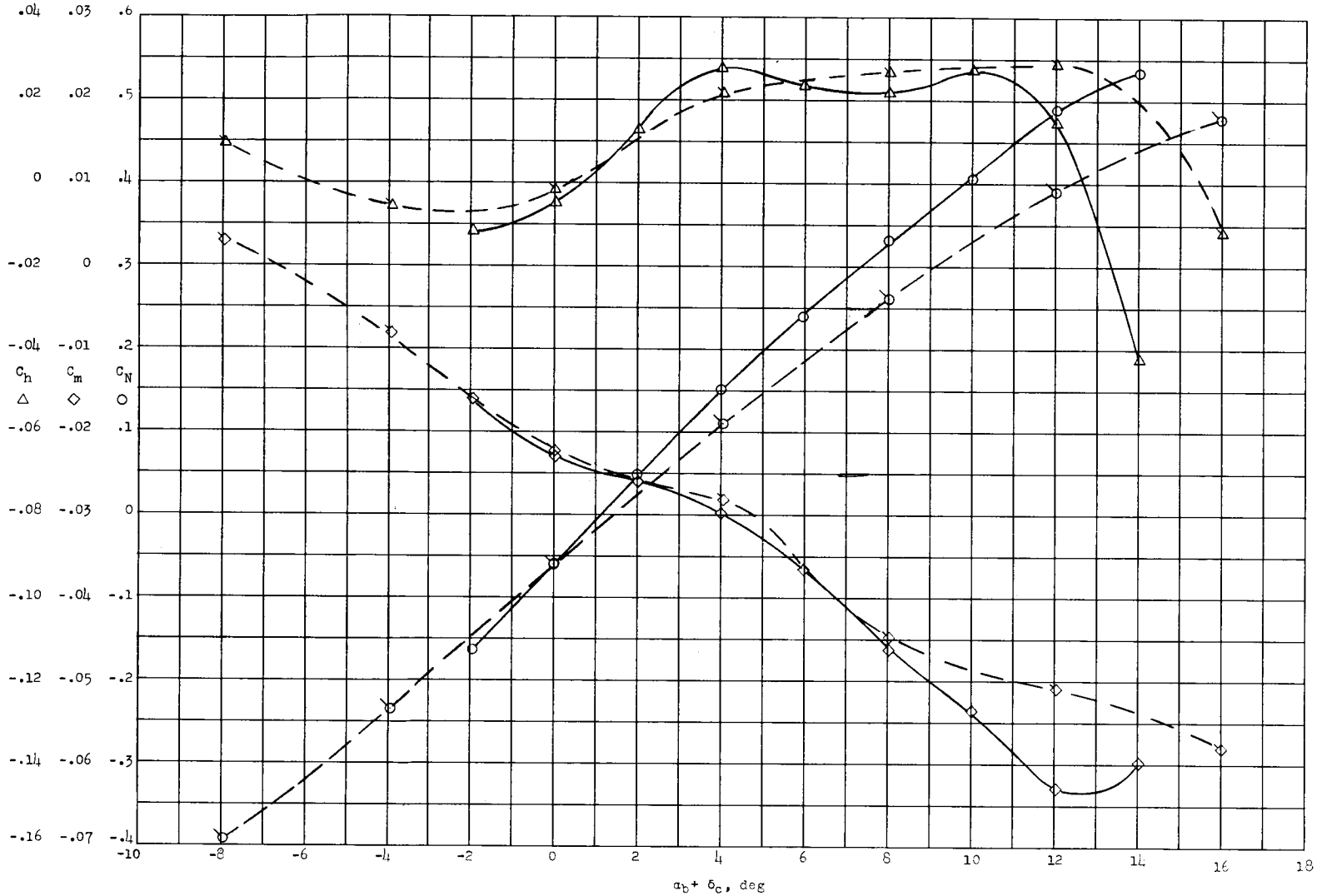

(c) M = 0.90.

Figure 45.- Continued.

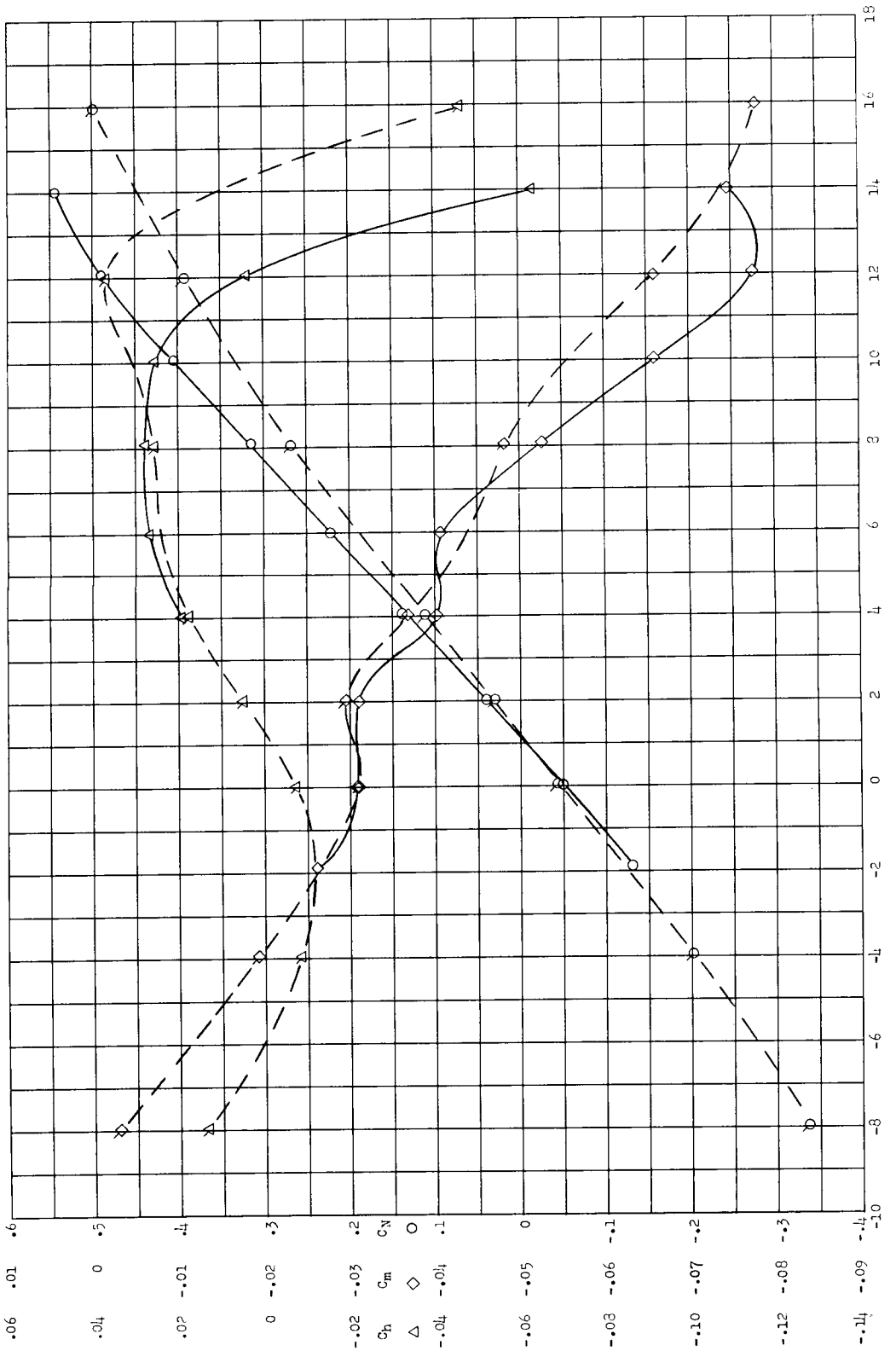

(d) M = 0.92.

Figure 45.- Concluded.

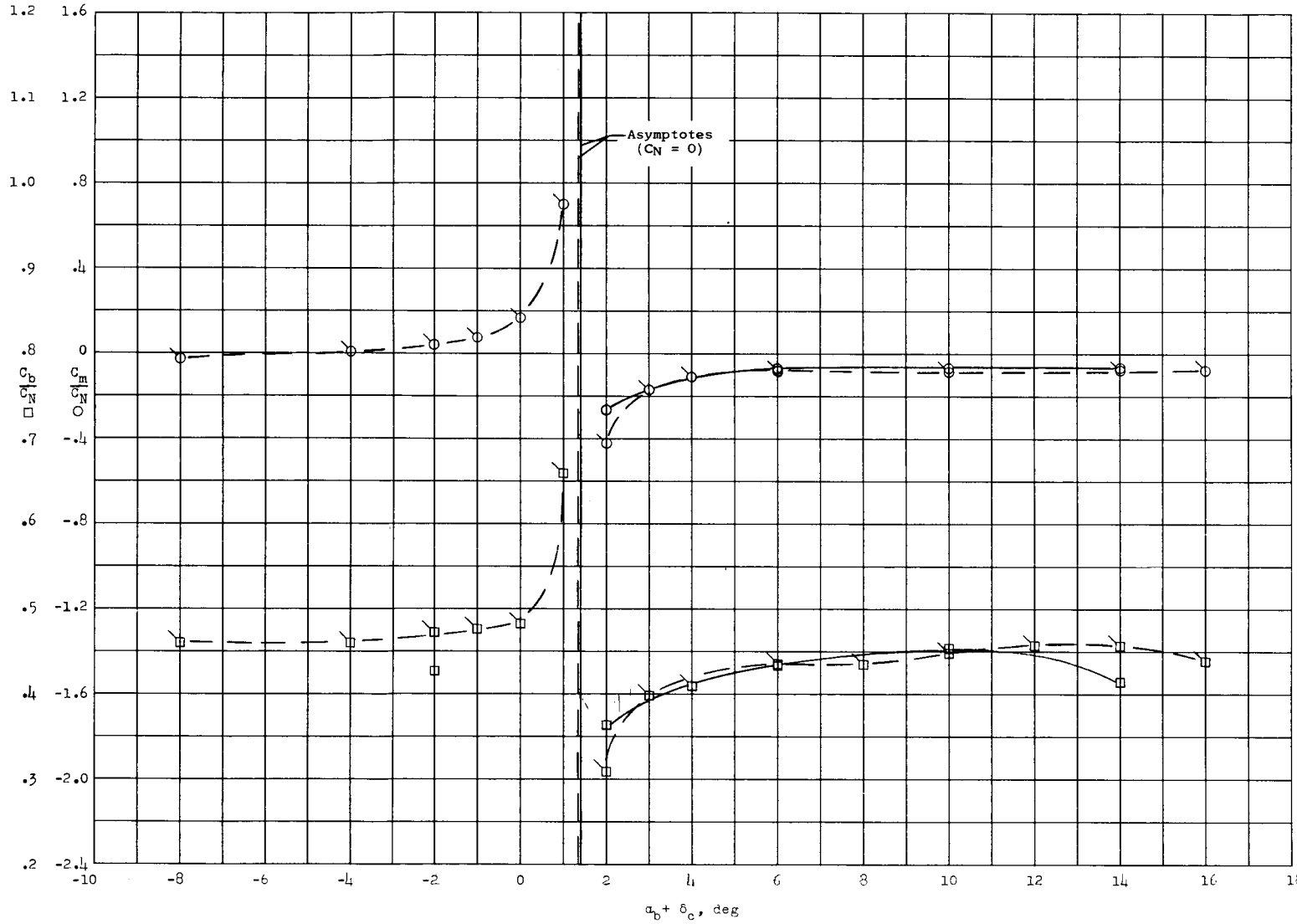

(a) M = 0.60.

Figure 46.- Comparison of center-of-pressure positions obtained with $\delta_c = 0^\circ$ (plain symbols) and with $\alpha_b = 0^\circ$ (flagged symbols). Tests of restrained canard in air at $q = 100$ lb/sq ft with $\delta_t = 0^\circ$.

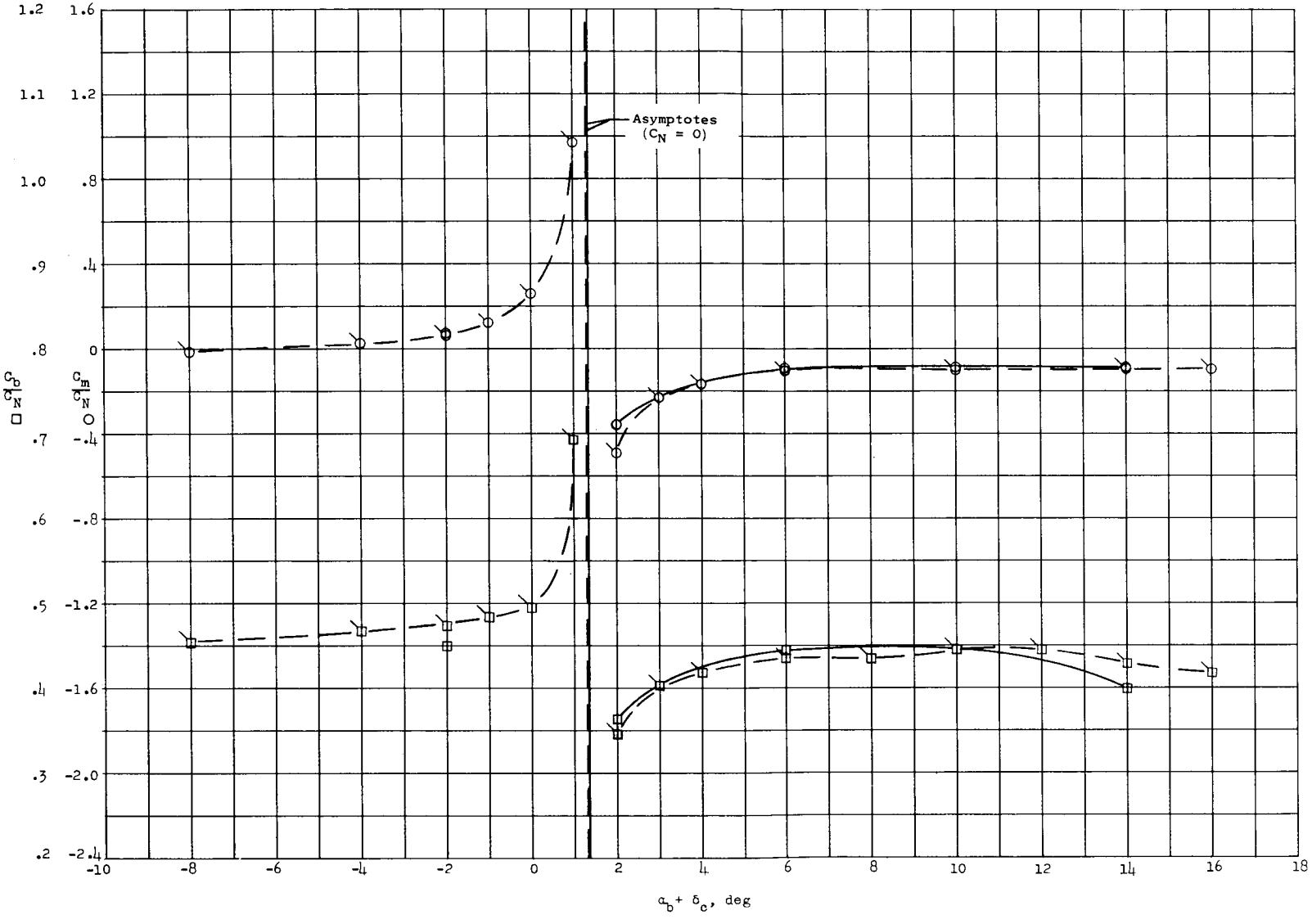

(b) M = 0.80.

Figure 46.- Continued.

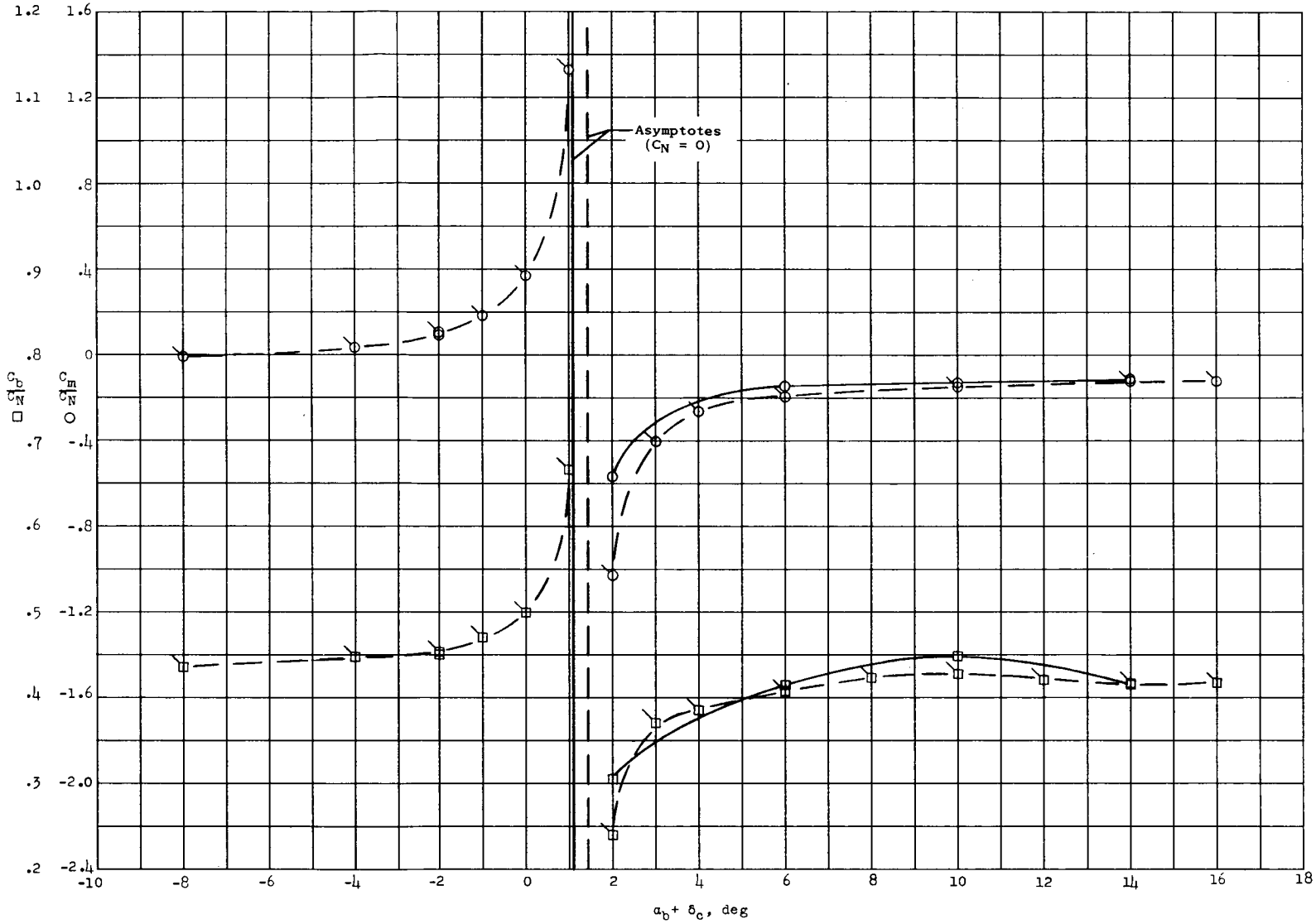

(c) M = 0.90.

Figure 46.- Continued.

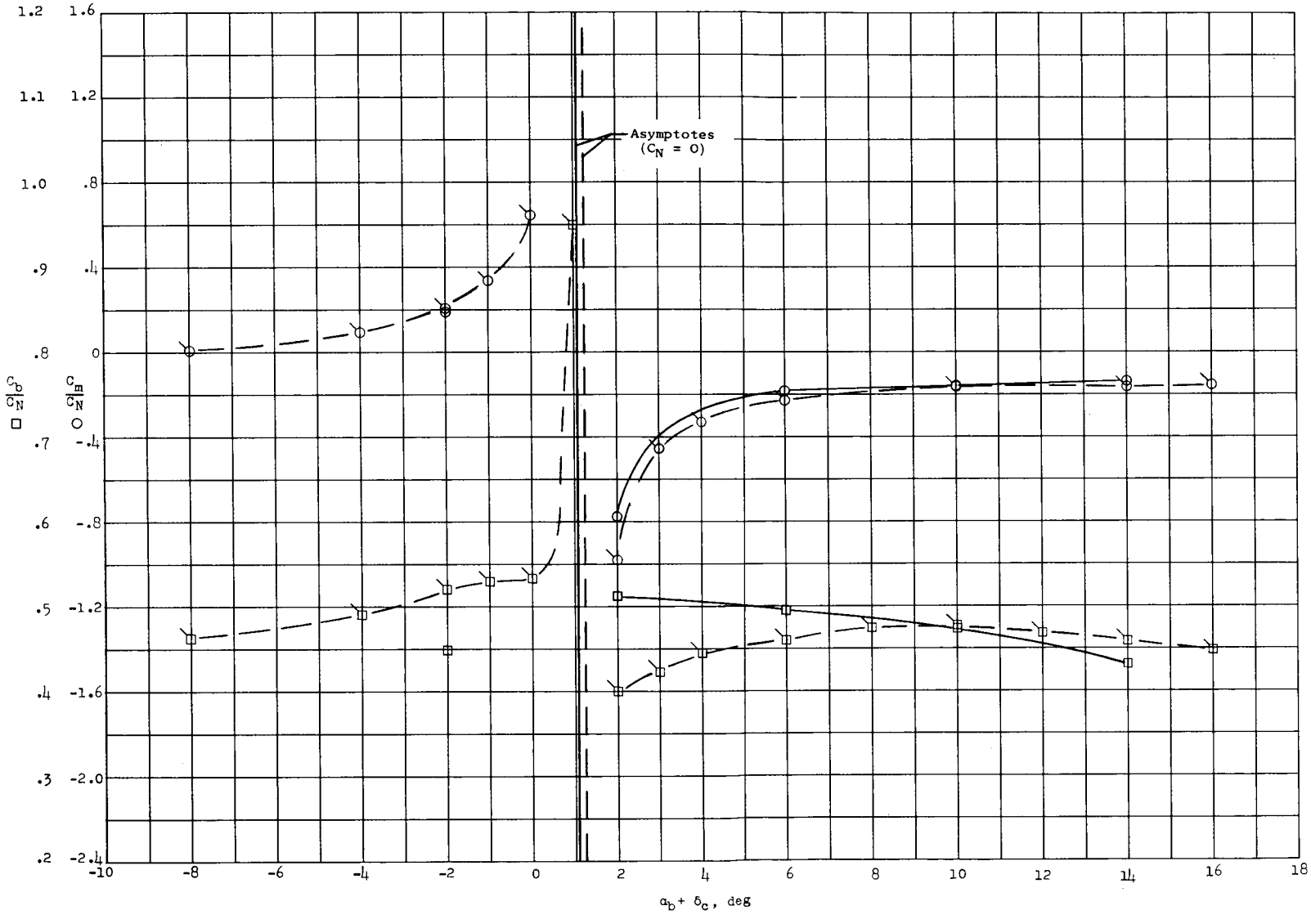

(d) M = 0.92.

Figure 46.- Concluded.

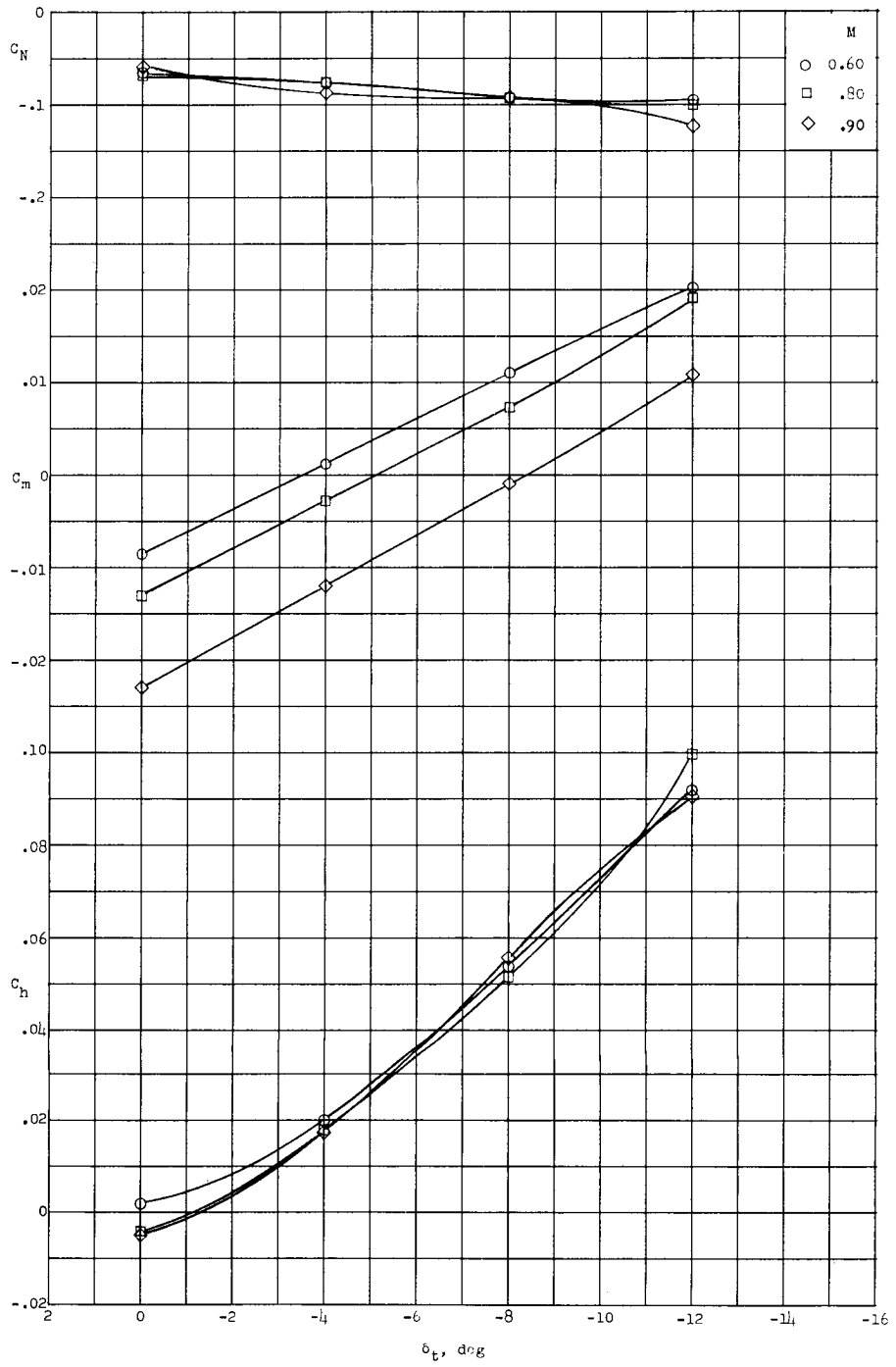

(a) Restrained canard; $\delta_c = 0^\circ$; $\alpha_b = 0^\circ$.

Figure 47.- Effect of tab deflection on aerodynamic characteristics measured in air at q = 100 lb/sq ft.

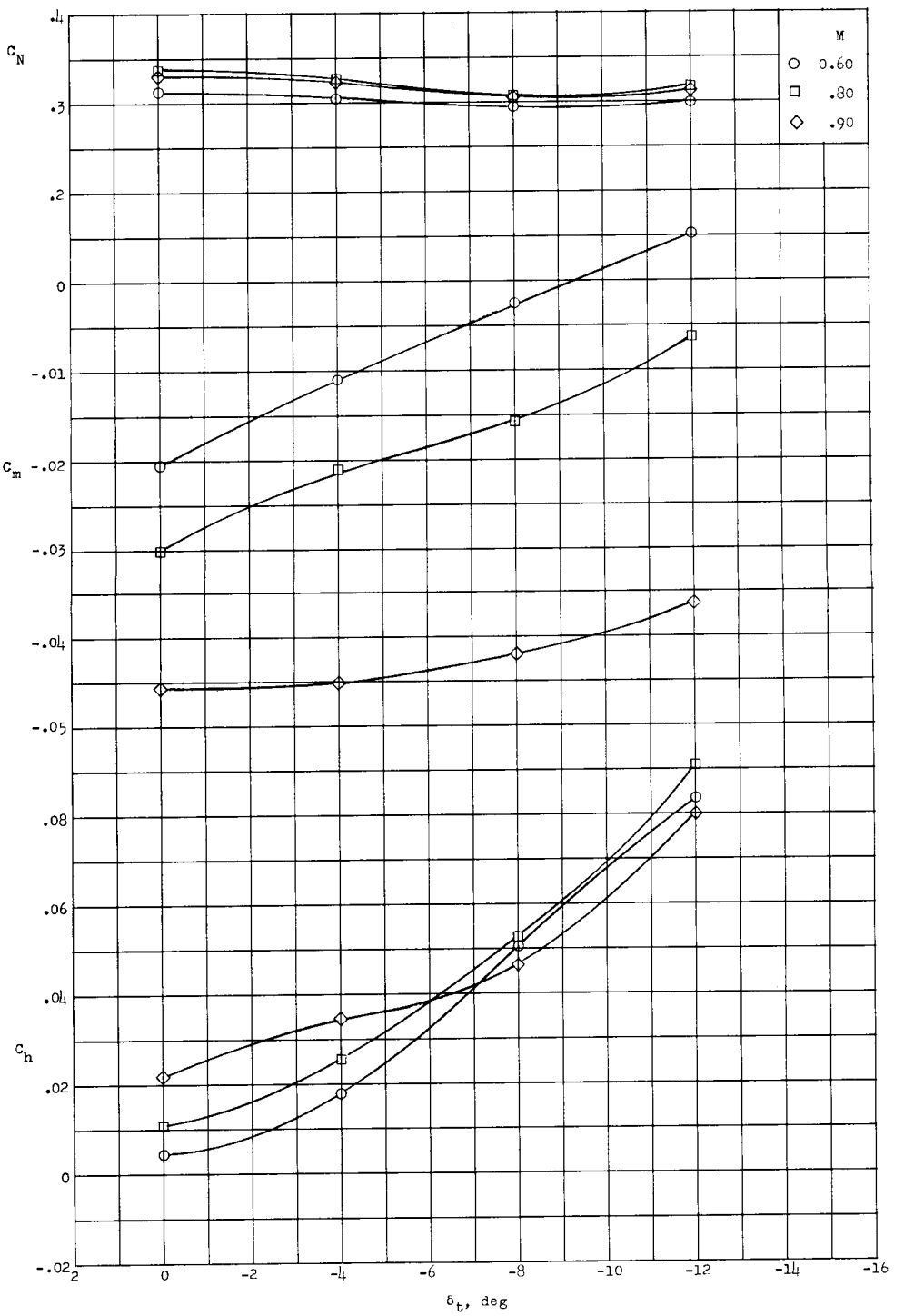

(b) Restrained canard; $\delta_c = 0^\circ$; $\alpha_b = 8^\circ$.

Figure 47.- Continued.

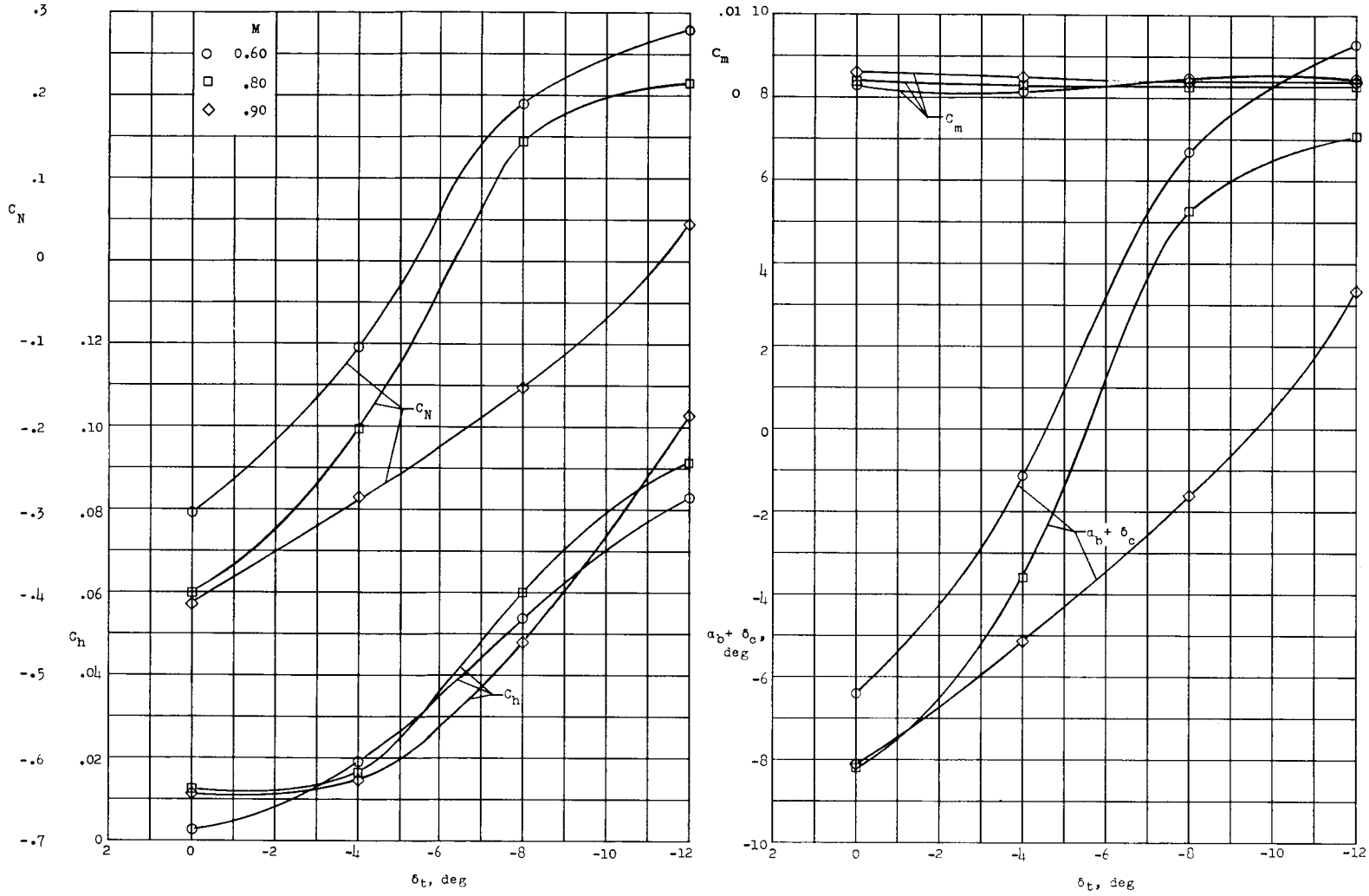

(c) Free canard; $\alpha_b = 0^\circ$.

Figure 47.- Continued.

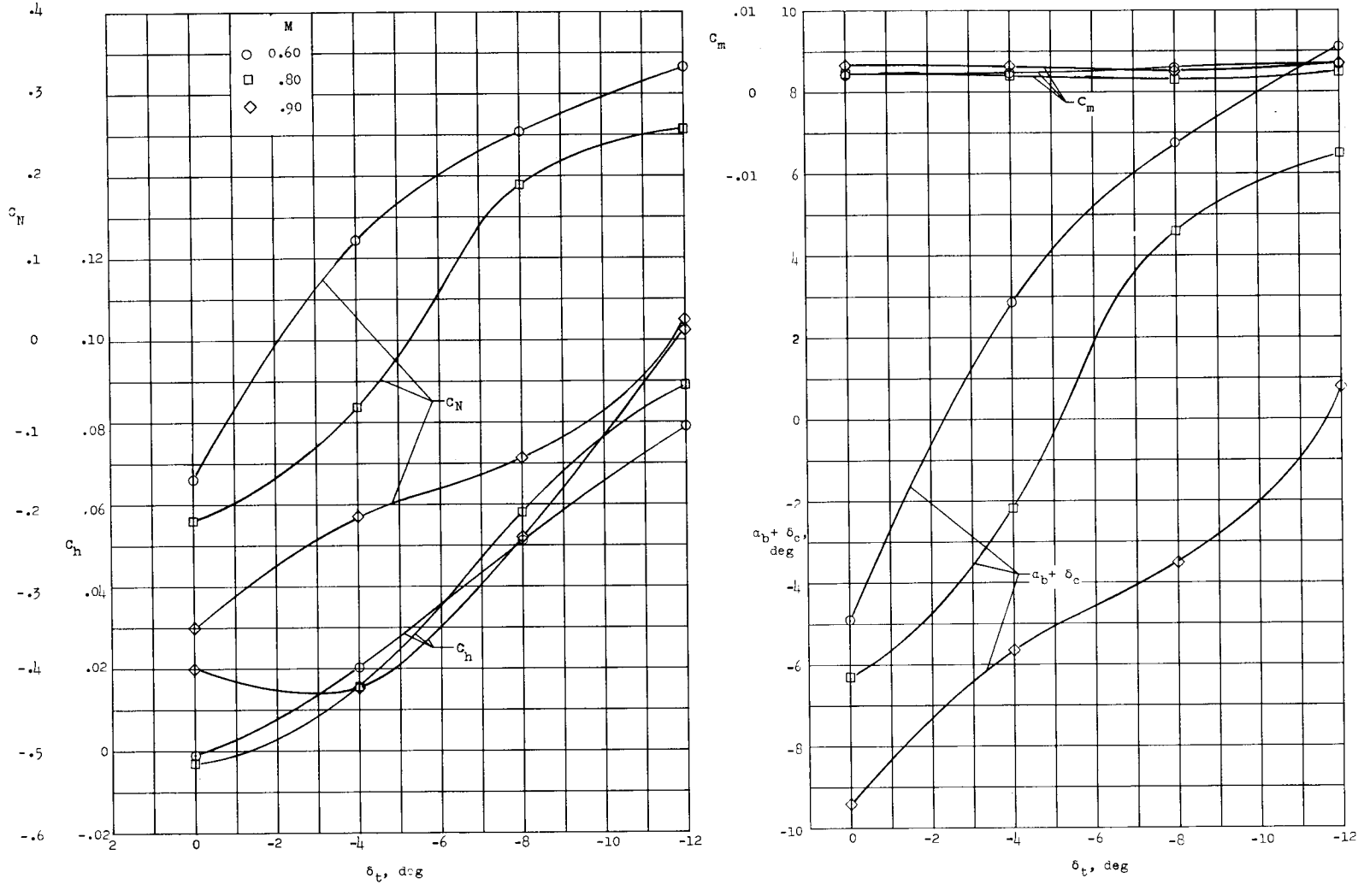

(d) Free canard; $\alpha_b = 8^\circ$.

Figure 47.- Concluded.

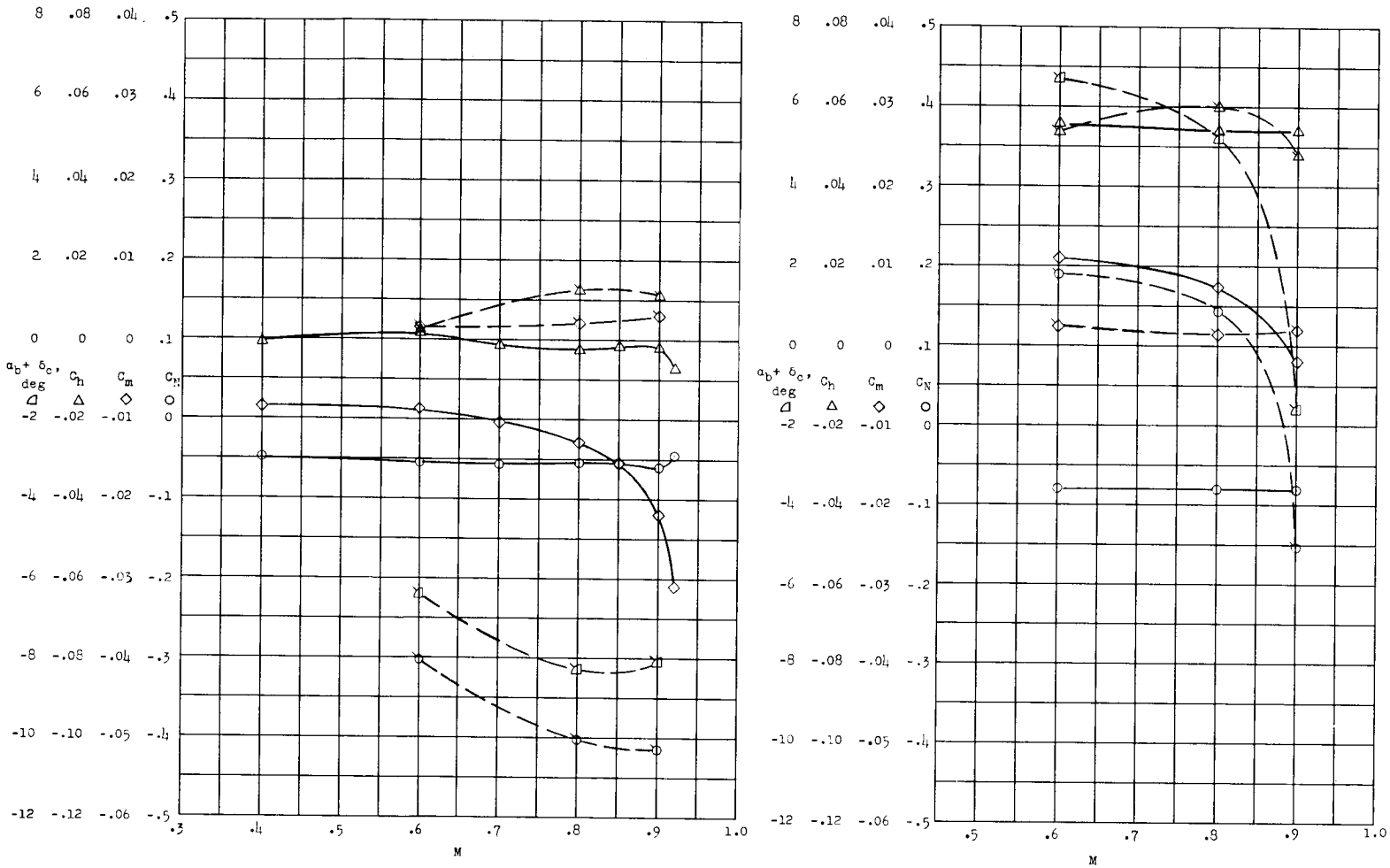

(a) $\alpha_b = 0^\circ$; $\delta_t = 0^\circ$.

(b) $\alpha_b = 0^\circ$; $\delta_t = -8^\circ$.

Figure 48.- Effect of Mach number on aerodynamic characteristics measured in air at $q = 100$ lb/sq ft. Plain symbols indicate restrained canard with $\delta_c = 0^\circ$; flagged symbols indicate free canard.

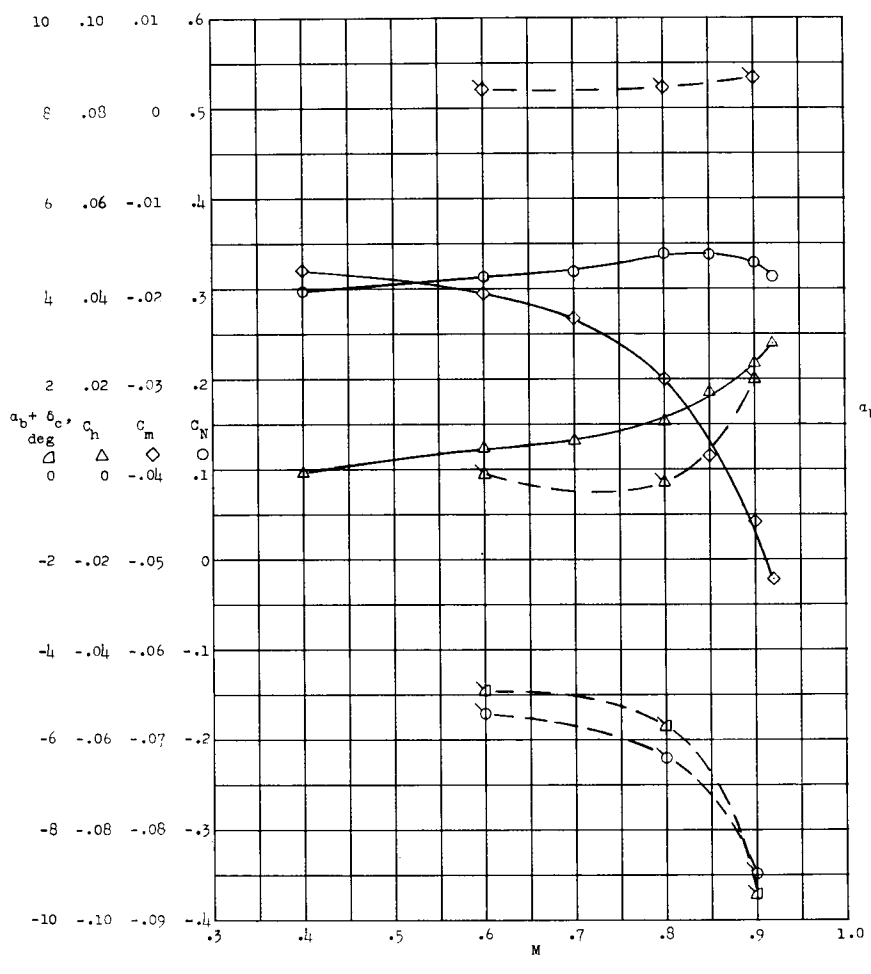

(c) $\alpha_b = 8^\circ$; $\delta_t = 0^\circ$.

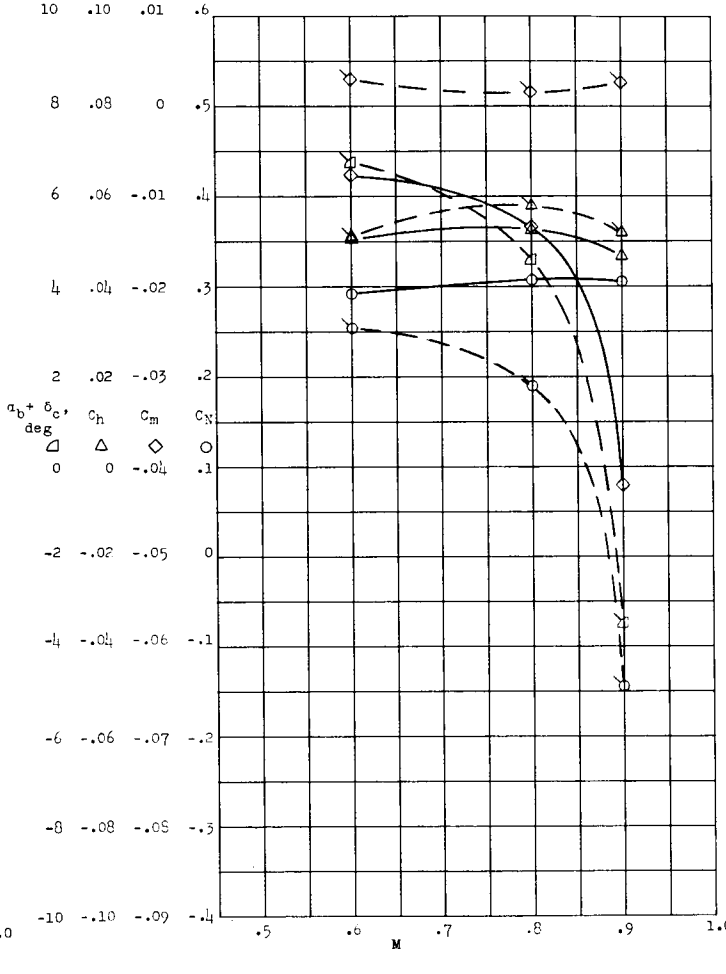

(d) $\alpha_b = 8^\circ$; $\delta_t = -8^\circ$

Figure 48.- Concluded.

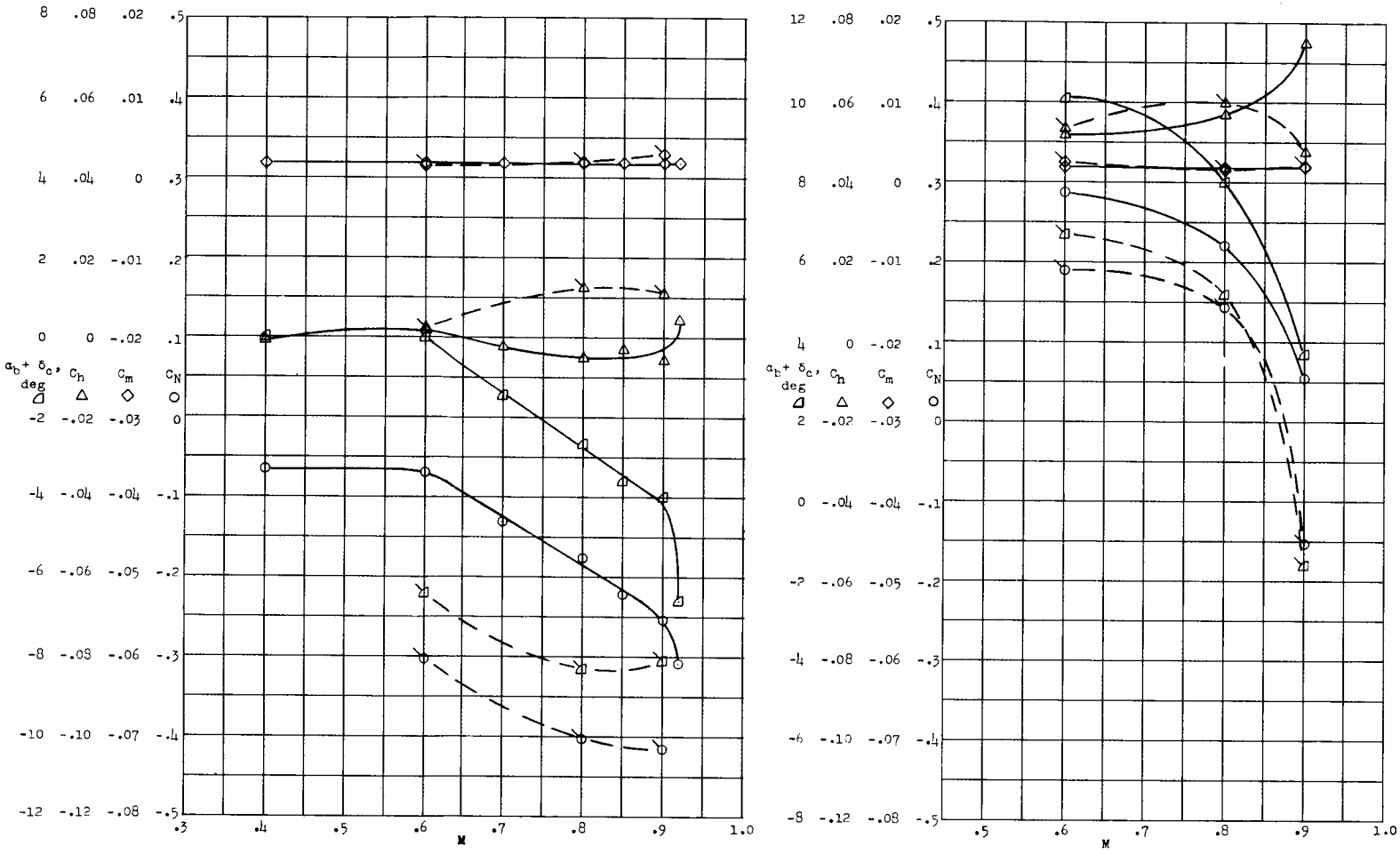

(a) $\delta_t = 0^\circ$.

(b) $\delta_t = -8^\circ$.

Figure 49.- Comparison of aerodynamic properties in air for free canard with trailing-edge ballast (plain symbols) and corresponding properties for free, balanced canard (flagged symbols).

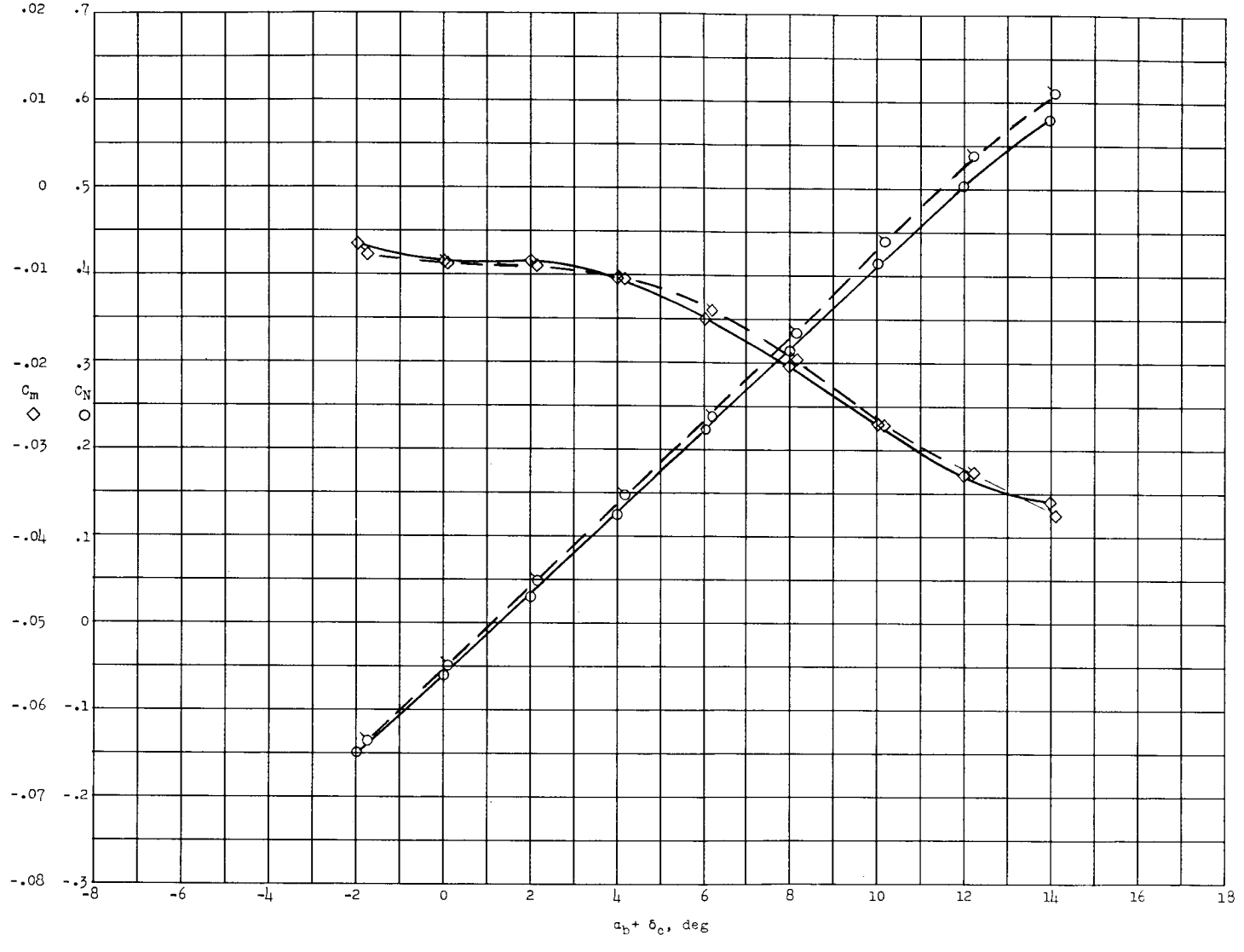

(a) M = 0.60.

Figure 50.- Comparison of normal force and pitching moment obtained from tests of restrained canard in air (plain symbols) and in Freon-12 (flagged symbols). q = 100 lb/sq ft; $\delta_c = 0^\circ$; $\delta_t = 0^\circ$.

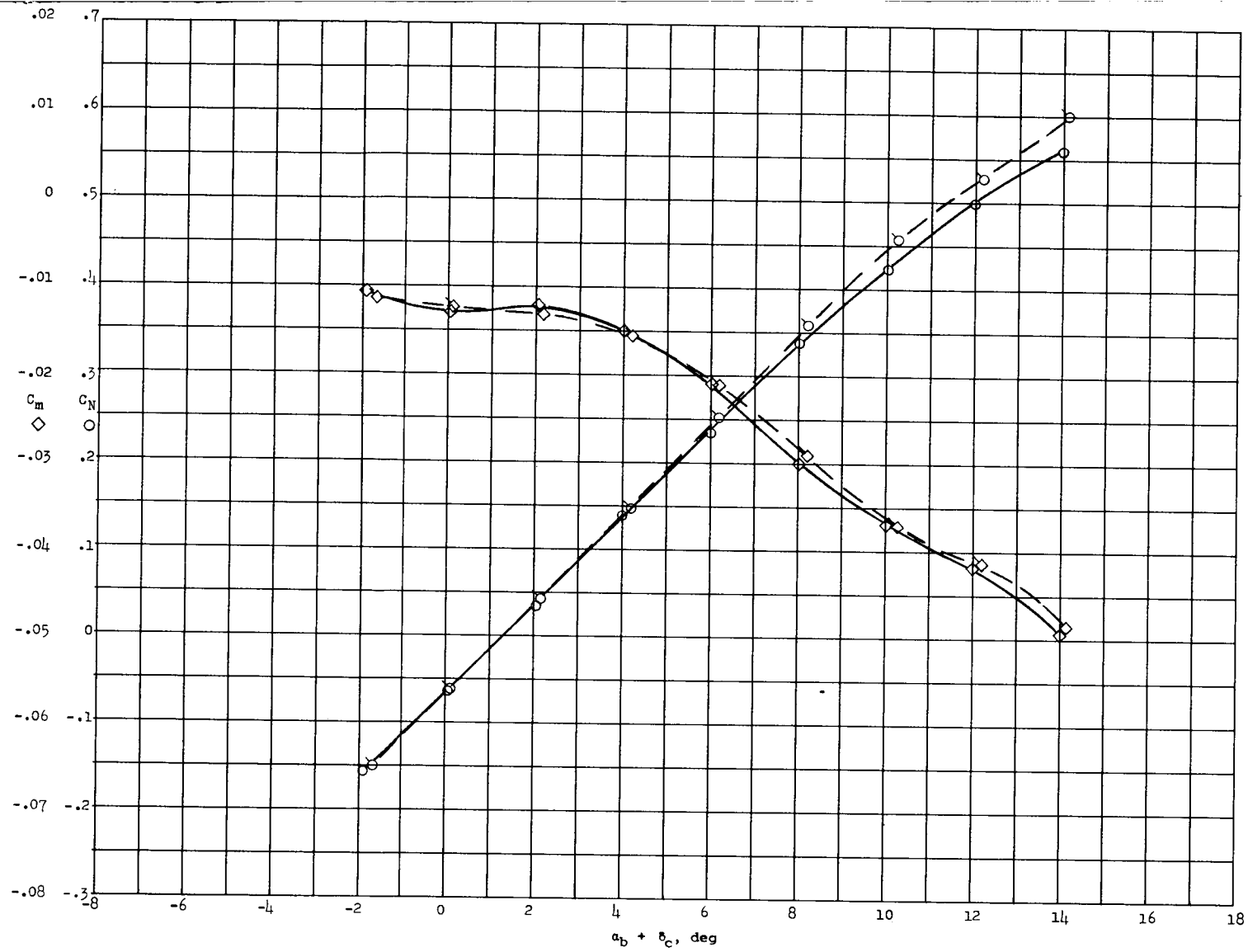

(b) M = 0.80.

Figure 50.- Continued.

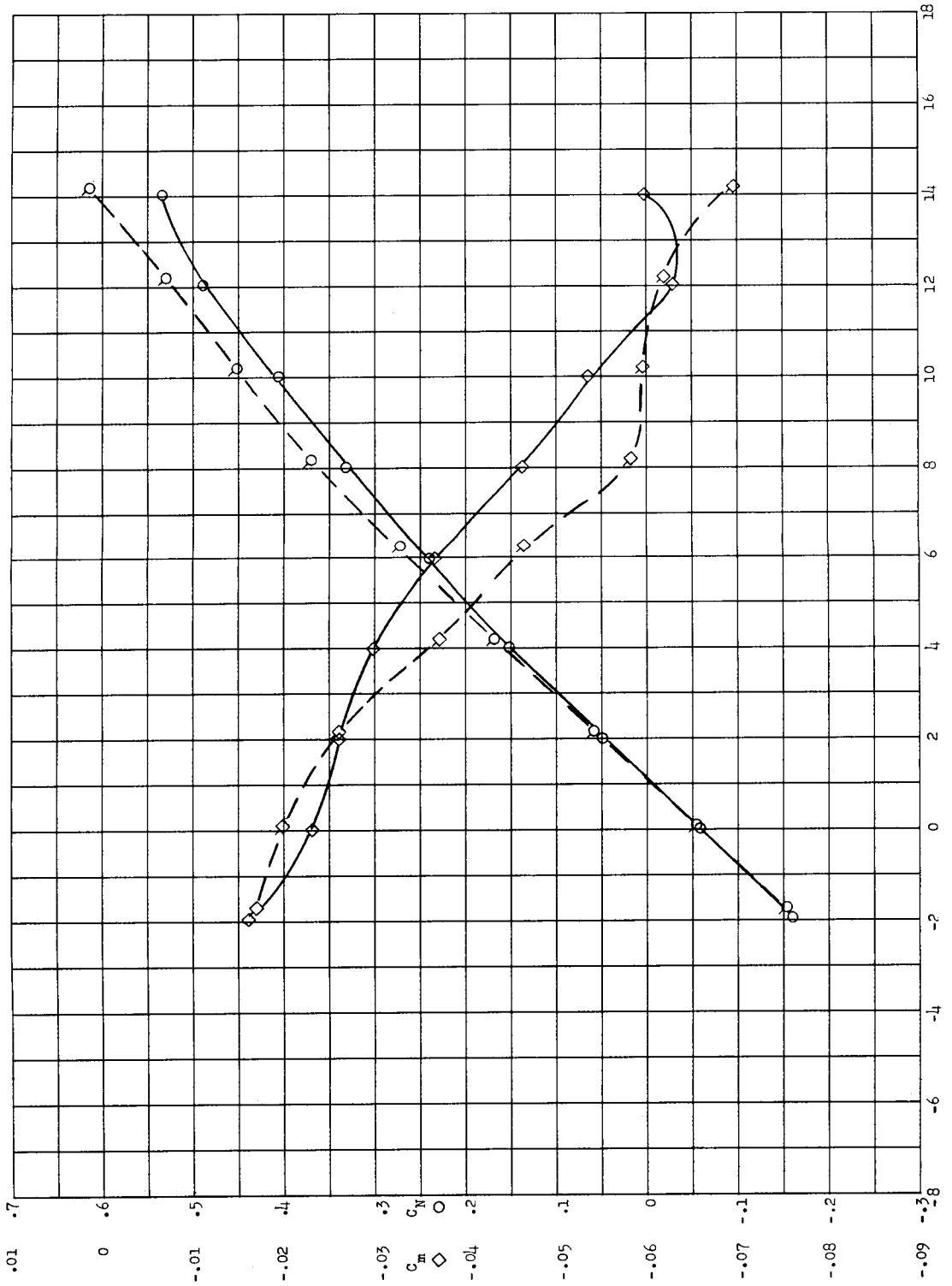

(c) M = 0.90.

Figure 50.- Continued.

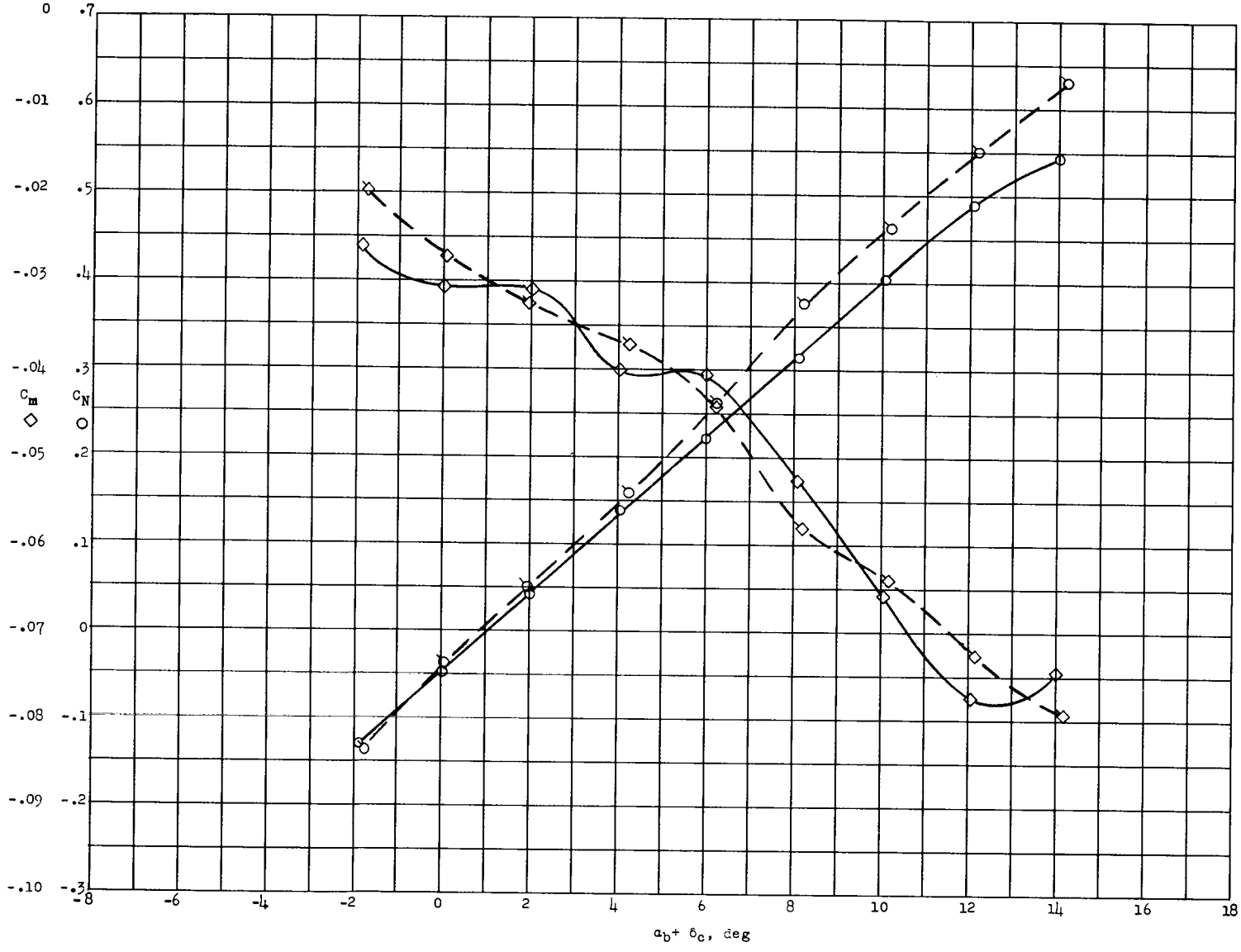

(d) M = 0.92.

Figure 50.- Concluded.

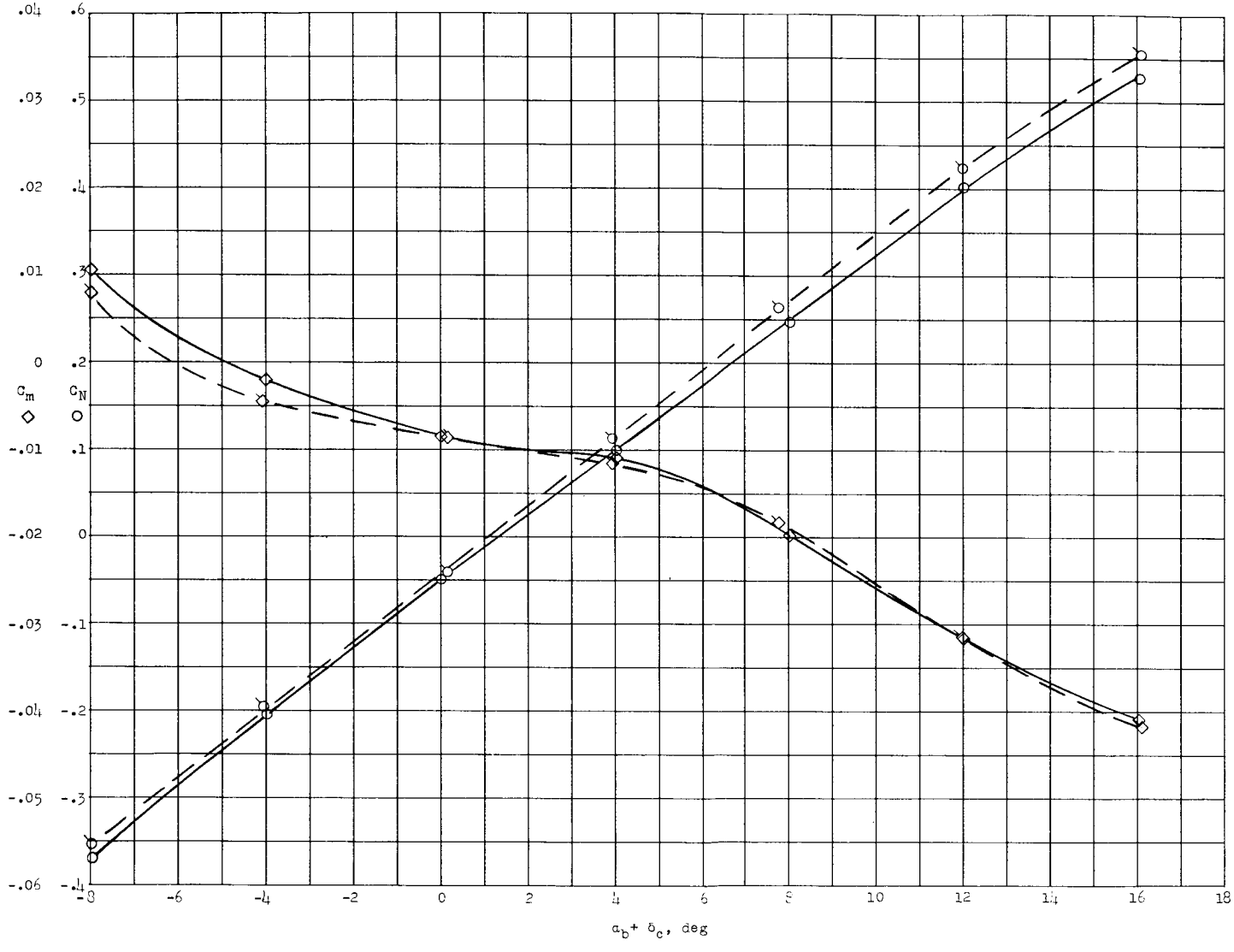

(a) M = 0.60.

Figure 51.- Comparison of normal force and pitching moment obtained from tests of restrained canard in air (plain symbols) and in Freon-12 (flagged symbols). q = 100 lb/sq ft; $\alpha_b = 0^o$; $\delta_t = 0^o$.

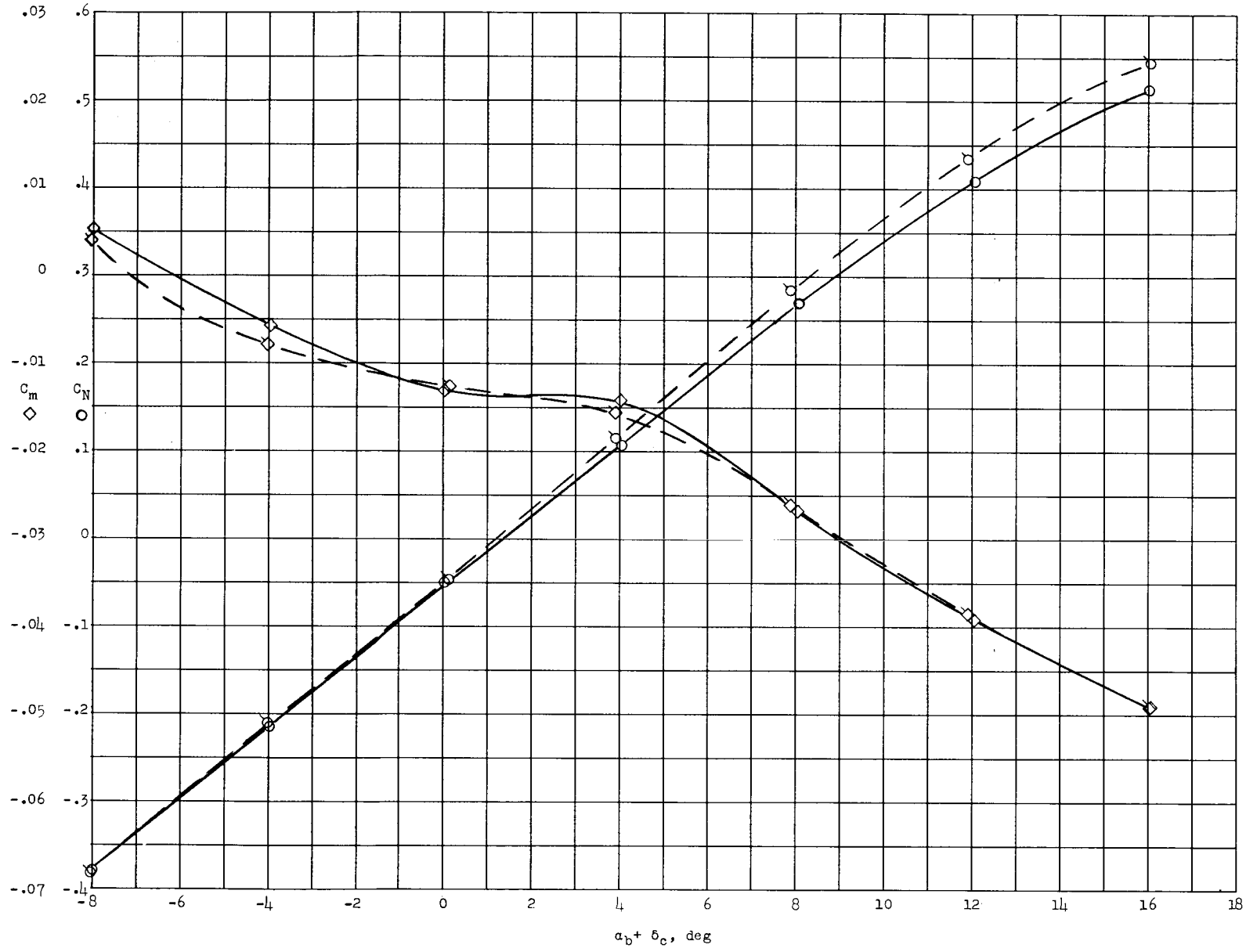

(b) M = 0.80.

Figure 51.- Continued.

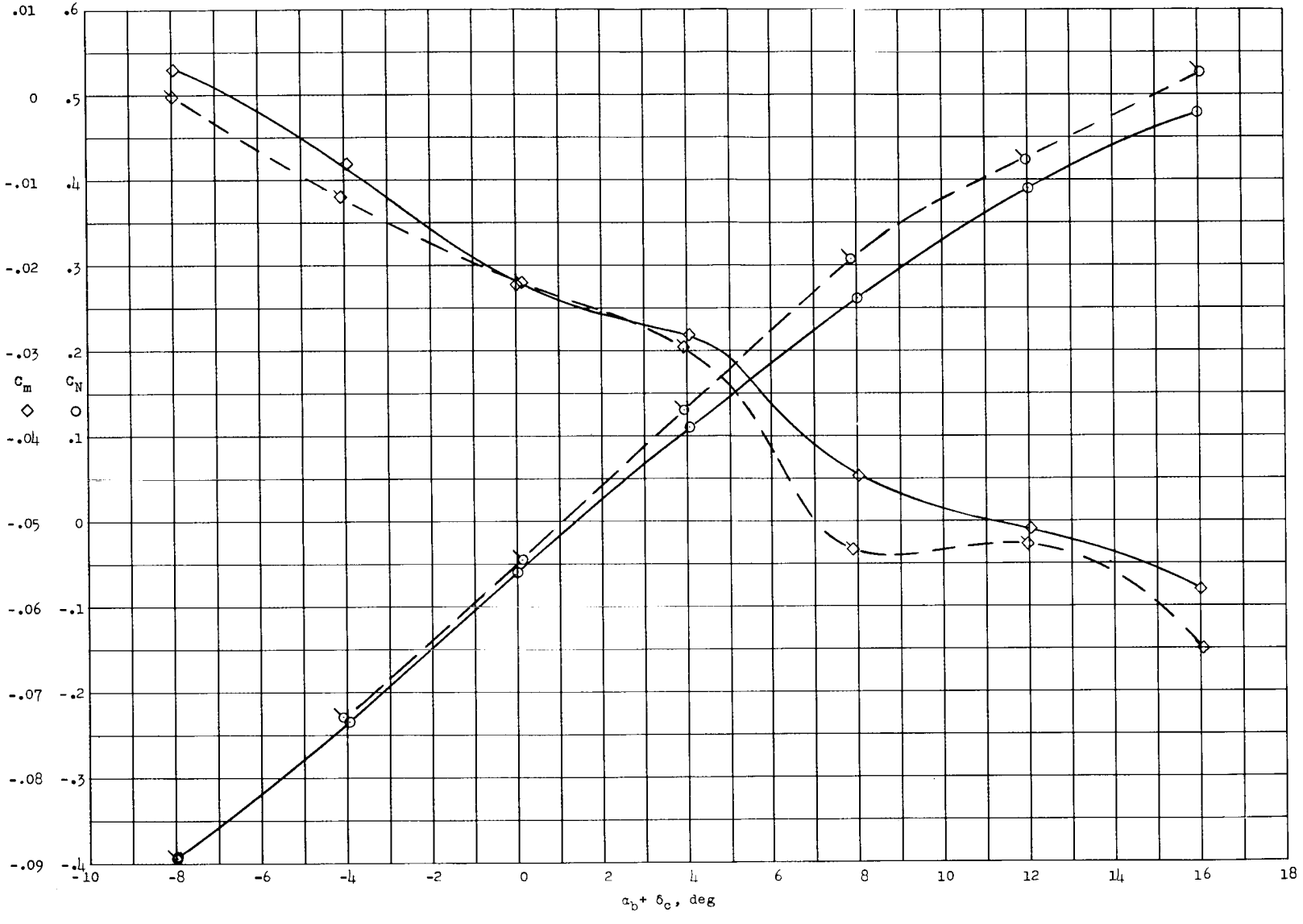

(c) M = 0.90.

Figure 51.- Continued.

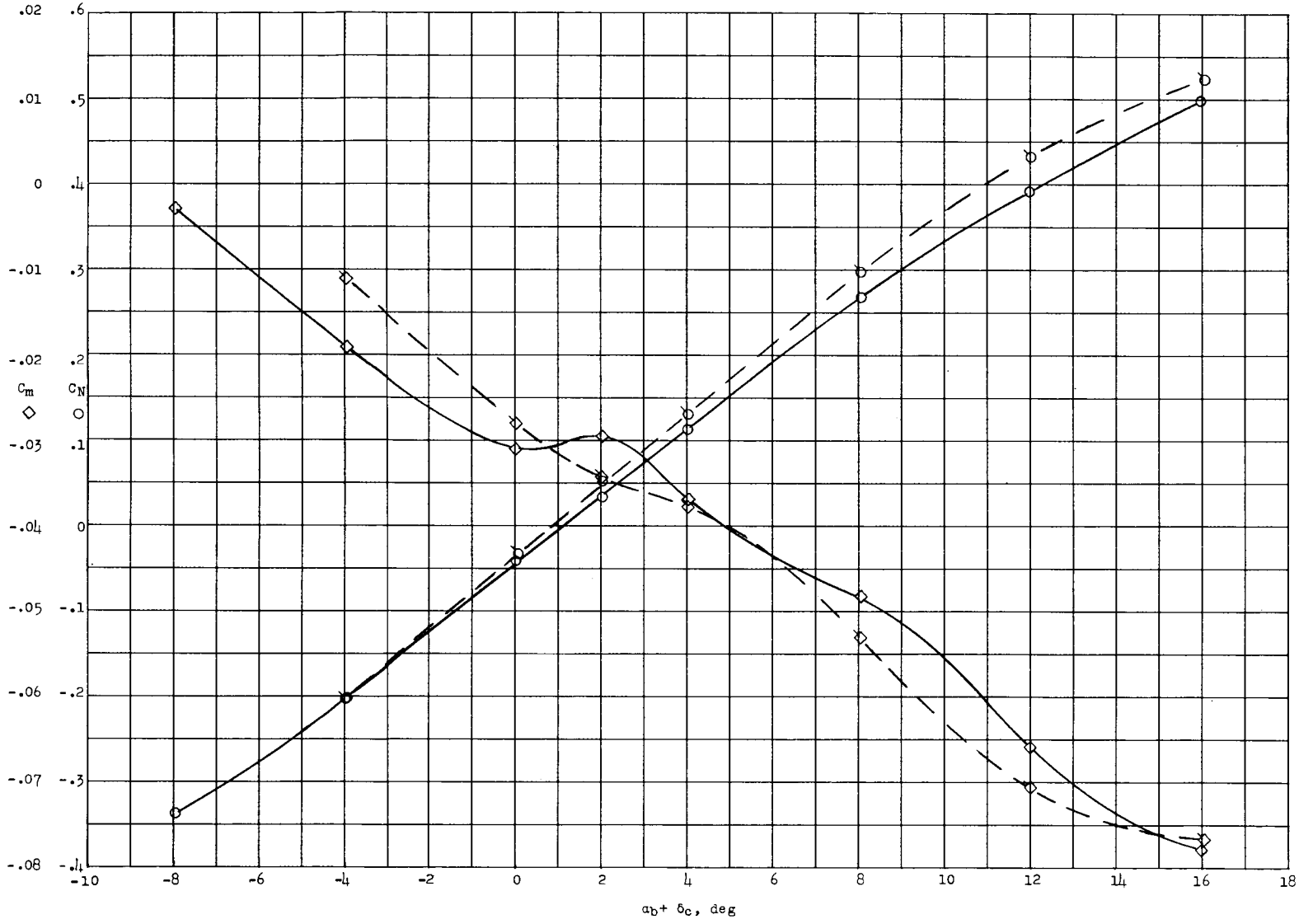

(d) M = 0.92.

Figure 51.- Concluded.

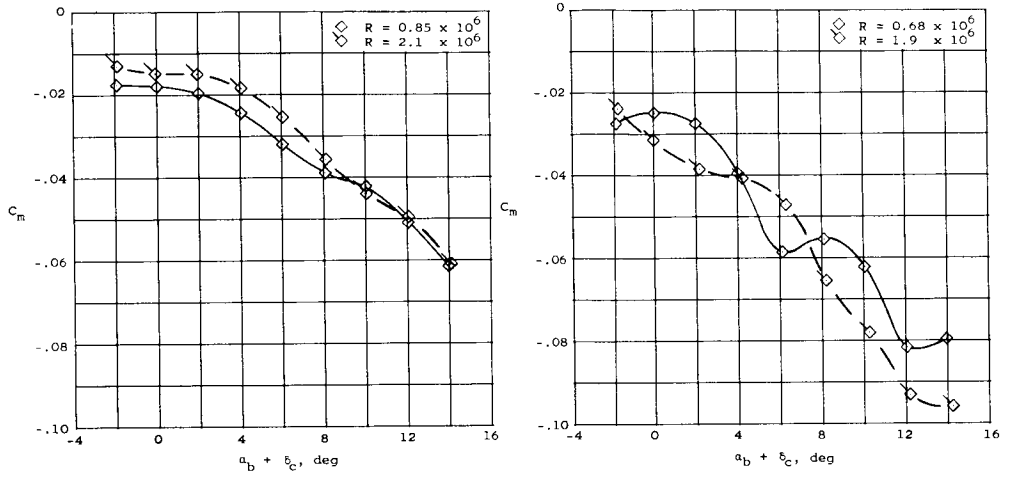

(a) M = 0.80; q = 50 lb/sq ft.

(b) M = 0.92; q = 50 lb/sq ft.

(c) M = 0.80; q = 100 lb/sq ft.

(d) M = 0.92; q = 100 lb/sq ft.

Figure 52.- Comparison of pitching-moment coefficients for restrained canard in air (plain symbols) and in Freon-12 (flagged symbols). $\delta_t = 0^\circ$; $\delta_c = 0^\circ$.

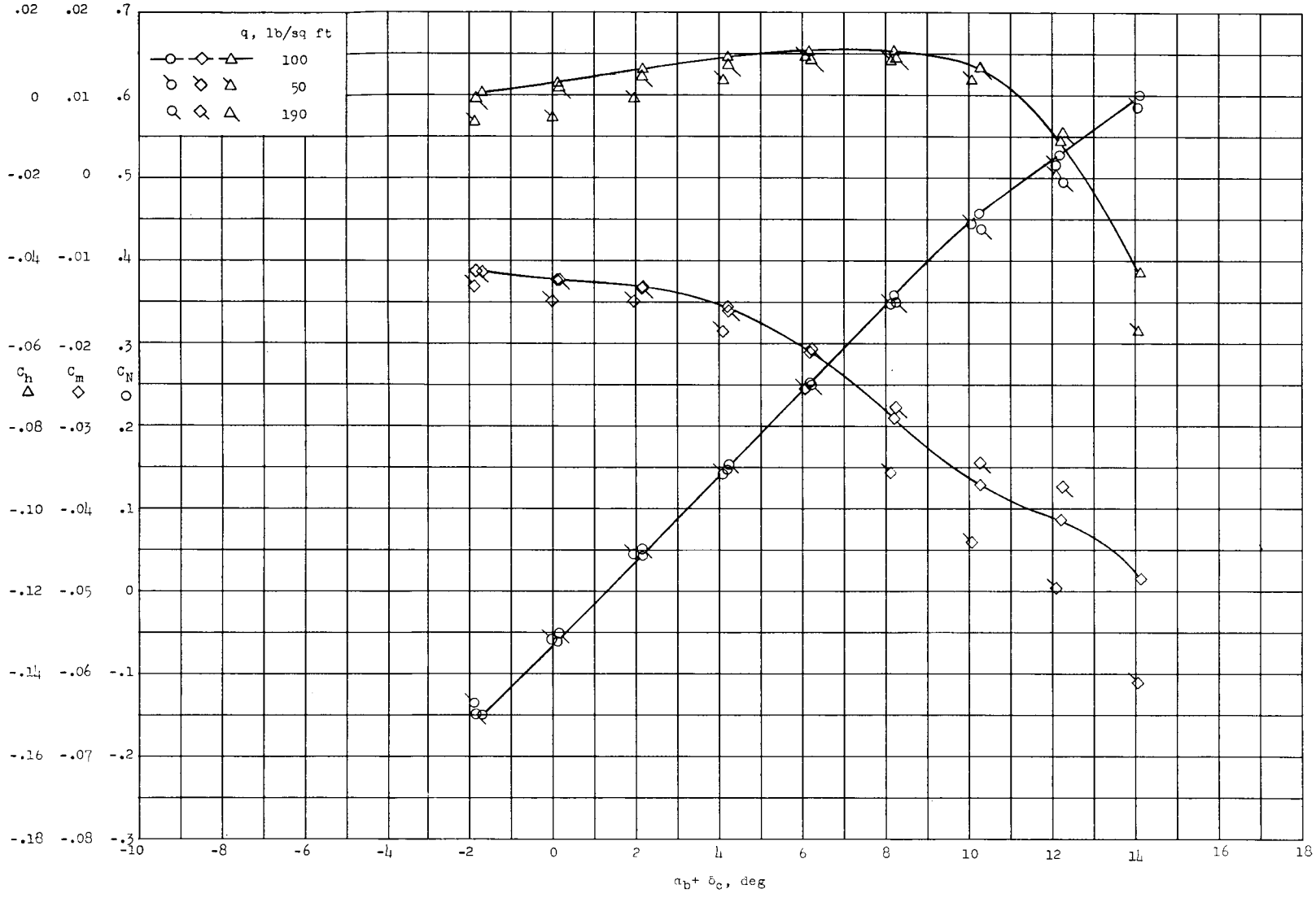

(a) M = 0.80.

Figure 53.- Comparison of aerodynamic characteristics for restrained canard in Freon-12 at different levels of dynamic pressure. $\delta_c = 0^o$; $\delta_t = 0^o$.

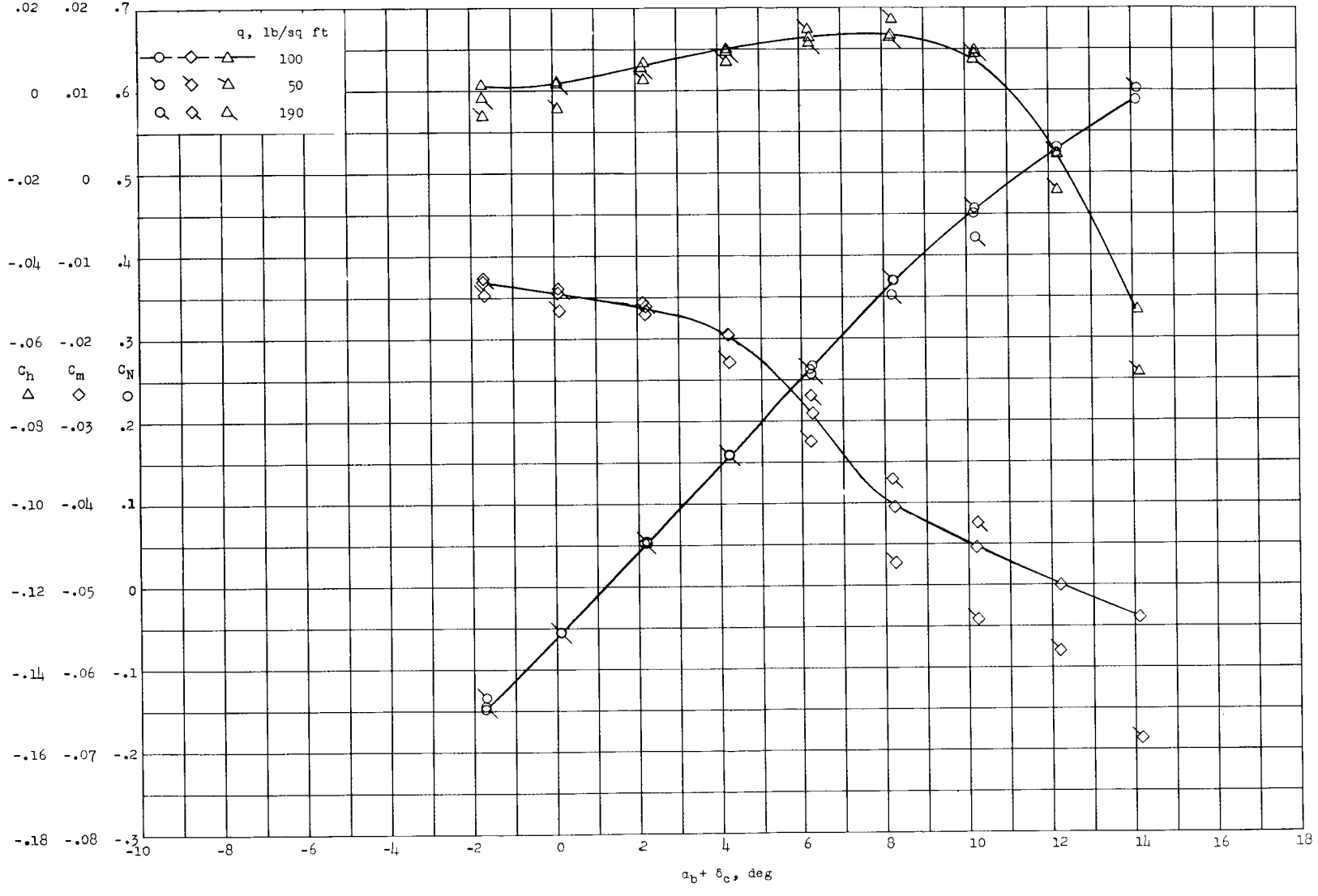

(b) M = 0.85.

Figure 53.- Continued.

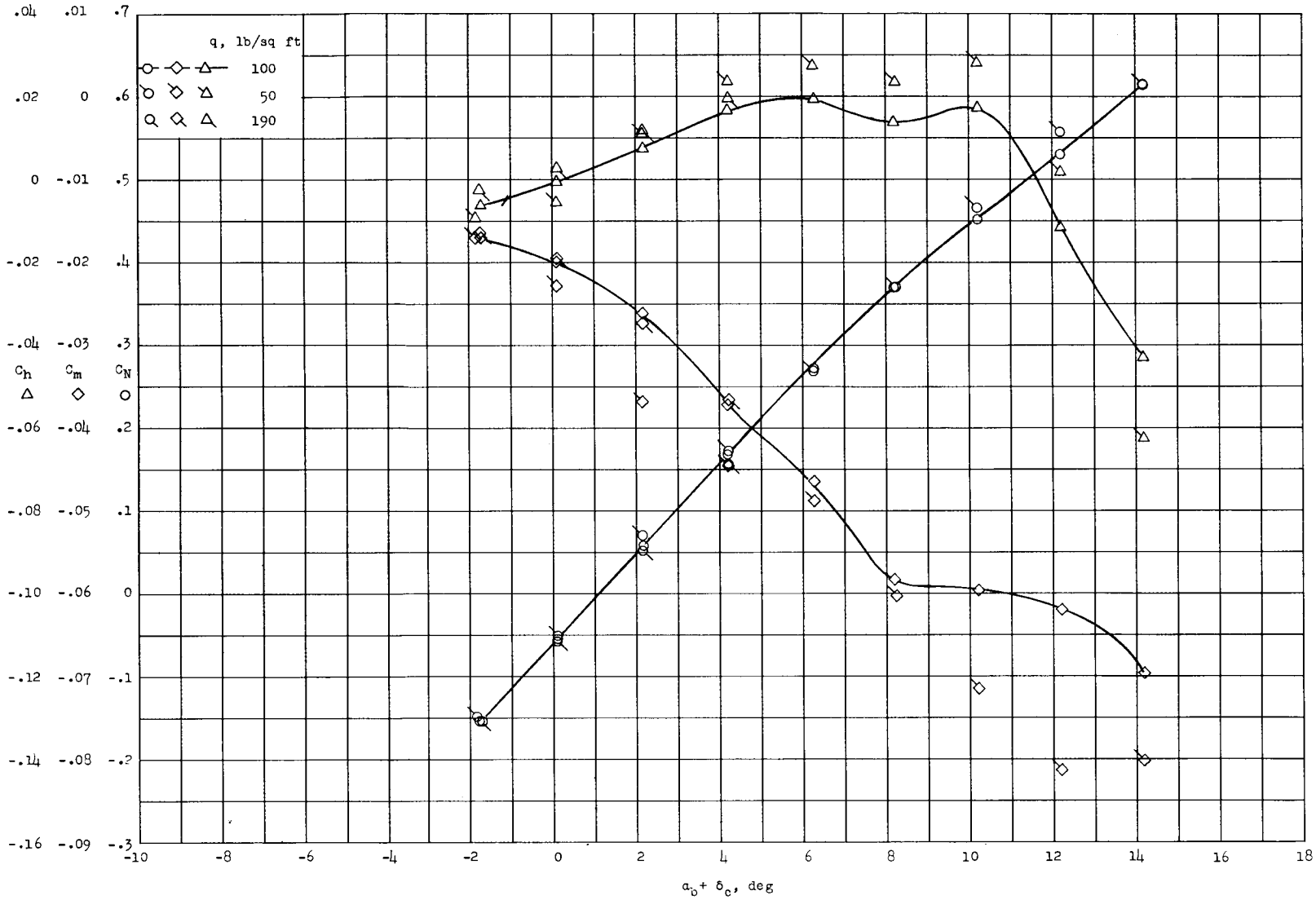

(c) M = 0.90.

Figure 53.- Continued.

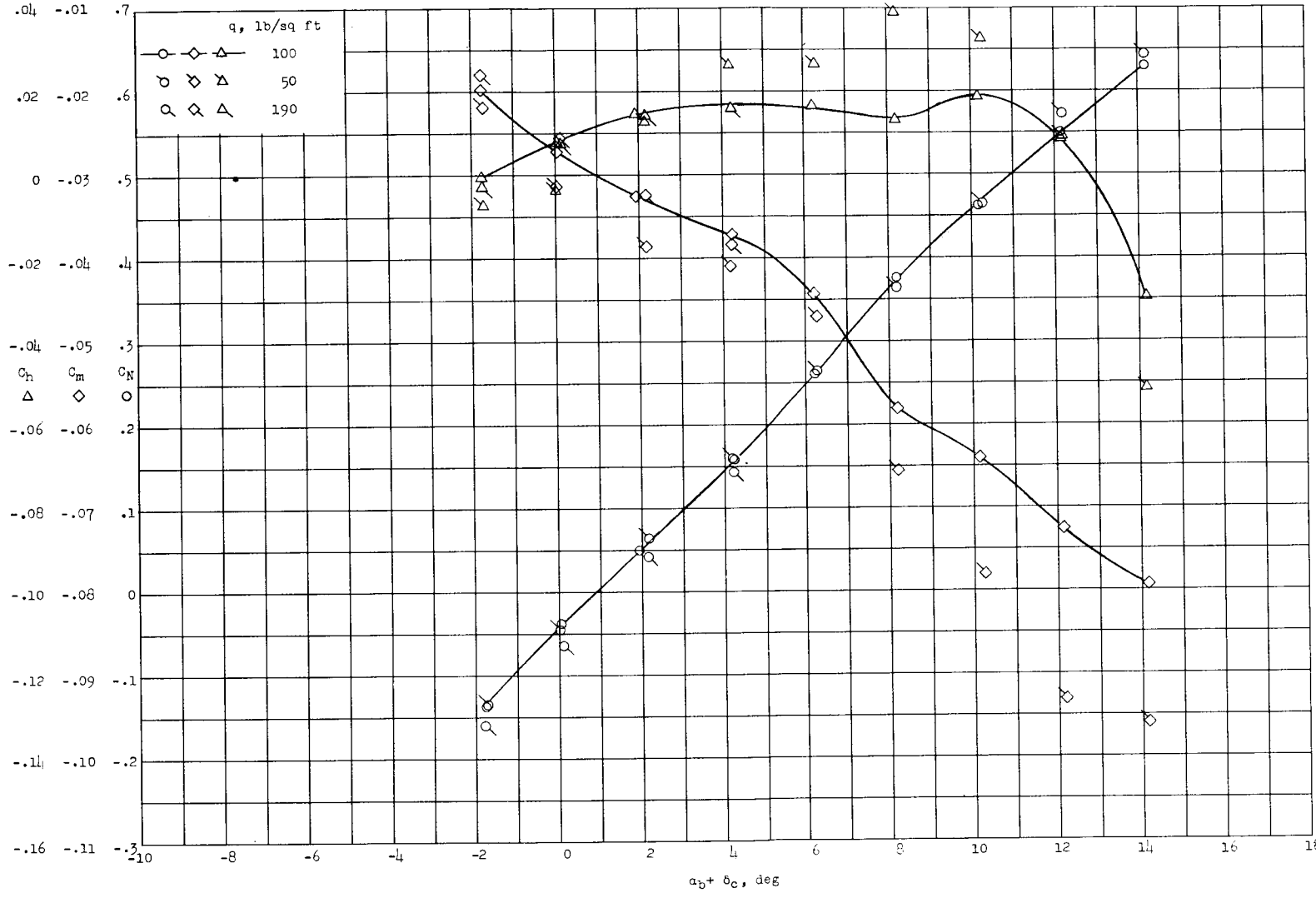

(d) M = 0.92.

Figure 53.- Concluded.

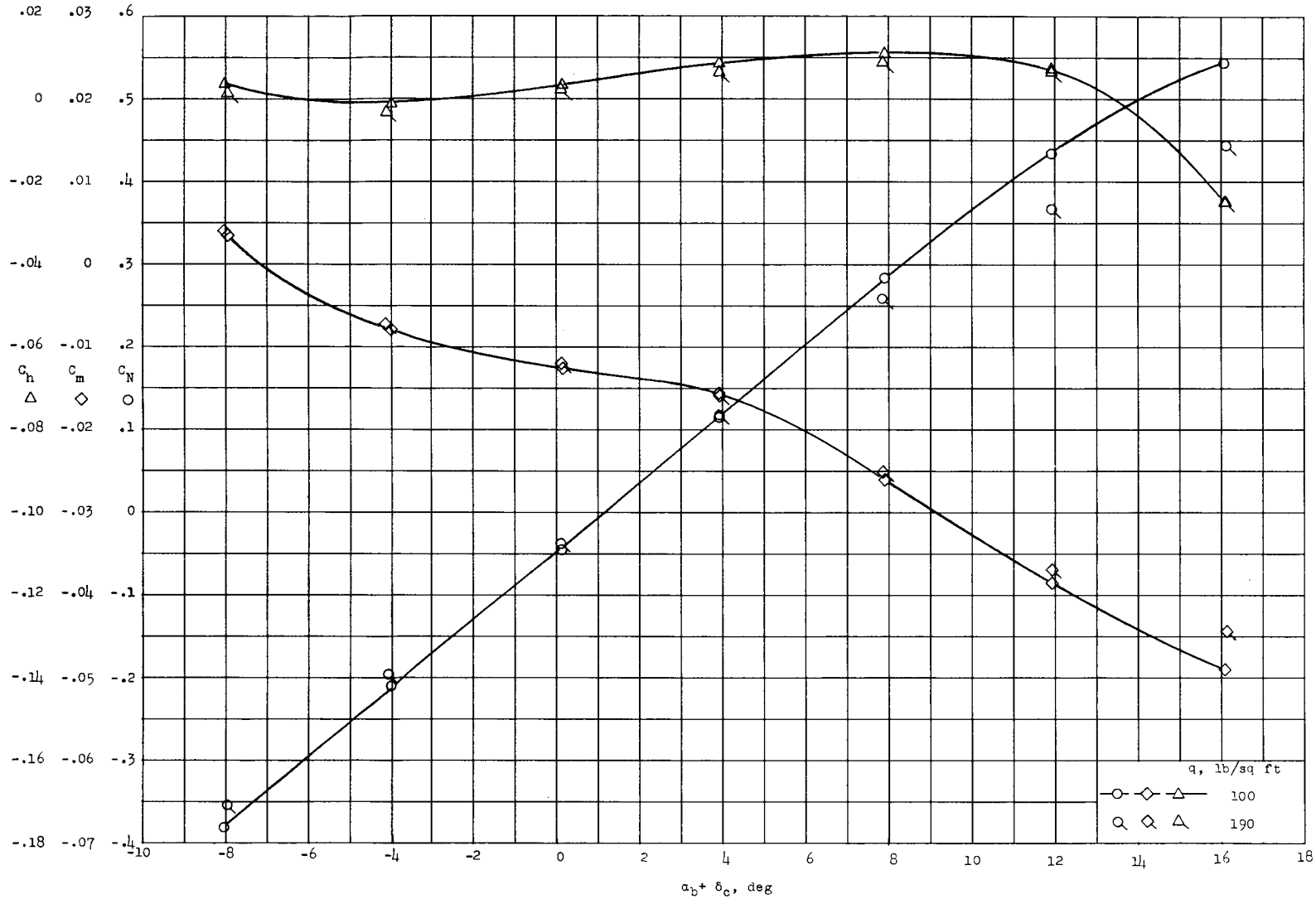

(a) M = 0.80.

Figure 54.- Comparison of aerodynamic characteristics for restrained canard in Freon-12 at different levels of dynamic pressure. $\alpha_b = 0^\circ$; $\delta_t = 0^\circ$.

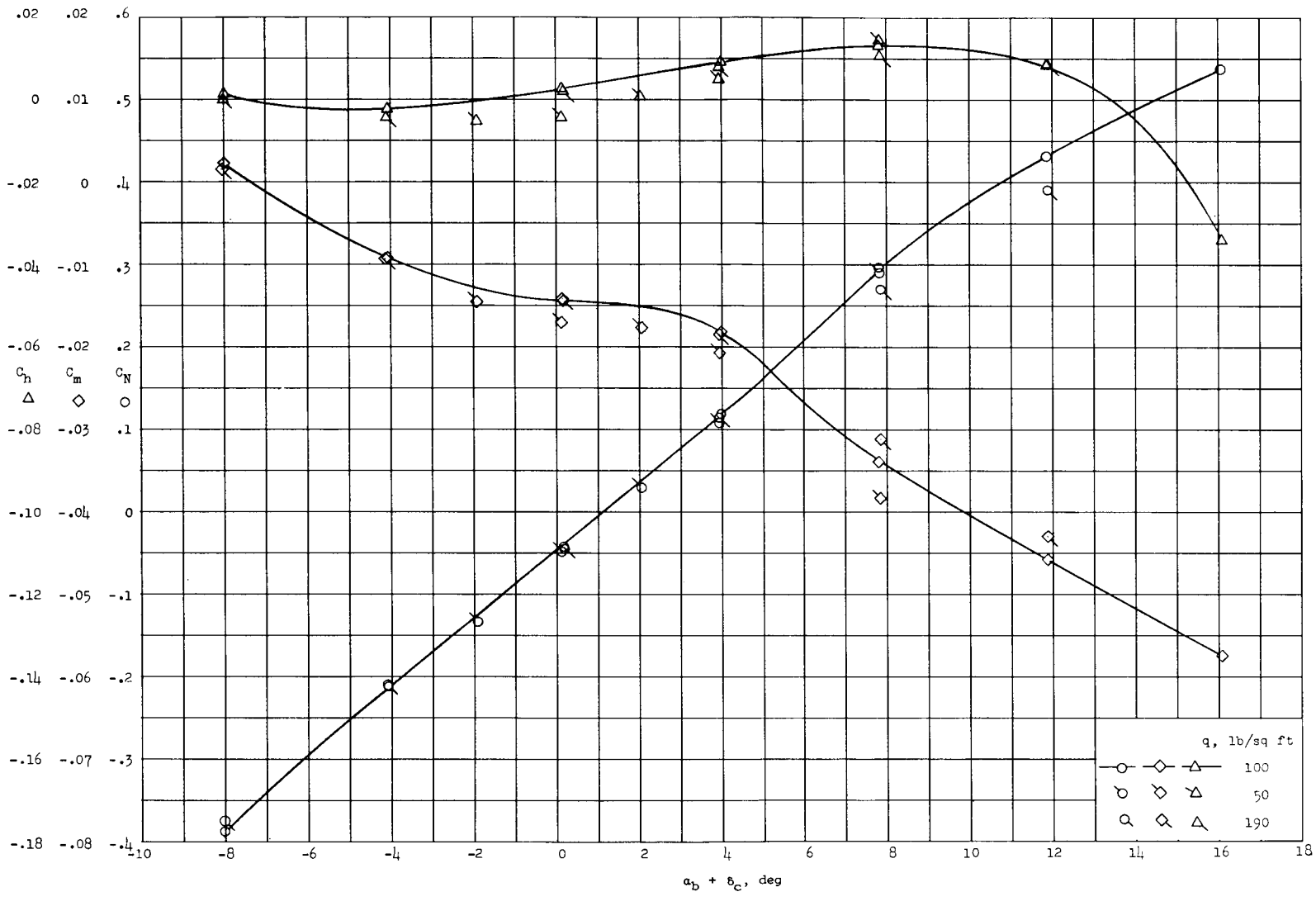

(b) M = 0.85.

Figure 54.- Continued.

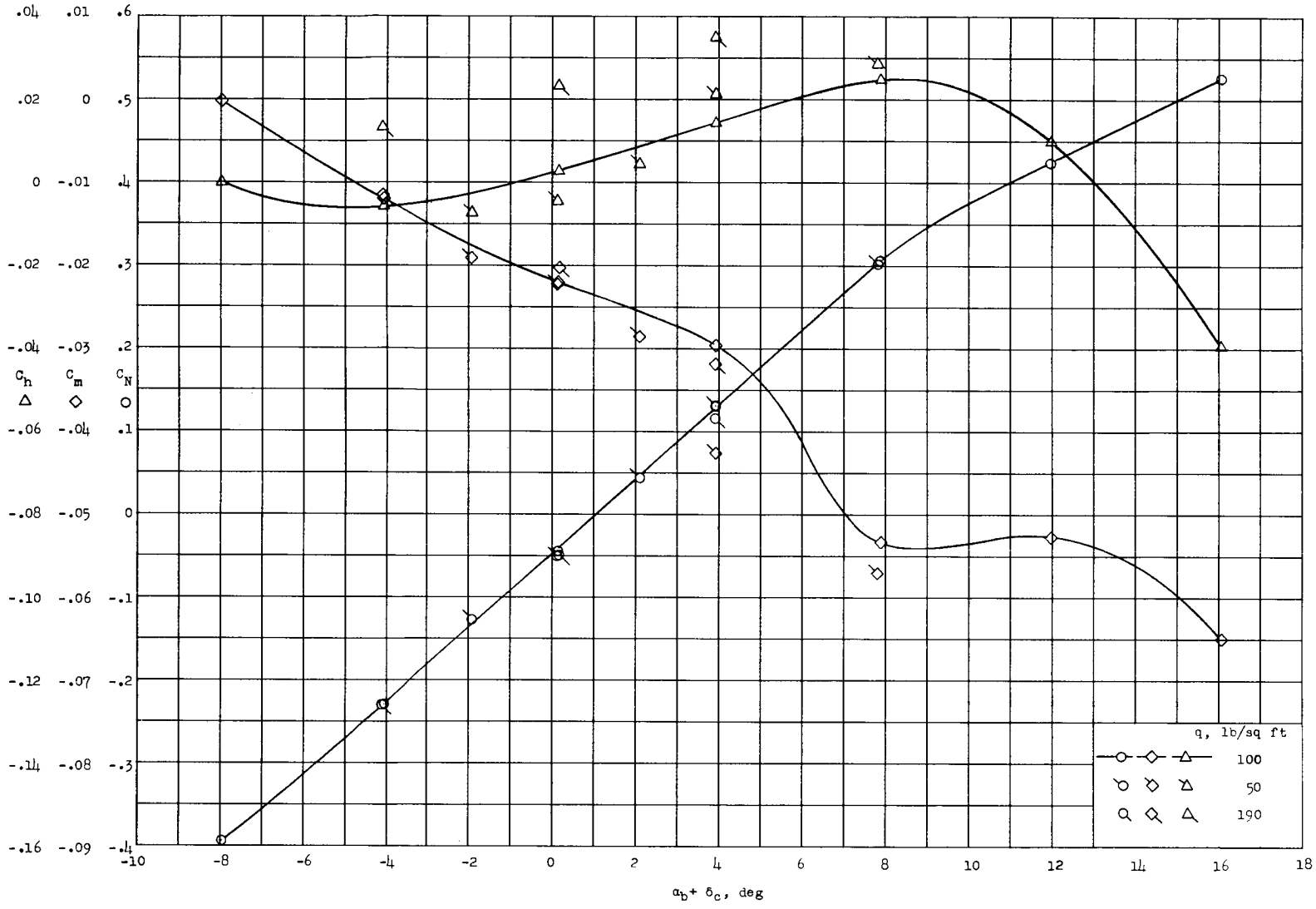

(c) M = 0.90.

Figure 54.- Continued.

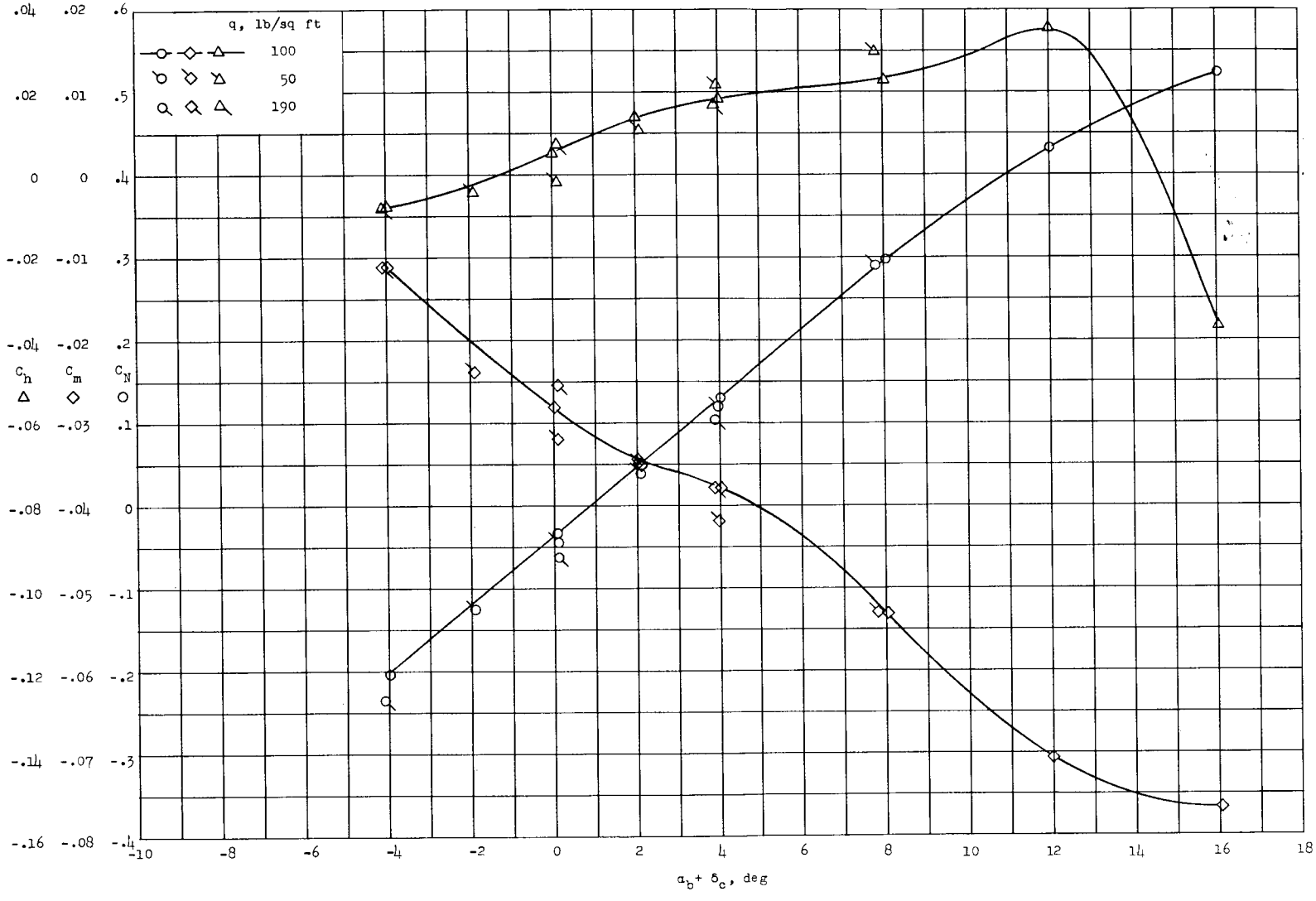

(d) M = 0.92.

Figure 54.- Concluded.

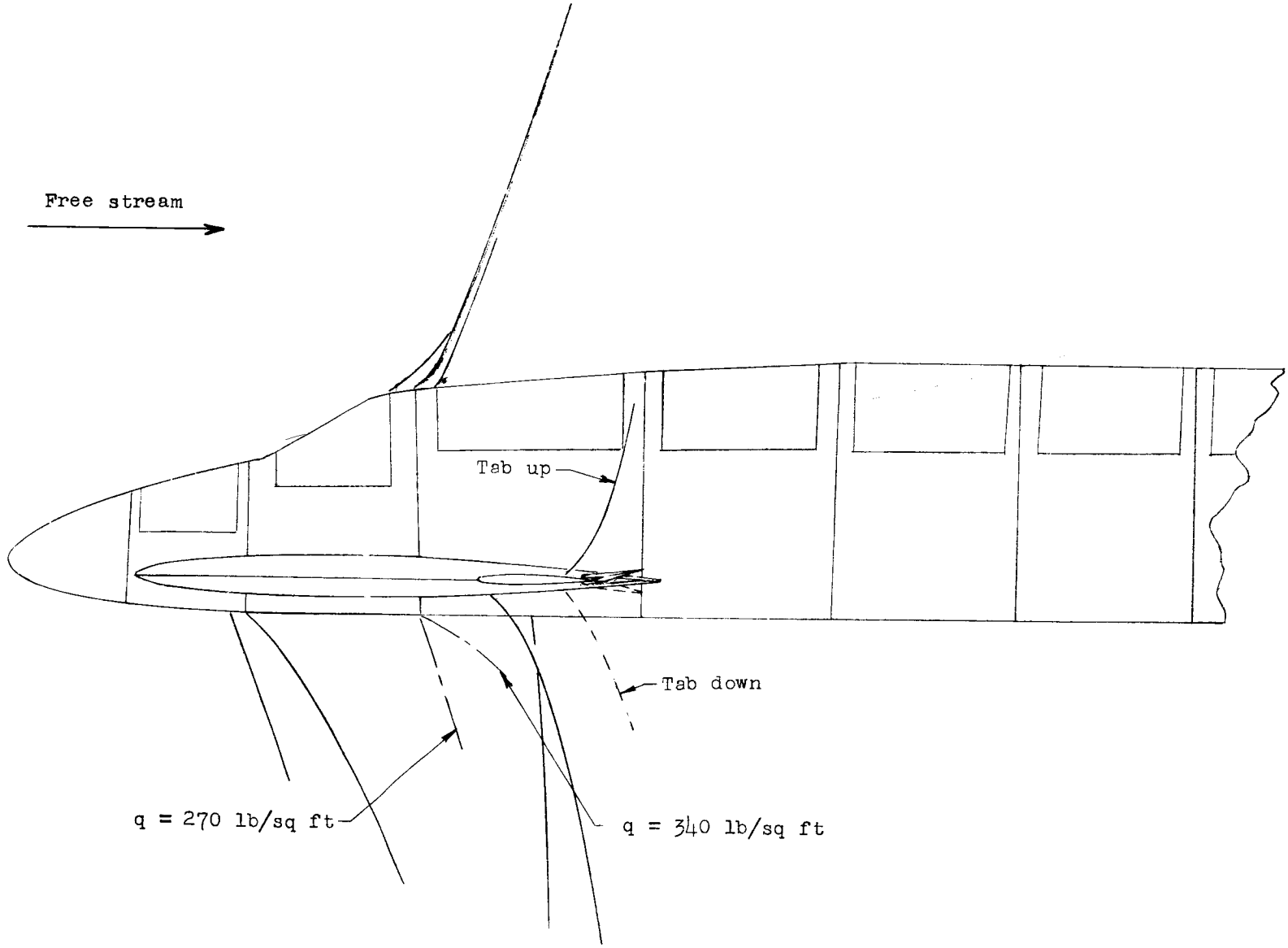

Figure 55.- Sketch of visible shock-wave pattern for restrained canard in Freon-12. $\alpha_b = 0^\circ$; $\delta_c = 0^\circ$; M = 0.92; q = 270 to 340 lb/sq ft.